



UNIVERSIDAD DE GRANADA

PROGRAMA OFICIAL DE DOCTORADO EN BIOMEDICINA

Departamento de Química farmacéutica y Orgánica

TESIS DOCTORAL

CELLULAR MODELS WITH EXTREME METABOPHENOTYPE TO STUDY TUMOR METABOLIC REPROGRAMING: DEVELOPMENT OF ANTITUMOR NANODEVICES FOCUSED ON METABOLIC TARGETS

Patricia Altea Manzano

Directores de la tesis:

Rosario M^a Sánchez Martín

Miguel Martín Hernández

Granada 14 de Julio del 2017



CENTRO PFIZER-UNIVERSIDAD DE GRANADA-JUNTA DE ANDALUCÍA
DE **GENÓMICA E INVESTIGACIÓN ONCOLÓGICA**

Editor: Universidad de Granada. Tesis Doctorales

Autora: Patricia Altea Manzano

ISBN: 978-84-9163-329-7

URI: <http://hdl.handle.net/10481/47537>

La doctoranda / *The doctoral candidate*: **Patricia Altea Manzano** y los directores de la tesis / *and the thesis supervisors*: **Rosario M^a Sánchez Martín y Miguel Martín Hernández**.

Garantizamos, al firmar esta tesis doctoral, que el trabajo ha sido realizado por el doctorando bajo la dirección del director de tesis y hasta donde nuestro conocimiento alcanza, en la realización del trabajo, se han respetado los derechos de otros autores a ser citados, cuando se han utilizado sus resultados o publicaciones.

//

Guarantee, by signing this doctoral thesis, that the work has been done by the doctoral candidate under the direction of the thesis supervisor and, as far as our knowledge reaches, in the performance of the work, the rights of other authors to be cited (when their results or publication have been used) have been respected

Lugar y fecha / *Place and date*:

España, Granada, 14 de Julio de 2017

Directores de la Tesis / *Thesis supervisors;*
candidate

Rosario M^a Sánchez Martín
Manzano

Miguel Martín Hernández

Doctorando / *Doctoral*

Patricia Altea

Firmado / *Signed*

Firmado / *Signed*

Firmado / *Signed*

QUALITY CRITERIA TO AIM FOR THE DEGREE OF “INTERNATIONAL Ph.D” FROM THE UNIVERSITY OF GRANADA:

1. An accepted or published scientific article in a relevant journal on the field of the knowledge of the doctoral thesis, here signed by the candidate, including part of the thesis results.

Patricia Altea-Manzano, Juan Diego Unciti-Broceta,* Ma Victoria Cano-Cortes, María Paz Ruiz-Blas, Ma Teresa Valero-Griñan, Juan Jose Diaz-Mochon and Rosario Ma Sanchez-Martin*. Tracking cell proliferation using a nanotechnology based approach. Nanomedicine. (2017) May 15, Year Impact Factor: 4.889 - BIOTECHNOLOGY & APPLIED MICROBIOLOGY

2. International stay in a foreign research centre.

A three months period working in the MRC Institute of Genetics & Molecular Medicine (MRC IGMM) at the Cancer Research UK Edimburgh Centre (United Kingdom) under the supervision of Andrew Finch, group leader and senior chancellor’s fellow. This fellowship was fully funded by “programa de movilidad de estudiantes de doctorado UGR-CEIBIOTIC”.

> Dates: From March 2015 to June 2015.

NOTA

El grueso del texto ha sido desarrollado en inglés debido a que se opta para la distinción de “doctorado internacional” y por la lógica del desarrollo de la mayoría de la investigación en este idioma. En la mayoría de textos científicos, los términos, acrónimos y abreviaturas que se utilizan día a día están en inglés. Para evitar confusión y aportar coherencia dentro de lo posible, el texto de la tesis se ha desarrollado íntegramente en inglés, y de la misma forma será presentada ante el tribunal. Además, se incluye un apartado donde se describen las abreviaciones y conceptos que puedan dar lugar a duda en caso de que el lector no esté familiarizado con ellos.

NOTE

According to University of Granada’s requirements to obtain an “international doctorate” degree, this thesis has been written in English and it will be defended in that language as well. As the vast majority of scientific texts, English have been selected as the language to avoid misconception within scientific terminology, abbreviation and acronyms. Nevertheless, and abbreviation and acronym table is included to facilitate the reader to go through the text in case they are not familiar with the terminology used.

TABLE OF CONTENTS

RESUMEN.....	13
SUMMARY.....	15
INTRODUCTION	17
SECTION I: Reprogramming tumor metabolism.....	17
1. From Warburg effect to current metabolic reprogramming paradigm	
1.1. Metabolism of quiescent and normal proliferating cells	
1.2. Rewiring of cellular metabolism in cancer	
1.3. Glycolysis	
1.4. The key role of anaplerosis and cataplerosis for TCA cycle function/oxidative versus reductive branch of TCA cycle.	
1.5. Glutamine: major metabolic and biosynthetic fates	
1.6. Branching pathways for macromolecular biosynthesis	
1.6.1. Nucleotides biosynthesis	
1.6.2. Lipid biosynthesis	
1.6.3. Amino acid biosynthesis	
2. Regulation of cancer cell metabolism by oncogenes and tumor suppressors	
2.1. Oncogenic alterations involved in metabolic reprogramming: glycolytic promoters and mitochondrial functional capacity assistants	
2.1.1. The PI3K/AKT/mTOR pathway	
2.1.2. c-Myc	
2.1.3. Ras	
2.2. Oncogenic stress sensors as metabolic checkpoints: promoting tumor growth	
2.2.1. Hypoxia inducible factors (HIFs)	
2.2.2. p53	
2.2.3. AMPK	
2.3. Oncogenic mutations in metabolic enzymes: changes in mitochondrial metabolism	
3. Bioenergetics and Redox-Cofactors	
3.1. Energy production in cancer cells	
3.1.1. Contribution of glycolysis and OXPHOS to ATP supply	
3.1.2. Alternative energy substrates for ATP synthesis pathways in cancer cell	
3.2. NAD(H) and NADP(H): The Universal Redox-Cofactors	

3.2.1. Major NADP/NADPH role in tumor metabolism: reductive biosynthesis and cellular defense against oxidative damage	
3.2.2. Major NAD ⁺ /NADH role in tumor metabolism: cellular metabolism regulation and energy production	
3.2.3. Movement of reducing equivalents: Cellular Shuttle Systems	
4. Aspartate and pyruvate as key growth factors in cell proliferation	
4.1. Aspartate	
4.2. Pyruvate	
5. Tumor models under alterations in metabolism	
5.1. Fumarate hydratase deficient (FH ⁻ /FH ⁻) cells	
5.2. SDH-deficient cells	
5.3. Oncogenic Kras model of pancreatic ductal adenocarcinoma (PDAC)	
5.4. VHL-deficient cells and clear-cell renal carcinoma (ccRCC)	
6. Tumor model to study reprogramming tumor metabolism: Respiration deficient cells	
SECTION II: Targeted drug delivery based on tumor metabolism.....	44
1. Strategies for targeting metabolic pathways for cancer treatment	
1.1. Targeting cancer metabolism	
1.2. Current status and future prospects of metabolism-based therapy	
1.3. Nanoparticles as promising alternative in metabolism-based therapy	
2. Nanotechnology-based Drug Delivery in cancer	
2.1. Nanotechnology approaches to cancer therapy	
2.2. Engineered Nanoparticles for Drug Delivery in cancer therapy	
2.3. Targeted therapy: monoclonal antibodies in cancer therapy	
3. Functionalized polystyrene nanoparticles as a platform for cancer therapy	
3.1. Polystyrene nanoparticles	
3.2. Multi-functionalisation strategy	
3.3. Amino-functionalised nanoparticles as carrier systems	
SECTION III: DEVELOPMENT OF AN EFFICIENT NANOTECHNOLOGY FLUORESCENCE-BASED METHOD TO TRACK CELL PROLIFERATION.....	61
1. Measurement of cell proliferation in biomedical research	
2. Fluorescent polystyrene nanoparticles as a platform for monitoring cell proliferation	
THESIS RATIONALE.....	64
THESIS MAIN AIMS.....	65
RESULTS & DISCUSSION	66

Aim 1. Understanding the overall metabolic status in the comparative tumor cell model of respiration deficient cells with extreme metabolic phenotypes	
Results.....	66
Discussion.....	82
Aim 2. Development of nanotechnology approaches based on tumor metabolism.	
Results.....	88
Discussion.....	108
Aim 3. Development of an efficient nanotechnology fluorescence-based method to track cell proliferation.	
Results.....	113
Discussion.....	125
CONCLUSIONS.....	128
CONCLUSIONES.....	130
MATERIALS AND METHODS	133
REFERENCES	147

RESUMEN

Las células tumorales, deben adaptarse y evolucionar eficientemente en un nicho celular hostil, sometido frecuentemente a un microambiente hipóxico y con fluctuaciones en la disponibilidad de nutrientes. Estas adaptaciones metabólicas en cáncer no han surgido como consecuencia de una adaptación accidental, sino debido a un muy preciso proceso regulado fundamental para la transformación celular y la oncogénesis. Por lo tanto, nos proponemos estudiar muchas de las principales rutas y dianas metabólicas que están aún sin descifrar, particularmente en algunos subtipos específicos de cáncer como son las células tumorales deficientes en respiración, que puedan desempeñar un papel fundamental en la evolución tumoral. Además, el descubrimiento de algunos de estas dianas metabólicas clave puede mejorar el desarrollo y la optimización de nuevas estrategias terapéuticas mediante el uso de aproximaciones nanotecnológicas.

El objetivo general que se propone para este proyecto es: (a) Elucidar cuales son las adaptaciones y dianas metabólicas más importantes en las células tumorales fundamentalmente en modelos de células cancerígenas deficientes en respiración, como el del fenotipo metabólico extremo propuesto en este trabajo. (b) Aprovechar el conocimiento metabólico para identificar dianas terapéuticas susceptibles de aplicaciones nanotecnológicas, que permitan un impacto selectivo y específico en las células cancerígenas utilizando nuestros modelos celulares para desarrollar una nueva aproximación para el estudio de proliferación celular mediante el uso de nanopartículas. (c) Desarrollar un método eficiente de nanotecnología basado en la fluorescencia para monitorizar la proliferación celular, ya que la proliferación celular no controlada es un sello distintivo de las células cancerosas, siendo cruciales los ensayos de proliferación celular para estudiar la influencia de los cambios metabólicos en la progresión del cáncer.

Se ha realizado un estudio profundo del mapa del estado metabólico en modelos de células tumorales de acuerdo con los siguientes parámetros de estudio para corroborar los metabofotos propuestos (Objetivo 1). Se han obtenido resultados que incluyen (i) análisis del grado de "adicción" tumoral a ciertos metabolitos que juegan un papel central en la bioenergética celular, (ii) estudio de la dependencia de estos metabolitos estableciendo perfiles de resistencia / susceptibilidad a inhibidores de la clave Enzimas de su metabolismo. (iii) estudiar la expresión y los perfiles de actividad de ciertos oncogenes para determinar su relevancia en el proceso de reprogramación metabólica de los modelos celulares. Además, en esta sección se describe una aproximación metabólica por espectrometría de masas para identificar las rutas metabólicas más importantes y objetivos. Para implementar estas estrategias nanotecnológicas basadas en el metabolismo tumoral (Objetivo 2), los resultados obtenidos son: (i) evaluación de la eficiencia de nanodispositivos en un modelo de células cancerígenas basado en células deficientes en respiración con un fenotipo metabólico extremo, (ii) desarrollo y evaluación de un sistema controlado (iii) desarrollo y validación de nanodispositivos multifuncionalizados para el sistema de administración de fármacos dirigidos a células tumorales con perfiles metabólicos selectivos. Para desarrollar un nuevo método de seguimiento basado en nanopartículas (Objetivo 3), el método ha sido validado en varias células adherentes y también en células en suspensión incluyendo células difíciles de transfectar. Aún más interesante es el hecho de que el monitoreo de la proliferación celular de

linfocitos se ha logrado con éxito (hasta el momento el único método eficaz para realizar este monitoreo de linfocitos es la tinción CFSE). El método también se validó en un ensayo basado en células que determinó la detención celular inducida a través del efecto MMC, mostrando la potencia del método para ensayos celulares a largo plazo. Además, este nuevo método no altera el ciclo celular, por lo que no presenta efectos citotóxicos.

ABSTRACT

Tumor cells need to adapt and evolve efficiently in a hostile cellular niche, frequently subjected to a hypoxic microenvironment and with fluctuations in availability of nutrients. These metabolic adaptations of cancer cells have not arisen as a consequence of an accidental adaptation, but due to a very precise regulated process for cell transformation and oncogenesis. Therefore, we intend to study many of the metabolic targets that are still to be deciphered, particularly in some cancer-specific subtypes such as respiratory deficient tumoral cells that can play a key role in tumor evolution. In addition, the discovery of these key metabolic targets can improve the development and optimization of new therapeutic strategies through the use of nanotechnology based approaches.

The main aims of this project are: (a) to elucidate the most important adaptations and metabolic targets in tumor cells, mainly in models of carcinogenic cells deficient in respiration, such as the extreme metabolic phenotype proposed in this work; (b) to take advantage of the metabolic knowledge to identify therapeutic targets susceptible of nanotechnological applications, that allow a selective and specific impact in the cancerous cells using our cellular models to develop a new approach for the study of cell proliferation through the use of nanoparticles.; (c) To develop an efficient nanotechnology fluorescence based method to track cell proliferation as the uncontrolled cell proliferation is a hallmark of cancer cells, being crucial cell proliferation assays to study the influence of metabolic changes in cancer progression.

A deep study of the map of metabolic status in tumor cell models according to the following study parameters to corroborate the proposed metabotypes has been carried out (Aim 1). Results has been achieved that include (i) analysis of the degree of tumor "addiction" to certain metabolites that play a central role in cellular bioenergetics, (ii) study of the dependence of these metabolites establishing profiles of resistance / susceptibility to inhibitors of key enzymes of their metabolism. (iii) study the expression and activity profiles of certain oncogenes to determine their relevance in the metabolic reprogramming process of the cellular models. Additionally in this section a metabolomic approximation by mass spectrometry to identify the most important metabolic routes and targets is described. To implement these nanotechnology approaches based on tumor metabolism (Aim 2), the results achieved are: (i) evaluation of nanodevices efficiency in cancer cell model based on respiration deficient cells with an extreme metabolic phenotype, (ii) development and evaluation of a controlled drug delivery system for combined metabolic-based therapy and (iii) development and validation of multifunctionalized nanodevices for targeted drug delivery system to tumor cells with selective metabolic profiles. To develop a novel tracking method based on nanoparticles (Aim 3), the method has been validated in several adherent cells and also in suspension cells including hard-to-transfect cells. Even more interesting is the fact that monitoring of cell proliferation of lymphocytes has been successfully achieved (so far the only efficient method to do this lymphocytes monitoring is CFSE staining). The method was also validated in a cell-based assay which determined the induced cellular arrest through MMC effect, showing the power of the method for long-term cellular assays. Furthermore, this new method does not alter the cell cycle hence presenting no cytotoxic effects.

SECTION 1: REPROGRAMMING TUMOR METABOLISM

1. From Warburg effect to current metabolic reprogramming paradigm

1.1. Metabolism of quiescent and normal proliferating cells

Metabolism covers the sum of all chemical reactions that take place within a cell or organism. It is divided into two antagonistic series of reactions: catabolism, which refers to the breakdown of molecules into smaller metabolites in order to release energy; and anabolism, which describes the consumption of energy in order to build macromolecules needed for cell proliferation (DeBerardinis and Thompson, 2012). The ratio between these opposing reactions depends on cellular context and differentiation state. Likewise, metabolic strategies vary greatly between resting versus proliferating cells. On the one side, quiescent cells are metabolically active, adopting catabolic metabolism focused on maximizing the ATP production efficiency from limited nutrients. In contrast, growth-factor-stimulated cells increase their nutrient uptake and adopt an anabolic metabolism. These proliferating cells take up nutrients in excess, convert them into biosynthetic building blocks in the form of amino acids, fatty acids and nucleotides, to generate macromolecules for cell growth and division (Lunt and Vander Heiden, 2011; Ward et al., 2012). Cancer cells are proliferating cells which can have the instructional signaling pathways downstream of growth factor receptors constitutively even in the absence of extracellular growth factors (**Fig. 1**). That enables them to sustain their aberrant metabolic needs (Ward et al., 2012).

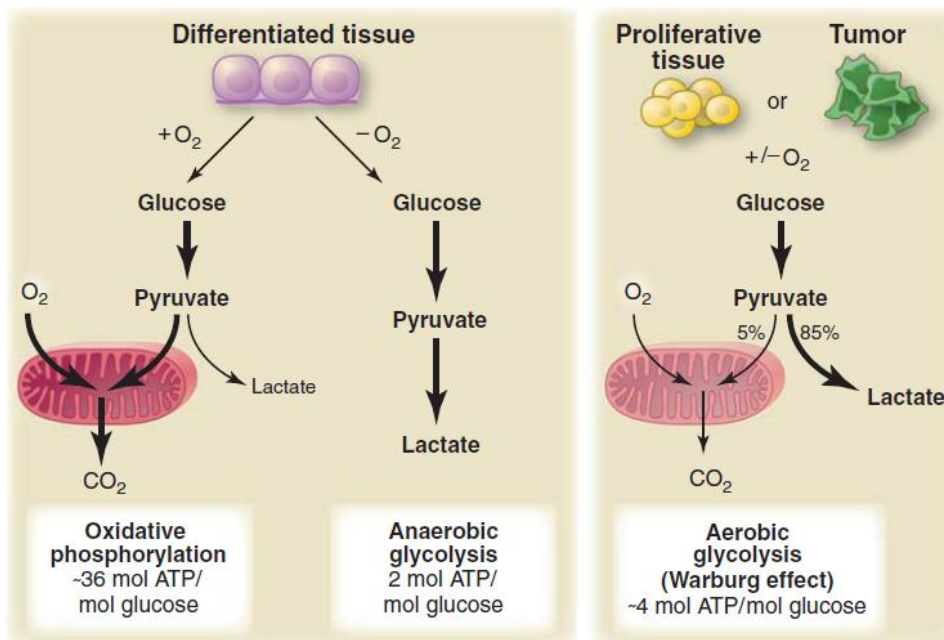


Figure 1. Overview of metabolic activity in quiescent and proliferating cells. Schematic representation of the metabolism in quiescent cells, proliferating normal cells and proliferating cancer cells. Quiescent cells rely mainly on mitochondrial respiration for ATP production. Proliferating cells use glucose for the conversion to pyruvate-derived lactate. They also divert carbons from glycolysis to accumulate building blocks for macromolecule biosynthesis and to maintain their redox potential. Nonmalignant cells are embedded in an environment that provides sufficient nutrients and oxygen for normal cell function. In contrast, cancer cells may be exposed to nutrient and oxygen withdrawal during same stages of tumorigenesis (Vander Heiden et al., 2009).

1.2. Rewiring of cellular metabolism in cancer

In the presence of oxygen, most differentiated cells primarily maximize ATP production by oxidative phosphorylation, with minimal production of lactate. For this purpose, they metabolize glucose to carbon dioxide by oxidation of glycolytic pyruvate in the mitochondrial TCA cycle (**Fig. 1**). Historically, the field of cancer metabolism has been dominated from the 1920s by the German biochemist Otto Warburg discoveries. He observed that cancer cells consume glucose at surprisingly high rate compared to normal cells. Furthermore, cancer cells metabolize it predominantly through glycolysis, producing high levels of lactate even in oxygen-rich conditions (Warburg, 1924, 1956a). This increase in glycolytic activity is known aerobic glycolysis or “Warburg effect” (DeBerardinis et al., 2008a; Vander Heiden et al., 2009). This glucose fermentation is far less efficient than the TCA cycle coupled to oxidative phosphorylation in generating ATP (Vander Heiden et al., 2009) (**Fig. 1**).

Predominant aerobic glycolysis observation in cancer cells led Warburg to suggest that these cells arise from a defect in mitochondrial respiration. According to that, tumor cells exhibit a permanent oxidative metabolism deficiency that causes them to rely on enhanced glycolysis (Warburg, 1956b). However, it is now clear that respiration is not impaired in most cancer cells (Fantin and Leder, 2006; Moreno-Sánchez et al., 2007; Zu and Guppy, 2004). Even then, aerobic glycolysis has been observed in a wide variety of tumors coming from different cell types. But most normal cells in adult tissues from which cancer cells arise generally do not utilize aerobic glycolysis (Lunt and Vander Heiden, 2011). Thus, the fact that cancer cells revert to a metabolic phenotype characteristic of rapidly dividing cells suggested that aerobic glycolysis must provide proliferative advantages (Coller, 2014).

Later, similar glucose metabolism patterns were observed in proliferating primary lymphocytes studies (Brand, 1985; Hedeskov, 1968; Wang et al., 1976), rejecting the possibility that aerobic glycolysis is tumor cell exclusive, or that the Warburg effect only develops when oxidative capacity is damaged (DeBerardinis et al., 2008a). These studies suggested that aerobic glycolysis is a common phenomenon among many proliferating cells.

Over years, it was thought that cancer was a disease of genetic alterations, where Warburg effect was considered an indirect secondary phenomenon consequence of tumorigenesis (Levine and Puzio-Kuter, 2010). However, the question as to why cancer cells favor the much less efficient process of aerobic glycolysis over oxidative phosphorylation remained open. Remarkably, after a long absence of interest, research done in the past fifteen years has begun to answer this question. The key lay in the discovery that oncogenes and tumor suppressors are intricately linked to the regulation of cancer metabolism (Vander Heiden et al., 2009; Kroemer and Pouyssegur, 2008). Both oncogenes and tumor suppressor gene products can influence the switch between aerobic glycolysis and a more extensive use of the TCA cycle to generate ATP. Furthermore, several transcription factors and metabolic enzymes have been demonstrated crucial in mediating the aberrant metabolic behavior of tumor cells (Kroemer and Pouyssegur, 2008; Levine and Puzio-Kuter, 2010; Ward et al., 2012). Therefore, in 2011, the importance of energy metabolism reprogramming to tumor progression was signified by its addition as an emerging hallmark to the revised list of hallmarks of cancer (Hanahan and Weinberg, 2011a).

Thus, a renewal view under the concept “metabolic reprogramming” has emerged in last few years. This term describes conventional metabolic pathways whose activities are enhanced or suppressed in tumor cells relative to benign tissues as a consequence of tumorigenic mutations and/or other factors (DeBerardinis and Chandel, 2016). Recent studies have provided a further understanding of cancer metabolism and the underlying rewiring of tumor metabolic pathways are being elucidated. Some of the most striking changes of tumor cell metabolism are detailed below.

1.3. Glycolysis

Glucose is converted to two pyruvate molecules through a series of nine enzymatic reactions collectively called glycolysis, resulting in a net gain of two molecules of ATP and two molecules of NADH. The fate of glycolytic product pyruvate depends on the cellular oxygen status. In well-oxygenated differentiated tissue, pyruvate enters the mitochondria and is completely oxidized to CO₂, a process that generates approximately 36 molecules of ATP per molecule of glucose. Under oxygen deprivation, pyruvate is converted to lactic acid by lactate dehydrogenase (LDH) and facilitates the conversion of NADH to NAD⁺, which is a necessary cofactor for the glycolytic flux (**Fig 2**). As mentioned, in proliferating tissue and cancer cells, pyruvate is mainly converted to lactate regardless of the oxygen concentration (Lunt and Vander Heiden, 2011). This reaction is beneficial for cancer cells as it help regenerate NAD⁺ to accelerate glycolysis and reduces intracellular oxidative stress, promoting tumors survival (DeBerardinis et al., 2008a; Vander Heiden et al., 2009). Previously, the excess production of lactate by cancers was considered simply to be a byproduct of the Warburg effect, but now it is known that lactate mediates a considerable number of effects in the tumor, such as promoting growth, invasion, and metastasis (Hirschhaeuser et al., 2011).

To prevent intracellular acidification and death due to high amount of intracellular lactate, this metabolite is exported from the cell by a family of passive proton-lactate membrane symporters called the monocarboxylate transporters (MCTs). It has been demonstrated that MCTs, especially the MCT1 and MCT4 isoforms, are over-expressed in most cancers to facilitate the overload of lactate production that occurs with the Warburg effect (Kennedy and Dewhirst, 2010). Indeed, decreasing breast cancer cell proliferation *in vitro* and tumor growth *in vivo* by MCT loss-of-Function has been recently reported, providing further support for use of MCTs inhibitors as anti-cancer therapeutics (Hong et al., 2016).

On the other hand, glycolytic-derived-ATP is certainly important for cellular functions and plays a significant role in proliferating cell biosynthesis. However, the importance of aerobic glycolysis extends beyond ATP production to allow nutrient assimilation into biosynthetic precursors (Lunt and Vander Heiden, 2011). This fact was reinforced by the discovery of the embryonic M2 isoform of pyruvate kinase (PK) enzyme is the isoform expressed in both cancer cells and normal proliferating cells. Recently, several papers reported that PK plays a crucial role in reprogramming of glycolytic metabolism (Chaneton et al., 2012; Christofk et al., 2008a; Hitosugi et al., 2009; Wong et al., 2013). It is a rate-limiting enzyme that catalyzes the final reaction of glycolysis, converting phosphoenolpyruvate (PEP) to pyruvate and producing ATP (**Fig. 2**). It has been demonstrated PKM2 is less active than PKM1 both *in vitro* and *in cells* (Vander Heiden et al., 2010). In addition, PKM2 effect on glycolysis depends on whether it

exists as a highly active tetramer favoring formation of pyruvate and ATP, or a less active dimer, which predominates in tumor cells (Anastasiou et al., 2012; DeBerardinis et al., 2008b). Indeed, cancer cells may revert to the highly regulated M2 isoform because it can switch between active and inactive forms to control the flow of glycolytic carbons between biosynthesis and mitochondrial ATP production (Lunt and Vander Heiden, 2011).

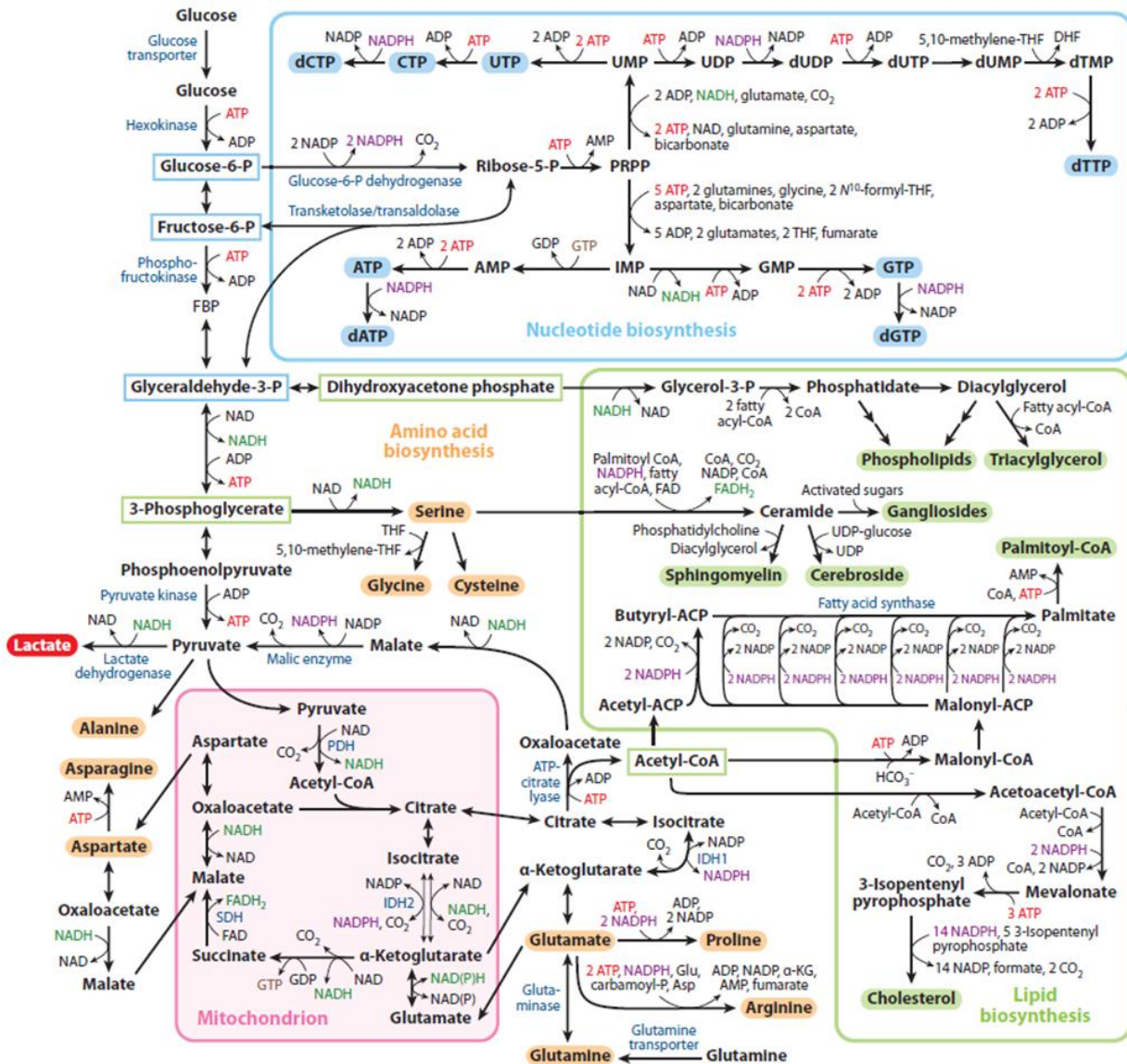


Figure 2. Metabolic pathways active in proliferating cells. This schematic represents our current understanding of how different pathways in central carbon metabolism contribute to biomass precursors. Enzymes that control critical steps and are often overexpressed or mutated in cancer cells are shown in blue. Abbreviations (other than standard nucleotide or amino acid abbreviations): PDH, pyruvate dehydrogenase; SDH, succinate dehydrogenase; IDH, isocitrate dehydrogenase; P, phosphate; PRPP, phosphoribosyl pyrophosphate; CoA, coenzyme A; ACP, acyl carrier protein; THF, tetrahydrofolate; DHF, dihydrofolate; aKG, a-ketoglutarate. (Vander Heiden et al., 2011).

Replacement of PKM2 isoform by constitutively active tetrameric form PKM1 in tumor cell lines renders them less glycolytically active, and diminishes tumor xenograft growth, suggesting that PKM2 promotes both aerobic glycolysis and anabolic metabolism (Christofk et al., 2008a). The suppression of PKM2 by phosphotyrosine-catalyzed release of FBP from the enzyme impairs pyruvate formation, resulting in accumulation of upstream intermediates.

These glycolytic intermediates above PK may be further directed towards anabolic processes for nucleic acid, phospholipid and amino acid synthesis, increasing substrate availability for rapidly growth (Christofk et al., 2008b). Until now, it has been described aerobic glycolysis is not selected for increased ATP production, otherwise a major function for proliferating cells likely extends beyond rapid ATP production to support macromolecular synthesis providing biosynthetic precursors.

Many glycolytic enzymes have been shown to be upregulated during tumorigenesis. The increased glucose uptake capacity in cancer cells is due to the upregulation of glucose transporters GLUT1 and GLUT3 (Au et al., 1997; Suzuki et al., 1999).

1.4. The key role of anaplerosis and cataplerosis for TCA cycle function

In quiescent cells glycolysis-derived-pyruvate is converted to acetyl-CoA and is oxidized in the TCA cycle generating ATP by oxidative phosphorylation. In cancer cells, acetyl-CoA tends to be introduced into a truncated TCA cycle, where it is converted into intermediates that can be used for macromolecular biosynthesis (**Fig 1**). The truncated TCA cycle appears to support cell proliferation (Mullen et al., 2014). This underscores the dual roles for cell growth: it generates reducing equivalents for oxidative phosphorylation by the electron transport chain while also supplying carbons for precursor production. That is possible by both oxidative and reductive branch of TCA cycle.

Entry and exit of TCA cycle carbons is carried out through reciprocal and correlative reactions termed anaplerosis and cataplerosis. Cataplerosis includes reactions involved in the conversion of TCA cycle intermediates to a product that is used in biosynthetic pathways (Owen et al., 2002). In quiescent cells, maximization of ATP production from oxidizable substrates is the main role of the TCA cycle. However, in proliferating cells much of the carbon that enters the TCA cycle serves as an important source of biosynthetic pathways. That results in a continuous efflux of TCA intermediates (DeBerardinis et al., 2008a). Most cataplerotic substrate TCA intermediate-derivate is citrate, which is transferred to the cytosol to be converted to oxaloacetate. This oxaloacetate can be transformed in the lipogenic precursor acetyl-CoA in order to produce fatty acids, cholesterol, and isoprenoids, resulting in truncated TCA cycle (DeBerardinis et al., 2008a). Furthermore, oxaloacetate and also α -ketoglutarate supply intracellular pools of nonessential amino acids (aspartate, asparagine, glutamate, and proline) to be used in the synthesis of proteins and nucleotides (**Fig. 2**) (Lunt and Vander Heiden, 2011).

For cataplerosis to be sustainable, the TCA cycle intermediates must be replenished. That TCA intermediates are replaced by a process called anaplerosis (Owen et al., 2002). There are several mechanisms that cells can use to produce

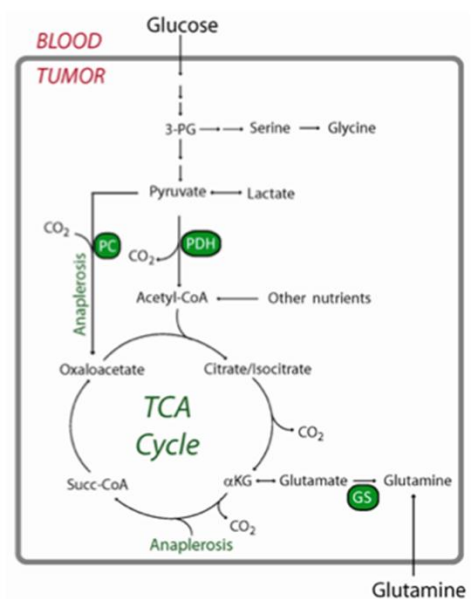


Figure 3. Predominant pyruvate and glutamine dependent anaplerotic activity in cancer cells. Adapted from E.A Maher et. al. 2012.

anaplerotic activity, remain prominent pyruvate and various amino acids in tumor metabolism (**Fig. 3**). Pyruvate carboxylase, which synthesizes oxaloacetate from pyruvate in the mitochondrial matrix, has been reported as an important anaplerotic enzyme (Cheng et al., 2011). Amino acids can enter the TCA cycle via pyruvate, acetyl-CoA, acetoacetyl-CoA, α -ketoglutarate, succinyl-CoA, fumarate, and oxaloacetate (Owen et al., 2002). The amino acid glutamine is the major contributor to anaplerotic flux, providing carbons for TCA cycle intermediates that serve as precursors of many macromolecules/nonessential amino acids (DeBerardinis et al., 2007a). Glutamine is catabolized to glutamate and glutamate can enter the TCA cycle through its conversion to α -ketoglutarate (glutaminolysis) or via numerous transamination reactions. In addition, by reductive carboxylation, glutamine-derived α -ketoglutarate is reduced through the consumption of NADPH in the non-canonical reverse reaction, to form citrate (Altman et al., 2016). Once in the TCA cycle, α -ketoglutarate is metabolized further to ultimately form oxaloacetate, an important anabolic precursor that will condense with acetyl-CoA to produce citrate.

1.5. Glutamine: major metabolic and biosynthetic fates

The other major source of energy and carbons for cancer cells besides glucose is glutamine (DeBerardinis et al., 2008a). Glutamine is a key substrate required for several important metabolic roles in the cell. It serves as a carbon source for energy production, contributes carbon and nitrogen to biosynthetic reactions, regulates redox homeostasis and modulates activity of signal transduction pathways (**Fig. 4**) (Daye and Wellen, 2012). These functions of glutamine metabolism that contribute to support cell growth and proliferation in cancer cells are detailed below.

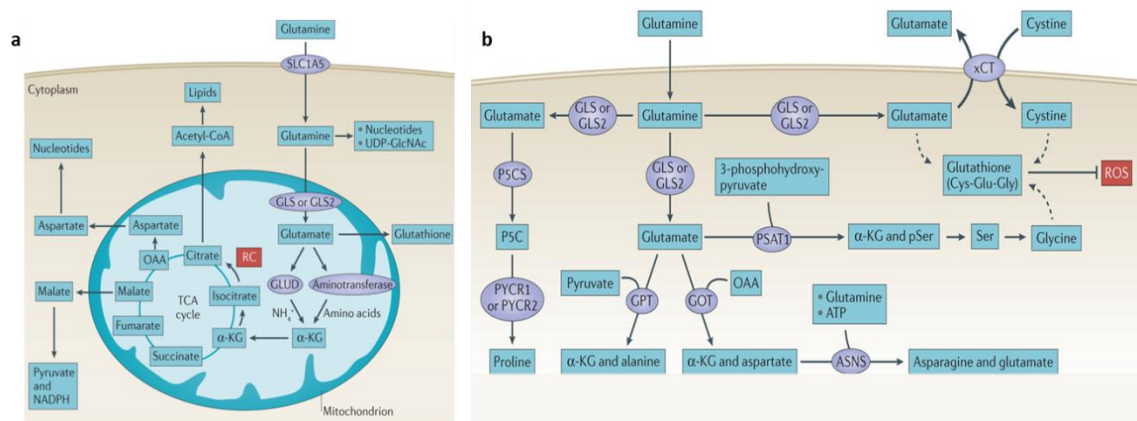


Figure 4. Glutamine metabolism. (a) Major metabolic and biosynthetic fates of glutamine. **(b)** Glutamine control of amino acid pools and reactive oxygen species.

As primary carbon source for energy production and biosynthesis. Role of glutamine in supporting mitochondrial metabolism has been previously mentioned. Glutamine serves as an important anaplerotic substrate in the replenishment of TCA intermediates. Based on ^{13}C isotopologues analyses, glucose-independent TCA cycle entirely supported by glutamine has been uncovered. This efficient glutaminolysis pathway, in which glutamine can be used either for anabolic purposes or for producing energy, involved the supply of acetyl-CoA and oxaloacetate to the TCA cycle (by the combined activity of ATP citrate lyase, malic enzyme, PDH, and/or pyruvate carboxylase) (**Fig. 4a**) (Le et al., 2012; Metallo et al., 2011).

Frequently, glutamine plays a supporting role in lipogenesis by allowing transfer of glucose-derived acetyl-CoA from the mitochondria to the cytoplasm through citrate. In addition to this, glutamine carbon can also support *de novo* lipogenesis supplying acetyl-CoA through two mechanisms. First, providing pyruvate from malate that can re-enter the TCA cycle as acetyl-CoA (Le et al., 2012). Second, glutamine, after conversion to α -ketoglutarate, can undergo reductive carboxylation to generate isocitrate, which is then converted into citrate (**Fig. 4a**) (Daye and Wellen, 2012; Scott et al., 2011). This direct contribution to *de novo* lipogenesis has been particularly observed under conditions of hypoxia or mitochondrial dysfunction, in which cells were shown to depend almost exclusively on the reductive metabolism of glutamine (Metallo et al., 2011; Mullen et al., 2011a).

As a nitrogen donor. The amido and amino groups of glutamine contribute to multiple biosynthetic pathways, including synthesis of non-essential amino acids, nucleotides, and hexosamines. On the one hand, nitrogen from glutamine via glutamate supports the levels of many amino acid pools in the cell through the action of aminotransferases (Hosios et al., 2016). It has been demonstrated that various glutamine-derived amino acids, particularly alanine, aspartate and serine, contribute to cancer cell survival (**Fig. 4b**) (Wise and Thompson, 2010). On the other hand, glutamine role in nucleotide biosynthesis as a nitrogen donor for both purine and pyrimidine synthesis, has been implicated in ongoing support of proliferation (Lane and Fan, 2015) (**Fig. 4a**). The importance of glutamine as a nitrogen reservoir was demonstrated by the fact that glutamine-deprived cancer cells undergo cell cycle arrest that cannot be rescued by TCA cycle intermediates but can be rescued by exogenous nucleotides (Gaglio et al., 2009).

As a regulator of redox homeostasis. Several glutamine metabolic pathways lead to products that directly control ROS levels. In addition to glutamine metabolism contributing to mitochondrial ROS production through its oxidation in the TCA cycle, the important glutamine-ROS-control is through synthesis of glutathione. Glutathione is a tripeptide (Glutamate-Cysteine-Glycine) that serves to neutralize peroxide free radicals (**Fig. 4b**). It has long been appreciated that glutamine input is the rate-limiting step for glutathione synthesis, and also is responsible for the synthesis of two of its components (Altman et al., 2016). In its antioxidant role, glutathione donates electrons, becoming oxidized. In order to restore glutathione to its reduced form, NADPH is required, and glutamine metabolism can also lead to increased production of NADPH, through its metabolism through malic enzyme (Daye and Wellen, 2012; Wise and Thompson, 2010).

As a modulator cell signalling pathways. In order to control cell survival and growth, cells have developed glutamine-dependent mechanisms that include the modulation of signal transduction pathways. Glutamine metabolism has been related to the integrated stress response, protein folding and trafficking, and endoplasmic reticulum stress (Altman et al., 2016; DeBerardinis and Cheng, 2010).

1.6. Branching pathways for macromolecular biosynthesis

Glucose and glutamine both serve as the primary nutrients to fuel cancer cell proliferation. Metabolism relation of these two nutrients and their active coordination in reprogramming metabolism of proliferating cells has been recently reported (Daye and Wellen, 2012).

Glucose-derived carbon has diverse fates. By glycolytic intermediates, glucose can provide the precursors for the chemical constituents required for building macromolecules essential for cell division. Besides replenishing TCA cycle intermediates, glutamine contributes most to protein biosynthesis (**Fig. 2**) (Hosios et al., 2016). Changes in branching pathways thus leading to higher levels of biosynthesis activities most commonly studied in cancer metabolism are discussed in the following section.

1.6.1. Nucleotides biosynthesis

To generate ribose 5-phosphate for nucleotide biosynthesis, cells divert carbon from glycolysis into either the oxidative or non-oxidative arm of the pentose phosphate pathway (PPP) (DeBerardinis et al., 2008b). Both the salvage and *de novo* synthesis pathways of purine and pyrimidine biosynthesis lead to production of nucleoside-5'-phosphates through the utilization of an activated sugar intermediate (5-phosphoribosyl-1-pyrophosphate, PRPP). PRPP is generated from ribose-5-phosphate diverted from the glycolytic flux to the PPP, and requires energy in the form of ATP (**Fig. 5**).

The purine and pyrimidine bases are constructed from various nonessential amino acids and methyl groups donated from the one-carbon/folate pool. The TCA cycle contributes oxaloacetate, which is transaminated to aspartate, intermediate required to synthesize both purine and pyrimidine bases. Aspartate is becoming essential in this pathway in order to maintain high flux of nucleotide biosynthesis (**Fig. 5**) (DeBerardinis and Chandel, 2016). In addition, glutamine is the obligate nitrogen donor in as many as three independent enzymatic steps for purine synthesis and in two independent enzymatic steps for pyrimidine synthesis (**Fig. 5**) (Wise and Thompson, 2010).

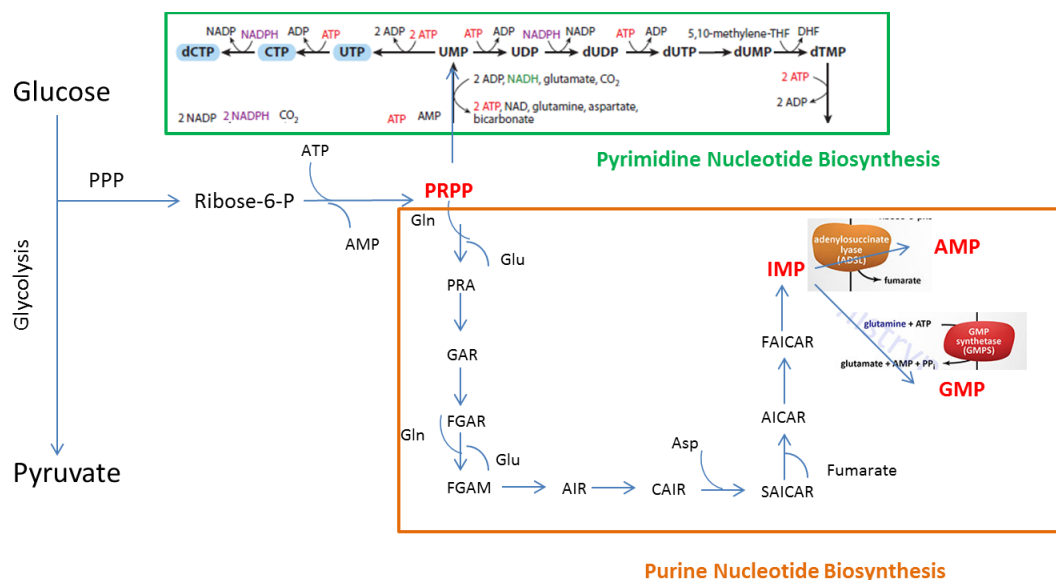


Figure 5. Nucleotide biosynthesis pathways. The *de novo* pathways for purine (orange) and pyrimidine (green) biosynthesis.

It has long been known that tumor cells depend on *de novo* nucleotide synthesis to support increased RNA production and DNA replication. Furthermore, elevated nucleotide biosynthesis has been observed in many cancers. Altered nucleotide metabolism in tumor cells compared

with normal cells has been shown, as manifested by the larger size of the nucleotide pool, higher activity of the nucleotide anabolic pathway as well as the activity of different enzymes involved in the nucleotide synthetic pathway (Tong et al., 2009). That means high adaptation requirements to increase nucleotide biosynthesis rate in order to support cancer cell proliferation. This adaptation involves ATP consumption (**Fig. 5**), suggesting proliferative cells are able to sacrifice energy towards the maintenance of purine and pyrimidine cellular pulls. Furthermore, aspartate and glutamine play a key role in these pathways as precursors, therefore making them more indispensable for proliferating cells (Sullivan et al., 2015; Wise and Thompson, 2010).

1.6.2. Lipid biosynthesis

Interestingly, as proliferative cells, cancer cells rely on *de novo* fatty acid synthesis, while it is suppressed in adult cells due to the nutritional excess availability (Narayanan Vijayakumar et al. 2015). Tumor tissue also takes up lipids from the tissue environment, but nevertheless it has been observed that *de novo* lipogenesis provides the majority of lipids required for the rapid proliferation of cancer cells (Medes et al., 1953).

Lipid synthesis describes the processes that convert nutrient-derived carbons into fatty acids (FA). FAs are carboxylic acids containing a long hydrocarbon chain and are the precursors of phospholipids, cholesterol-esters and triacylglycerides. FA synthesis requires integration with other carbon pathways and redox metabolism, in order to obtain sources of acetyl-CoA and reducing power in the form of cytosolic NADPH (**Fig. 2**).

Glucose is the most prominent acetyl-CoA source for FA synthesis (DeBerardinis et al., 2007a). Glycolysis-derived-acetyl-CoA obtained in the mitochondrial matrix is used to synthesize citrate in the TCA cycle. Citrate is transported into the cytosol where acetyl-CoA is recaptured from citrate and used as the carbon source for the growing acyl chains (**Fig. 6a**). Acetyl-CoA, which can also be synthesized in the cytosol by acetyl-CoA synthetase, is carboxylated to malonyl-CoA. Malonyl-CoA is converted to palmitate, a saturated fatty acid which is the origin of many saturated and unsaturated fatty acids (Currie et al., 2013). Acetyl-CoA can also be used to generate cholesterol via the mevalonate pathway, an important building block for steroid synthesis and membranes (**Fig. 2**) (Baenke et al., 2013). In addition, glucose-alternative carbon sources such as glutamine, to generate citrate for FA biosynthesis can be used when access to glucose-derived acetyl-CoA is impaired by hypoxia or mitochondrial dysfunction (**Fig. 6b**) (Metallo et al., 2011; Mullen et al., 2011a).

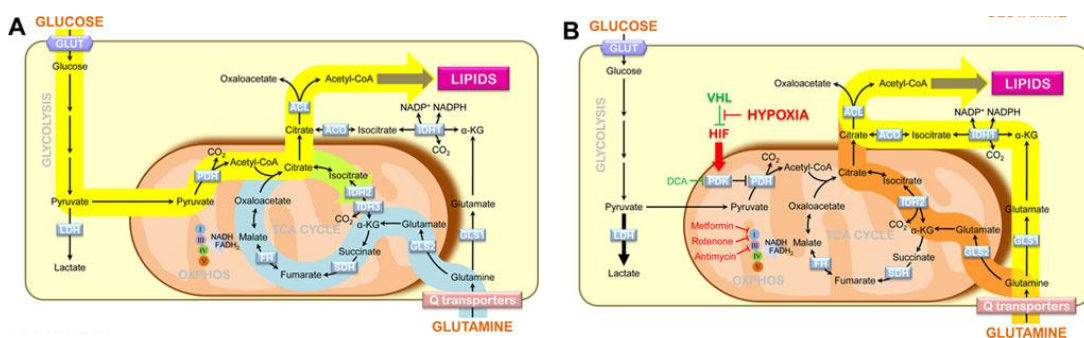


Figure 6. A metabolic switch in carbon source for lipid synthesis. (a) Under conditions when mitochondrial respiration is fully functional, glucose is the major source of carbons for acetyl-CoA to synthesize lipids. The yellow

block arrow indicates the route of carbons from glucose to lipids. The blue block arrow indicates oxidative glutamine metabolism (anaplerosis). The green block arrow shows the metabolic pathway of citrate generated from glucose-derived acetyl-CoA and glutamine-derived oxaloacetate. (b) Under conditions where HIF is stabilized (such as hypoxia or upon VHL deletion) or when mitochondrial respiration is limited, glutamine predominantly provides carbons for lipogenic acetyl-CoA either via cytoplasmic IDH1 (yellow block arrow) or mitochondrial IDH2 (orange block arrow). This pathway is referred to as reductive glutamine metabolism. (Anastasiou and Cantley, 2012)

Another carbon sources from glycolytic pathway needed for lipogenesis is dihydroxyacetone phosphate. This glycolytic intermediate is the precursor to glycerol-3-phosphate, which is crucial for the biosynthesis of the phospholipids and triacylglycerols that serve as major structural lipids in cell membranes. Other glycolytic intermediate, 3-phosphoglycerate, is the precursor of sphingolipids, another major class of lipids in cells (**Fig. 2**) (Lunt and Vander Heiden, 2011).

Importantly, cell growth is supported by the increased rate of fatty acid synthesis in multiple ways. In one side, it provides lipids for membrane biogenesis. Also, it provides cancer cells with fuel that can be mobilized in times of nutrient deprivation through fatty acid oxidation and lipid synthesis precursors. In the other side, these products can also function as second messengers and signalling molecules (Baenke et al., 2013; Phan et al., 2014). Aberrant activation of *de novo* lipogenesis owing to increased expression of metabolic enzymes involved in lipogenesis has been reported in numerous studies (Baenke et al., 2013; Menendez and Lupu, 2007; Yahagi et al., 2005). Indeed, inhibition of different enzymes within the FA biosynthesis pathway can block cancer cell growth (Abramson, 2011; Röhrig and Schulze, 2016)

1.6.3. Amino acid biosynthesis

Amino acids are the building blocks for proteins and can be mostly provided by the cell environment (essential amino acids). However, some of them are synthesized by intracellular reactions (non-essential amino acids). The major pathways involved in amino acid synthesis are glycolysis, the TCA cycle and glutaminolysis (**Fig. 2**).

On the one hand, glycolytic intermediates are direct precursors for the biosynthesis of some amino acids. 3-phosphoglycerate provides the carbons for cysteine, glycine, and serine, and pyruvate provides the carbons for alanine (Lunt and Vander Heiden, 2011). On the other hand, glutamine-derived glutamate is the primary nitrogen donor for the most nonessential amino acids synthesis through transamination reactions. Transaminases generate a large intracellular glutamate pool available for nonessential amino acid synthesis. These enzymes transfer the amine group from glutamate to α -ketoacids. These α -ketoacids can come from carbon catabolites of glucose or glutamine and are used to synthesize alanine, serine, aspartate, and ornithine (Wise and Thompson, 2010). Particularly, upregulation of glutamate-dependent transaminases—PSAT1, GPT, and GOT has been observed in cancer cells (Coloff et al., 2016).

Alanine is used in protein synthesis, but is also avidly secreted by tumor cells, moving some of the excess carbon from glycolysis (DeBerardinis et al., 2007b). In contrast, aspartate remains inside the cell. It is a precursor for asparagine biosynthesis and contributes to the synthesis of proteins and nucleotides and to electron transfer reactions through the malate-aspartate shuttle (DeBerardinis and Cheng, 2010), as discussed in greater detail below. Serine, for its

part, is required for biosynthetic and signaling pathways, including amino acids synthesis such as glycine and cysteine and the phospholipids production such as sphingolipids and phosphatidylserine (Lunt and Vander Heiden, 2011).

Serine is also involved in folate metabolism as carbon donors for many biosynthetic reactions through one-carbon metabolism. Serine-derived one-carbon units are used for the *de novo* synthesis of adenosine, guanosine and thymidylate, and to support the methionine cycle (Yang and Vousden, 2016). Furthermore, serine and the one-carbon metabolism (folate pathway) can regenerate cofactors such as NADPH, NADH and ATP (Tedeschi et al., 2013). Therefore, alterations in serine metabolism has been shown in numerous studies to have profound effects that may contribute to cancer development/to be crucial in cancer metabolism (Yang and Vousden, 2016).

2. Regulation of cancer cell metabolism by oncogenes and tumor suppressors

While tumor metabolism was initially thought to be an indirect secondary effect to oncogenic mutations, there is growing evidence to suggest that one of the main primary functions of activated oncogenes and inactivated tumor suppressors is to reprogram cellular metabolism. It is becoming increasingly evident that many key oncogenic signaling pathways converge to adapt tumor metabolism in order to support growth and survival in cancer cells (Ward et al., 2012). In contrast to their normal counterparts, cancer cells accumulate oncogenic alterations that confer them independence from external requirements and growth-factor-driven signaling inputs (Pavlova and Thompson, 2016). These oncogene activation and tumor suppressor lost that ensure metabolic robustness and stress resistance are described below.

2.1. Oncogenic alterations involved in metabolic reprogramming: glycolytic promoters and mitochondrial functional capacity assistants

2.1.1. The PI3K/AKT/mTOR pathway

The master regulator of glucose metabolism is the PI3K/Akt/mTOR pathway. The phosphoinositide 3-kinases (PI3Ks) are a family of lipid kinases that propagate intracellular signaling cascades regulating a wide range of cellular processes (Cantley, 2002). In non-transformed cells, the PI3K pathway is activated in response to growth signals. However, it was reported that the PI3K pathway is constitutively activated by several different mechanisms in a sizable fraction of all cancers. These mechanisms include mutations in tumor suppressor genes, such as PTEN, mutations in the components of the PI3K complex itself or aberrant signaling from tyrosine kinase receptors (EGFR, IGF-1, Her-2, etc.) (Wong et al., 2010).

Once activated, subsequent Akt and mTOR kinases activation is induced. The growth-promoting metabolic program activated by PI3K/Akt/mTOR system supports cellular biosynthesis through several pathways: (a) increasing expression and membrane translocation of nutrient transporters, enabling increased uptake of glucose, amino acids, and other nutrients; (b) Akt increases glycolysis, by phosphorylating key glycolytic enzymes, and stimulates lactate production, being sufficient to induce a Warburg effect in either nontransformed cells or cancer cells; (c) enhancing the biosynthesis of macromolecules. PI3K and Akt stimulate expression of lipogenic genes and lipid synthesis whereas mTOR functions as

key regulator of nutrient availability (Cairns et al., 2011; DeBerardinis et al., 2008a). Activated mTOR stimulates protein and lipid biosynthesis, activates glycolysis and *de novo* lipid biosynthesis by transcription factors such as HIF-1 and SREBP (Düvel et al., 2010).

2.1.2. c-Myc

In addition to its well-established roles in the regulation of cell growth and proliferation, the oncogenic transcription factor c-Myc, commonly amplified in human tumors, also has several important effects on tumor cell metabolism. In the one side, c-Myc plays an important role in regulation of glycolysis. Highly expressed oncogenic c-Myc has been related to the activation of several glucose transporters and glycolytic enzymes, as well as LDHA (Shim et al., 1997) and PDK1 (Dang et al., 2008). Regarding proliferation, c-Myc drives the accumulation of cellular biomass by activating transcription of targets that increase nucleotide biosynthesis (Tong et al., 2009), ribosome and mitochondrial biogenesis (Li et al., 2005). Furthermore, c-Myc controls many components of intermediary metabolic pathways that are confined to the mitochondria, thereby affecting mitochondrial function. Affected components in these pathways include enzymes involved in purine and pyrimidine synthesis, in folate pathways and the vast majority of the TCA cycle enzymes (Stine et al., 2015).

In the other side, c-Myc also promotes glutamine metabolism by inducing the expression of glutamine transporters and indirectly by up-regulating glutaminase levels via repression of the miRNA miR-23 (Dang, 2010; Gao et al., 2009). Requirement of high level expression of c-Myc to maintain the glutaminolytic phenotype has been observed. In fact, this c-Myc overexpression results in the concurrent glucose conversion mainly to lactate and the oxidation of glutamine via the TCA cycle. As a result, some c-Myc-transformed cells have shown an absolute requirement for glutamine as a bioenergetic substrate to maintain continuous replenishment of TCA cycle intermediates and mitochondrial integrity (Stine et al., 2015; Wise et al., 2008).

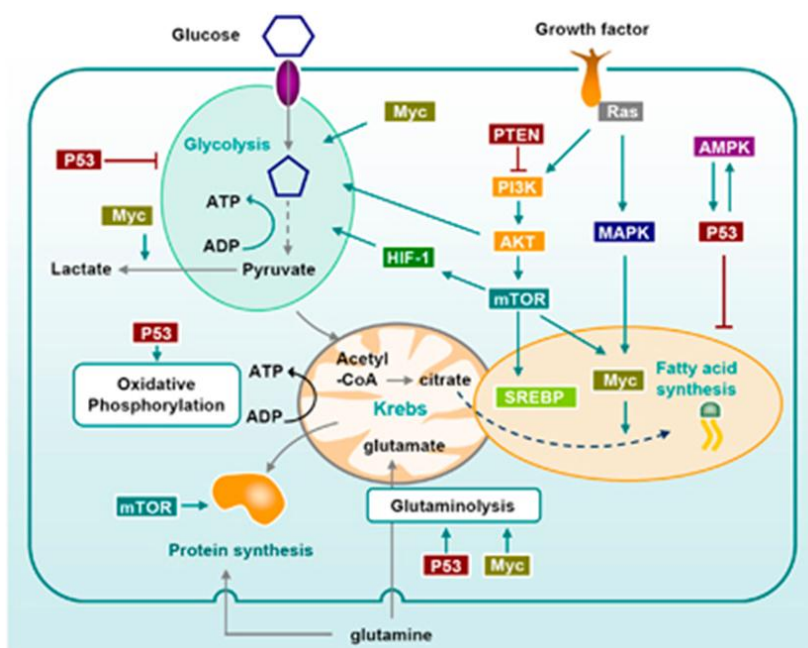


Figure 7. Signaling pathways that regulate metabolism of proliferating and cancer cells. Growth factors influence metabolism through Ras and PI3K. Both PI3K/Akt and MAPK increase glycolysis. They also induce the upregulation

of the transcription factor SREBP which promotes lipogenesis. mTOR, downstream of PI3K/Akt also plays a central role in the metabolic switch observed in highly proliferating cells: it activates protein translation, glycolysis (through HIF-1 dependent and independent pathways) and lipogenesis through the transcription factors SREBP and Myc. Myc is also the main oncogene implicated in glutamine addiction of cancer cells, through the upregulation of glutamate synthesis. It also contributes to the Warburg effect by increasing glycolysis and lactate production. AMPK activation, which is often impaired in tumors, allows the cells to switch their metabolism to catabolism when the nutrients are scarce. p53 regulates metabolism at multiple steps, notably through the upregulation of glutamate synthesis and inhibition of fatty acid synthesis and glycolysis. (Muñoz-Pinedo et al., 2012).

2.1.3. Ras

RAS proteins function as binary molecular switches through interaction with signaling molecules that regulate cell activities such as proliferation, differentiation, apoptosis, and cell migration (Pasca et al., 2013). Ras is stimulated by growth factors, and it is very often mutated leading to its hyperactivation in cancer. Among Ras-mediated metabolic effects is the activation of several effector pathways like PI3K/Akt/mTOR and MAPK pathways, involved in lipid biosynthesis (Muñoz-Pinedo et al., 2012). More evidence for the role of oncogenic isoform K-Ras in the cancer cells metabolic reprogramming has been reported. K-Ras supports the decoupling of glycolysis and TCA metabolism with glutamine supplying carbon to drive the TCA cycle (Gaglio et al., 2011). In K-Ras-transformed cells, the decoupling between glucose and glutamine metabolism leads to an efficient utilization of both carbon and nitrogen from glutamine into biomass building blocks (amino acids and nucleotides) and glutathione. Furthermore, K-Ras reprograms glutamine metabolism by downregulating GLUD1 and upregulating GOT1 to support malic-enzyme dependent NADPH production for redox balance (Son et al., 2013). Glucose metabolism is also K-Ras-promoted by enhancing glucose uptake and channeling of glucose intermediates into the hexosamine biosynthesis and pentose phosphate pathways to generate nucleotide precursors (Ying et al., 2012).

2.2. Oncogenic stress sensors as metabolic checkpoints: promoting tumor growth

2.2.1. Hypoxia inducible factors (HIFs)

Variation of oxygen availability is frequently observed in tumors, based on the distance of tumor cells from a functional blood vessel. Low oxygen condition or hypoxia arises through the rapid proliferation of cancer cells in the absence of an efficient vascular bed. One main mechanism allowing cells to adapt to hypoxia is mediated through the stabilization of the hypoxia-inducible factor 1 (HIF-1) transcription factor complex (Semenza et al., 2008). Cells, which are more distant from the vessel, are poorly oxygenated and express high levels of HIF-1. HIF-1 is a heterodimer composed of HIF-1 α and HIF-1 β subunits, and the biological activity of HIF-1 is determined by presence of the HIF-1 α subunit. HIF-1 α stability is regulated by oxygen levels through the inactivation of a family of prolyl hydroxylases (PHDs) (Eales et al., 2016; Lunt and Vander Heiden, 2011).

Orchestration of intermediary metabolic fluxes in conditions where HIF-1 α is stabilized has been reported. Capacity of tumor cells to consume glucose and produce lactate by carrying out glycolysis is increased. HIF-1 induces the expression of proteins that increase: uptake of glucose (GLUT1); conversion of glucose to pyruvate (glycolytic enzymes) (Iyer et al., 1998; Semenza, 2009); generation of lactate (LDHA); and efflux of these molecules out of the cell (MCT4) (Kroemer and Pouyssegur, 2008). In addition, HIF-1 will activate Pyruvate

Dehydrogenase Kinase 1 (PDK1), which phosphorylates and inhibits the mitochondrial PDH complex and thereby reduce the flow of pyruvate used by the TCA cycle. This limits entry of glycolytic carbon into the TCA cycle, decreasing the rate of oxidative phosphorylation and oxygen consumption, reinforcing the glycolytic phenotype (Kim et al., 2006; Papandreou et al., 2006).

HIF1 can be stabilized even under normoxic by oncogenic signalling pathways, including PI3K, and by mutations in tumour suppressor proteins (DeBerardinis et al., 2008a). In one side, inactivating mutation in the VHL tumor suppressor impairing HIF1 ubiquitination and degradation has been observed. Other mutations in SDH and FH stabilize HIF-1a by interfering with HIF-1a hydroxylation, which is competitively inhibited by accumulation of TCA cycle metabolites succinate or fumarate (Cairns et al., 2011; DeBerardinis et al., 2008a)

2.2.2. p53

The p53 tumor suppressor is best known for its function in apoptosis, DNA damage and cellular stress response. p53 is also being reconsidered from a metabolic perspective as regulator of glycolysis and oxidative phosphorylation (Vousden and Ryan, 2009). In its normal function, p53 decreases the glycolytic rate. This function that might enforce metabolic changes include down-regulation of glucose transporters, up-regulation of a fructose-bisphosphate-phosphatase that lowers levels of glycolytic activator fructose-2,6-bisphosphate, repression of lactate transporters, repression of PDKs, induction of the mitochondrial oxidation regulator and synthesis of cytochrome c oxidase complex of the electron transport chain (Cairns et al., 2011; Collier, 2014; Muñoz-Pinedo et al., 2012). In contrast, in cancer cells, control loss of its functions by mutation or suppression is frequently occurred, thus promoting glycolysis. Mutant p53 cells have shown higher rates of glycolysis, producing more lactate, and exhibiting decreased mitochondrial respiration compared with wild-type cells (Matoba et al., 2006), indicating that wild-type p53 suppresses an aerobic glycolysis phenotype. Therefore, the loss of p53 has been recognised as one of the major force behind the acquisition of the glycolytic phenotype (Cairns et al., 2011).

2.2.3. AMPK

The AMP-activated protein kinase (AMPK) complex thus functions as a metabolic checkpoint, regulating the cellular response to energy availability. AMPK is activated in response to an increased AMP/ATP ratio during periods of energetic stress and is responsible for changing to oxidative metabolic phenotype, downregulating anabolic pathways and promoting catabolism (Cairns et al., 2011). In addition, AMPK participates in inactivation of mTOR working against effects of AKT (Muñoz-Pinedo et al., 2012). Several oncogenic mutations and signalling pathways overcome AMPK checkpoint, which uncouples fuel signals from inappropriate growth signals, allowing tumour cells to proliferate under abnormal nutrient conditions (Shackelford and Shaw, 2009). Accordingly, many cancer cells exhibit a loss of appropriate AMPK signalling, contributing to a glycolytic phenotype.

2.3. Oncogenic mutations in metabolic enzymes: changes in mitochondrial metabolism

Many of the metabolism genes whose mutations can cause cancers are mitochondrial genes. Disruption of mitochondrial respiration can also occur through mutations in TCA cycle and electron transport chain proteins. Mutations in TCA cycle enzymes succinate dehydrogenase (SDH, which also functions as complex II of ETC), isocitrate dehydrogenase (IDH2) and fumarate hydratase (FH) have been documented in variety of cancers (Pavlova and Thompson, 2016; Wu and Zhao, 2013).

Both SDH and FH have been regarded as tumor suppressors (Gottlieb and Tomlinson, 2005; King et al., 2006). Tumors that exhibit SDH and FH loss, elevated levels of HIF1 α are commonly observed. Tumorigenicity induced by SDH and FH mutations through activation of HIF1 α pathway has been hypothesized (Isaacs et al., 2005; Selak et al., 2005). Indeed, mutations of SDH and FH were found to accumulate succinate and fumarate, structural analogs of α -KG that may inhibit PHDs and activate HIF pathway (Wu and Zhao, 2013).

In the case of IDH2, or its cytosolic counterpart IDH1, specific mutations linked to tumorigenesis have recently been found. These mutations cause IDH1 and IDH2 to acquire a novel enzymatic activity that converts α KG to 2-hydroxyglutarate (2-HG) switching from NADPH production to NADPH consumption (Dang et al., 2009; Ward et al., 2010). 2-HG is accumulated to massive increased levels in IDH-mutant cancer cells, producing wide-ranging effects on metabolism and signalling that promote tumorigenesis (Sullivan et al., 2016).

Nevertheless, FH, SDH or IDH mutant cells still rely on mitochondrial metabolism, reprogramming metabolic pathways to provide the necessary TCA cycle intermediates and ROS for cell proliferation- as it will be discussed in section four.

3. Bioenergetics and Redox-Cofactors

3.1. Energy production in cancer cells

All tumor cell types show an altered energy metabolism in comparison to their tissue of origin. Conventional view that the enhanced glycolysis is induced by a decreased oxidative phosphorylation has been assumed for years. However, a renewed dynamic view of tumor bioenergetics has been lately observed. Different cancer cell types undergo different bioenergetic alterations, from exclusively glycolytic to mainly OXPHOS, depending in part on the energy substrate utilization according to tumor stage, serial oncogene activation and fluctuating microenvironmental substrate conditions (Jose and Bellance, 2011). In addition, contrary to traditional presumption, mitochondrial function is not impaired and has a key role for the cancer cell. Although mitochondrial genes mutations in cancer cells have been reported, now it is known that they do not inactivate mitochondrial energy metabolism but rather alter the mitochondrial bioenergetic and biosynthetic state (Wallace, 2012). This bioenergetics and reducing power process needed to sustain tumor cell proliferation are discussed in this section.

3.1.1. Contribution of glycolysis and OXPHOS to ATP supply

Cellular energetics is primarily supplied by either glycolysis or mitochondrial oxidative phosphorylation (OXPHOS). In terms of ATP production, aerobic glycolysis is less efficient than the complete oxidative metabolism of glucose. The ATP yielded through OXPHOS is 18 times greater than that generated via glycolysis, but the rate of ATP production through glycolysis is 100 times faster than via OXPHOS (Lunt and Vander Heiden, 2011). Nevertheless, it has been demonstrated that oxidative phosphorylation supplies the majority of ATP for most proliferating cells. That comparison of several cell lines found that glycolysis ATP contributions are entirely dependent on the cell context and have a wide range (0.3%–64%) depending on cell/tissue type, thereby not supporting the hypothesis that cancer cells could exhibit aerobic glycolysis to generate ATP faster (Zu and Guppy, 2004). As commented before, it was observed that limiting glycolytic ATP production by inhibiting the activity of pyruvate kinase fails to prevent tumorigenesis, suggesting that the major role of high glycolysis ratio is not to supply ATP (Israelsen et al., 2013).

Thus, most cancer cells generate the majority of ATP through mitochondrial function, with the exception of tumors bearing mutations in enzymes involved in mitochondrial respiration. In these cells, nicotinamide adenine NAD⁺ from NADH is highly required for high glycolytic flux maintenance. This NAD may be efficiently generated from the conversion of pyruvate into lactate by lactate dehydrogenase isoform A (LDHA). This metabolic conversion, maintaining ratio NADH/NAD⁺, makes glycolysis self-sufficient as long as elevated glucose uptake is possible (Feron, 2009).

3.1.2. Alternative energy substrates for ATP synthesis pathways in cancer cells

The importance of cancer cells maintaining their ATP/ADP ratio to sustain viability in nutrient- and oxygen-poor environments has been reported. Consequently, it has been observed that cancer cells exhibit metabolic flexibility afforded by multiple possible inputs into the TCA cycle, allowing adequate response to the fuels available in the changing microenvironment during the evolution of the tumor. In this way, apart from pyruvate derived from glycolysis, fatty acids, amino acids and ketone bodies can supply substrates to the TCA cycle to sustain mitochondrial ATP production. In one side, breakdown of fatty acids in the mitochondria generates acetyl-CoA and the reducing equivalents NADH and FADH₂, which are used by the ETC to produce ATP. Glutamine can generate glutamate and subsequently α -KG to fuel the TCA cycle by glutaminolysis (Le et al., 2012). Furthermore, the branched-chain amino acids isoleucine, valine, and leucine can be converted into acetyl-CoA and other organic molecules that also enter the TCA cycle (Mayers et al., 2014). In the other side, ketones bodies by-pass cytoplasmic glycolysis and directly enter the mitochondria where they are oxidized to acetyl-CoA, contributing to ATP production (Seyfried and Mukherjee, 2005).

3.2. NAD(H) and NADP(H): The Universal Redox-Cofactors

Energy transduction through catabolic pathways and also biosynthetic processes depend on the ability to carry redox equivalents. The pyridine nucleotides NAD(H) and NADP(H) play pivotal roles in metabolic redox reactions, not only serve as electron acceptors in the breakdown of catabolic substrates but also provide the cell with the reducing power needed in energy-conserving redox reactions. They can accept electrons when present in their oxidized state (NAD⁺ and NADP⁺) or donate electrons from their reduced state (NADH and NADPH).

The relative abundance of the oxidised and reduced forms of these cofactors is also an important regulator of metabolic activity (Feron, 2009).

Both nicotinamide enzymes act as coenzymes of dehydrogenases. NAD linked dehydrogenases are involved in the oxidative pathways of metabolism like in glycolysis, TCA cycle and in the mitochondrial respiratory chain. In the other hand, NADP linked dehydrogenases, are involved in reductive biosynthetic reactions like fatty acid synthesis and cholesterol synthesis. In addition, coenzyme flavin adenide dinucleotide (FAD), also linked dehydrogenases, has an important role in TCA cycle through succinate dehydrogenase and β -oxidation of fatty acid by acyl-CoA dehydrogenase.

3.2.1. Major NADP/NADPH role in tumor metabolism: reductive biosynthesis and cellular defence against oxidative damage

In the one hand, NADPH is used to drive anabolic reactions as a reducing agent for nucleotide biosynthesis (in the deoxynucleotides conversion from ribonucleotides, a source of NADPH is required), for amino acid production (such as proline and arginine), and largely for lipid biosynthesis (Lunt and Vander Heiden, 2011) (**Fig. 2**). In the other hand, the reducing equivalent NADPH plays a key role maintaining multiple antioxidant defense systems (DeBerardinis and Chandel, 2016). NADPH is required to generate the reduced form of glutathione, which is a major intracellular defense against damage mediated by reactive oxygen species (ROS) (Vander Heiden et al., 2009). It has been demonstrated that reduced activity of isoform PKM2 allows sustaining antioxidant responses, increasing the production of NADPH and reduced glutathione through enhancement of glycolytic intermediates entry into the PPP pathway (Anastasiou et al., 2011).

In contrast to NAD⁺/NADH, the NADPH/NADP⁺ ratios are maintained high in both cytosol and mitochondrial compartments in favor of the reduced form, to maintain a reducing environment (Pollak et al., 2007). Recent years, it has been revealed tumor cells show upregulated metabolic pathways in order to maintain NADPH in different subcellular compartments. Cytosolic sources of NADPH include the oxidative arm of PPP via G6PD, conversion of isocitrate to α -ketoglutarate by the cytosolic isoform IDH1, conversion of malate to pyruvate by the cytosolic isoform ME1, and one-carbon metabolism. Mitochondrial sources of NADPH include also one-carbon metabolism and IDH2 (DeBerardinis and Chandel, 2016; Fan et al., 2014). In addition, metabolism of glutamine through malic enzyme has been reported as a significant source of NADPH (DeBerardinis et al., 2007a). Thus, depending on the context, cells show a preference for one mechanism of NADPH production over another. For instance, in *KRAS*-mutated PDAC cells it has been observed a glutamine-dependent carbon flux via malate dehydrogenase and malic enzyme producing malate and pyruvate, respectively, with the latter reaction also producing NADPH. Suppression of any of several enzymes in this pathway results in oxidation of the glutathione pool, enhanced ROS levels and reduced PDAC tumor growth (Son et al., 2013).

3.2.2. Major NAD⁺/NADH role in tumor metabolism: cellular metabolism regulation and energy production

NAD⁺ modulates the activity of compartment-specific pathways such as glycolysis in the cytosol, and TCA cycle, OXPHOS, fatty acid and amino acid oxidation in the mitochondria. On one side, NAD⁺ is converted to NADH at the glyceraldehyde 3-phosphate dehydrogenase (GAPDH) step of glycolysis. This NADH can be oxidized to NAD⁺ during LDH catalysed reaction. This reduction is required since NAD⁺ is a necessary substrate for GAPDH, without which glycolysis will cease. In addition, the electrons of cytoplasmic NADH can be transferred to mitochondrial carriers of the OXPHOS pathway by aspartate-malate shuttle, generating a continuous pool of cytoplasmic NAD⁺. On the other side, in the mitochondrial compartment, NAD⁺ is converted to NADH at multiple steps in the TCA cycle (**Fig. 2**) and NADH is then oxidized by providing reducing equivalents to complex I in the ETC through a series of redox reactions that generate ATP by OXPHOS (Alano et al., 2007; Chiarugi et al., 2012). Besides, glutamine metabolism can be regulated by NAD/NADH through glutamate dehydrogenase enzyme. GDH utilizes NADH in the direction of nitrogen incorporation for protein synthesis, and also catalyzes the NAD⁺-consuming backward anaplerotic reaction of the glutamate to α KG, providing an oxidizable carbon source used for the energy production as well as a reduced electron carrier (NADH) (Bunik et al., 2016).

The NAD⁺/NADH ratio thus regulates multiple metabolic pathway enzymes that are relevant to tumor cell survival and proliferation, including GAPDH, pyruvate dehydrogenase, isocitrate dehydrogenase, α -ketoglutarate dehydrogenase and malate dehydrogenase (Alano et al., 2007). Highly glycolytic cells display increased NADH levels relative to NAD⁺ levels. This leads to a constraint in their metabolic activity and cancer cells need to regenerate NAD⁺ to maintain a balanced NAD⁺/NADH ratio. Major mechanisms to regenerate NAD⁺ are upregulated in tumor cell, such as LDHA that preferentially converts accumulating pyruvate to lactate thereby maintaining glycolysis flux, and shuttle systems that move reducing equivalent between subcellular compartments (Liberti and Locasale, 2016; Locasale and Cantley, 2011).

3.2.3. Movement of reducing equivalents: Cellular Shuttle Systems

Due to the impermeability of the inner mitochondrial membrane to NAD⁺ and NADH, NADH generated by glycolysis depends on the indirect transfer of reducing equivalents into the mitochondria via special shuttle systems. Such shuttles involve the movement of oxidizable material between subcellular compartments accomplished by antiporter-based mechanisms. Two such shuttle systems that can lead to the transport of reducing equivalent from the cytoplasm into mitochondria have been described: malate-aspartate shuttle and glycerol phosphate shuttle (Locasale and Cantley, 2011).

➤ Malate-aspartate shuttle

In the malate-aspartate shuttle (**Fig. 8a**), the reducing equivalents of cytosolic NADH are first transferred to cytosolic oxaloacetate to yield malate by cytosolic malate dehydrogenase, and in the process, NAD⁺ is generated from NADH, eliminating the cytosolic NADH/NAD⁺ imbalance that results from glycolysis. Malate is transported across the inner membrane by an antiporter mechanism coupled to mitochondrial α KG export to the cytosol. Upon entering the mitochondria, malate is converted back to OAA by mitochondrial malate dehydrogenase. In this reaction, reducing equivalents carried by malate are then transferred to mitochondrial NAD⁺ thereby generating NADH. By a transamination reaction, OAA is converted to aspartate

with the nitrogen donor glutamate converted back to α KG, and is then transported to the cytosolic side in exchange for cytosolic glutamate via amino acid antiporter. In the cytosol, a reversal of the aspartate aminotransferase reaction gives rise to oxaloacetate from aspartate, and simultaneously converts cytosolic GLU to α KG, thereby completing the shuttle system. The redox imbalance from glycolysis is satisfied by NADH to NAD⁺ conversion in the cytosol and NADH generated in the mitochondria enters the electron transport system to ultimately generate more ATP (Locasale and Cantley, 2011).

The malate-aspartate shuttle is active in the neoplastic cells of several types of tumors (Greenhouse and Lehninger, 1976; López-Alarcón and Eboli, 1986). Indeed, about one-third of the respiratory ATP was demonstrated to be generated by electron flow originating from cytosolic NADH via the malate-aspartate shuttle (Greenhouse and Lehninger, 1977). Furthermore, malate dehydrogenase and aspartate aminotransferase has been highlighted as key enzymes required for this shuttle system in cancer cells.

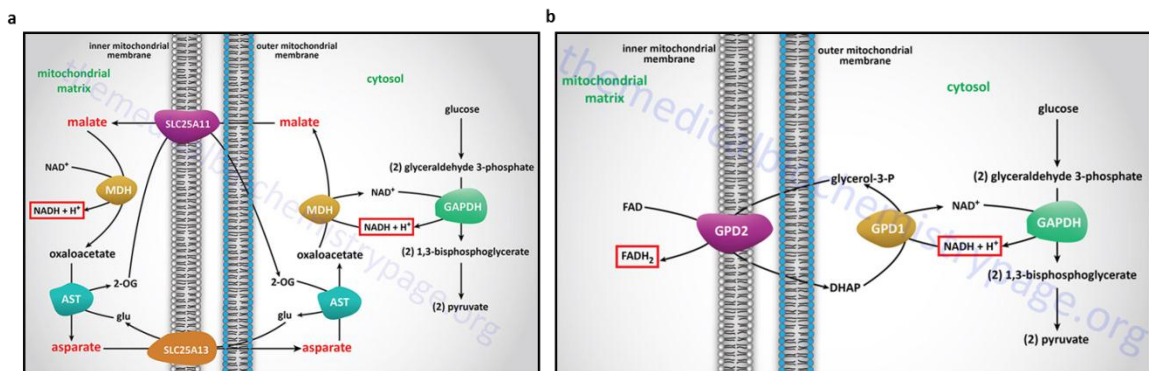


Figure 8. Shuttle mechanisms for cytoplasmic NADH. The malate-aspartate shuttle (a) produces NADH in the matrix for entry into the ETC at NADH-Q reductase. The glycerol phosphate shuttle (b) produces FADH₂ in the mitochondrial inner membrane so that it enters the ETC at complex II by reducing coenzyme Q.

On one side, MDH represents a key link enzyme between mitochondrial and cytosolic pools of metabolic intermediates. This is the case of glutamine oxidation, which generates several TCA cycle intermediates that may be shuttled from the mitochondrial matrix to the cytoplasm involving conversion to and from malate (DeBerardinis et al., 2007b). Moreover, elevated MDH expression has been observed in prostate cancer cell lines compared to benign prostate epithelial cells and its inactivation induced metabolic inefficiency, decreasing cell proliferation and increasing drug sensitivity (Liu et al., 2013). Additionally, MDH inhibitors which demonstrated strong anti-tumor activity, are being tested in order to mediate cancer cell drug resistance (Ban et al., 2016; Lo et al., 2015).

On the other side, transamination reactions are becoming increasingly important in tumor metabolism due to studies of transaminases inhibition by genic silencing or using amino-oxyacetic acid (AOA) have shown cytotoxic effect in certain cancer cell lines (Lyssiotis et al., 2013; Thornburg et al., 2008; Wise et al., 2008). Last years, aspartate aminotransferase has emerged as critical enzyme for reprogramming tumor pathways. Strongly dependence on the GOT transaminases for metabolism of the glutamine carbon skeleton has been reported in PDAC (Son et al., 2013). Thus, reprogrammed glutamine metabolism through kras-mediated

GOT1 activation and GLUD1 repression, leads glutamine flux through the aspartate aminotransferase pathway in pancreatic cancer cells, decoupling canonical malate-aspartate shuttle from TCA reactions (Lyssiotis et al., 2013). What is more, a synthetic lethal interaction between GOT1 loss and with ETC dysfunction has been recently proposed. This lethality is generated by disabled of aspartate biosynthesis since upon ETC inhibition cells use the reductive carboxylation of glutamine to fuel compensatory aspartate synthesis via a GOT1-requiring pathway (Birsoy et al., 2015). The activity of malate-aspartate shuttle system becomes essential in the presence of an excess of cytosolic NADH not efficiently removed when the respiratory chain is impaired. In addition, from these findings, the main role of aspartate biosynthesis in tumor metabolism has begun to emerge.

➤ Glycerol phosphate shuttle

This shuttle is a secondary mechanism for the transport of electrons from cytosolic NADH to mitochondrial carriers of the OXPHOS pathway. A similar concept is in place with the glycerol phosphate shuttle in which glycerol-3-phosphate is shuttled into the mitochondria where is re-oxidized to dihydroxyacetone phosphate, regenerating NAD⁺ from NADH in the cytosol and producing reducing equivalents for oxidative phosphorylation in the form of FADH₂ (**Fig. 8b**) (Locasale and Cantley, 2011).

Two enzymes are involved in this shuttle, cytosolic (GPD1) and mitochondrial glycerol-3-phosphate dehydrogenase (GPD2). It has been demonstrated that GPD2 activity is elevated in several human prostate cancer cell lines compared with normal prostate epithelial cells, leading to increased cancer progression-related ROS levels (Roy Chowdhury et al., 2007). Furthermore, inhibitors of mitochondrial GPD2 activity have displayed anti-proliferative effects on cancer cells (Singh, 2014).

4. Aspartate and pyruvate as key growth factors in cell proliferation

As noted before, in cancer cells, importance of malate-aspartate shuttle beyond the classical role of reducing equivalents movement for energy production has been reported. This importance lies in the fact that aspartate and pyruvate have a fundamental role in several metabolic pathways that are upregulated in cancer metabolism. Thus, both metabolites directly involved in malate-aspartate shuttle system, have emerged as key metabolites linked to tumor reprogramming.

4.1. Aspartate

It has been widely recognized that this non-essential amino acid contributes to protein production and is one of the major precursors for the nucleotides that compose DNA. Within its classical role, in cell proliferation process it has been remarkable the following key fate of aspartate:

De novo purine nucleotide synthesis pathway, through a series of reactions utilizing ATP, this pathway yields IMP, which represents a branch point for purine biosynthesis. This nucleotide can serve as a precursor for both AMP and GMP synthesis. Aspartate is involved in the ATP-consuming synthesis of SAICAR from CAIR (**Fig. 5**).

Purine nucleotide cycle, that amino group of aspartate is transferred to purine nucleotide IMP to generate adenylosuccinate, which is broken down by the activity of a lyase to generate fumarate and AMP. Fumarate performs the anaplerotic function of replenishing the TCA cycle by being converted to oxaloacetate (**Fig. 5**).

Pyrimidine nucleotide biosynthesis. Glutamine-derived carbamoyl phosphate is condensed with aspartate in the cytosol in one of the steps from UMP synthesis by trifunctional enzyme CAD (carbamoyl-phosphate synthetase 2, aspartate transcarbamoylase and dihydroorotase) (**Fig. 6**).

Precursor of ornithine for the Urea cycle. In the cytosol, aspartate can also serve as substrate for argininosuccinate synthase (ASS1) producing argininosuccinate to continue the urea cycle. It has been demonstrated ASS1 deficiency in cancer increases cytosolic aspartate levels, which increases CAD activation and pyrimidines synthesis. ASS1 downregulation is presented as a novel mechanism supporting cancerous proliferation, showing a metabolic link between the urea cycle enzymes and pyrimidine synthesis (Rabinovich et al., 2015).

Instead, in recent years, a renewal role of aspartate in reprogramming tumor metabolism has emerged, focusing it as a key regulator malate-aspartate shuttle (Birsoy et al., 2015; Sullivan et al., 2015). Aspartate biosynthesis has taken on a leading role in tumor metabolism instead of aspartate consumption. These studies have revealed that the main role of respiration in cell proliferation is not energy production, but rather making aspartate. In addition, aspartate biosynthesis involves coordination of mitochondrial and cytoplasmic compartmentalized transamination enzymes and mitochondrial transporters, members of the mentioned malate-aspartate shuttle (**Fig. 9**). Upon ETC inhibition, it was demonstrated cells use this

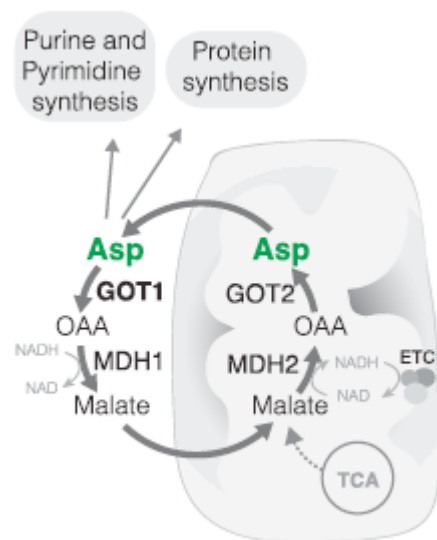


Figure 9. Schematic depicting the malate-aspartate shuttle. Normally, the malate-aspartate shuttle runs in the forward direction to transfer reducing equivalents across the mitochondrial membrane. GOT1 is part of the malate-aspartate shuttle and consumes aspartate to generate oxaloacetate (OAA). Aspartate produced by mitochondria is a precursor for protein and nucleotide biosynthesis. (Birsoy et al., 2015)

GOT1-dependent pathway to generate aspartate, indicating that GOT1 loss has a synthetic lethal interaction with ETC dysfunction. However, not fully compensation for loss of mitochondrial aspartate synthesis was observed, allowing other possible key pathways or metabolites implicated (Birsoy et al., 2015). This primary role for mitochondrial respiration in cell proliferation has been focused on providing access to electron acceptors in support of aspartate synthesis (Sullivan et al., 2015). Furthermore, aspartate transaminases have been suggested as promising cancer target (Son et al., 2013; Thornburg et al., 2008). In the other hand, it has been demonstrated that not only is a functional TCA cycle key for generating aspartate, but that a differential ability to utilize aspartate as anaplerotic sources can dictate the ability of cells to survive and grow in disrupted TCA cycle conditions (Allen et al., 2016).

Additionally, aspartate is becoming to be used as diagnostic view. It has been demonstrated that breast cancer is associated with significantly lowered plasma aspartate levels, and what is more, higher level of aspartate in breast cancer tissues than in adjacent non-tumor tissues has been found. These findings have suggested that depleted level of aspartate in blood of breast cancer patients is due to increased tumor aspartate utilization and lowered circulating aspartate could be a key metabolic feature of human breast cancer (Xie et al., 2015).

4.2. Pyruvate

Pyruvate, glucose-oxidized product, is the branch point molecule of glycolysis. Pyruvate has been noted as a key intersection in the network of metabolic pathways. Traditionally it has been located at a crucial crossroad of cellular metabolism between aerobic and anaerobic pathway. In the presence of oxygen, pyruvate can be converted into acetyl-coenzyme A and shuttled into the mitochondria to participate in the TCA cycle. In addition, pyruvate can be converted to oxaloacetate by an anaplerotic reaction and further broken down to carbon dioxide. Pyruvate can also be converted to carbohydrates via gluconeogenesis, to fatty acids or energy through acetyl-CoA and to the amino acid alanine (Roudier and Perrin, 2009).

If oxygen is not sufficiently available, pyruvate from glycolysis is thus converted to lactate in a reaction that regenerates NAD⁺ from NADH, which is reduced during glycolysis. In cancer cell this flux, observed even under aerobic conditions (Warburg effect), is increased due to the need of NAD⁺ replenishment to maintain a high flux of glucose metabolism (Hay, 2016). The alterations of pyruvate metabolism observed in tumor (glycolysis and glutaminolysis increased and pyruvate oxidation decreased) are known to increase lactate and alanine yield (DeBerardinis et al., 2007a). It has been demonstrated that the decrease in the rate of pyruvate entering the TCA cycle and the concurrent increase in lactate production is vital for the growth and survival of tumors (Tennant et al., 2010a). Even more, reduction in tumor growth in xenograft models has been observed by knocking down LDHA or inhibiting PDK1 (using RNAi or dichloroacetate) (Fantin et al., 2006; Sun et al., 2010), strongly supporting that the fate of pyruvate play a determinant role in the tumorigenic process.

However, novel roles in tumor metabolic reprogramming have been associated with pyruvate. Evidences that pyruvate can regulate hypoxia-inducible gene expression independently of hypoxia by stimulating the HIF-1 α accumulation have been reported (Lu et al., 2002). Thus, through its ability to stabilize HIF-1 α , pyruvate can inhibit the PDH complex in cancer cells enhancing Warburg metabolism and malignant phenotype, besides promoting resistance to anti-cancer therapies (Roudier and Perrin, 2009). Furthermore, most recently revolutionary role of pyruvate as electron acceptor in respiratory deficient cells has been discovered (Birsoy et al., 2015; Sullivan et al., 2015). It has been observed that cells with defects in their electron transfer chains become dependent on pyruvate as an alternative electron acceptor for GOT1-catalyzed aspartate synthesis. Moreover, cellular aspartate levels recovery has been observed by addition of exogenous pyruvate, which increases the cellular NAD⁺/NADH ratio normalizing redox levels and restores proliferation in cells with severe ETC defects (Gui et al., 2016).

5. Tumor models under alterations in cell metabolism

For decades, dominant glycolytic metabolism and defective mitochondrial respiration both have been hallmark in tumor cell metabolism. However, a growing body of evidence is now challenging this assumption, and also implying that tumors are metabolically less homogeneous than previously supposed. Because of that, the need arises to find suitable study models that enable to take in account tumor metabolic heterogeneity. Last years, it has been considerable utility to establish preclinical cell and xenograft models for studying energy metabolism reprogramming, as well as their use in development of new therapeutic approaches targeting of metabolic enzyme-mutant human cancers.

In essence, these models are based on tumor cell lines which present one or several mutations, either metabolic enzymes or metabolic pathways-related proteins. In some cases, these mutations may implicate altered metabolism as an underlying hallmark of neoplastic transformation (Gaude and Frezza, 2014). But, in any case, these mutations have caused metabolic adaptations that reprogrammed cell metabolism, so these models are representative of extreme metabolic phenotypes. The commonly used mutant tumor cellular models in recent years are described below.

5.1. Fumarate hydratase deficient (FH⁻/FH⁻) cells

FH is an enzyme of the TCA cycle that catalyzes the reversible conversion of fumarate into malate. It has been reported that germline mutations of *FH* are responsible for hereditary leiomyomatosis and renal-cell cancer (HLRCC) and were also found in glioblastoma and sporadic clear cell carcinoma (Gaude and Frezza, 2014). The dependence of HLRCC tumors on glycolysis, coupled with their impaired mitochondrial respiration, marks its reprogramming as hallmark of study.

In order to elucidate metabolic alterations and adaptations of FH-mutant tumors, Fh1-deficient cells have been highly used (Yang et al., 2010, 2012). In the one hand, FH-deficiency derived tumorigenic activity has been proved using this model. It was demonstrated that the absence of FH leads to the accumulation of fumarate, which activates hypoxia-inducible factors (HIFs) at normal oxygen tensions (Isaacs et al., 2005b; Pollard et al., 2007). Furthermore, mechanism that explains the ability of cells to survive without a functional TCA cycle has been provided with this model. As a consequence of absence of Fh1, truncated TCA cycle was shown, causing an accumulation of fumarate and succinate paralleled by a decrease of malate and citrate. This metabolites accumulation in *Fh1*^{-/-} cells diverts TCA metabolites into heme biosynthesis and degradation, engaging a linear metabolic pathway beginning with glutamine uptake and ending with bilirubin excretion (Frezza et al., 2011). This work allowed for developing a new potential target based on synthetically lethal inhibition of haem oxygenation when combined with Fh1 deficiency.

In the other side, an additional metabolic adaptation was identified studying human FH-deficient cells. It was demonstrated that, by reversing parts of the TCA cycle, citrate and malate from glutamine can be generated by reductive carboxylation of alpha-ketoglutarate to isocitrate, thus providing anabolic building blocks required for cell proliferation (Mullen et al., 2011b). Other studies have demonstrated that arginine depletion decreased the production of argininosuccinate in FH-deficient cells, and cell survival and proliferation reduced was observed. Argininosuccinate was found to be produced from arginine and fumarate by the

reverse activity of the urea cycle enzyme argininosuccinate lyase, making these cells auxotrophic for arginine and argininosuccinate as a common metabolic biomarker of FH deficiency (Adam et al., 2013; Zheng et al., 2013).

5.2. SDH-deficient cells

Succinate dehydrogenase (SDH) is a heterotetrameric nuclear-encoded complex responsible for the oxidation of succinate to fumarate in the TCA cycle. In addition to its role in the Krebs cycle, SDH also functions as complex II of the electron transport chain (ETC), catalyzing the oxidation of succinate to fumarate in a reaction that generates FADH₂, and donates electrons to the ETC for ATP production. Inactivating mutations in the human genes for any of the SDH subunits have been associated with susceptibility to develop neuroendocrine neoplasms, gastrointestinal stromal tumors and renal cell carcinoma (Cardaci et al., 2015). SDH mutant was originally discovered as a TCA cycle enzyme with tumor suppressor properties (Gottlieb and Tomlinson, 2005). However, its defect as central mitochondrial enzyme complex has raised its emergence as an ideal genetic model for deciphering how metabolic adaptation fuels cell growth and proliferation.

ast years, mutation-derived metabolic consequences and the molecular mechanisms enabling survival and growth of SDH-defective cells have been largely explored (Bardella et al., 2011). It has been demonstrated that accumulated succinate, observed in SDH-deficient cells, inhibits the activity of enzymes such as HIF α prolyl hydroxylases (PHDs) in the cytosol, leading to the induction of a hypoxic response under normoxic conditions (Briere et al., 2005). Several studies have demonstrated that amino-acid metabolism is altered in SDH-deficient cells as a result of re-wiring of mitochondrial metabolic pathways. In the one hand, pyruvate carboxylase has been identified as essential for the proliferation and tumorigenic capacity of SDH-deficient cells, by diversion of glucose-derived carbons into aspartate biosynthesis, thus sustaining cell growth (Cardaci et al., 2015). In the other hand, the highly dependent upon mitochondrial aspartate from SDH-deficient cells provokes that aspartate constitutes a key metabolic hub in these cells, being a major precursor for other 'non-essential' amino acids such as arginine and asparagine. It has been observed that SDH-deficient cells shows limited means of producing aspartate that provokes reduction in their metabolic plasticity, and suggesting vulnerabilities that can be used therapeutically (Lussey-Lepoutre et al., 2015a).

5.3. Oncogenic Kras model of pancreatic ductal adenocarcinoma (PDAC)

Pancreatic ductal adenocarcinoma, the most common type of pancreatic cancer, is highly lethal and has a poor prognosis (Hidalgo, 2010). It has been shown PDAC supports major metabolic challenges, principally hypoxia and nutrient deprivation. Constitutively activated K-Ras, which is present in wide majority of these tumors, results in aberrant activation of proliferative and survival signaling pathways. As mentioned before, oncogenic K-Ras has a key role in metabolic reprogramming and particularly in the glycolytic switch. Last years, this PDAC connection with *KRAS* oncogenic alterations has brought metabolic reprogramming to the forefront of PDAC therapeutic research (Cohen et al., 2015).

Preclinical models of pancreatic ductal adenocarcinoma have been developed (Hwang et al., 2016) and widely employed to analyze K-Ras-dependent metabolic alterations. Firstly, using an

inducible oncogenic K-Ras model of PDAC, it was demonstrated that K-Ras oncogene has a fundamental role in reprogramming tumor metabolism by selectively activating biosynthetic pathways to maintain tumor growth (Ying et al., 2012). Moreover, a non-canonical pathway of glutamine required for tumor growth was identified in PDAC cells. This glutamine metabolism redirection relies on a distinct pathway in which glutamine-derived aspartate is transported into the cytoplasm where it is converted into oxaloacetate by GOT1. This metabolic reprogramming is thought to facilitate regeneration of NADPH for reductive biosynthesis and redox homeostasis as well as NAD⁺ for maintaining glycolysis (Son et al., 2013).

On the other hand, evidence that inhibition of mitochondrial function may effectively target cells that survive after suppression of oncogenic K-Ras signaling was also demonstrated in PDAC tumor *in vitro* and *in vivo* (Viale et al., 2014). Finally, more recently it was observed that enhanced mitochondrial glutamine anaplerosis markedly inhibits PDAC growth and induces apoptotic cell death, therefore identifying a new aspect of glutamine metabolism in PDAC growth and survival (Jeong et al., 2016).

5.4. VHL-deficient cells and clear-cell renal carcinoma (ccRCC)

The von Hippel-Lindau (VHL) protein, a tumor suppressor, regulates HIF-1 α levels through specific binding and induces its proteasomal degradation. Under hypoxic conditions or in the absence of functional VHL, HIF-1 α is accumulated and different hypoxia-response pathways are triggered (Gossage et al., 2014). In some aggressive tumors, such as most ccRCC, the VHL protein is mutated, thus becoming ineffective in promoting HIF-1 α degradation and driving tumorigenesis. Indeed, kidney cancer has been considered as metabolic disease due to dysregulated genes related to this tumors (such as VHL) are involved in metabolic pathways that respond to metabolic stress or nutrient stimulation (Linehan et al., 2010).

In this regard, several studies have used VHL-deficient cells in order to elucidate possible molecular mechanisms underlying metabolic reprogramming led to HIF-1 α . Thus, preferential use of reductive glutamine metabolism for citrate and lipid synthesis, even under normal oxygen levels exposition, has been reported in VHL-deficient ccRCC cell lines, whereas those expressing wild-type VHL behaved similarly to other carcinoma cell lines (Metallo et al., 2011). Furthermore, selective sensitivity to glutamine deprivation and glutaminase inhibitors was exhibited by VHL-deficient cells. *In vivo* reductive carboxylation activity in VHL-deficient tumors growing as xenografts in mice has been demonstrated. These VHL-deficient tumor models have enabled to prove systemic administration of glutaminase inhibitors suppressed the growth of ccRCC cells as xenografts, suggesting reductive glutamine metabolism may fuel tumor growth (Gameiro et al., 2013).

On the other hand, molecular pathway by which glucose metabolism is reprogrammed in VHL-deficient renal carcinoma cells has been delineated. This pathway is triggered by loss of VHL function and the consequent dysregulated activity of HIF-1, which leads to the inhibition of c-MYC transcriptional activity. Mitochondrial DNA content, mitochondrial mass, cellular O₂ consumption, and ROS production are significantly reduced as a result, being loss of VHL function responsible for the dramatic decrease in respiration observed in renal carcinoma cells (Zhang et al., 2007).

6. Tumor model to study reprogramming tumor metabolism: Respiration deficient cells

As has been detailed before, most cells that engage in aerobic glycolysis are not only capable of respiration, but also require respiration for proliferation. Impaired proliferation has been early observed in cultured cancer cells during exposition of respiration inhibitors (Kroll et al., 1983; Löffler and Schneider, 1982). Diminished tumorigenic phenotype after depletion of mitochondrial DNA was described in several tumors of different origins (Cavalli et al., 1997). In vivo, it was observed that functional mitochondrial electron transport chain by maintenance of mtDNA is required for tumorigenesis (Weinberg et al., 2010).

Nevertheless, under specific culture conditions proliferation is possible even in the absence of respiration. This is the case of p0 cells, which had been completely depleted of mitochondrial DNA by long-term exposure to low-dose ethidium bromide (King and Attardi, 1989, 1996). In its initial generation, they were found to be dependent on uridine and pyruvate for growth and this fact was attributed to the absence of a functional respiratory chain (King and Attardi, 1989). Uridine is needed to produce pyrimidines since that enzyme dihydroorotate dehydrogenase activity is impaired by loss of electron transport to ETC required in this reaction (Sullivan et al., 2015). However pyruvate dependence was initially undefined, arguing energy demand fulfilments. Until recently, it has not begun to be elucidated possible explanations for pyruvate auxotrophy in respiratory deficient cells. As mentioned before, novel studies have attributed to pyruvate an alternative electron acceptor role for generating aspartate. According to that, high demand of extracellular pyruvate is a matter of aspartate production in order to support proliferation in cells with severe ETC defects (Birsoy et al., 2015; Gui et al., 2016; Sullivan et al., 2015).

In addition, these studies have made aspartate into the spotlight in the tumor metabolic reprogramming of respiratory deficient cells. They demonstrated that aspartate levels decrease dramatically when respiration is blocked in cancer cells, and addition of high levels of this amino acid is sufficient to restore proliferation of respiration-defective cancer cells (Sullivan et al., 2015). The fact that specific nutrients adding has been able to substitute for respiration has suggested respiration fulfills specific metabolic requirements for proliferating cells. However, other than dihydroorotate to orotate conversion, the metabolic functions that become limiting for proliferation in the absence of respiration are unknown. Nowadays, this question still remains unresolved and it will be widely discussed in this work.

Furthermore, as commented before, mitochondria carry out many essential metabolic processes, such as ATP generation by the respiratory chain, aspartate synthesis by matrix aminotransferases and long-chain fatty acid catabolism by the beta-oxidation pathway (Chen et al., 2016). What is more, it has been demonstrated tumor cells with mitochondrial defects are able to fulfil bioenergetic and anabolic demands even if any of its function is truncated (Frezza and Gottlieb, 2009). Moreover, defects in mitochondrial metabolism have been related to tumor formation and growth (Gaude and Frezza, 2014). Therefore, we decided to study functional effects of cancer mitochondria on energy metabolism and tumorigenesis. For that purpose, we have considered highly useful to utilize p0 cells as an extreme metabolic phenotype of respiratory deficient cells. As a result of lack of mitochondrial DNA (mtDNA), these cells are not able to assemble respiratory complex and they turn into completely knock

out for mitochondrial OXPHOS. It is known that encoded OXPHOS genes are essential for cancer cell survival and growth. Mutations in mitochondrial genes must therefore be altering cellular bioenergetics and metabolism so that contribute to neoplastic transformation (Wallace, 2012). Even so, $\rho 0$ cells are not only able to survive, but also proliferate at the same level as respiration fully active cells through effective reprogrammed metabolism.

Over the years, these cells have been widely used to investigate relationships between mtDNA mutation, mitochondrial function, and a variety of cellular processes (Chandel and Schumacker, 1999; Ishihara et al., 2016; Scarlett et al., 2004). In cancer, $\rho 0$ cells have been utilized for studying selective advantages of mtDNA mutations in tumorigenesis and metastasis (van Gisbergen et al., 2015; Petros et al., 2005; Weinberg et al., 2010).

In summary, using this extreme metabophenotype model, we will try to find the most essential metabolic functions for proliferation provided by mitochondrial respiration. In addition, new therapeutic approaches targeting tumor metabolism will be applied using nanotechnology. These nanoparticle based strategies will be discussed in the next section.

SECTION II: TARGETED DRUG DELIVERY BASED ON TUMOR METABOLISM

1. Strategies for targeting metabolic pathways for cancer treatment

The specificities of tumor metabolism targeting and the difficulties of translating this basic knowledge to clinic for the design of efficient drug screening and preclinical therapeutic anti-cancer strategies will be described. Furthermore, some recent advances and insights in the field are mentioned, as well as our proposed alternative in metabolism-based therapy.

1.1. Targeting cancer metabolism

As it has been discussed in section one, accumulating evidence supports that cancer is not only a disease of genetics, but also a disease of dysregulated bioenergetic metabolism. During the past decade, this cancer-associated metabolic rewiring has been viewed as a promising source of novel drug targets. Several approaches focused on tumor metabolic specificities or vulnerabilities have been explored, which has allowed the discovery of novel targets now considered for preclinical therapy programs or even for clinical trials. The main chemotherapeutic approaches that are being used to target the aberrant metabolism observed in tumors are detailed below and summarized in Table 1.

Targeting bioenergetic metabolism: several cancer-associated alterations in bioenergetic metabolic pathways (including glycolysis, TCA cycle, mitochondrial respiration, glutaminolysis and fatty acid oxidation) have been investigated as potential drug targets (Galluzzi et al., 2013) (**Fig. 11**). Many enzymes and transporters involved in these pathways have been suggested as promising targets by a large body of preclinical researches. These include HK2 (Wolf et al., 2011), PFKFB3 (Clem et al., 2013), GAPDH (Nicholls et al., 2012), PKM2 (Goldberg and Sharp, 2012), LDHA (Le et al., 2010), PDK1 (Shen et al., 2013), glucose transporters (Liu et al., 2012; Zhan et al., 2011), and monocarboxylate transporters (Birsoy et al., 2012; Sonveaux et al., 2008). Inhibition of both TCA cycle and mitochondrial respiration has been known to possess anti-tumor activity for many years (Fulda et al., 2010), as in the case of antineoplastic activity of OXPHOS and mitochondrial translation inhibitors (Zhang et al., 2015). In addition, targeting agents related to glutamine addiction, such as GLS1 (Seltzer et al., 2010; Wang et al., 2010) and GLUD1 (Yang et al., 2009), have been noted as possible key metabolic therapeutics for clinical use. Accordingly, pharmacological or genetic inhibition of these enzymes has been associated with antineoplastic effects *in vivo* in several tumor models, and few of these approaches have entered clinical development (**Table 1**).

Targeting anabolic metabolism: the strong new biomass demand to sustain high proliferative capacity in cancer cells focused attention on lipid, protein and nucleotide biosynthesis pathways (**Fig. 11**). In one hand, drugs that target one-carbon metabolism in tumor cells, thus reducing nucleotide biosynthesis, ATP generation, and altering redox balance, formed the foundation for modern chemotherapy (Martinez-Outschoorn et al., 2016). Currently, inhibitors of folate metabolism, thymidine synthesis, and nucleotide synthesis and nucleotide-strand elongation, which are collectively named as antimetabolites, inhibit cell proliferation via interference with RNA and DNA synthesis, and are all used as standard chemotherapeutic agents in the treatment of many cancers (**Table 1**). These antimetabolic therapies are being improved by blocking early stages that supply intermediates to be used in nucleotide

biosynthesis, such as ribose-5-phosphate (R5P) production in the PPP pathway (Hitosugi et al., 2012; Yuan et al., 2010). In this regard, activators of PKM2 have also been shown to limit tumor growth in xenograft models by promoting the glycolytic flux at the expense of the PPP (Anastasiou et al., 2012). On the other hand, tumor cells of different origins have been suggested to be auxotrophic for non-essential amino acids beyond glutamine, including asparagine, arginine glycine and serine, which are the building blocks of proteins and also intermediate metabolites that fuel other biosynthetic pathways (Galluzzi et al., 2013) (**Table 1**). Amino acids deprivation has been already exploited as an anticancer therapy: rapidly induced tumor regression has been observed due to further decrease glutamine concentrations by phenylacetate (Samid et al., 1994); bacterial variant of L-asparaginase, which reduces the availability of circulating asparagine, was approved by the FDA for the treatment of acute lymphoblastic leukemia (Müller, 1998); pegylated variant of arginine deiminase, which converts circulating L-arginine into L-citrulline, is being investigated in tumors auxotrophic for arginine with promising preliminary results in clinical trials (Ott et al., 2013). Furthermore, efforts to target the contribution to amino acid production through transamination reactions are currently preclinical studies. Even if retards tumor growth in breast cancer xenograft models by aminooxyacetate treatment has been reported (Korangath et al., 2015), there is a notable absence of inhibitors that are selective for individual transaminases. Lastly, targeting *de novo* lipogenesis or steroidogenesis also represents a rational approach for anticancer therapy because of high demand for the novel phospholipid bilayers generation. Several enzymes involved in these pathways, including fatty acid synthase (FASN) (Flavin et al., 2010), ATP citrate lyase (ACLY) (Hatzivassiliou et al., 2005), Acetyl-CoA carboxylase (ACCs) (Harwood et al., 2004) and choline kinase (Clem et al., 2011) have been attributed critical roles in tumor oncogenesis and their inhibition are being tested as anticancer therapy (**Table 1**).

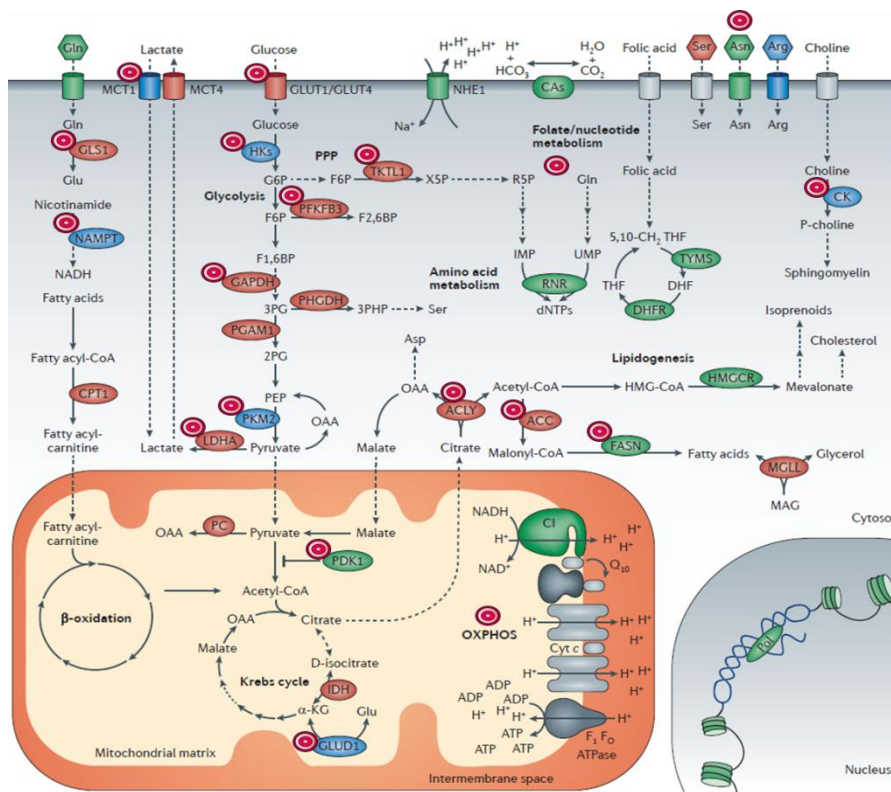


Figure 10. Schematic illustration of several branches of the bioenergetic and anabolic metabolism of malignant cells that offer targets that can be drugged to inhibit oncogenesis or tumour progression. Some of the metabolic enzymes that are currently being considered as therapeutic targets for cancer are marked with a target (shown as a pink circle in the figure). Adapted from (Galluzzi et al., 2013).

Targeting processes regulating metabolism: additional pathways that are involved in the adaptation to metabolic stress may be drug targets for anticancer therapy, such as NAD⁺ metabolism and growth factor signaling networks. Because of high need for regenerating NAD⁺ to enable the continued flow of glucose carbon via glycolysis, cells that are treated with NAMPT inhibitors, enzyme that is involved in regenerating NAD⁺ via a salvage pathway, die as a result of NAD⁺ depletion (Garten et al., 2009). Thus, NAMPT inhibition has shown activity as an anticancer agent in preclinical cancer models. However, dose-limiting toxicity was observed so far in early clinical trials of NAMPT inhibitors, remaining necessary to develop target therapies (Vander Heiden, 2011). On the other hand, HIF1-orchestrated responses have highlighted possible antitumor drug targets. Several cytotoxic agents have been developed to block HIF-1 α expression, transcription, translation, target-binding disruption and other associated signaling and are being tested in oncology clinical trials (**Table 1**). However, despite the promise of HIF-1 inhibitors as anticancer agents, preclinical and clinical development of many of these agents has been halted because of toxicity or safety concerns (Talekar et al., 2014). Furthermore, mTOR-targeted therapy has been extensively investigated during the past decade. Despite the fact that mTOR is believed to have a crucial role in tumor development, the clinical outcome in trials using mTOR inhibitors as monotherapy has shown only modest results owing to induction of autophagy (Tennant et al., 2010b). A new generation of drugs has recently been developed (**Table 1**), and combination therapy with other autophagy modulators might constitute a good approach to negating resistance to mTOR inhibitors (Martinez-Outschoorn et al., 2016).

Target	Drug	Development stage	Observations
Bioenergetic metabolism			
Glycolysis			
GLUT1	<ul style="list-style-type: none"> • WZB117 • Silibinin 	Preclinical studies	Anticancer activity <i>in vitro</i> and <i>in vivo</i>
Hexokinases	<ul style="list-style-type: none"> • 2-deoxyglucose • Lonidamine • 3-bromopyruvic acid • Methyl jasmonate 	Preclinical and clinical studies	Anticancer activity <i>in vitro</i> and <i>in vivo</i> . Discontinued clinical development. Lonidamine, tested in phase II clinical trials
PFKFB3	<ul style="list-style-type: none"> • PFK158 	Preclinical studies	Anticancer activity <i>in vivo</i>
PKM2	<ul style="list-style-type: none"> • TLN-232 	Phase II clinical studies	Anticancer activity <i>in vitro</i> and <i>in vivo</i>
LDHA	<ul style="list-style-type: none"> • GNE-140 • FX11 • Galloflavin 	Preclinical studies	Anticancer activity <i>in vitro</i> and <i>in vivo</i>
MCTs	<ul style="list-style-type: none"> • AZ93 • AZD3965 • CHC 	Preclinical and clinical studies	Reduced tumor-cell growth <i>in vitro</i> and <i>in vivo</i> . Being tested in Phase I in patients with advanced-stage solid tumors
TCA cycle/mitochondrial metabolism			
PDK1	<ul style="list-style-type: none"> • DCA 	Approved for the treatment of lactic acidosis. Phase II clinical trials	Well tolerated in glioblastoma patients. A phase II trial in previously treated other cancer was terminated early owing to toxicity
IDH	<ul style="list-style-type: none"> • AG-120 • AG-221 • AG-881 	Preclinical and clinical studies	Anticancer effects via decreased production of 2-hydroxyglutarate
Mitochondrial complex I	<ul style="list-style-type: none"> • Metformin • Phenformin 	Approved agent (not for cancer)	Anticancer activity <i>in vitro</i> and <i>in vivo</i> . Phase II clinical trials, with results mixed. Ongoing phase III clinical trials.
Glutamine metabolism			

GLS1	<ul style="list-style-type: none"> • CB-839 • 968 • BPTES 	Preclinical and phase I clinical studies	Inhibition of TCA anaplerosis. Anticancer activity <i>in vitro</i> and <i>in vivo</i>
GLUD	<ul style="list-style-type: none"> • EGCG 	Preclinical studies	Tool compound
Aminotransferases	<ul style="list-style-type: none"> • AOA 	Preclinical studies	Clinically used to treat tinnitus. Toxic at higher doses
Anabolic metabolism			
Nucleic acid synthesis			
Folate metabolism (DHFR)	<ul style="list-style-type: none"> • Methotrexate • Pemetrexed • Pralatrexate 	Approved as anticancer agents	Effective therapies for various cancers
Thymidine synthesis (TYMS)	<ul style="list-style-type: none"> • 5-Fluorouracil • Capecitabine • S-1 (pyrimidine analogues) 	Approved as anticancer agents	Effective therapies for various cancers
Adenine/adenosine deaminase	<ul style="list-style-type: none"> • Pentostatin, • 6-mercaptopurine • Cladribine (purine analg) 	Approved as anticancer agents	Used mainly to treat haematological malignancies
Nucleotide incorporation (DNA polymerase/ribonucleotide reductase)	<ul style="list-style-type: none"> • Gemcitabine • Fludarabine • Cytarabine • Hydroxyurea 	Approved as anticancer agents	Gemcitabine is a widely used agent in clinical oncology practice, pancreatic and lung cancer. Rest are used mainly in patients with haematological malignancies
Amino acid metabolism/protein synthesis			
Asparagine availability	<ul style="list-style-type: none"> • L-asparaginase 	Approved agent	An effective therapy for acute lymphoblastic leukaemia
Arginine availability	<ul style="list-style-type: none"> • Pegylated arginine deiminase (ADI-PEG20) 	Clinical development	Multiple phase II clinical trials are ongoing
Lipid synthesis			
FASN	<ul style="list-style-type: none"> • TVB-2640 	Preclinical studies	Anticancer effects <i>in vitro</i>
ACL	<ul style="list-style-type: none"> • Hydroxycitrate 	Preclinical studies	Anticancer effects <i>in vitro</i>
ACC	<ul style="list-style-type: none"> • NDI-010976 	Preclinical and clinical studies	Phase I clinical trials in hepatocellular carcinoma are ongoing
Choline kinase	<ul style="list-style-type: none"> • TCD-717 • CK37 • MN58b • RSM932A 	Preclinical and clinical studies	Anticancer effects <i>in vitro</i> and <i>in vivo</i> . Phase I trial completed for TCD-717
Other metabolic pathways			
HIF	<ul style="list-style-type: none"> • Topotecan • Irinotecan • Digoxin • Ganetespib • Bortezomib • CRLX101 • Acriflavine • PX478 • BAY 87-2243 	Preclinical and clinical studies	Clinical development of PX478, acriflavine, and BAY 87-2243 has been discontinued owing to toxicity and safety concerns
mTOR	<ul style="list-style-type: none"> • Everolimus • Temsirolimus (rapalogues) 	Preclinical and clinical studies	Approved for renal-cell carcinoma, breast cancer, and neuroendocrine tumors
NAMPT (synthesis NAD)	<ul style="list-style-type: none"> • FK866 • CHS828 • GMX1778 • AU-315 • CB30865 	Preclinical and phase II clinical studies	Modest anticancer efficacy with haematological and gastrointestinal adverse effects

Table 1. Strategies to target biological processes regulating metabolism for cancer treatment.

(Adapted from Galluzzi et al., 2013; Martinez-Outschoorn et al., 2016).

1.2. Current status and future prospects of metabolism-based therapy

Metabolic reprogramming in cancer is now widely recognized as an important target for cancer treatment. For the last years, many metabolic enzymes have been identified as targets to block biosynthesis or induce energy stress in cancer cells. As mentioned, targeted metabolic drugs that influence these pathways have been tested in humans (Table 1). Nevertheless, this strategy has not fully translated into clinical results (Garber, 2016). A number of these agents had considerable systemic toxicity and a lack of therapeutic benefit in clinical studies, which has restrained further development (Martinez-Outschoorn et al., 2016).

Consequently, there are certain limitations that should be considered before translating a metabolism-based anticancer approach from bench to bedside. Firstly, diversity in cellular bioenergetics profiles within the same tumor mass due to intratumoral heterogeneity (different level of glycolysis and oxidation) and metabolic plasticity should be taken in consideration. Cells can meet specific energy and biosynthetic needs by metabolizing preferentially a given carbon substrate over another (Lehuédé et al., 2016; Stanley et al., 2014). In fact, fast metabolic plasticity in response to changing tumor cell microenvironments has been observed in cells which use OXPHOS efficiently during optimal growth conditions and reversibly shut down OXPHOS during transient hypoxia and/or glutamine deprivation (Simões et al., 2015). Furthermore, that depends also on the microenvironmental/nutritional niche in which cancer cells reside (Lukey et al., 2016). Recent studies have reported that different key molecules in tumor metabolism such as aspartate, pyruvate or NAD⁺, are often fluctuating, and highlight that consideration of the metabolic environment is critical for the development of cancer therapies that target metabolism (Gui et al., 2016).

Apart from that, it is widely known multidrug resistance (MDR) is one of the most critical problems that have been found in chemotherapy. MDR in cancer refers to a state of resilience against structurally and functionally unrelated drugs (Stavrovskaya, 2000). Several studies pointed to a relation between MDR and alterations in cellular metabolism. Extremely high glycolytic rates, such as mitochondrial defects or under hypoxic conditions scenarios, have been associated with cellular resistance to conventional anti-cancer drugs and radiation therapy (Lopes-Rodrigues et al., 2017; Pelicano et al., 2006). This fact, together with unsuccessful results in glycolytic inhibitors as single agent chemotherapy, has led to implement effective strategies by using traditional drugs along with glycolysis inhibition. Nowadays, there are an increasing number of reports showing that targeting the Warburg effect may overcome tumor resistance to commonly used chemotherapeutic agents in an effort to eradicate as much cancer cells as possible and prevent survival of chemoresistant cells (Li et al., 2002; Nakano et al., 2011).

On the other side, whether metabolic reprogramming in cancer is intrinsically different from the metabolic response to proliferative stimuli in non-transformed cells still remains unclear. However it has been recognized that certain proliferative cells and normal tissues including brain, retinae and testis, also use glucose as the main energy source, and is unclear whether instead can effectively use alternative energy sources (fatty acids, amino acids, etc.). Thus, glycolysis inhibition may be potentially toxic to these tissues due to failure to generate sufficient ATP to support their cellular function when the glycolytic pathway is inhibited during therapy. Likewise, toxic side effects may be restricted to metabolic tissues, such as liver, but may also have marked effects on whole body metabolism, such as decreased body weight by fatty-acid synthase inhibitors (Schulze and Harris, 2012).

Recently, different alternatives have been proposed in order to overcome some of these metabolic therapy limitations. First, a deeper understanding of the tumor reprogramming mechanisms still remains in the vanguard to identify new key signaling nodes to be targeted for cancer therapy. Moreover, current available metabolic inhibitors are generally not very potent, and high doses are required, which may cause high levels of systemic toxicity limiting their use in humans. Alteration of one single pathway in the metabolic network may be

inducing compensatory pathways that can compensate metabolites loss by generating alternative sources. Combined pharmacologic strategies simultaneously targeting multiple metabolic pathways became providing a rational approach to treat cancer. In this context, metabolic synthetic lethality, refers to a principle in which the combination of two metabolic perturbations are lethal, whereas each individually is not, has emerged as the possibility of reaching undruggable targets indirectly (Beijersbergen et al., 2017). Recently, the concept of synthetic lethality has been applied to cellular metabolism. A clear example of this effect is the combination of LDHA inhibitor with a drug that blocks the NAD⁺ synthesis through the salvage pathway. This LDHA inhibition results in the depletion of NAD⁺, which is crucial to maintain high glycolytic flux observed in cancer cells. Reduction of NAD⁺ cellular pool has been observed in the combination of LDHA inhibition with small inhibitor FX11 and FK866 (**Table 1**), resulting in tumor regression (Le et al., 2010).

As it has been discussed, besides these clear genetic alterations in metabolic enzymes, various types of cancers display defects in the respiratory chain (Gaude and Frezza, 2014). Therefore, synthetic lethality strategies based on the metabolic reprogramming triggered by these defects have been proposed. Accordingly, mitochondria-based synthetic lethality interactions to target cancer was enhanced by the recent observation that, through its ETC complex I inhibition activity, the anti-diabetic drug metformin acts as an anticancer agent (Wheaton et al., 2014). Respiration inhibition in combination with drugs which blocks the possible escape routes in the reprogrammed metabolism has been shown to prevent tumor growth (Birsoy et al., 2014). In this respect, in a preclinical study, a combination of metformin and 2-deoxyglucose, a specific glycolysis inhibitor (**Table 1**), was effective in a wide range of tumor types impairing the growth of cancer cells (Cheong et al., 2011).

On the other hand, decreased mtDNA content is also detected in tumor-initiating cells, a subpopulation of cancer cells that are believed to play an integral role in cancer recurrence following chemotherapy (Guerra et al., 2017). Thus, our respiration deficient cell model, which has been entered in the previous section, provides certainly an excellent feature for studying both synthetic lethality, such as metformin effect observed, and potential role of defective mtDNA in the cancer chemoresistance development. Besides that, we propose to enhance metabolism-based therapeutic efficacy through nanotechnology approaches. This strategy could enable overcome the drug resistance and also simultaneously achieve a target delivery preserving the survival of normal proliferating cells.

1.3. Nanoparticles as promising alternative in metabolism-based therapy

In recent years, nanotechnology has been increasingly applied to the area of drug development. Specifically, nanoparticles (NPs) are receiving great attention in the diagnostic and therapeutic fields as biocompatible carriers for tracing molecules or drugs. This is due not only they can access biological systems and compartments, but also to can be engineered with precise functional properties. NPs are defined as being submicronic (<1 μm) colloidal systems and may act as a drug vehicle able to target tumor tissues or cells while protecting the drug from degradation or inactivation during its transport (Brigger et al., 2002).

The main advantages of anticancer drugs delivery through a nanoparticle-based platform compared with traditional chemotherapeutics include: (a) improved insoluble drugs delivery

and enables delivery of high dose into cancerous cells; (b) better drug protection from untoward environments before targets have been reached, leading to an extended drug plasma half-life in the system; (c) targeted delivery of drugs in a cell- or tissue specific manner, maximizing treatment efficacy and reducing systemic side effects; (d) controlled drug release using a stimuli-responsive system; and (e) co-delivery of multiple types of drugs and/or diagnostic agents for combination therapy, which potentially allows to overcome multidrug resistance and synthetic lethality strategies (Desai, 2012; Sun et al., 2014). Hence, the NPs-induced huge intracellular drug loading should elude the many resistance processes related to drug uptake, metabolism and efflux, and thus markedly improve chemotherapies efficiency.

Several studies have been reported using nanoparticles in an effort to take advantage of the therapeutic efficacy of traditional drugs avoiding MDR and reducing toxicities due to dosage (Gao et al., 2012; Piktel et al., 2016). NPs can be used to reverse MDR phenotype both by inhibition of efflux pumps and MDR-associated proteins, and enhancing intracellular drug retention. The mechanism of nanosystem internalization facilitates undetected entry into cells, bypassing the increased drug efflux mechanism of drug resistance in tumor cells (Fig. 11). Epidermal growth factor receptor (EGFR) targeted nanoparticles encapsulating lonidamine and paclitaxel were developed and tested in orthotopic MDR-positive breast cancer xenografts. Reduced tumor growth compared to treatment with blank nanoparticles was observed and higher liver toxicities were arisen in animals treated with soluble drugs compared to drugs bound to nanoparticles (Milane et al., 2011).

In this regard, it is desired to take advantage of using NPs in order to improve metabolism-based cancer treatment. More specifically, in this work it has been proposed to redesign metabolic therapies focusing on emerging targets (for instance, MCTs, GOT and CD147) and implement traditional chemotherapeutic drugs (such as doxorubicin) with new key roles. Although doxorubicin mainly suppresses cell proliferation through DNA intercalation, it has also been known this drug plays an important role in oxidative stress, increasing the intracellular levels of ROS (Gilliam et al., 2012; Thorn et al., 2011). Enhanced anticancer efficacy of doxorubicin *in vitro* and *in vivo* through GOT1 suppression using the shRNA, which inhibits drug-induced oxidative stress, has been recently reported (Yang, 2016). Accordingly, this enhancement in therapeutic efficacy is based on the inability of the cells to detoxify doxorubicin-stimulated ROS, thus confirming targeting metabolic strategies can improve conventional chemotherapeutics efficiency.

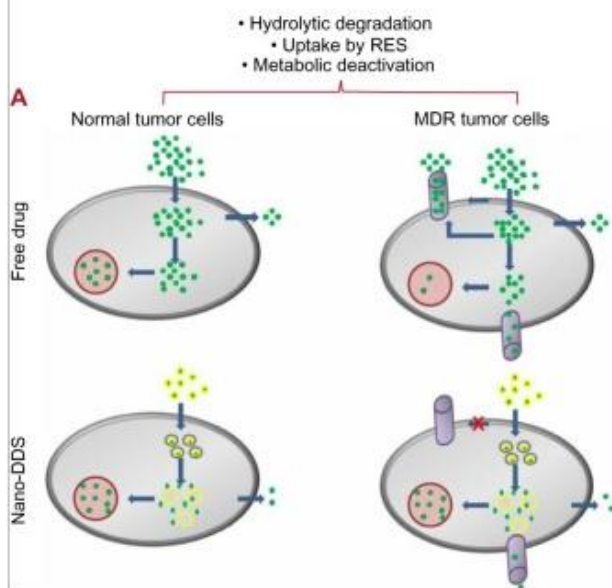


Figure 11. Diagrammatic comparison of the internalization mechanisms of free drug and nanodrug delivery systems in normal tumor cells and multidrug-resistant tumor cells. (Frank et al., 2014)

In this new overview, taking advantage of metabolic approaches, we expect to improve the efficacy of traditional antiproliferative therapies such as doxorubicin, which present an important metabolic role that promotes antitumoral drug capacity, and also be personalized depend on tumor type and patient condition. The final goal will be to achieve main effectiveness in current metabolic therapies together with reduction of secondary effects.

2. Nanotechnology-based Drug Delivery in cancer

Nanotechnology, which is the study and application of materials on the nanometer scale, is rapidly expanding its reach into many areas with great impact, including medicine. The nanomedicine field embraces the development of new materials and their manipulation for devices, drugs and diagnostics. In this section, we will briefly review recent translational advances in the use of nanosystems to develop therapeutic agents focusing on cancer treatment, with special regard to targeted delivery systems. Finally, we will introduce an alternative to current antibody-based therapies using nanotechnology approaches.

2.1. Nanotechnology approaches to cancer therapy

Medical potential of nanoparticles comes from the broad spectrum of unique physicochemical and biological features, including large surface area/volume ratio, specific structural properties, high ability to carry compounds on their surface, capability to pass biological barriers and long circulation time in blood (Piktel et al., 2016). Their design (shape, size, surface characteristics) and material from which nanoparticles are made determine their theranostic potential, employment in medical applications and effect on pharmacokinetic parameters *in vivo* conditions (Fig. 12) (Piktel et al., 2016; Shi et al., 2016).

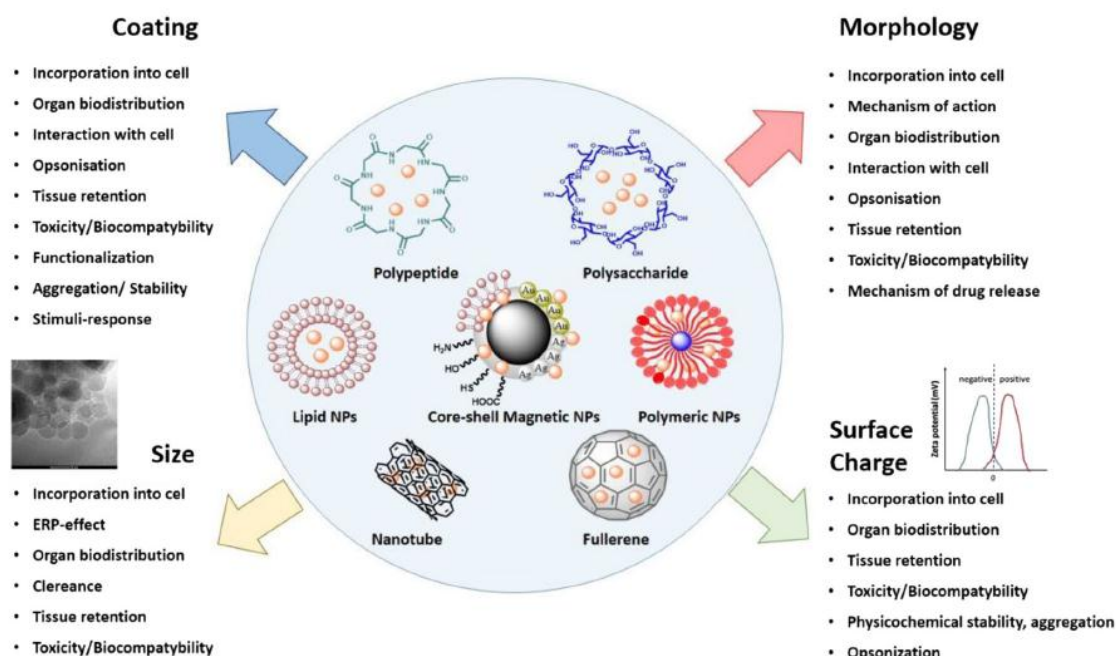


Figure 12. Physicochemical features of different nanomaterials with medical potential use. NP properties affect the biological processes involved in the delivery to tumor tissues (such as interactions with serum proteins, blood circulation, biodistribution, extravasation to perivascular tumor microenvironment and penetration), tumor cell targeting and intracellular trafficking (Piktel et al., 2016).

A variety of nanostructures have been investigated to be employed in a number of biomedical applications, such as drug delivery systems (Wilczewska et al., 2012), contrast agents for magnetic resonance imaging or computer tomography imaging and as diagnostic tools (Niemirowicz et al., 2012; Scheinberg et al., 2017). In cancer treatment, several therapeutic nanoparticle platforms have already been approved, and many other nanotechnology-based modalities are under clinical investigation, including chemotherapy, radiation therapy, gene or RNA interference (RNAi) therapy and immunotherapy (Table 2) (Shi et al., 2016).

Name	Nanotechnology platform	Drug	Application	Development stage
Chemotherapy: non-targeted delivery				
Doxil	Pegylated liposome	Doxorubicin	Kaposi sarcoma, ovarian cancer, multiple myeloma	Approved by FDA
DaunoXome	Liposome	Daunorubicin	Kaposi sarcoma	Approved by FDA
Marqibo	Liposome	Vincristine sulfate	Acute lymphoblastic leukemia	Approved by FDA
Onivyde or MM-398	Pegylated liposome	Irinotecan	Post-gemcitabine metastatic pancreatic cancer	Approved by FDA
Myocet	Liposome	Doxorubicin	Metastatic breast cancer	Approved in Europe and Canada
Abraxane	Albumin NP	Paclitaxel	Breast, lung and pancreatic cancer	Approved by FDA
Mepact	Liposome	Muramyl tripeptide phosphatidylethanolamine	Nonmetastatic, resectable osteosarcoma	Approved in Europe
Genexol-PM	Polymeric micelle	Paclitaxel	Breast cancer and NSCLC	Approved in Korea
Oncaspar	Polymeric PEG-L-asparaginase	Asparaginase	Acute lymphoblastic leukemia	Approved by FDA
Chemotherapy: targeted delivery				
MM-302	HER2-targeting liposome	Doxorubicin	HER2-positive breast cancer	Phase II/III
Anti-EGFR immunoliposomes	EGFR-targeting liposome	Doxorubicin	Solid tumors	Phase I
BIND-014	PSMA-targeting polymeric NP	Docetaxel	NSCLC and mCRPC	Phase II
Radiotherapy				
NBTXR3	Hafnium oxide NP	--	Adult soft tissue sarcoma	Phase II/III
Gene or RNAi therapy				
SGT53	TfR-targeting liposome	Plasmid encoding normal human wild-type p53 DNA	Recurrent glioblastoma and metastatic pancreatic cancer	Phase II
PNT2258	Liposome	DNA oligonucleotide against BCL-2	Non-Hodgkin lymphoma and diffuse large B-cell lymphoma	Phase II
DCR-MYC	Lipid NP	Dicer-substrate siRNA against MYC	Hepatocellular carcinoma	Phase I/II
CALAA-01	TfR-targeting polymeric NP	siRNA against ribonucleotide reductaseM2	Solid tumors	Phase I
Immunotherapy				
dHER2 + AS15	Liposome	Recombinant HER2 antigen +AS15 adjuvant	Metastatic breast cancer	Phase I/II
Tecemotide	Liposome	MUC1 antigen	NSCLC	Phase III

Table 2. Examples of clinical-stage of nanoparticle-based therapeutics for cancer therapy. (Adapted from (Shi et al., 2016; Sun et al., 2014).

Although the translation to clinic of just few nanoparticles have been successful achieved (Couvreux, 2013), several new and promising nanoparticles are currently in development. In this regard, studies have been focused on the thorough physiochemical, pharmacological and immunological NP characterization before evaluated them in clinics. Furthermore, design of

multifunctional nanoparticles, which enable combination of various strategies, is certainly another exciting future challenge in the field, discussed in the next section.

2.2. Engineered Nanoparticles for Drug Delivery in cancer therapy

After several decades of technological developments, drug-delivery systems based on engineered nanoparticles have started to show great promise. As the platforms for these drug delivery systems liposomes, solid lipids nanoparticles, dendrimers, silicon nanostructures, polymer conjugates, micelles, carbon nanomaterials and protein or nucleic acid-based nanoparticles (**Fig. 12**) have been tested (Piktel et al., 2016). However, despite a variety of described nanotechnology-based formulations for cancer therapy, only a limited number of liposomes and polymeric nanodevices were clinically approved (**Table 2**). Because of lipid-based NPs represent a large proportion of clinical-stage nanotherapeutics, emerging efforts have been focused on improvement already used drugs by encapsulation. Thus, multiple studies with formulations of encapsulated nanoparticles for improved therapeutic effects have been reported (Cabeza et al., 2017; Sadhukha and Prabha, 2014; Yallapu et al., 2010; Zhou et al., 2017). However, although encapsulating drugs have been broadly shown to improve pharmacokinetics and biodistribution, several disadvantages such as stability and early degradation have not yet been overtaken (Fontana et al., 2017). In addition, recent study has shown that as yet antitumor efficacy of liposomal therapeutic agents over conventional drug in preclinical studies generally did not translate to the clinical trial setting (Petersen et al., 2016).

In this context, engineered nanoparticles offer a powerful alternative in the development of cancer nanotherapies (Sun et al., 2014). Multifunctionality allows for the creation of more complex drugs that might modulate and act through different pathways and diverse mechanisms. Furthermore, appropriately designed multifunctional nanoparticles could have components that enable selectivity to the target by decoration of nanoparticles with ligands able to recognize a specific biological target overexpressed on tumor cells, and allowing active binding. To that end, surface of nanodevices can be functionalized by a number of tumor targeting agents including small molecules, peptides, monoclonal antibodies or their fragments, aptamers and nucleic acids (Piktel et al., 2016). Beyond increase of intracellular uptake by the target cells, biofunctionalized targeted nanoparticles also preferentially are accumulated in tumors when compared with non-targeted nanoparticles (Wang et al., 2008), which an important point for this thesis research pipeline.

Strategies based on the antibody-antigen or ligand-receptor interactions have been designed for targeted cancer therapy (Wang et al., 2014), and some of them have progressed into clinical trials (van der Meel et al., 2013). The main therapeutic targets of the nanotechnologies currently studied in human are the transferrin receptor (Davis et al., 2010), EGFR (Mamot et al., 2012), PSMA (Hrkach et al., 2012), the surface of gastric cancer cells (Matsumura et al., 2004) and HER-2 (Espelin et al., 2016) (**Table 2**). These promising clinical trials open the door to look for new alternative biomarkers overexpressed on cancer cells to use in targeting cancer therapy. In addition, in the next years, thanks to the experience acquired on NP-based clinical trials in patients, our understanding of the parameters determining active targeting will hopefully improve.

On the other hand, targeted delivery strategies have also been shown to achieve greater efficacy in cancer treatments. Towards this end, substantial efforts have recently been directed towards developing stimuli-sensitive nanodevices to trigger drug delivery (**Fig. 13a**). These approaches offer better spatial and temporal control of drug release in response to external factors or by changes in local endogenous conditions in the precise target tissue. To date, a number of stimulus factors, including light, temperature, magnetic field, enzymes, redox potential or alternation in pH value, have been explored (Jhaveri et al., 2014; Mura et al., 2013). To conjugate drug molecules and enable controlled drug release from nanoparticles, chemical conjugation approach has been extensively investigated. According to that, acid-labile chemical bonds are widely used to trigger drug release, due to their pH-responsive hydrolysis (**Fig. 13b**). These chemical bonds remain intact at neutral pH, while at acidic environment, the chemical bonds can be hydrolyzed, and drugs attached through the linkage can be released (Sun et al., 2014). This strategy is based on microenvironment in tumors is generally more acidic compared to normal or blood physiological pH (Piktel et al., 2016), therefore allowing pH-sensitive drug release (**Fig. 13c**).

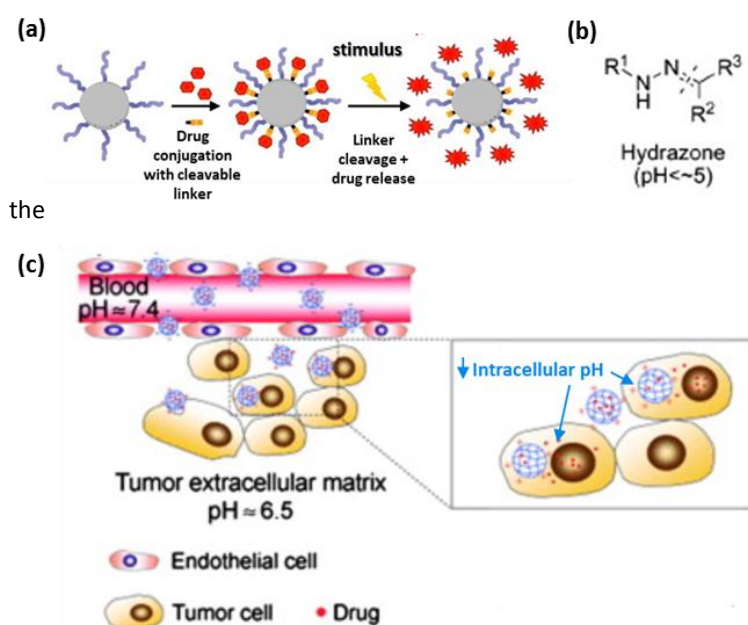


Fig. 3. Multifunctional, stimuli-sensitive nanodevices for drug delivery. (a) General scheme of a stimuli-responsive engineered NP for transport of active compounds. (b) One of the usually cleavable linkers used for stimuli-responsive nanocarriers. The dashed line shows the bond that is broken upon activation by lower pH. (c) Schematic illustration of the behavior of the drug-loaded pH-responsive NPs, showing NP internalization by tumor cells from vessel with

subsequent intracellular drug release. Adapted from (Fleige et al., 2012).

Hydrazone bond is often used as cleavable linker for stimuli-responsive depending on pH (**Fig. 13b**) (Sun et al., 2014). It has been widely investigated to covalently attach some drugs to different nanodevices in order to overcome drug side effects. Doxorubicin, which is one of the most effective traditional antitumor agents in clinical practice, is a hydrophilic molecule. That has restricted its transport through the cellular membrane leading to minimal drug internalization. Besides, development of MDR is a common limitation with doxorubicin based-chemotherapy (Xu et al., 2014). Doxorubicin conjugated NPs-based drug delivery system via stimuli-responsive cleavable bond has been proved to reduce these limitations (Lu et al., 2009; Meng et al., 2014; Ren et al., 2011, 2014; Zohreh et al., 2016). This concept is relevant for the focus of this thesis, since that will be the strategy chosen to address metabolic therapy developed.

2.3. Targeted therapy: monoclonal antibodies in cancer therapy

Over the past two decades, therapeutic antibodies have demonstrated promising results in the treatment of a wide range of diseases, in particular in cancer and immunological disorders (Li and Zhu, 2010). Many of the forty-seven monoclonal antibody products approved and marketed in the United States and Europe are used in cancer therapy (Ecker et al., 2015). These approved targeted therapies include antibodies directed against the cell surface markers cluster of differentiation (CD20, CD33, and CD52), which are present on lymphoma and leukemia cells, and extracellular components of upregulated molecular pathways, such as EGFR, VEGF and HER2 (Li and Zhu, 2010). Some of these molecules may be present in normal tissues, but they are often mutated or overexpressed in tumors.

However, antibody-based therapy has several disadvantages which limit its application, such as limited stability of antibodies, low level of tissue penetration and multiple administrations together with a high cost of antibody production, resulting in costly therapy. Accordingly, the use of nanoparticles as carriers and delivery systems for antibodies can allow for a reduction in antibody dosing and may represent a suitable alternative to increase antibody stability (Sousa et al., 2016).

As biomedical application, antibody-conjugated nanoparticles can be used principally in therapy and diagnosis. Among others, in diagnosis the applications include contrast agents for magnetic resonance imaging, sensing, cell sorting, bioseparation, enzyme immobilization, immunoassays, gene delivery and purification (Arruebo et al., 2009). In therapy, the development of targeted drug delivery represents the main applications of antibody-conjugated nanoparticles. While antibodies have the ability to serve as carriers for drug delivery systems for even more effective and less intrusive cancer therapy, as was discussed in previous section, they can also prove to be therapeutic agents in their own right. That is known as antibody-based therapy or targeted therapy, whereby cell proliferation is blocked by interfering with specific molecules required for tumor development and growth. The inhibition may occur at multiple levels: by binding and neutralizing ligands; by occupying receptor-binding sites, thereby preventing ligand binding; by blocking receptor signaling within the cancer cell; or by interfering with downstream intracellular molecules (Gerber, 2008).

In line with the rationale of this thesis, use of antibodies directed against new metabolic key targets opens a new window of opportunity to develop alternative cancer therapies. Furthermore, novel metabolic approaches of current drugs can be considered in order to improve targeted therapy. In this context, cancer metabolism rewired has been recently found in cetuximab (anti-EGFR antibody therapy)-resistant tumor xenografts by upregulation of acetyl-CoA carboxylase (Luo et al., 2017). Thus, targeting both traditional molecules and metabolic pathways, which are implied in cancer reprogramming of resistant tumors in these treatments, could improve current antibody-based therapies. In addition, nanoparticle based-platforms are proposed as a new technology to increase the efficacy of therapeutic antibodies.

3. Functionalized polystyrene nanoparticles as a platform for cancer therapy

Because of polystyrene nanoparticles allow the use of solid-phase methodology that simplifies their functionalization and derivatization, they are emerging as a useful platform in

nanomedicine. In addition, the non-endocytotic nature of their cellular uptake makes these remarkable delivery vehicles suitable for all cell types and allow the direct cargo exposure inside the cell. In this section, potential of polystyrene nanoparticles and their use as carrier system will be discussed.

3.1. Polystyrene nanoparticles

Among the nanodevices currently on the market or in preclinical development, liposomes, polymer-drug conjugate and polymeric nanospheres are the predominant classes (Table 2), while others nanocarriers such as micelles and dendrimers has been more recently developed. Polymeric nanoparticles represent the ideal hybrid technology because they possess chemical and physical properties similar to those of the polymers and their surface can be coated with recognition molecules such as those of the liposomes (Wilczewska et al., 2012). Particularly, the surface chemistry of the nanoparticles is crucial for their durability and solubility in biological media as well as for their biocompatibility and biodistribution. The aromatic polymer polystyrene is biocompatible, does not degrade in the cellular environment and exhibits no short-term cytotoxicity (Loos et al., 2014a).

Polystyrene nanoparticles can be easily synthesized in a wide range of sizes with different surface functionalization. Specifically surface-modified polystyrene nanoparticles are homogeneous, exhibit a low polydispersity index, and form stable colloids in biological fluids (Loos et al., 2014a; Stephen R. Popielarski et al., 2005). Our research group has developed a chemistry methodology that allows the preparation of a range of mono-disperse, cross-linked, functionalized polystyrene nano and microparticles (Fig. 14) in a variety of user defined sizes (100 nm-2 μm) (Unciti-Broceta et al., 2012a), which show both chemical and biological compatibility and wide application to the biomedical field.

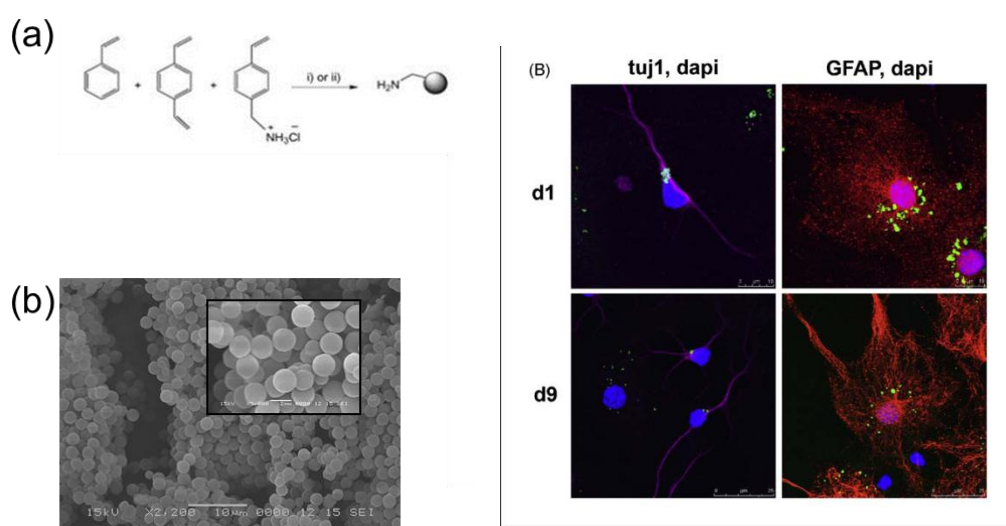


Figure 14. Amino-functionalized polystyrene nanoparticles. (a) Synthesis of amino-functionalized polystyrene nanoparticles by polymerization. (b) SEM images of the well-defined, amino- cross linked nanoparticles. (Sanchez-Martin et al., 2005) (c) Nanoparticles internalization by mouse neuronal stem cells (mNSCs). Immunofluorescent-staining for Tuj1 (purple), S100b (red) and DAPI (blue) of mNSCs fixed on day 17 of neural differentiation, after beadfection (500 nm ahx-FAM beads, green) on day 1 or day 9 of differentiation. (*New Biotechnol.*, **2009**, 25, 442-449).

Such systems have previously been tested either for their toxicity or for the uptake efficiency on a large number of human and murine cell lines, such as embryonic stem cells (HEK293T, hES and mES, tumor cell lines (HeLa, A375M, K562, MDAMB231, B16F10) and primary cells (L929 and ND11), including primary neurons (Alexander et al., 2010; Borger et al., 2011; Cardenas-Maestre et al., 2011; Cárdenas-Maestre et al., 2014; Gennet et al., 2009; Tsakiridis et al., 2009; Unciti-Broceta et al., 2015). In these studies has been demonstrated that nanoparticles are neither toxic to the cells nor mobile; once within a cell, the bead is stably retained. Furthermore, the most incontrovertible proof about the non-toxicity of the microspheres, as well as their ability to leave unchanged the normal cellular function, has been the generation of mice alive and vital from murine embryonic stem cells previously nanofected with polystyrene NPs (Tsakiridis et al., 2009)

Polystyrene NPs trafficking across Madin Darby canine kidney cell II monolayers (MDCK-II) and rat alveolar epithelial cell monolayers (RAECM) has been investigated, thereby transcellular translocation was observed (Fazlollahi et al., 2011a; Yacobi et al., 2008). Furthermore, NP externalization observed by exocytosis rate has been negligible, showing NPs are not exported from the cells (Kim et al., 2011a). The nanoparticle uptake mechanism has been studied by chemical modulation, fluorescence microscopy and gene profiling technology and it was found to be size and time dependent, but independent of depletion of both ATP and cholesterol, equally required for endocytosis process (Alexander et al., 2010). The results obtained have led to the hypothesis according to which the polystyrene NPs anchor and cross the phospholipid bilayer and diffuse in the cytoplasm, thereby a process that involves rearrangements of the actin cytoskeleton and does not require ATP hydrolysis. Additionally their intracellular localization has been proved (Cárdenas-Maestre et al., 2014; Unciti-Broceta et al., 2015).

In the other hand, gene-expression profiling studies have reported that the transcriptome of nanofected cells is only partially affected (Alexander et al., 2010). The involved genes mainly encode for membrane proteins or for related proteins to cellular metabolism and cytoskeleton rearrangements. What is more, recent proteomic studies showed no key regulators of cell cycle were affected by the NPs internalization, confirming that this system is harmless and well tolerated by the cells (Pietrovito et al., 2015).

3.2. Multi-functionalisation strategy

Surface functionalization of nanoparticles is crucial for the stability of the particle suspensions in biological media, biocompatibility, and biodistribution, in addition to the importance for their controlled and targeted biomedical applications. Depending on the particular use of the nanospheres, different chemical approaches have been developed to the coupling of cargos to the polymeric particle. In this thesis, surface functionalisation will be achieved applying solid-phase synthesis protocols previously optimized by Sánchez-Martínez's group (Sanchez-Martin et al., 2005; Unciti-Broceta et al., 2012a). The main strategy used consists of an Fmoc solid-phase synthesis protocol (**Fig. 15**), which is based on simple coupling and deprotection steps, where coupling is normally carried out in DMF (dimethylformamide) with standard coupling agents such as ethyl 2-cyano-2-(hydroxyimino) acetate (oxyma) and N,N'-diisopropylcarbodiimide (DIC). Fmoc chemistry allows spacers of a variety of different lengths and hydrophilicities, such as Fmoc-polyethylene glycolic acid (Fmoc-PEG-OH), to be coupled to

the NPs in order to alter their physical properties (for instance the hydrophilicity), and to distance the cargo from the bead itself (Sanchez-Martin et al., 2005).

Additionally, in order to achieve a controlled synthesis of functionalized NPs, both the N- α -amino group and the side chain amino functionality of the lysine derivative should be blocked with orthogonal protecting groups. In this regard, for this thesis, Fmoc-Dde full

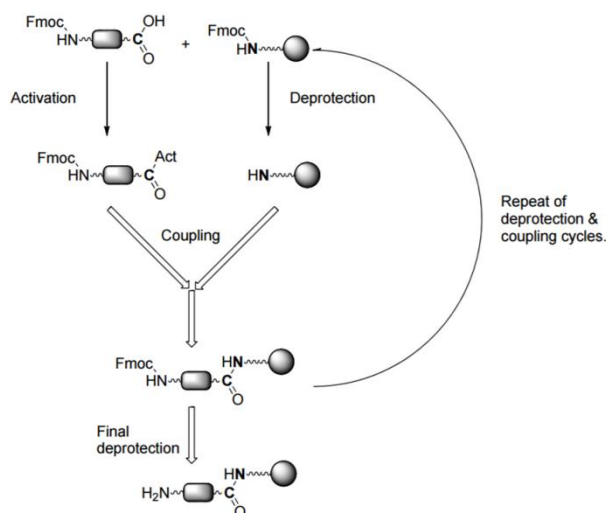


Figure 15. Basic steps in Fmoc chemistry approach.

orthogonality strategy has been implemented to obtain dual

functionalized NPs that allow carrying two cargos simultaneously (for instance, a biologically relevant cargo and a tracking fluorophore) (Fig.16). Sánchez-Martínez's bifunctionalization protocol is based on the use of a two orthogonal protective groups (PG1 and PG2). N-Fmoc group (PG1) for protection of the α -amino and a nucleophilically labile protecting group on the side chain (1-(4,4-dimethyl-2,6-dioxacyclohexylidene) ethyl, Dde, PG2) (Díaz-Mochón et al., 2004). Subsequently, selective cleavage of PG1 (Fmoc) or PG2 (Dde) allow the directed coupling of the cargo so that its position can be known, and facilitates the introduction of a scaffold that could be easily attached to the NPs and elongated using Fmoc protocols in a directed manner. In fact, thanks to their stability in organic solvents provided by the cross-linking structure, numerous chemical reactions can be carried out easily on these NPs.

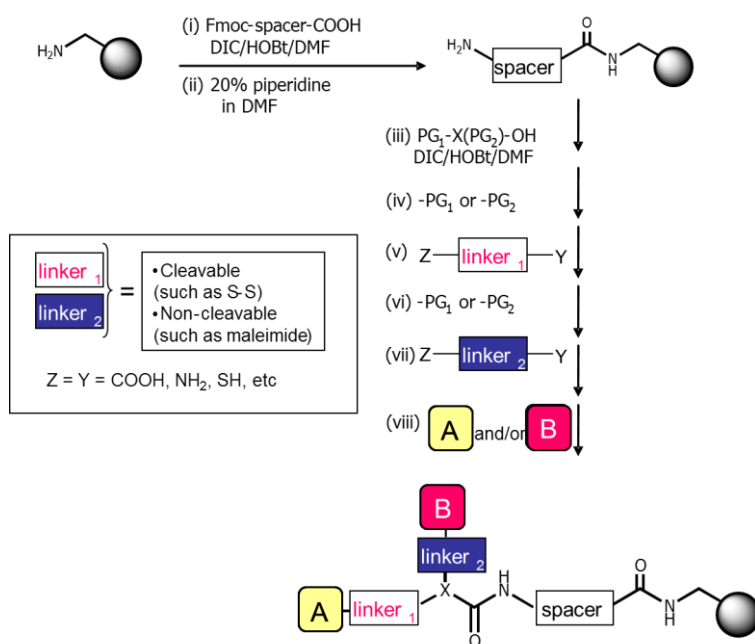


Figure 16. Conjugation protocol for multifunctionalisation of nanoparticles. A and B are bioactive molecules conjugated to nanoparticle (protein, nucleic acid, fluorophore, sensor, drug, etc), PG: protecting group.

3.3. Amino-functionalised nanoparticles as carrier systems

The Sánchez-Martín's group is pioneer in the synthesis and application of multi-functionalized, cross-linked, polystyrene nanoparticles. The synthesis is performed by dispersion-polymerization following a protocol described by Martín-Sánchez's group (Unciti-Broceta et al., 2012a). This method allows obtaining monodispersed populations of robust crosslinked size-defined nanoparticles (from 180 nm to 2 µm), which can be readily functionalized using solid-phase methodology previously described. This opens a great number of possibilities for the application of these NPs because it means that many different molecules could be bound to them. In addition, crosslinked NPs offer greater advantages over non-crosslinked NPs because they exhibit much improved mechanical stability in various organic solvents, allowing a wide spectrum of possible reactions that can be carried out on them (Sanchez-Martin et al., 2005).

Amino-functionalized nanoparticles have been used for covalent couplings of a broad range of cargos following different protocols optimized by the group. Importantly, NPs have been successfully labelled with several dyes to be able to follow their movement inside cells and to study their cellular uptake. Some of the applications that this group has been studying over the last years include:

- *Analysis of Microsphere-Based Intracellular Calcium Sensing:* By using amino-functionalized polystyrene NPs changes in the concentration of intracellular Ca^{2+} ions in single living cells in real time has been measured. The fact that NPs are firmly retained for several days also allows NPs acting as carriers of sensors for long term enzymatic activity assays (Sánchez-Martín et al., 2006).
- *pH Sensing in Living Cells Using Fluorescent Microspheres:* The employment of fluorescein-loaded NPs as intracellular pH sensors in living cells has been successfully proven, and covalent binding of fluorescein to NPs significantly improved the stability of the indicator over time and eliminated escape (Bradley et al., 2008a).
- *Cellular uptake of Fluorescent Labelled Biotin-Streptavidin Microspheres:* The use of streptavidin-loaded NPs as a carrier system able to enter living cells and biotinylated oligonucleotide uptake were successfully demonstrated. This strategy opens the door to a huge variety of applications, such as intracellular detection of a diverse number of targets (Bradley et al., 2008b).
- *Microsphere Mediated Protein Delivery into Cells:* The ability of protein-loaded NPs to go through cell membranes was demonstrated and protein activity while attached to the beads "expressed" within the cellular environment was maintained (Sanchez-Martin et al., 2009a).
- *Knocking Anti-Sense into Cells:* Green fluorescent protein expressed in HeLa cells has been successfully silenced using amino-functionalized siRNA linked to NPs via cleavable and non-cleavable linkers (Alexander et al., 2009).
- *Microsphere-based tracking and molecular delivery in embryonic stem cells:* Amino functionalized polystyrene microspheres were employed for efficient delivery of a variety of

cargos, including proteins, siRNAs and fluorescent dyes, into both undifferentiated and differentiated embryo derived stem cells (Tsakiridis et al., 2009).

- *Selective activation of biomolecules inside living cells by carrying on palladium (Pd)-catalyzed chemical reaction.* Pd-NPs were loaded into amino-polystyrene NPs and tested on HeLa cells as innovative catalysis/delivery system, showing a promising highly effective therapeutic system (Yusop et al., 2011).
- *DNA transfection:* delivery of plasmid DNA was successfully developed by conjugation of pDNA to microspheres. A noninvasive, nontoxic, and efficient gene delivery method with the potential to be applied to transfection-resistant, nondividing primary cells, including naïve T cells has been achieved. (Borger et al 2011)
- *Delivery of thiolated bioactive cargoes:* sulfhydryl reactive polymeric nanoparticles were successfully functionalised to successfully conjugate a thiolated fluorophore and siRNA which silence GFP expression. The high efficiency of siRNA–microsphere conjugates as gene silencing devices has been demonstrated by microscopy and flow cytometry. (Cardenas-Maestre et al, Journal of material chemistry)
- *Apoptosis nanosensors by conjugating fluorogenic specific substrates of caspases to NPS.* Polystyrene NPs were decorated with sensors of caspase-3/7 to monitor apoptosis by flow cytometry (Cárdenas-Maestre et al., 2014). Using this nanotechnology platform improved stability and sensitivity, avoiding the dilution of the signal over time was achieved.

In summary, polystyrene NPs have a number of advantages over other cell release systems, including the following: (a) A variety of biologically relevant structures such as small molecules (drugs, biosensors and fluorophores), peptides, proteins, RNAs and DNA can be attached to the nanoparticles by using efficient conjugation protocols without damage of the transported biological material. (b) Several molecules can be attached simultaneously to the nanoparticles following protocols developed in our group, allowing the use of this system to carry out the controlled and efficient release of the bioactive charge. (c) high concentrations of the captured molecule on the nanoparticle; (b) fluorescent NPs can be efficiently evaluated by standard techniques such as flow cytometry and microscopy; (c) loading of bioactive cargoes on the nanoparticle can be tuned, then desired loadings may be achieved depending on the specific application; (d) a variety of cell lines have been successfully nanofected without cytotoxic effects and (e) when desired, as in the case of diagnosis, the charge can be held together with the nanoparticles, whereby the signal is not diluted. (f) Selective activation of biomolecules can be accomplished by the intracellular release of palladium microcatalysts designed from this nanotechnology. Therefore, nanosystem presented here proved to be an efficient and controlled delivery system, able to efficiently target different cargoes in diverse cell lines, without altering the vitality. Given the many possibilities and applications of this methodology, this nanotechnology approach has been chosen for the development of this thesis.

SECTION III: DEVELOPMENT OF AN EFFICIENT NANOTECHNOLOGY FLUORESCENCE-BASED METHOD TO TRACK CELL PROLIFERATION

As has been seen in Section I, methods for cell proliferation measurement are fundamental to deeper study of metabolic impact on cellular growth. Based on the experience gained from previous work using polystyrene nanoparticle, we decided to develop a novel nanotechnology-based approach to track efficiently cellular proliferation by flow cytometry. This proof of concept could be implemented in future work accomplished in our group. In addition, this approach has recently been reported in a research article, constituting the main published work of this thesis.

1. Measurement of cell proliferation in biomedical research

Cell division, as the default status, is a *sine qua non* condition for life (Sonnenschein and Soto, 1999). Cell proliferation is the process by which the number of cells is increased, and is defined by the balance between cell divisions and cell loss through cell death or differentiation. Many biological responses are related to changes in cell proliferation. In normal cells, the cell growth and division processes are tightly controlled by complex mechanisms (Rhind and Russell, 2012). However, in cancer cells, these mechanisms are deregulated allowing cancer cells to acquire the ability to sustain a chronic proliferation (Evan and Vousden, 2001). This becomes the abnormal and uncontrolled cell proliferation in a hallmark of cancer cells (Hanahan and Weinberg, 2011b). For this reason, cell proliferation assays are crucial to control the division rate in cancer research (Yadav et al., 2001). By contrast, the lack of proliferative ability of immune cells may indicate an immunodeficiency disorder. A key feature of the adaptive immunity is the T-cell proliferative responses to antigen stimuli (Rezaei et al., 2017). Therefore, the measure of cell proliferation is essential in the assessment of the immune status.

Among the wide variety of methods for measuring dividing cells, there are commercially available cell-labelling fluorescent dyes for monitoring proliferation in living cells (Progatzky et al., 2013). These exogenous reporters are chemical entities which interact with cellular components providing fluorescence to the cells allowing the direct visualisation by fluorescent techniques. There are three conventional types of exogenous fluorescent reporters depend on labelled cellular component: i) *Membrane dyes*: lipid bilayer inserting dyes which stain the whole cell membrane (e.g., PKH lipophilic dyes); ii) *Cytoplasmic dyes*: cytoplasmic coupling dyes which stain cytoplasmic cellular proteins through covalent bounds (e.g., carboxyfluorescein diacetate succinimidyl ester, CFSE); and iii) *Nuclear dyes*: dyes with high affinity for double-

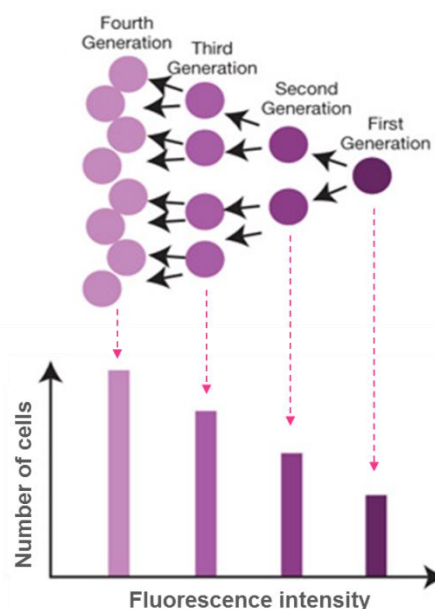


Figure 27. Mechanism of cell labeling. Top panel: illustration of proliferation analysis by dye dilution. Cell divisions result in larger numbers of cells, each with half the fluorescence intensity of its parent cell. Bottom graph: fluorescent signal from the initial population of cells is decreased during proliferation. Adapted from Thermo Fisher CellTrace-Cell Proliferation guide.

stranded DNA which provide a bright nuclear signal (e.g., Hoechst 33342) (Progzatzky et al., 2013; Tario et al., 2012). After each cell division, the fluorescent molecules conjugated to their target cellular components, pass and distribute to daughter cells, in a theoretically equal distribution, resulting in a progressive halving of the progeny fluorescence. This fluorescence intensity reduction can be quantified by conventional fluorescent techniques, the most used one being flow cytometry (Progzatzky et al., 2013; Tario et al., 2012).

These cell-labelling fluorescent dyes are the best alternative to gene transfer fluorescent protein-based endogenous reporters to monitor cell proliferation in long-term assay (Progzatzky et al., 2013). On the other hand, as alternative apart from fluorescent protein reporters, there are many different methods to test cellular proliferation, based on measurement of DNA levels or synthesis (e.g., BrDU), cellular metabolism (e.g., MTT), or proliferation-specific protein (e.g., Ki67). However, all of them provide information of end time point, preventing growth monitoring. Because of fluorescent dyes enable to monitor cell proliferation in long-term assay, they have become in a useful tool applied in biomedical research field. One of the most outstanding is CFSE, which enables calculate the absolute number of cells in each culture well that have undergone different numbers of cell divisions even in *in vivo* experiments (Quah et al., 2007), while others determine bulk population growth.

Although, these fluorescent reporter are widely recognized by the scientific community as a powerful method for the measurement of cell proliferation, they present some limitations such as alteration of the normal function of the cells to be tracked, irregular distribution in the progeny, rapid dilution during cell proliferation or high cytotoxic effect (Progzatzky et al., 2013), (Tario et al., 2012). Consequently, the search for new approaches to track successfully cell proliferation, avoiding these limitations, continues.

2. Fluorescent polystyrene nanoparticles as a platform for monitoring cell proliferation

As has been detailed in the previous section, over the last decade, our research group has developed several nanotechnologies for preparing functionalised polystyrene nanoparticles which are then conjugated to cargoes of different nature from small molecules (fluorophores, sensors, small drugs) to biomolecules (proteins and nucleic acids and their mimics). The main benefits of using polystyrene nanoparticles are cellular environment is not degraded and there is no apparent toxicity to cells even in long term studies (Loos et al., 2014b). Specifically surface-modified polystyrene nanoparticles are homogeneous, exhibit a low polydispersity index, and form stable colloids in biological fluids.

These nanodevices exhibit a number of appropriate characteristics by which become an excellent tool to develop novel biomedical approaches. Briefly, they have been extensively used as systems for *in vitro* applications (Borger et al., 2011; Loos et al., 2014b; Yusop et al., 2011). Furthermore, these NPs enable solid phase multistep chemistries to become compatible with different bio-orthogonal strategies (Cardenas-Maestre et al., 2011; Unciti-Broceta et al., 2012b). Their easy entry in a broad range of cell types including adherent, suspensions and primary cell lines has been extensively reported (Borger et al., 2011; Cardenas-Maestre et al., 2011; Tsakiridis et al., 2009; Unciti-Broceta et al., 2012b; Yusop et al., 2011). On the other

hand, gene-expression profiling studies showed that these NPs did not induce any significant alteration in nanofected cell transcriptomes (Alexander et al., 2010). Recent proteomic studies showed no key regulators of cell cycle were affected by the internalisation of these NPs, resulting in a parent-progeny transfer of the nanofection load. Furthermore, NPs are not exported from the cells because externalization- exocytosis rate is negligible, allowing long-term monitoring (Kim et al., 2011b), and their intracellular localization has been proved (Cárdenas-Maestre et al., 2014). These properties make NPs ideal to be used as cell proliferation devices.

THESIS RATIONALE

Metabolic adaptations in cancer are not emerged consequence of an accidental adaptation, but very precise regulated process fundamental for cell transformation and oncogenesis. In this context, many of the major metabolic pathways and targets remain still to be deciphered, particularly for specific cancer types such as respiration deficient models.

Accordingly, we propose the metabolic reprogramming characterization of comparative cell models based on cancer cell lines with extreme metabolic phenotypes undergoing a permanent metabolic challenge (switching off the mitochondrial oxidative metabolism by permanent mitochondrial DNA depletion, ρ^0 cells). We aim to enhance our knowledge of cancer metabolic reprogramming, thus contributing to a breaking review of cancer paradigm.

Furthermore, finding some of these key metabolic targets may improve the discovery and optimization of novel therapeutic strategies by using novel nanotechnology approaches. Our interest covers the development of targeted metabolic therapies in order to induce specific and selective impact in cancer cells. Finally, we aim to take advantage of nanotechnology knowledge in order to implement new technical approaches in cancer studies.

THESIS MAIN AIMS

Aim 1. UNDERSTANDING THE OVERALL METABOLIC STATUS IN THE COMPARATIVE TUMOR CELL MODEL OF RESPIRATION DEFICIENT CELLS WITH EXTREME METABOLIC PHENOTYPES

- 1.1. Identify the major pathways and metabolite-dependency, responsible for the metabolic reprogramming of respiration deficient cells compared to parental cell model.
- 1.2. Study the expression profile of oncogenes and the activity of key enzymes implicated in metabolic reprogramming process of our cell models.
- 1.3. Analyze the dynamic metabolic distribution in the identified key pathways in respiration deficient cells with regard to parental cell model.

Aim 2. IMPLEMENTATION OF NANOTECHNOLOGY APPROACHES BASED ON TUMOR METABOLISM.

- 2.1. Check possible differences on the efficiency of nanodevices in the respiration deficient comparative cancer cell model
- 2.2. Develop and evaluate a controlled drug delivery system for combined metabolic-based therapy.
- 2.3. Develop and validate multifunctionalized nanodevices for targeted drug delivery system to tumor cells with selective metabolic profiles.

Aim 3. DEVELOPMENT OF AN EFFICIENT NANOTECHNOLOGY FLUORESCENCE-BASED METHOD TO TRACK CELL PROLIFERATION.

- 3.1. Optimize a novel nanotechnology approach to track cellular proliferation by flow cytometry using fluorescence labelled nanoparticles.
- 3.2. Validate and implement the method in different cell types and cell proliferation assays.

AIM 1. UNDERSTANDING THE OVERALL METABOLIC STATUS IN THE COMPARATIVE TUMOR CELL MODEL OF RESPIRATION DEFICIENT CELLS WITH EXTREME METABOLIC PHENOTYPES

RESULTS

As part of the first aim, by using respiration deficient cells as extreme metabophenotype model, we try to find the most essential metabolic functions for proliferation provided by mitochondrial respiration in the context of cancer metabolic reprogramming. Despite of the importance of respiration in mammalian cell proliferation, ρ^0 cells display a high proliferation ratio under specific culture conditions, even in the absence of a functional mitochondrial electron transport chain. The ρ^0 206 cell line was reproduced by our research group through serial passage in low-dose ethidium bromide of human osteosarcoma 143B cell line, producing cells devoid of mtDNA (King and Attardi, 1989, 1996). Accordingly, ρ^0 206 cells were maintained in supra-physiological levels of uridine and pyruvate. Different approaches were employed in order to understand their metabolic adaptations.

1.1. IDENTIFICATION OF THE MAJOR PATHWAYS AND METABOLITE-DEPENDENCY RESPONSIBLE FOR THE METABOLIC REPROGRAMMING OF RESPIRATION DEFICIENT CELLS

Initially, we wanted to address what would be the most limiting metabolite dependency to sustain the proliferative capacity of the respiration deficient cells

1.1.1. Checking proliferative features in respiration deficient cells.

Initially, a comparative analysis of the basic features of ρ^0 cells was made, aiming to check whether in our hand, the respiration deficient cells behave as originally described by King and Attardi (**Fig. 18**). Firstly, absence of mitochondrial DNA (mtDNA) was checked by PCR amplification of DLP6, a segment of the mtDNA main control region for replication. No amplification product was observed in ρ^0 206 DNA, whereas 143B DNA displayed a clear amplification product of 365bp (**Fig. 18a**). This result confirmed the total depletion of mtDNA in ρ^0 206 cells. Then, proliferative capacity was studied by growth curve analysis for 143B and ρ^0 206 cell lines. Minimal differences in cellular proliferation were observed between both cell lines; being their doubling times 18.25 hours and 20.65 hours respectively (**Fig. 18b**).

In addition, proliferation data were completed by flow cytometry analysis of cell cycle following propidium iodine staining. Both cell lines displayed almost similar cell cycle profiles (**Fig. 18c**), and no significant differences were observed between the distribution percentages in each phase of the cycle (**Fig. 18d**). In general, these data confirm in our hands what was previously described: that not only respiration deficient cells are able to adapt and survive, despite of their irreversible mDNA depletion, but indeed maintaining high proliferative rates like the parental cell line.

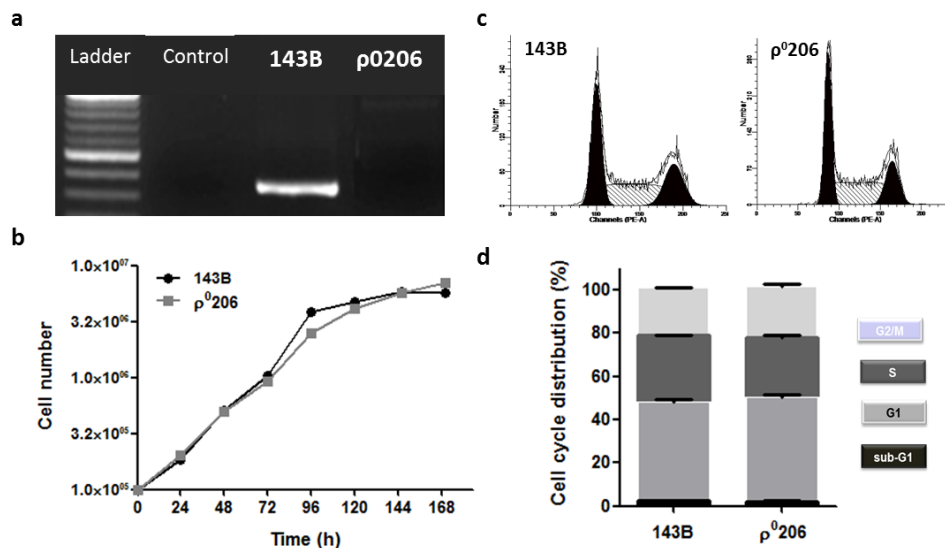


Figure 18. Checking mtDNA genotype and proliferative capacity of respiration deficient cells. (a) PCR products for mitochondrial DNA amplification of the control region fragment DLP6. **(b)** Cell growth curve plots of 143B (parental) and ρ^0 206 (respiration deficient) cells. Each point represents the mean of quadruplicates. **(c)** Cell cycle and ploidy analysis of both cell lines. Representative histograms are displayed, plotting cell count versus DNA content. In the histogram, the first peak represents cells in G0/G1 with 2N DNA content, and the second peak represents cells in G2/M with 4N DNA content. Cells traversing S phase are between the two peaks with DNA content ranging from 2N to 4N. **(d)** The data indicate the percentage of cells in each phase of cell cycle. For all experiments $n=3$, and bars indicate the mean + SEM.

1.1.2. *In vitro* tumorigenic potential is partially sustained in cells with suppressed respiration

Further to confirm previously described features of respiration deficient cells, we wanted to determine whether respiration is necessary to maintain the neoplastic growth potential *in vitro*. To this effect, *in vitro* tumorigenic potential was studied by anchorage-independent capacity growing tumorspheres in soft agar, and the subsequent enrichment in stemness factor. Firstly, in order to characterize the clonogenicity and spheroid formation capacity, 143B and ρ^0 206 cells were selectively expanded using a specific stem cell medium formulation (Fig. 19a). After 48-72h, a proportion of the cells were already observed, growing into spheres in stem cell medium. Then, the culture was observed over days to check the quality of the growing spheres: number, morphological and size features, and the invasive index. Both cell lines showed prominent sphere-forming ability, while proliferative capacity was higher in the parental cell line 143B, displaying spheres of higher size. Moreover, according to the already described features of tumor initiating cells growing in spheroids, the expression of stemness genes was found to be increased in both sphere-forming cell lines compared with the adherent growth cells control (Fig. 19b). Interestingly, expression of stemness markers was maintained in ρ^0 206 despite impaired respiration function, even significantly higher in the key biomarker of cancer stem cells CD133.

On the other hand, migration and invasiveness capacity was assessed by using the real time cell analyzer system xCELLigence device, a bioimpedance-dependent platform (described in materials and methodology section 7). ρ^0 206 showed a significant decrease in the migration capacity compared to parental cell model, thereby indicating that respiration somehow contributes to tumor cell invasion (Fig. 19c).

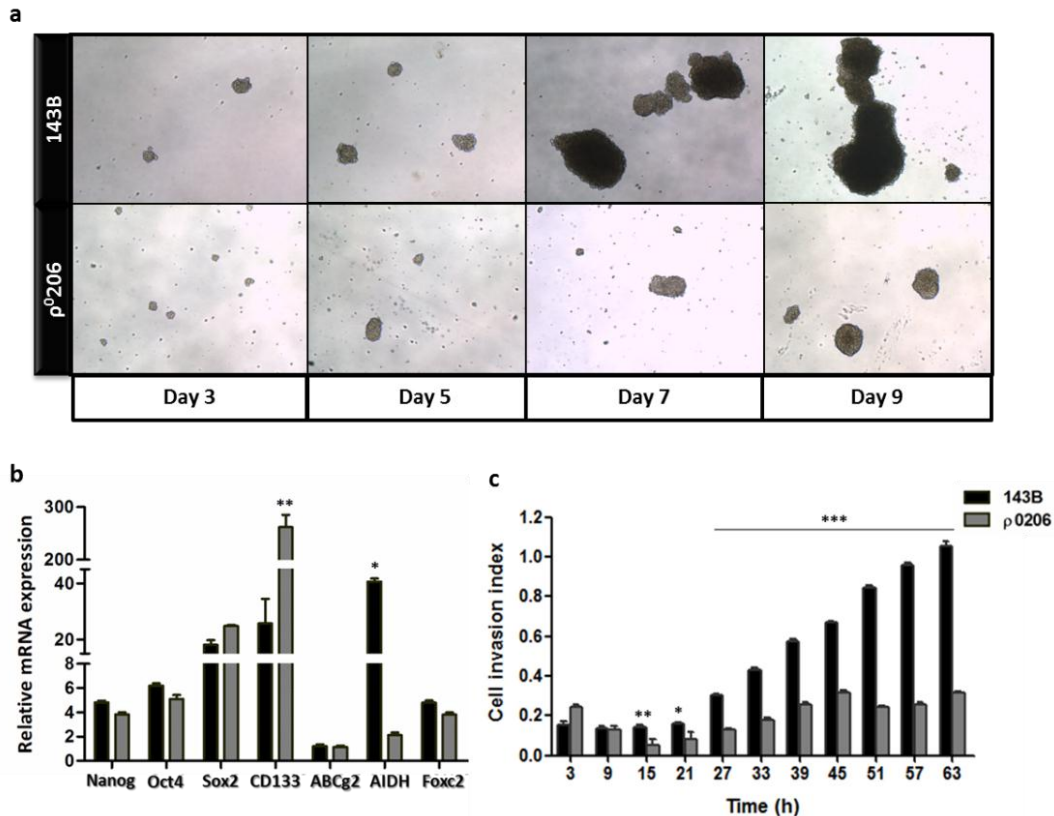


Figure 19. Reduced tumorigenic potential in absence of full mitochondrial respiration capacity. (a) Representative microscopy images of tumor initiating cell spheroids, 3, 5, 7 and 9 days after plating 143B and p⁰206 cells in non-adherent conditions. (b) Stemness-related biomarker expression of tumor spheres after 9 days of growth. Expression levels are relative to adherent control cultures. (c) 143B and p⁰206 invasive capacity was analyzed by the real time cell analyzer system (xCELLigence) with four biological replicates. Data are expressed as cell invasion index units by using xCELLigence software algorithm. For statistical analysis, Student's t-test was performed (*p value <0.05, **p value <0.01, ***p value <0.001).

These results indicate that impaired mitochondrial respiration does not affect tumor-initiating capacity, suggesting that tumor stem cells are characterized by predominantly glycolytic metabolism OXPHOS-independent. However, respiration seems to display a key role in migration and invasion process since p⁰206 migrated less efficiently than parental cell line.

1.1.3. Respiration deficient cells present pyruvate and glutamine dependence to sustain high proliferation ratio

Regarding early observations of cells lacking a functional mitochondrial ETC, that require pyruvate to sustain viability and proliferative capacity (King and Attardi, 1989), we wanted to confirm this data, and to test whether respiration deficient cells displayed stronger dependence to key nutrients. For this purpose, cellular viability and proliferation under selective culture conditions (deprivation of essential metabolites) were assessed in respiration deficient cells and the parental cell line (Fig.20a). Both cell lines displayed total glucose-dependency for growth, thus indicating that metabolism is primarily sustained by glycolytic pathway. However, when cells were cultured with lower glucose concentration (1mM) than control conditions (25mM), 143B cells were able to maintain proliferation, whereas p⁰206 viability eventually decreased. Conversely, a sharp decline of viability was observed in 143B cells cultured in absence of glutamine, suggesting that glutamine plays an important additional

role to glucose sustaining viability. Similar glutamine-dependence was shown in respiration deficient cells, where glutamine was not sufficient to rescue cell proliferation during glucose deprivation. Finally, unlike 143B cells, p⁰206 cells were also profoundly sensitive to pyruvate deprivation, confirming that pyruvate auxotrophy accompanies loss of mitochondrial respiration (**Fig.20a**).

Additional analysis of cellular viability under selective culture conditions was performed following 96h incubation by using Annexin V/7AAD double staining (**Fig.20b**). According to proliferation results, in 143B increased apoptosis and cell death was principally found when cells were cultivated in glutamine deprivation. In addition, apoptosis was observed in cell incubated in lower glucose levels, which could not be appreciated in the previous cell viability analysis. In p⁰206 cells, high apoptosis rates were observed for all the selective culture conditions, displaying a dramatic impact when pyruvate is absent (**Fig.20b**). These data confirmed that glucose, glutamine or pyruvate depletion induced apoptosis in respiration deficient cells, suggesting that these metabolites are critical for cellular viability and proliferation maintenance during impaired mitochondrial respiration.

To further analyze the role of these key metabolites in a respiration deficient context, we tried to determine the possible fates of pyruvate and glutamine in their reprogrammed metabolism. In one hand, we focused on glutamine, which can be converted into α -KG to replenish the TCA cycle through two mechanisms, either by glutamate dehydrogenase or transaminases. To check the importance of these pathways, we treated 143B and p⁰206 cells with either aminooxyacetate (AOA), a pan-inhibitor of transaminases (Wise et al., 2008), or epigallocatechin gallate (EGCG), an inhibitor of glutamate dehydrogenase (GDH) (Son et al., 2013). Surprisingly, in standard culture conditions, AOA treatment robustly inhibited the growth of 143B whereas displayed a minimal effect in p⁰206 viability (**Fig.20c**). EGCG impaired cellular growth in both cell lines, although the effect was significantly more dramatic in 143B viability. Likewise, we wanted to study two potential fates of pyruvate. Firstly, we used dichloroacetate (DCA), a small molecule which activates PDH by inhibition of PDK, resulting in increased oxidative decarboxylation of pyruvate to acetyl-CoA into the mitochondria (Michelakis et al., 2008). Again, both cell lines showed to be sensitive to DCA inhibition, but stronger effect was observed in 143B viability. This result suggested a greater reliance on the pyruvate incorporation in the TCA cycle of these cells. Lastly, pyruvate efflux via lactate was indirectly checked. Cells were treated with p-Chloromercuribenzenesulphonate (pCBMS), which specifically inhibits lactate transport via the basigin-associated monocarboxylate transporters MCT1 and MCT4 (Wilson et al., 2005). Interestingly, 143B were resistant to pCBMS, whereas p⁰206 viability was dramatically affected by pCBMS treatment, suggesting that respiration deficient cells are strongly dependent on pyruvate-lactate efflux (**Fig.20c**).

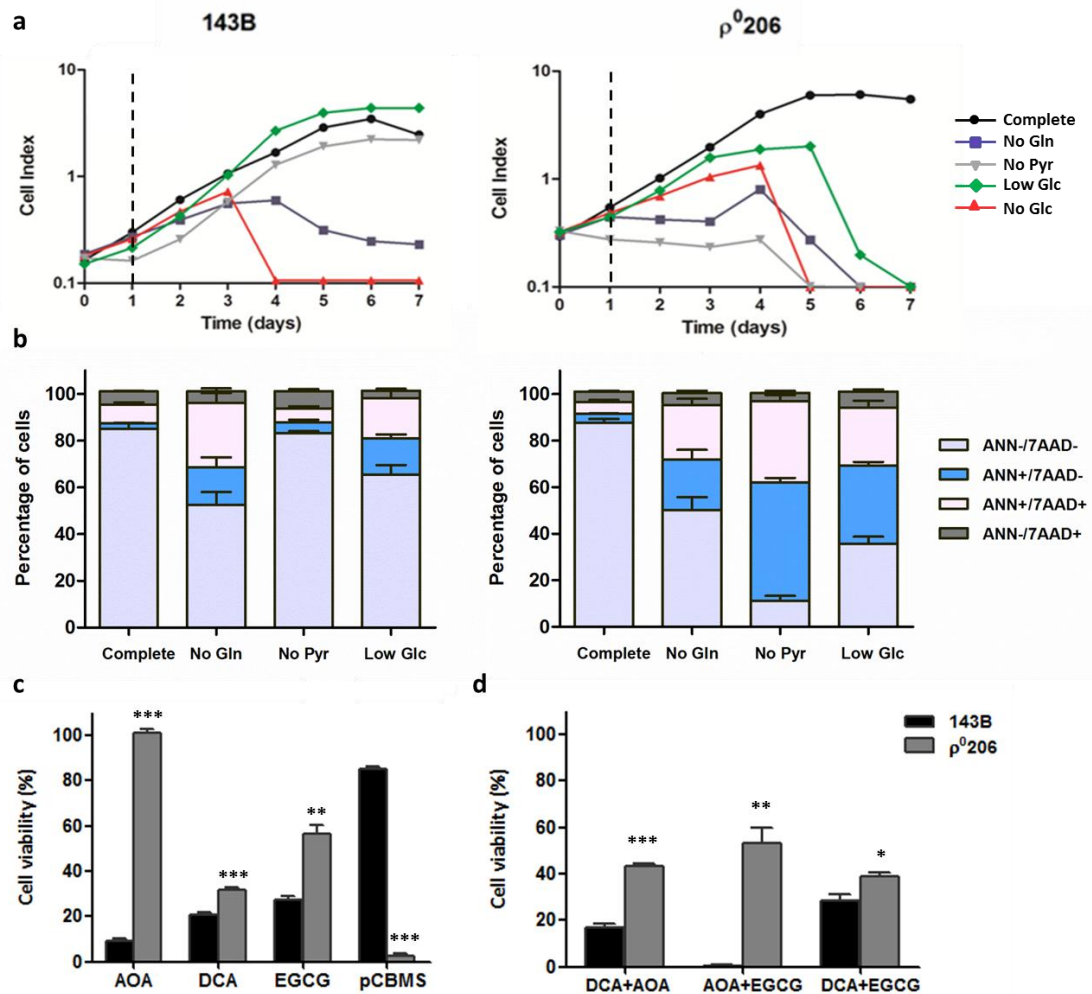


Figure 20. Glucose, glutamine and pyruvate dependence of 143B and ρ^{0206} cells for growth. (a) Relative proliferation of 143B and ρ^{0206} expressed as cell index arbitrary units using the xCELLigence real time analyzer. Cells were maintained in selective culture media under the conditions indicated. Dashed line represents time-point when complete culture media was replaced with selective conditions. (b) The viability of 143B and ρ^{0206} cells under different culture conditions was determined by Annexin V-FITC/7AAD staining, followed by flow cytometric analysis. Viable cells are negative for both Annexin V-FITC and 7AAD. Cells that are in early apoptosis are Annexin V-FITC positive and 7AAD negative. Cells that are in late apoptosis, or dead, are both Annexin V-FITC and 7AAD positive. 7AAD positive corresponds to dead cells. (c) Both, 143B ρ^{0206} were treated with different metabolic enzyme inhibitors during 96h, and cell viability was assayed. The percentages of cell viability under each graph are expressed as mean \pm SEM from three independent experiments. For statistical analysis, Student's t-test was performed, *p value <0.05, **p value <0.01, ***p value <0.001. Complete: normal growth media; No Glc: glucose depletion; No Gln: glutamine depletion; No Pyr: pyruvate depletion; Low Glc: 1mM glucose. AOA: aminooxyacetate; DCA: dichloroacetate; EGCG: Epigallocatechin gallate. pCBMS: p-Chloromercuribenzenesulphonate.

Finally, we also wanted to assess combination of inhibitors in order to elucidate possible alternative pathways that become decisive for cell survival during key enzyme impairment (Fig.20d). Respiration deficient cells became more susceptible to AOA when it was used in combination with DCA or EGCG, whereas no differences were observed in cell viability between single treatment and DCA and EGCG combination.

From these results, we can conclude that besides high glycolytic profile, respiration deficient cells are strongly dependent on glutamine and pyruvate. However, the pathways where these

metabolites are mostly being used remain unclear. Thus, a deeper study of pyruvate and glutamine fates is necessary to understand their key role in metabolic reprogramming during mitochondrial respiration impairment.

1.2.COMPARATIVE STUDY OF ONCOGENES AND TUMOR METABOLISM-RELATED GENE EXPRESSION PROFILES. ACTIVITY OF KEY ENZYMES IMPLICATED IN METABOLIC REPROGRAMMING

We next performed a comparative study between the parental and the respiration deficient cell lines, aiming to determine what key oncogenic signaling pathways are involved in the metabolic reprogramming of respiration deficient cells to support their growth and survival (**Fig. 21**). First, the expression of oncogenes involved in metabolic reprogramming by enhancement of glycolysis, or mitochondrial capacity, was assessed by immunoblotting and qPCR. No expression of HIF-1 α protein in normoxia was detected in 143B, since HIF-1 α is usually degraded through the ubiquitin/proteasome system, whereas its expression was maintained in hypoxic conditions. However, interestingly respiration deficient cells displayed high expression level of HIF-1 α protein even in normoxia, suggesting that the stable HIF-1 α expression is triggered in response to mitochondrial respiration defect (**Fig. 21a**). On the other hand, c-myc protein level was increased in p⁰206 in both normoxia and hypoxia conditions. Surprisingly, c-myc protein expression was dramatically reduced in 143B cells under hypoxia, whereas expression was maintained in p⁰206 cells without regard to oxygen conditions (**Fig. 21a**).

Furthermore, the status of the oncogene KRAS, which supports the decoupling of glycolysis and TCA metabolism, with glutamine supplying carbon to drive the TCA cycle, was examined using a Ras GTPase-specific pulldown assay. The abundance of active, GTP-bound, KRAS was slightly greater in respiration deficient cells (**Fig. 21b**) compared to parental model. Further, KRAS-GTPase amount corresponding to active KRAS is in line with total KRAS protein, according to the presence of previously reported KRAS oncogenic mutations in several osteosarcoma cell lines (Choy et al., 2012).

Last, we wanted to corroborate if there was any difference in PI3K/Akt/mTOR pathway caused by lack of full respiration capacity in tumor cells. Phosphorylation of mTOR at Ser2448 is carried out directly by AKT kinase as well as p70S6 kinase acting as a feedback signal. Phosphorylation at this site is a biomarker for the activation state of the PI-3 kinase pathway as well as the activation status of mTOR. Thus, mTOR pSer2448 relative levels in 143B and p⁰206 cell lysates were detected by ELISA. No significant differences in mTOR phosphorylation of respiration deficient cells in comparison with parental cell model were found (**Fig. 21c**), indicating impaired respiration does not affect to mTOR phosphorylation in this AKT-target site.

The study of key oncogenes expression profiles was followed by an extensive gene expression analysis of major enzymes implicated in the pyruvate and glutamine fate, aiming to highlight possible key targets in ρ^{0206} metabolic reprogramming. In line, we evaluated the relative gene expression to a non-transformed human cell line of several transaminases and dehydrogenases in our cell models (**Fig. 21d**). All transaminases were drastically overexpressed in both cell lines compared to control, except mitochondrial aspartate aminotransferase (GOT2). Alanine aminotransferase (ALAT) and phosphoserine aminotransferase 1 (PSAT1) expression was significantly higher in 143B, whereas cytosolic aspartate aminotransferase (GOT1) was significantly increased in ρ^{0206} . In the case of dehydrogenases, expression increased only in glutamate dehydrogenase (GDH), remaining stable in pyruvate dehydrogenase kinase (PDK) in both cell lines. Moreover, Hif-1 α was remarkably overexpressed in respiration deficient cells, correlating with the protein expression levels (**Fig. 21a**).

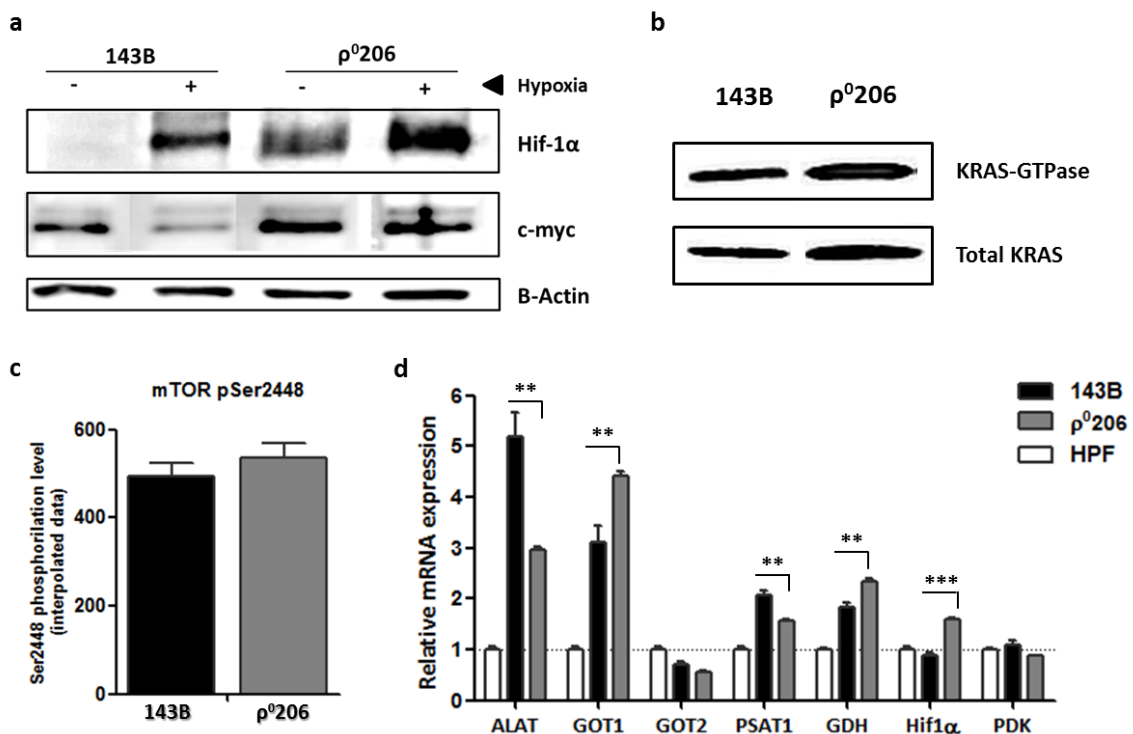


Figure 21. Comparative study of oncogenes and tumor metabolism-related gene expression profiles. (a) Immunoblotting of nuclear (HIF-1 α) and total lysates obtained from 143B and ρ^{0206} cells, using antibodies against HIF-1 α , c-myc and beta-actin (as a loading control). (b) KRAS GTPase-specific pulldown assay showing stably activated KRAS in both cell models. (c) Protein level of phosphorylated mTOR (pSer2448) quantified by enzyme-linked immunosorbent assay. Data values were obtained interpolated from a standard curve. (d) Relative mRNA expression by q-PCR analysis ($2^{-\Delta\Delta C_t}$ value) of tumor metabolism-related genes for 143B and ρ^{0206} cells. Data were calculated relative to non-transformed control (HPF, human pulmonary fibroblasts). Bars from graphs are expressed as mean \pm SEM from three independent experiments. For statistical analysis, Student's t-test was performed, *p value <0.05, **p value <0.01, ***p value <0.001.

Collectively, these data demonstrate that different pathways are predominant under mitochondrial respiration impairment. Both, Hif-1 α and c-myc could be orchestrating the overexpression of key metabolic enzymes related to pyruvate metabolism. Indeed, transaminases seem to have a key role in tumor metabolism and more specifically GOT1 appears closely associated to respiration deficiency adaptation.

1.3. IDENTIFICATION OF THE DYNAMIC METABOLIC DISTRIBUTION IN THE IDENTIFIED KEY PATHWAYS BY ISOTOPOMERIC ANALYSIS OF METABOLIC FLUX PROFILING

Our very first findings, highlighting differences in the metabolic network of respiration deficient cells comparing with fully mitochondria active cells, were found in the requirement of pyruvate and glutamine. Further investigation to decipher where is primarily being used these key metabolites might shed important information about the metabolic reprogramming of respiration deficient cells. In line, it is important to reveal what are the most essential metabolic functions for proliferation provided by mitochondrial respiration. Such pathways could be deeper studied by metabolic flux analysis using dynamic labeling and metabolic modelling. To this extent, we performed targeted and untargeted metabolomics in order to decipher the global metabolic profiling of respiration deficient cancer cells.

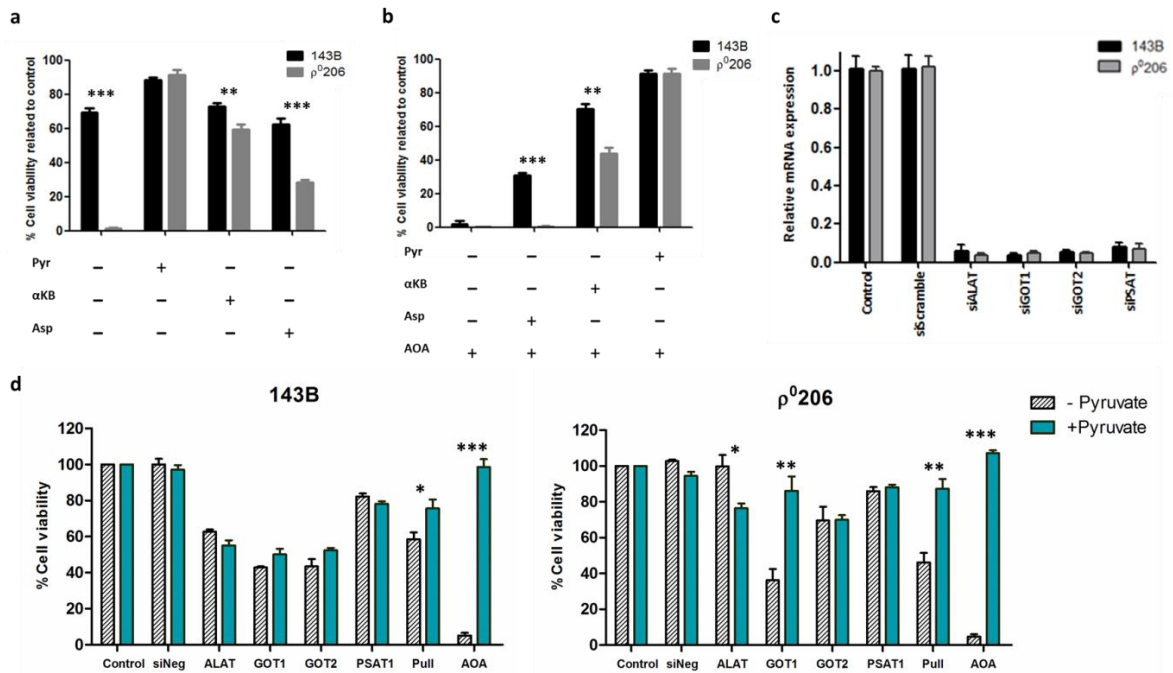
1.3.1. Pyruvate is sufficient, and more efficient than aspartate, to maintain viability in respiration deficient cancer cells

While conducting the work for this thesis goal, a primary role for mitochondrial respiration supporting cell proliferation was reported. Respiration mainly functions like a key provider of NAD⁺ as an electron acceptor, which is required for supporting aspartate synthesis (Sullivan et al., 2015). This unprecedented observation likewise gave to tumor niche available pyruvate the main role as NAD⁺ supplier in respiration deficient cells.

Hence, we wanted to test pyruvate and aspartate capacity to maintain viability of respiration deficient cancer cells. Once again, ρ^{0206} cells displayed absolute dependency for pyruvate as (Fig. 22a). Conversely, no significant differences were observed in 143B cells cultured with or without pyruvate, confirming that pyruvate auxotrophy is associated with loss of mitochondrial respiration. Then, to check whether at least in part the pyruvate importance is due to its ability as an electron acceptor, the use of the alternative electron acceptor alpha-ketobutyrate (α KB) was sufficient to restore ρ^{0206} proliferation, although remained under 143B levels yet. Even more surprisingly, we found that aspartate supply under no availability of exogenous pyruvate displayed only an unexpected moderate rescue, whereas pyruvate behaved much more efficiently, reaching a total rescue of cell viability (Fig. 22a).

Further demonstration that pyruvate is sufficient for cell viability was the inhibition of the aspartate transamination to OAA by aminooxyacetate, which is the main catalytic reaction for aspartate synthesis and metabolism. Even under AOA inhibition, only pyruvate, but not addition of supra-physiological concentration of aspartate (20mM), nor the alternative electron acceptor α KB, could efficiently maintain ρ^{0206} cell viability (Fig. 22b).

Since AOA is a pan-inhibitor of pyridoxal phosphate-dependent enzymes, including transaminases (Son et al., 2013), further studies were performed to gain knowledge about what would be the key transaminase target(s) in ρ^{0206} . To identify the specific transaminase(s), the expression of pyruvate-related transaminases (aspartate and alanine phosphoserine transaminase) were individually and collectively (pull) silenced by using RNA interference (RNAi). Once knockdown of each transaminase was confirmed (Fig. 22c), their potential impact on cell growth was examined under enzyme impaired activity. Consistent with AOA results, transaminases knockdown also had no effect on respiration deficient cell growth



when exogenous pyruvate was supplied. Among this set of RNAi-silenced transaminases, the viability of ρ^0206 cells was significantly impaired by knockdown of the aspartate transaminase GOT1, but not GOT2, in the absence of exogenous pyruvate. Importantly, this knockdown could be rescued by pyruvate (Fig. 22d). On the other hand, the parental 143B cells displayed an exogenous pyruvate-independent profile, and no particular dependency was observed, as in the case of respiration deficient cells for GOT1. Rather, the parental cells showed a slight dependency on overall transamination. In particular, GOT1 and GOT2 are both required, which certainly concur, since respiration is unimpaired, and thus, aspartate-malate shuttle would be fully active and not truncated (Fig. 22d).

Figure 22. Pyruvate is sufficient, and more efficient than aspartate, to maintain cell viability in respiration deficient cells. (a) Cell viability measurements for 143B and ρ^0206 cells were determined in the presence or absence of pyruvate (Pyr), α KB, and aspartate (Asp). (b) Experiments of cell viability rescue under AOA treatment were determined for 143B and ρ^0206 cells in the presence or absence of pyruvate, α KB and aspartate (c) 143B and ρ^0206 cells were transfected with ALAT, GOT1, GOT2, PSAT1 and control siRNA, and examined for mRNA expression of these enzymes by qPCR. (d) Cellular viability referred to as % of control no pyruvate (lined) or pyruvate supplied (smooth) under transaminases knockdown. siNeg is referred to scramble siRNA sequence as experimental control. Values in all figure panels denote mean \pm SEM of three independent experiments with four biological replicates. T-student are represented (* $p < 0.05$, ** $p < 0.01$, *** $p < 0.001$).

Importantly, our own studies suggest that GOT1 partially counter acts the detrimental effect of pyruvate withdrawal in respiration deficient cells. Hence, there might be a metabolic pathway mediated by GOT1 that might be essential for these cells. At this point, many mechanisms could be attributed to the pyruvate rescue during respiration impairment, but we also aimed to continue further research into the role as exogenous electron acceptors to maintain NAD⁺ levels and to answer whether alternative pyruvate fates may be contributing to the ρ^0206 survival.

1.3.2. Exploring a new role of exogenous pyruvate in respiration deficient cells beyond electron acceptor

As already has been introduced, pyruvate has a major role as electron acceptor, maintaining NAD⁺ availability to sustain aspartate biosynthesis during mitochondrial respiration impairment. However, we observed that supplemented exogenous aspartate, or alternative electron acceptors, was not able to maintain ρ^0206 proliferation at the same level as control cells during pyruvate withdrawal. At this point, our main goal was to continue deciphering the pyruvate contribution into major pathways to sustain respiration deficient cell proliferation.

Comprehensive metabolic profiling of 143B and ρ^0206 cell extracts was performed using LC-MS to study the profiles of major compounds that are involved in pyruvate metabolism according to differences in isotopomeric labeling. Both cell lines were cultured in medium containing ¹³C₆-glucose and ¹³C₃-pyruvate separately, and the ¹³C-enrichment of intracellular metabolites was measured, aiming to investigate whether exogenous pyruvate was being driven to different pathways than pyruvate generated from glucose (**Fig. 23a**). Interestingly, several metabolites were found to be differently contributed by pyruvate labeling (**Fig. 23a,c**). We observed that glucose-derived pyruvate was metabolized via oxidative decarboxylation by PDH to form citrate m+2 (citrate containing two additional mass units from ¹³C) in both cell lines, resulting in a large amount of acetyl-CoA and citrate m+2. However, in ρ^0206 during exogenous pyruvate labeling, most citrate contained no labeled carbon (m+0), indicating reduced PDH contribution to acetyl-CoA from exogenous pyruvate metabolism (**Fig. 23c**). Furthermore, fatty acid production coming from pyruvate-derived citrate was observed in 143B, whereas respiration deficient cells displayed a lack of palmitate synthesis through exogenous pyruvate contribution, which is a likely consequence of reduced citrate synthesis (**Fig. 23b**).

Fumarate, malate and aspartate m+3 were increased in both 143B and ρ^0206 cells, revealing that exogenous pyruvate is catabolized by PC to generate the TCA intermediate and aspartate precursor oxaloacetate (OAA). On the other hand, exogenous pyruvate was not directly involved in serine-related transamination reaction. Likewise, alanine production from ¹³C₃-pyruvate was not significantly increased in respiration deficient cells. However, surprisingly, exogenous pyruvate-derived lactate m+3 was notably reduced compared to glucose-derived lactate, suggesting that NAD⁺ regeneration by exogenous pyruvate is mainly coming from an alternative pathway to LDH (**Fig. 23c**).

In general, our findings with pyruvate and glucose labeling correlated with a prominent pyruvate carboxylation metabolism for exogenous pyruvate in both cell lines, although prominently in respiration deficient cells. In line, the reduced contribution to citrate synthesis is corroborated by impaired palmitate synthesis. However, these labeling experiments did not reveal a clear distinct fate for exogenous pyruvate in ρ^0206 phenotype; thus denoting the major importance of pyruvate for maintaining NAD⁺ balance via transamination during mitochondrial respiration impairment.

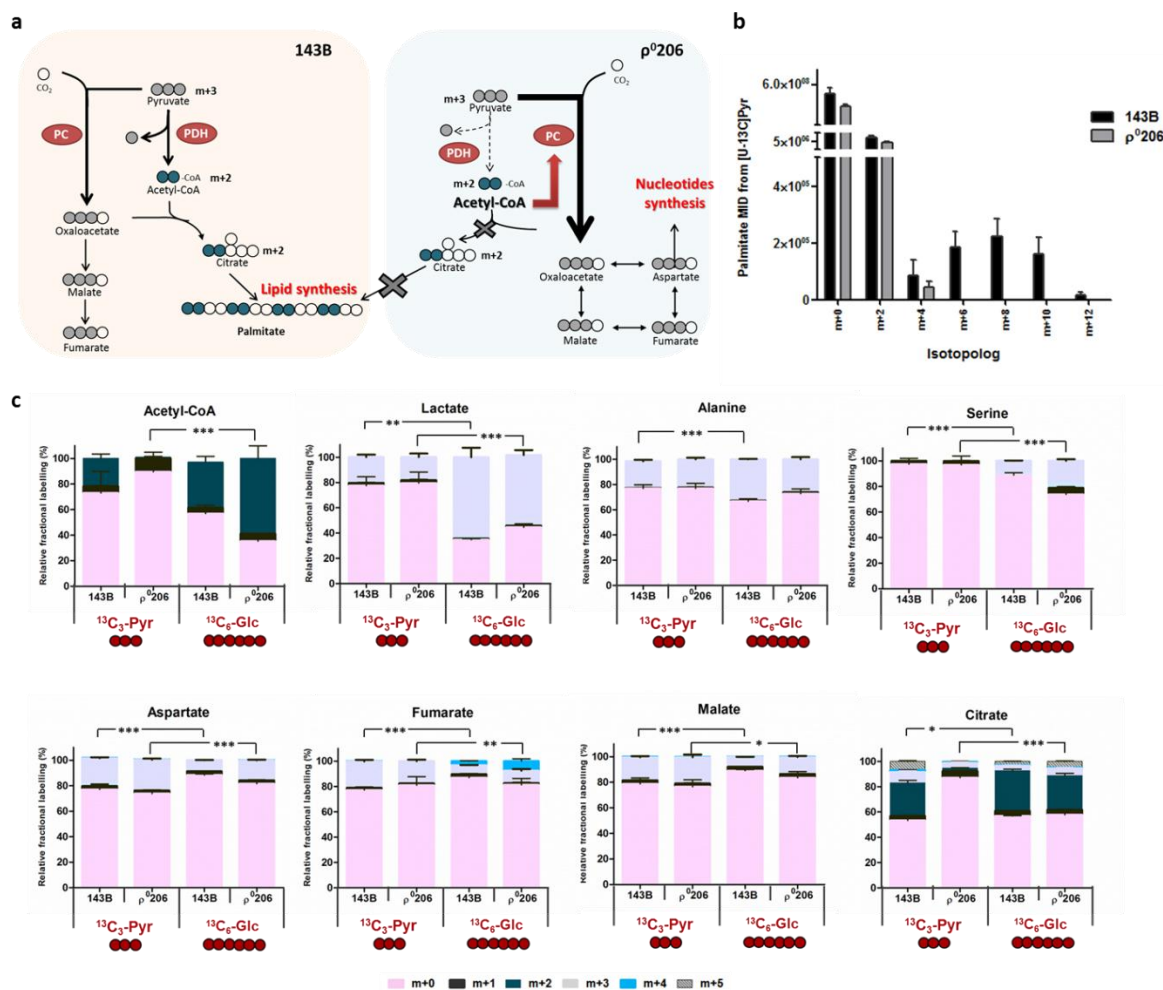


Figure 23. Comparative pyruvate metabolic profiling by LC-MS ¹³C₃-pyruvate or ¹³C₆-glucose isotopomeric labeling. (a) Schematic representation of metabolic fates and pathways for labeled pyruvate in 143B and p⁰206. **(b)** Mass isotopomer analysis of palmitate in cells cultured with ¹³C₃-pyruvate and unlabeled glucose. **(c)** ¹³C₃-pyruvate and ¹³C₆-glucose incorporation into different metabolites were measured by targeted LC-M. Data are presented as relative metabolite abundance by mean ± SEM for >4 independent cultures. Student's t-test of m+3 metabolites, and m+2 for Acetyl-CoA and Citrate is represented (*p < 0.05, **p < 0.01, ***p < 0.001). CoA, coenzyme A; PDH, pyruvate dehydrogenase; PC, pyruvate carboxylase. The color assignation for the different molecular mass species is displayed at the bottom of the figure.

1.3.3. Respiration and a pyruvate rich environment are required for supporting NAD⁺ availability to maintain high glycolytic flux and aspartate biosynthetic use

Our first observation of GOT1-dependence, in the respiration deficient metabophenotype of p⁰206 cells, made that the study of the pyruvate role by this aspartate transamination became a priority for us. Furthermore, the recently reported role of pyruvate as electron acceptor, also stand out its importance in relationship to aspartate biosynthesis. But, two key questions remain unresolved yet: why pyruvate is more efficient than other electron acceptors (for instance αKB) sustaining respiration-deficient viability and, why addition of even supraphysiological concentrations of aspartate did not rescue efficiently p⁰206 cells.

Accordingly, we thought to determine whether the levels of glycolytic intermediates are compromised due to NAD⁺ imbalance during lack of exogenous pyruvate, or to transamination inhibition. As expected, NAD⁺ levels were decreased in respiration deficient cells without the addition of exogenous pyruvate (NAD⁺ panel, **Fig. 24**). Surprisingly, when pyruvate is absent in the niche (culture media), then 3-phosphoglycerate, and phosphoenolpyruvate, were significantly decreased in ρ^0 206 cells comparing to 143B. Importantly, those are glycolytic intermediates downstream the GAPDH step, which is just the enzyme that require a continuous supply of NAD⁺ in the glycolytic pathway to be catalytically active. Importantly, supporting the fact that GAPDH acts as a short circuit for the glycolytic flux, upstream intermediate fructose-6-phosphate was increased (**Fig. 24**). Thus, by the dependency of GAPDH on NAD⁺ as an electron acceptor, the reduced NAD⁺ availability due to lack of pyruvate availability in the niche, may result in glycolytic flux deregulation when mitochondrial respiration cannot sustain the maintenance of the cofactor.

These observations suggest that cancer cell paradoxically require not only active respiration, but also a pyruvate rich environment, in order to maintain the glycolytic flux, which is required for supplying intermediary metabolites for biosynthetic purposes. In fact, the reduction in the glycolytic flux provokes a lack of ATP in respiration deficient cells when no exogenous pyruvate was available. However, parental 143B cells has no problem at all to maintain ATP levels, thanks to the OXPHOX supply, even under no exogenous pyruvate supply (ATP panel, **Fig. 24**).

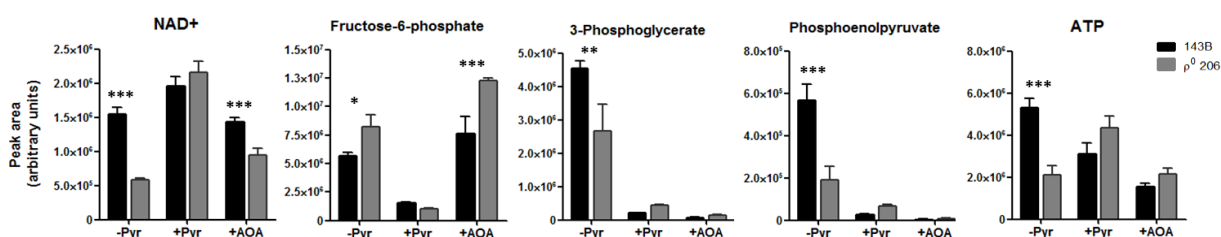


Figure 24. Respiration and a pyruvate rich environment are required for supporting NAD⁺ availability to maintain high glycolytic flux. Quantification by LC/MS of intracellular metabolite levels in 143B and ρ^0 206 cells, n = 6. Aspartate was supplemented in supra-physiological concentration (20mM) in all scenarios. Conditions tested are: without exogenous pyruvate supply (-Pyr), supplemented pyruvate (+Pyr), and AOA inhibition under exogenous pyruvate withdrawal. For statistical analysis, Student's t-test was performed, *p value <0.05, **p value <0.01, ***p value <0.001.

Now, beyond the recently reported role for pyruvate as an electron acceptor, providing NAD⁺ which is required to support aspartate biosynthesis (Birsoy et al., 2015; Sullivan et al., 2015); we have just identified the importance of a pyruvate rich niche in respiration deficient cells, maintaining redox balance, and sustaining glycolytic flux for biosynthetic intermediates supply, and ATP production. Accordingly, we next wanted to address how the aspartate metabolic fate can be adapted in respiration deficient cells to sustain their viability in the absence of pyruvate. In addition, we aimed to understand why aspartate supply cannot fully rescue ρ^0 206 cells when pyruvate is absent. To that end, to determine the aspartate metabolic fate, ¹³C-Aspartate isotopomeric labeling for LC/M dynamic metabolic flux experiments were conducted in absence or presence or exogenous pyruvate. Untargeted metabolomic workflow revealed that aspartate contribution to malate and citrate generation was significantly different in absence of exogenous pyruvate for ρ^0 206 as compared to 143B cells (**Fig. 25**). Most malate is synthesized from aspartate when pyruvate was absent (**Fig. 25a**), whereas in this condition

aspartate is no longer contributing to citrate formation (**Fig. 25b**). Therefore, this data importantly support a reductive metabolism of aspartate. Fumarate, another malate-downstream metabolite, was also checked, finding no differences (with or without pyruvate addition) on its amount derived from aspartate contribution for ρ^{0206} . However, interestingly, aspartate input to fumarate was much more representative than in the respiration-competent parental cells (**Fig. 25c**).

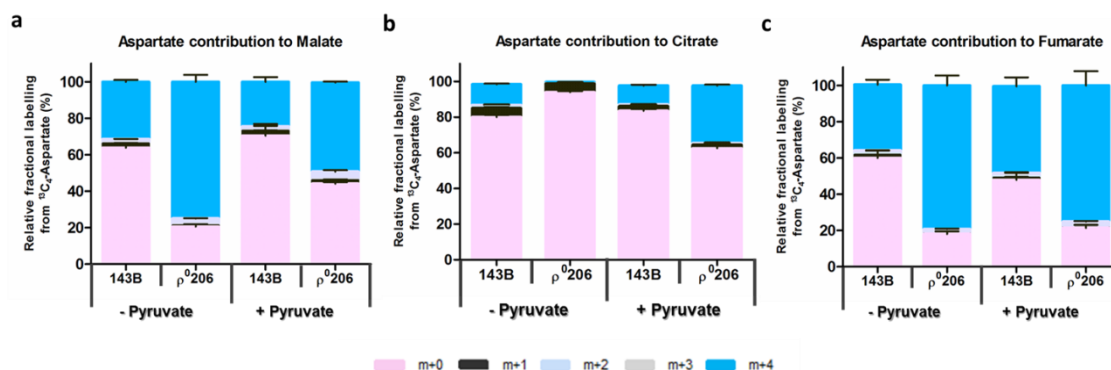


Figure 25. Aspartate is deviated from its canonical biosynthetic use to be reductively consumed upon pyruvate withdrawal. Aspartate m+4 contribution to (a) malate, (b) citrate and (c) fumarate in presence or absence of exogenous pyruvate from 143B and ρ^{0206} cells cultured with $^{13}\text{C}_4$ -Aspartate for 12h. Values denote mean \pm SEM of relative metabolite abundance, n = 4. The color assignment for the different molecular mass species is displayed at the bottom of the figure.

From these results, we can argue that reprogramming of the aspartate metabolism indicates that pyruvate play a primary role in the aspartate metabolic fate. Thus, for respiration deficient cells, in the absence of pyruvate, even though aspartate is supplied in supra-physiological concentrations, now our results have demonstrated that is redirected to be consumed by reductive reactions to supply the absence of pyruvate. Importantly, it is pyruvate the one that more efficiently maintains cell viability of respiration deficient cells probably pointing to its direct molecular capacity to be reduced. Therefore, taken together, these data suggest that the electron acceptors avoid aspartate consumption out of its main biosynthetic role in respiration deficient cells.

1.3.4. Aspartate is consumed replacing pyruvate to supply NAD+ which implies a truncated reductive TCA branch

To further confirm our discovery on the key role of aspartate consumption in ρ^{0206} when pyruvate is absent in the niche, here we aimed to discern where would be the metabolic fate of the consumed aspartate by addressing targeted metabolomic analysis. As it is displayed in **Figure 26a**, $^{13}\text{C}_4$ -Aspartate was mainly directed to provide malate and fumarate in both cell lines. Of note, respiration deficient cells displayed a significant increase in $^{13}\text{C}_4$ -labeled m+4 succinate, coming from fumarate m+4, which is observed by a series of reductive reactions from aspartate to malate, then fumarate and succinate. Moreover, ρ^{0206} cells showed a dramatic reduction in flux of $^{13}\text{C}_4$ -Aspartate into the canonical oxidative TCA pathway, as it is displayed by the absence of citrate and αKG . Only the parental 143B cells, with functional

respiration, displayed canonical oxidative TCA reactions as denoted by citrate and α -KG produced from aspartate. Surprisingly, only ρ^0 206 cells showed labeled succinate m+4, and, moreover, these cells accumulated much more succinate than the parental counterpart in all tested conditions (**Fig. 26b**). Therefore, these data support that this alternative pathway of aspartate consumption in respiration deficient cells is mainly due to a mitochondrial truncated reductive branch of the TCA.

The observation of this unusual predominant pathway was further reinforced by two observations. On the one side, by the significant decrease found in the aspartate-derived $^{13}\text{C}_4$ -labeled succinate m+4 (blue bars represented in Fig 9c) under AOA treatment for ρ^0 206 cells, which nearly disappeared due to inhibition of the aspartate consumption through GOT1 (AOA treatment) (**Fig. 26c**). On the other side, $^{13}\text{C}_4$ -labeled 5-aminolevulinic acid (5-ALA) was only found in respiration deficient cells, predominantly observed in the absence of exogenous pyruvate (**Fig. 26d**). ALA is produced by the enzymatic mitochondrial conversion of $^{13}\text{C}_4$ -labeled succinate as part of the haeme synthesis pathway (**Fig. 26d**). Moreover, this flux from aspartate was once again undetectable during AOA treatment (data not shown).

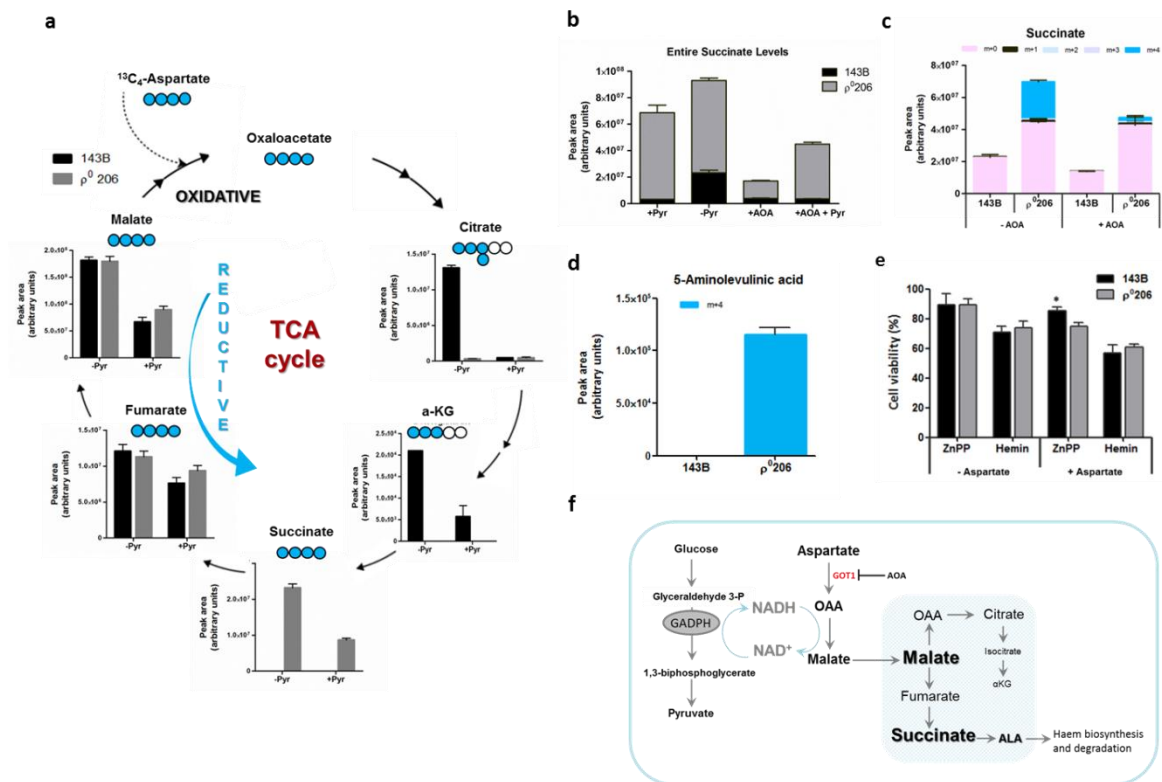


Figure 26. $^{13}\text{C}_4$ -Aspartate dynamic metabolic flux analysis revealed its metabolism through malate to succinate by a truncated reductive TCA branch in respiration deficient cells. **(a)** $^{13}\text{C}_4$ -Aspartate-incorporation into TCA intermediates was analyzed by targeted LC-MS in the presence or absence of exogenous pyruvate. Schematic representation of the four ^{13}C -labeled carbons contribution from aspartate to TCA intermediates (m+4, blue circles). **(b)** Total succinate production was predominantly observed for all tested condition in respiratory deficient cells. **(c)** Under AOA treatment, without any pyruvate exogenous supply, ρ^0 206 cells displayed a lack of succinate derived from aspartate (m+4, blue bar). **(d)** The graph displayed the strong production of m+4 aminolevulinic acid (ALA) from aspartate in ρ^0 206 cells during

exogenous pyruvate withdrawal. Values denote ion counts mean \pm SEM, n = 4. **(e)** Inhibition of Heme pathway in absence of exogenous pyruvate. **(f)** Schematic summary graph depicting the alternative truncated reductive TCA branch. Normally, the TCA cycle runs in the forward direction to oxidize intermediates generating precursors for protein and nucleotide biosynthesis such as aspartate. However, respiration deficient cells reverse this pathway by consuming aspartate in a reductive metabolism in order to sustain NAD⁺ production. In addition, succinate is significantly accumulated, and further transformed to ALA.

This finding of the accumulation of succinate prompted us to predict a possible synthetic lethality between mitochondrial respiration and haem pathway. To test this possibility, we aimed to answer whether inhibition of the haeme pathway, thus resulting in an hypothetical toxic accumulation of succinate, could impact on the viability of ρ^0 206 cells. In line, the cells were treated with zinc protoporphyrin (ZnPP), an inhibitor of the haeme oxygenase 1, the rate-limiting enzyme in the haeme synthesis pathway (Labbé et al., 1999). By this approach, no differences were observed between 143B and ρ^0 206 cells (**Fig. 26e**). However, slight toxicity arose in respiration deficient cells compared to parental cells when aspartate was supplemented. This fact may be related to ρ^0 206 need for further aspartate consumption through haem pathway when this is abundant. On the other hand, to further examined the possibility of a synthetic lethality, the enzyme d-Aminolevulinic acid (ALA) synthase, which is the entry point and rate-limiting step of haeme biosynthesis, was also inhibited by using hemin, an approved drug used for acute porphyria (Frezza et al., 2011) (**Fig. 26e**). Likewise to the ZnPP experiments, inhibition of ALAS had similar effect on both cell models, suggesting that the haeme pathway is not synthetically lethal under conditions of defective ETC.

In general, these findings demonstrate that, in respiration deficient cells, malate is produced by reductive conversion of aspartate, generating cytosolic NAD⁺ in absence of exogenous pyruvate. Malate excess is transported to mitochondrion to be subsequently metabolized up to succinate. This alternative pathway can be blocked when transamination by GOT1 is inhibited, causing cell death, therefore suggesting that aspartate transamination must allow NAD⁺ regeneration to sustain viability, as an alternative vital pathway if pyruvate is not present (**Fig. 26f**). In summary, these data support the fact that, a lack of available electron acceptors, not only restricts aspartate biosynthesis, but also primarily promotes its consumption to maintain NAD⁺ production as a vital pathway for respiration deficient cells.

1.3.5. Respiration deficient cells are totally dependent on glutamine anabolism to sustain alternative reductive truncated-TCA

Next, we wanted to perform further metabolomic experiments to verify the significant occurrence of this truncated reductive branch of the TCA, primarily observed in respiration deficient cells. ¹³C₅-glutamine was used to trace glutamine flux into the TCA cycle or alternatively by its reductive anabolic contribution (**Fig. 27a**). Consistent with the aspartate labeling, we observed that 143B cells showed oxidative metabolism of glutamine as anaplerotic substrate to replenish TCA intermediate metabolites. The ¹³C₄ glutamine-incorporation into the canonical oxidative TCA is traced by the presence of succinate, malate, fumarate and aspartate m+4, that is, with four ¹³C-labeled carbons donated by glutamine (**Fig. 27b**). However, oxidative TCA pathway was totally truncated in ρ^0 206 cells, since ¹³C₄ glutamine

flux through was arrested in succinate m+4, thus respiration deficient cells did not display any fumarate or malate m+4 (**Fig. 27b**). Interestingly, these cells showed a fraction of malate, fumarate and aspartate m+3. These species are produced due to their synthesis from a reductive, rather than oxidative, glutamine metabolism (**Fig. 27b**). Glutamine-dependent reductive carboxylation was also observed in 143B cells although appeared less prevalent than oxidative pathways.

Now, in the parental 143B cells, the canonical oxidative anaplerotic contribution of glutamine clearly gives rise to citrate m+4 (**Fig. 27b**). In contrast, citrate m+5 might be expected ρ^{0206} cells, which can be generated through reductive carboxylation of glutamine-derived α -ketoglutarate, and the addition of an unlabeled carbon by isocitrate dehydrogenase (IDH) (**Fig. 27a**). But, surprisingly only trace quantities of citrate m+5 were detected in respiration deficient cells. However, acetyl-CoA m+2 was clearly observed in ρ^{0206} cells. This metabolite is produced by cleavage of citrate m+5 by ATP-citrate lyase. Therefore, the presence of acetyl-CoA m+2 is strikingly suggesting that glutamine-derived citrate (m+5) is rapidly consumed during mitochondrial respiration impairment (**Fig. 27b**).

We next determined whether reductive glutamine metabolism was also contributing to *de novo* lipid synthesis as one possible fate of the glutamine-derived citrate. Because fatty acids are synthesized by the sequential addition of two-carbon units, pair $^{13}\text{C}_5$ -glutamine incorporation in palmitate was investigated. There was a rightward shift of the ρ^{0206} isotopolog-labeling pattern in comparison with 143B, indicating that a higher percentage of palmitate carbon was sourced from glutamine in ρ^{0206} cells than parental cell line (**Fig. 27c**). This shift is highly indicative of an increased availability of glutamine-derived acetyl-CoA for fatty acid synthesis, and, importantly, shows that reductive branch can be a major nutritional source in respiration deficient cells.

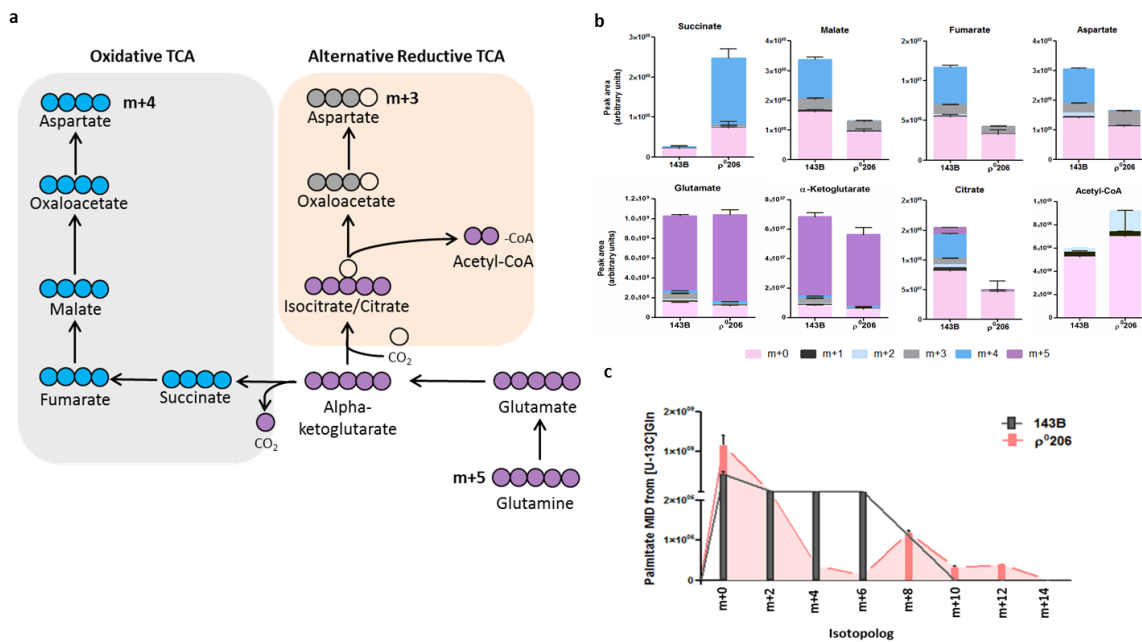


Figure 27. Glutamine contributes to TCA intermediates and fatty acids biosynthesis via reductive pathway in cancer cells lacking ETC activity. (a) Schematic representation showing expected TCA intermediates, and aspartate labeling patterns, synthesized from glutamine using oxidative TCA metabolism, or reductive carboxylation as

indicated in the scheme by the colored circles (purple circles represent m+5 labeled carbons; blue circles m+4, and grey circles m+3). **(b)** Mass isotopomer analysis of different metabolites in 143B and ρ^0 206 cells cultured with $^{13}\text{C}_5$ -glutamine. **(c)** Isotopolog distribution pattern for palmitate in 143B and ρ^0 206 cells cultured with U^{13}C -glutamine. Area under the curve is shown to highlight the shift in the isotopolog-labeling pattern induced by respiration impairment. Bars represent mean \pm SEM for six independent cultures.

As a summary of the results of this section we can conclude that ρ^0 206 cells have efficiently reprogrammed their metabolism to overcome the metabolic limitation caused by the lack of a full active mitochondrial respiration. This reprogramming is based on strong dependence of pyruvate and glutamine in order to sustain high demand of building blocks during tumor proliferation. Pyruvate is able to support aspartate consumption along with the recovery of affected NAD^+/NADH ratio due to lack of ETC activity, whereas glutamine serves as fundamental resource in a reductive truncated-TCA.

DISCUSSION

The current research in tumor biology has demonstrated the rising relevance of the tumor metabolism during the oncogenic process. Altered energy metabolism in cancer cells has been recognized to be essential to satisfy the high demands of growth and proliferation under so-called tumor metabolic reprogramming (Hanahan and Weinberg, 2011b). However, this reprogramming is not only a single effect caused by tumorigenesis, but also specific metabolic activities can participate directly in the transformation event or support the biological processes that enable tumor growth (Vander Heiden and Deberardinis, 2017). In fact, though rapid cell growth is a general neoplastic feature, variability within the underlying metabolic rewiring of a given cancer cell confer heterogeneity in the metabolic dependencies of the cell. This metabolic heterogeneity is driven by combination of genetic alterations and non-genetic factors such as the tumor microenvironment.

Decreased mitochondrial respiration, for instance triggered by key enzyme mutations or hypoxic environments, is one of these metabolic perturbations which dictate how proliferative adaptations are driven. Regarding the metabolic requirements of respiration deficient cells and their capacity to overcome the strong selective pressure generated by metabolic stress it has not been fully characterized. Therefore, in this section we aimed to decipher the specific metabolic requirements fulfilled by mitochondrial respiration to support proliferation.

Since ρ^0 cell model was generated by Giuseppe Attardi and collaborators, these cells been subsequently used to study mitochondrial disorders (Khan et al., 2007). Specifically in cancer research, ρ^0 cybrids (cytosolic mitochondria of one cell type becomes perpetually incorporated within the cytoplasm of the other cell type) with frameshift deletion in cytochrome B have been used instead of totally mtDNA depleted ρ^0 cells (Emerling et al., 2009; Sullivan et al., 2015; Weinberg et al., 2010). Nevertheless, though generally selective pressure in human cancers for retention of mitochondrial genome function has been reported (Stewart et al., 2015), we decided to use ρ^0 cells undergoing a permanent mitochondrial DNA depletion to continue deciphering the tumor metabolic reprogramming. In fact, these cells represent an excellent extreme metabolic phenotype due not only to their successful adaptation to overcome this pressure, but also supporting the large-scale biosynthetic programs that are

required for active cell proliferation. Some adaptive process, that conferring survival advantage on them, have already been described, such as the increase in the expression of antioxidant enzymes to resist against oxidative stress or chemotherapeutic agents (Park et al., 2004). In this context, we reasoned that deeper understanding the role of key metabolites pyruvate and glutamine in these cells would allow us to gain insight into how respiration supports the metabolic needs of proliferating cells.

Although the distinguishing aerobic glycolysis phenotype was initially hypothesized to result from diminished mitochondrial function (Warburg, 1956a), it is currently known that most cancer cells require respiration for proliferation beyond ATP production (Zong et al., 2016). Nevertheless, despite the importance of respiration in cell proliferation, we have demonstrated that ρ^0 cells, which undergo permanent loss of a functional mitochondrial electron transport chain (ETC), are able to not only survive but also proliferate at same level than respiration-competent cells under specific culture conditions. Since their generation, ρ^0 cells were found to be auxotrophic for uridine and pyruvate for growth in the absence of respiration (King and Attardi, 1989). Uridine auxotrophy was rapidly explained due to *de novo* pyrimidine biosynthesis impairment caused by loss of respiratory chain electron transfer. Nevertheless, the role for exogenous pyruvate in the metabolism of these cells was recently renewed (Birsoy et al., 2015; Sullivan et al., 2015). These authors reported that in proliferating cells, respiration serves a crucial anabolic role by providing access to electron acceptors to convert glutamine-derived glutamate into α -KG in order to support aspartate synthesis. Evidence includes the fact that α -Ketobutyrate (as an alternative electron acceptor) can also rescue growth and α -KG levels. However, we found that pyruvate is more efficient than α -Ketobutyrate to maintain high proliferation, suggesting that a contribution of carbon to aspartate also affects viability. In addition, even though aspartate partially maintained cell proliferation when exogenous pyruvate was not supplied, the efficiency of aspartate rescues resulted with certain variability to reach a total rescue. Regarding these observations, we assumed that role of pyruvate in mitochondrial respiration was not been fully understood.

In both cases α -Ketobutyrate and pyruvate, their role in NAD⁺ regeneration to allow continued glycolysis for ATP production is probably important. Indeed, mitochondrial ATP production appears dispensable in proliferating cells with access to sufficient glucose. Falling production levels of glycolytic intermediates downstream GAPDH and accumulation of those upstream GAPDH during exogenous pyruvate withdrawal demonstrated that lack of NAD⁺ blocked glycolysis, decreasing ATP levels in respiration deficient cells. Surprisingly, these levels were totally recovered when pyruvate was supplied, indicating that cancer cell can paradoxically adapt ATP production according to mitochondrial respiration availability. Importantly, this observed rescue was primarily attributed to the contribution of pyruvate, since supra-physiological aspartate concentration was provided, remaining unchanged even in the absence of pyruvate.

Furthermore, impaired transaminases activity using RNAi revealed that upon pyruvate withdrawal, GOT1 knockdown (but not GOT2 knockdown) markedly reduced ρ^0 206 cellular growth and this knockdown could be rescued by pyruvate. This suggests that GOT1 partially counters the detrimental effect of pyruvate withdrawal in respiration deficient cells and that there might be a metabolic pathway mediated by GOT1 that is of benefit to these cells. The

importance this enzyme in respiration deficient cell metabolism was also corroborated by significantly GOT1 overexpression observed compared to non-transformed cells or even parental cell model. Consistent with this observation, loss of GOT1 has been recently identified by CRISPR-based genetic screen to sensitize human cells to phenformin, a complex I of ETC inhibitor (Birsoy et al., 2015). These authors related this fact to a key mechanism through which pyruvate restores the proliferation of cells with ETC inhibition promoting GOT1-catalyzed aspartate synthesis. However, the inversion in the cytosolic side of the aspartate-malate shuttle (synthesis of aspartate from OAA catalyzed by GOT1) might be cause to an unnecessary, even toxic, increase of NADH in respiration deficient cells, where mitochondria is not able to supply NAD⁺. More importantly, if it were the case, presence of plenty of aspartate might be enough to sustain proliferation when respiration is impaired. In contrast, under AOA treatment, when transamination for aspartate synthesis is blocked, supplementation of aspartate could only rescue 143B, indicating an additional defect in ρ^0 206 cells that is independent of aspartate production. Thus, forwarded aspartate metabolism to nucleotide biosynthesis or asparagine is not supporting ρ^0 206 rescue, indicating that aspartate-to-oxaloacetate route must be an essential step in the reprogramming metabolism during mitochondrial respiration dysfunction.

Given that entire ρ^0 phenotype rescue during AOA inhibition using pyruvate was observed (in part through aspartate production) and aspartate was not, then we reviewed aspartate metabolism via transamination to check if this might be responsible for increased viability. As showed, we approached LC/MS-based metabolomics analysis in order to further investigate pyruvate rescue during transamination inhibition. These studies served to comprehensively characterize metabolic alterations due to lack of mitochondrial respiration, focusing on the metabolites involved in key pathways related to pyruvate and aspartate tumor intermediary metabolism including glycolysis, the TCA cycle as well as its anaplerotic pathways, aspartate-malate shuttling, glutaminolysis, and fatty acid biosynthesis.

¹³C₄-aspartate tracing revealed metabolism of aspartate through malate and fumarate to succinate. Both 143B and ρ^0 206 cells metabolized aspartate to malate and fumarate to similar extents, indicating a relatively free interconversion of these metabolites. However, the conversion of fumarate to succinate was only observed in respiration deficient cells. This suggests that in ρ^0 206 cells, the SDH reaction proceeds in reverse and is GOT-dependent, since aspartate derived-succinate became extinct during transaminases inhibition. Succinate derived mainly from the malate–aspartate shuttle and the purine nucleotide cycle (which is converted by the reversal of SDH) was found to specifically accumulate during ischemia in various tissues (Haas et al., 2016). On the other hand, inhibition of SDH also results in accumulation of succinate. SDH-mutant tumors exhibit a decreased abundance of alanine, aspartate, asparagine and glutamate (Lussey-Lepoutre et al., 2015b). However, levels of these amino acids were maintained in ρ^0 206 cells as long as exogenous pyruvate was present, suggesting not only SDH is not disabled, but also reversal activity of SDH is predominant during mitochondrial respiration impairment.

Nevertheless, this role of SDH would allow conversion of NADH to NAD⁺ to counter the accumulation of mitochondrial NADH that is being generated through lack of function of the NADH dehydrogenases due to absence of pyruvate as electron acceptor. This leads in addition

to possible mitochondrial conversion of oxaloacetate to malate (presumably mediated by malate dehydrogenase 2) that further absorbs electrons, allowing the regeneration of NAD⁺. The predominant α -KG species observed in 143B cells cultivated with ¹³C₄-aspartate was the m+3 isotopomer, indicating that aspartate would normally be converted to succinate through the oxidative TCA cycle when respiration is unimpaired. Thus, in p⁰206 cells, the m+4 succinate occurs through conversion of aspartate to succinate because of defective respiration. The most likely explanation for this metabolic reprogramming is to accommodate the conversion of mitochondrial NADH back to NAD⁺ to reverse the consequences of impaired respiration (and therefore mitochondrial NADH accumulation) in p⁰206 cells.

In consonance with our findings, we propose a novel role for pyruvate beyond electron acceptor to support aspartate synthesis (**Fig. 28**). As already described, respiration deficient cells experience a lack of NAD⁺ availability, and a pyruvate rich niche restores NAD⁺ (Normal conditions, **Fig. 28a**) (Birsoy et al., 2015; Sullivan et al., 2015). Surprisingly, to maintain the high glycolytic flux demanded for supplying biosynthetic intermediates, cancer cell paradoxically require not only active respiration, but also a pyruvate rich environment as we have demonstrated. Based on this reciprocal dependency on respiration and pyruvate rich niche to maintain NAD⁺ availability, we hypothesized that under restrictive conditions (for instance pyruvate poor niche and respiration impairment) aspartate could replace lack of electron acceptors to supply NAD⁺ (**Fig. 28b**). This is likely supported by the fact that inhibition of the aspartate transamination to OAA by AOA also collapsed the glycolytic flux, due to lack of NAD⁺ production by its further reduction to malate. Thus, aspartate is highly consumed in cytosol, producing OAA by GOT1, which in turns is reduced to malate. This might become a major supply of NAD⁺ supporting cytosolic homeostasis, mainly for respiration deficient cells under pyruvate-poor or absence environments. Accordingly, a main aspartate fate to support NAD⁺ homeostasis-dependent glycolysis operates by a reductive truncated-TCA branch for respiration deficient cells.

In contexts where respiration is inhibited, aspartate must behave as less efficient supplier of NAD⁺ than pyruvate, in part due to the fact that its support requires several metabolic reactions, whereas pyruvate can be directly reduced. In fact, we have demonstrated here that under no exogenous pyruvate conditions, aspartate is driven to a reductive alternative metabolic branch but not effective enough to maintain proliferation. Consequently, it is reasonable to argue that NAD⁺ consumption kinetics could be faster than the capacity of aspartate to supply it under restrictive conditions (pyruvate poor niche and respiration impairment). This argument might also explain why recovery on NAD⁺ levels was not observed when aspartate was supplied for respiration deficient cells with no exogenous pyruvate in the media (Sullivan et al., 2015).

Aspartate constitutes a key metabolic pivot in several biosynthetic pathways, being a major precursor for protein and nucleotide generation, as well as critical for the synthesis of other 'non-essential' amino acids such as arginine and asparagine. With limited means of consuming aspartate in respiratory deficient cells during pyruvate withdrawal, significant number of metabolic pathways are likely affected by reprogramed aspartate consumption. Altogether, our data indicated a significant loss of viability in respiration deficient cells when aspartate was forced to primarily replace the pyruvate contribution as electron acceptor (**Fig. 28c**).

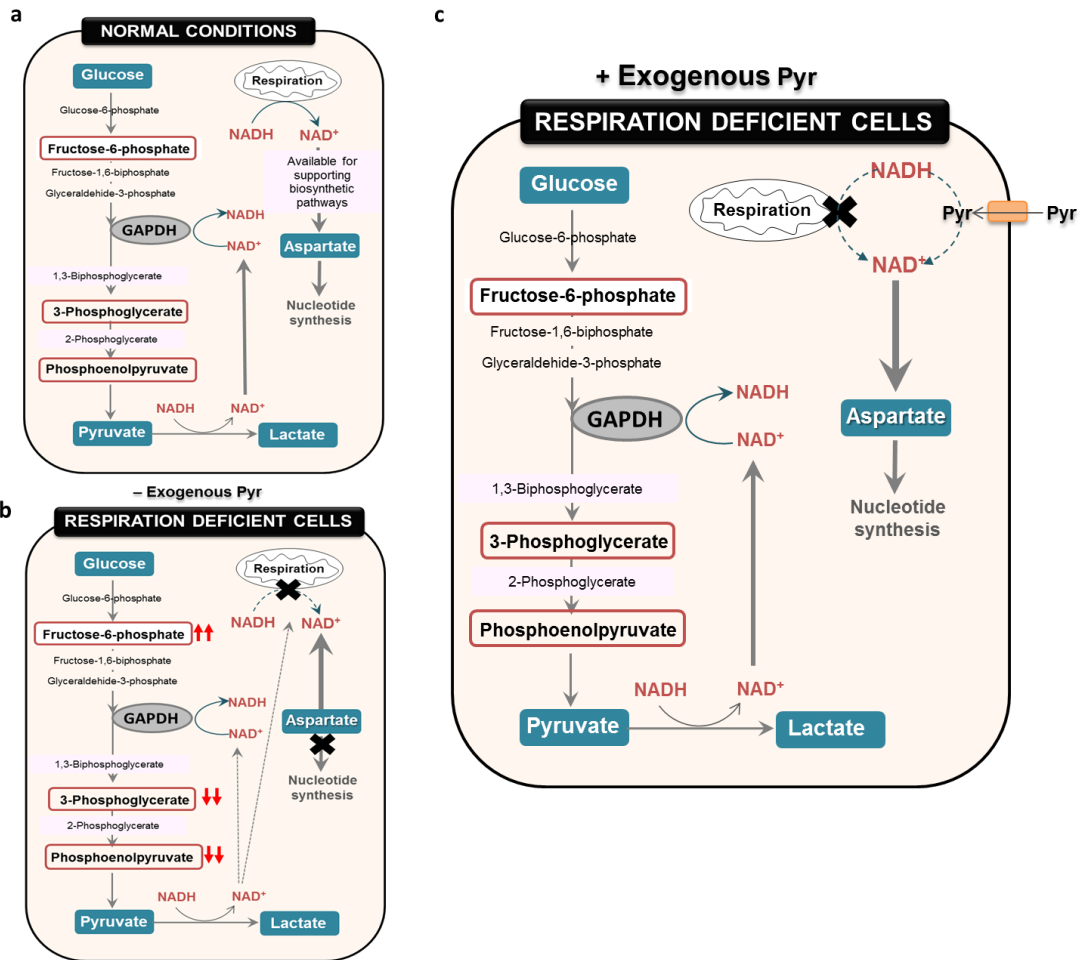


Figure 28. Representation of possible cellular scenario according to pyruvate availability and mitochondrial respiration function.

As reported, among others glutamine provides a carbon source to fuel the TCA and nitrogen for nucleotide (DeBerardinis and Cheng, 2010). Both 143B and p⁰206 cells showed to be dependent of glutamine to maintain cellular viability, implying a respiration-independent function for glutamine in cell growth. The reductive branch of glutamine metabolism is the predominant pathway in rapidly-growing malignant cells containing mutations in complex I or complex III of the ETC, as well as in patient-derived renal carcinoma cells with mutations in fumarate hydratase, and in cells with normal mitochondria subjected to synthetic lethality by ETC inhibition (Mullen et al., 2011c). Accordingly, similar to other glutamine-dependent cancer models (Cheng et al., 2011), 143B cells used glutamine as the major anaplerotic precursor to generate fumarate, malate, aspartate and citrate. In contrast, glutamine-dependent reductive carboxylation rather than oxidative metabolism was noticed in respiration deficient cells as previously reported. While glutamine-derived citrate was slightly detected, other TCA metabolites formed downstream of citrate m+5 and OAA m+3 were present, such as malate, fumarate, aspartate and acetyl-CoA, indicating these metabolites were generated from reductive, rather than oxidative glutamine metabolism. Furthermore, this tracing was also observed in 143B, suggesting reductive glutamine metabolism is not limited to mitochondrial defects adaptation. Indeed, glutamate dehydrogenase was overexpressed in both cell models, and cellular viability was affected during its enzymatic inhibition.

Prominent accumulation of succinate was constantly observed in respiration deficient cells. Succinate is synthesized from α -ketoglutarate (converted first to succinyl-CoA and then to succinate) and subsequently utilized as a substrate by succinate dehydrogenase (SDH) to produce fumarate. Although large proportion of succinate is provided by reductive glutamine metabolism in respiration deficient cells, important fraction of succinate was generated from aspartate during pyruvate withdrawal. Succinate production remained fundamental in respiration deficient cells since metabolites as important as glutamine and aspartate are contributing to its biosynthesis. Haem oxygenation was demonstrated as one of the fate of this succinate. Likewise inhibition of this pathway was synthetically lethal when combined with fumarate hydratase deficiency cells (Frezza et al., 2011), we raised if inhibition of this succinate flux further metabolized for excretion could be targeted during respiration impairment. In this case, high reductive production of succinate derived from aspartate consumption did not generate a synthetic lethality in the heme pathway, suggesting succinate detoxification is not a primary pathway during unable respiration.

Therefore, apart from its unavoidable accumulation in the onward metabolism to fumarate that is blocked because of the permanent reduced state of the ubiquinone that is required (due to a lack of electron transfer to cytochrome B in complex III), significantly higher levels of accumulated succinate must have highlighted role in respiration deficient cells. The oncogenic role of succinate has been initially linked to the inhibition of prolyl hydroxylases and the subsequent stabilization of Hif-1 α (Selak et al., 2005). Hif-1 α overexpression was evident both mRNA and protein level in respiration deficient cells compared to respiration-competent 143B, suggesting the role of succinate accumulation beyond enzymatic deficiency results in HIF stabilization. Since Hif-1 α is considered critical for metabolic adaptation to hypoxia through increased conversion of glucose to pyruvate and subsequently to lactate (Solaini et al., 2010), it must be not surprisingly related to overexpression of genes involved in supporting ρ^0 phenotype, such as activation of key glycolytic genes.

Interestingly, ρ^0 206 have shown an extremely efficient capacity to overcome selective pressure due to mitochondrial respiration impairment, operating their metabolic requirements primarily to enhance their anabolic pathways for supplying the necessary biomass supporting cell division. Importantly, many oncogenes must play a fundamental role orchestrating the tumor metabolic reprogramming observed.

Moreover, more importantly we have demonstrated that the fine reducing power balance control on tumor metabolism allows cancer cells getting over extreme metabolic stress, which can be caused well for the continuous pressure generated for satisfying their own aberrant physiological requirements, or well for alterations in the tumor microenvironment, such as nutrient starvation or hypoxia. In addition, in this thesis, we provide an explanation for the substantial exogenous pyruvate contribution to reprogrammed metabolism under mitochondrial respiration impairment beyond sustaining aspartate biosynthesis. Interestingly, we described for the first time that the loss of functional ETC triggers strict exogenous pyruvate dependence to the cells and its absence clearly causes diversion of aspartate to maintain high glycolytic flux demand. Taken together, this section present a model where reducing power requirements take precedent over specific metabolite biosynthesis.

AIM 2. DEVELOPMENT OF NANOTECHNOLOGY APPROACHES BASED ON TUMOR METABOLISM.

RESULTS

As discussed above, alterations in cancer cell metabolism are intricately linked to the principal hallmarks of cancer. After the completion of the first aim of this thesis, our findings studying reprogrammed respiration deficient cell metabolism indicated extreme phenotypes could be selectively targeted. Thus, as part of our second aim, we develop different nanotechnology approaches, taking advantage of several strategies established by our research group, in order to design new metabolism-based cancer therapies.

We focus on the improvements of current cancer treatment using polystyrene nanoparticle (NPs) as delivery system. The synthesis and characterization of these NPs has been previously optimized in our research team (see Introduction section). The batch of amino-functionalized polystyrene cross-linked nanoparticles use for the accomplishment of this aim were prepared by the chemistry team of our research group by dispersion polymerization following the protocol previously described (Unciti-Broceta et al., 2012a). A monodisperse population of 200 nm NPs was successfully synthesized and characterized (see Fig. 1).

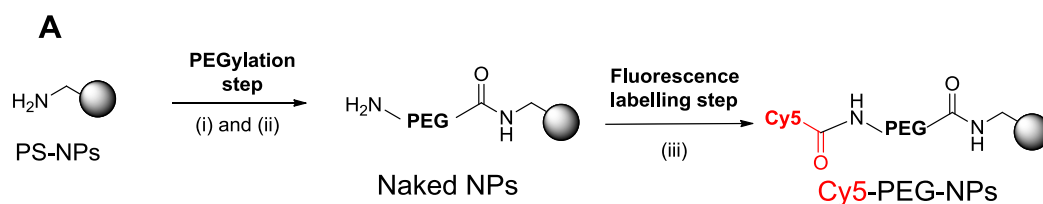
2.1 EVALUATION OF NANODEVICES UPTAKE EFFICIENCY IN CANCER CELL MODEL BASED ON RESPIRATION DEFICIENT CELLS WITH AN EXTREME METABOLIC PHENOTYPE

The first step in this aim was to determine whether these polystyrene nanoparticles (PS-NPs) could be taken up by parental and respiration deficient cell lines. Consequently, an initial analysis of the NP uptake efficiency and cell viability effects in our models was assessed.

2.1.1. Preparation of fluorescent labelled nanoparticles

To monitor the cellular uptake, NPs were labelled with a fluorophore to be able to track uptake efficiently by flow cytometry and confocal microscopy. In particular Cy5 was used (Ex (nm) 625 nm /Em (nm) 670). Cy5 is a cyanine derivative that yields brighter and stable fluorescence.

For this purpose 200 nm amino-methyl cross-linked polystyrene NPs (PS-NPS) were coupled with a NHS activated Cy5 following a PEGylation step of PS-NPs (Fig. 1a) using Oxyma/DIC as coupling reagents. This PEGylation increases the biocompatibility of the NPs, thereby facilitating their transport across cell membranes. It also reduces unfavorable interactions between NPs and the bioactive cargoes. Then, the size and monodispersity of these NPs was determined using standard techniques such as SEM and Dynamic Light Scattering analysis. (Fig.29).



Reagents and Conditions: (i) Fmoc-4,7,10-trioxa-1,13-tridecanediamine succinamic acid (PEG), Oxyma, DIC, DMF, 60 °C, 1400rpm, 2h, 100%; (ii) 20% piperidine in DMF; (iii) Cy5-NHS, DIPEA, DMF, RT, 1400rpm, O/N, 100%.

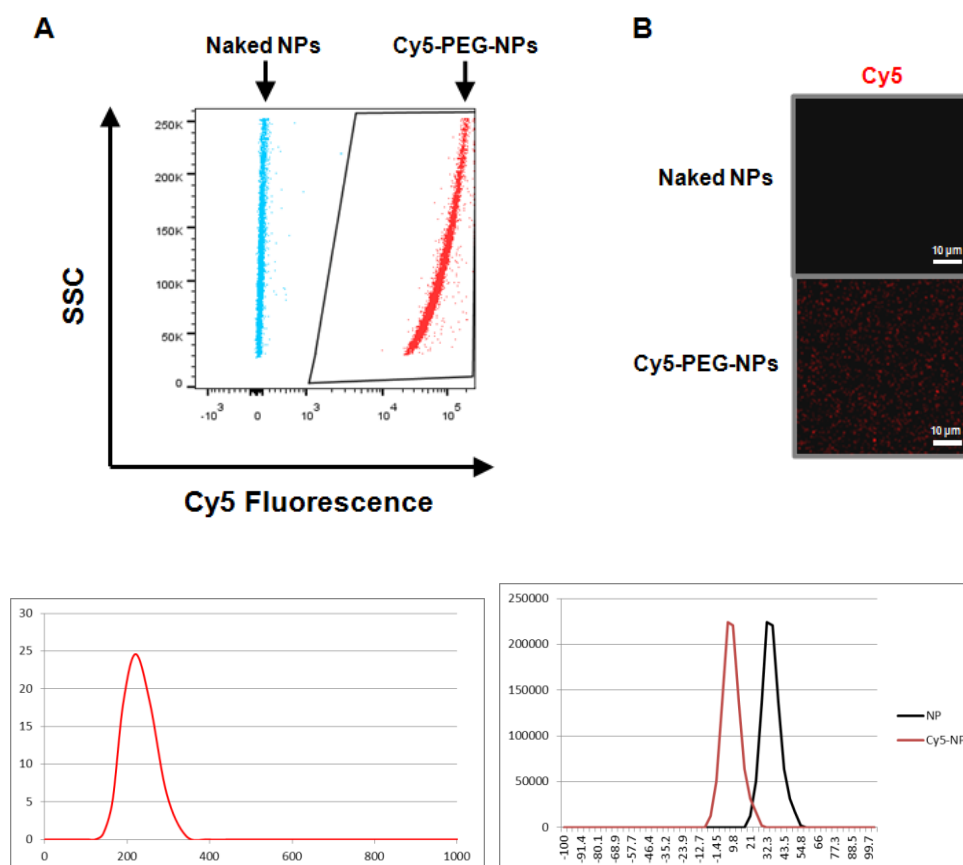


Figure 29. Fluorescence nanoparticles synthesis and characterisation. A. Scheme of synthesis of fluorescence PEGylated Cy5-NPs. B. Representative overlay dot plot obtained after flow cytometry analysis of naked NPs (blue) and Cy5-NPs (Red). C. Confocal fluorescence microscopy of naked NPs and Cy5-NPs. Scale bar, 10 μ m. D. Particle size distribution (nm) of Cy5-NPs. E. Zeta potential values of naked NPs (black) and Fluorescent labelled Cy5-NPs (red), SSC, side scatter. Abbreviations: PS, polystyrene; PEG, polyethylene glycol; NP, nanoparticle.

2.1.2. Assessment of uptake efficiency of NPs

To assess the efficiency of uptake of these NPs by 143B and p⁰206 cells, cells were incubated with Cy5-NPs and confocal microscopy was used to identify NP localization. Untreated and non-fluorescence NPs (Naked-NPs) treated cells were used as negative controls. Both cell lines were able to internalize NPs efficiently as observed in confocal imaging (**Fig. 30**).

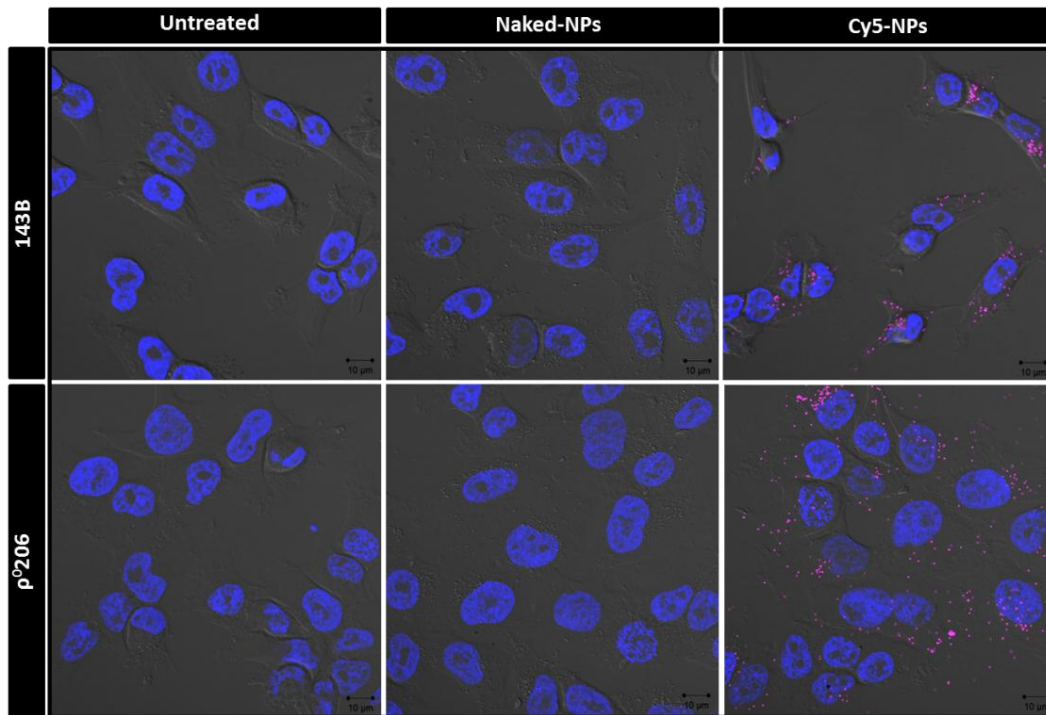


Figure 30. Confocal fluorescence microscopy to analyze Cy5-NPs cellular uptake by 143B and ρ^{0206} . Cells were incubated 1.5 hours with 10000 NPs/cell and analyzed by confocal microscopy. 63X magnification representative images show a composition of the three recorded channels (DIC–Differential interference contrast–; blue, DAPI – nuclei–; and red, Cy5-NPs). Black bar = 10 μ m.

After NP internalization was verified, a deeper study of the cellular uptake was performed using different ratios of Cy5-NPs added per cell and several incubation times. Following the appropriate treatment, cells were detached, fixed and analyzed by flow cytometry. To further describe the uptake capability of cell lines, we use a parameter previously reported by our group (Unciti-Broceta et al., 2015), Multiplicity of Nanofection Fifty index (MNF50), defined as the number of NPs capable of nanofecting 50% of the cell population. Percentages of nanofected cells versus NPs ratios were fitted to a hyperbola equation model (**Fig. 31a**) in order to obtain the 50% of positive cell populations given by the curve (MNF50). For 143B cell line MNF50 index was established as 103 ± 8.5 Cy5-NPs and three times lower MNF50 index was observed in ρ^{0206} cell line, 33 ± 1.9 Cy5-NPs. Furthermore, median of fluorescence intensity increments (Δ MFI = MFI sample/MFI untreated) of Cy5-positive cells was studied in order to reach more information about difference in uptake capability of cells lines. Once more, ρ^{0206} cells showed an increased uptake capability compared to 143B cells (**Fig. 31b**) under the same experimental conditions (3 hours of incubation time and different NP ratios). In this study, these data also revealed that the larger number of nanoparticles, the greater cellular uptake and although cells are nanofected, nanoparticles uptake continues (**Fig. 31c**). The percentage of Cy5-positive cells increased gradually from the lowest to the higher both NP ratio and incubation. These studies suggest that respiration deficient cells show a more “permeable” behavior to be nanofected than the parental cell line.

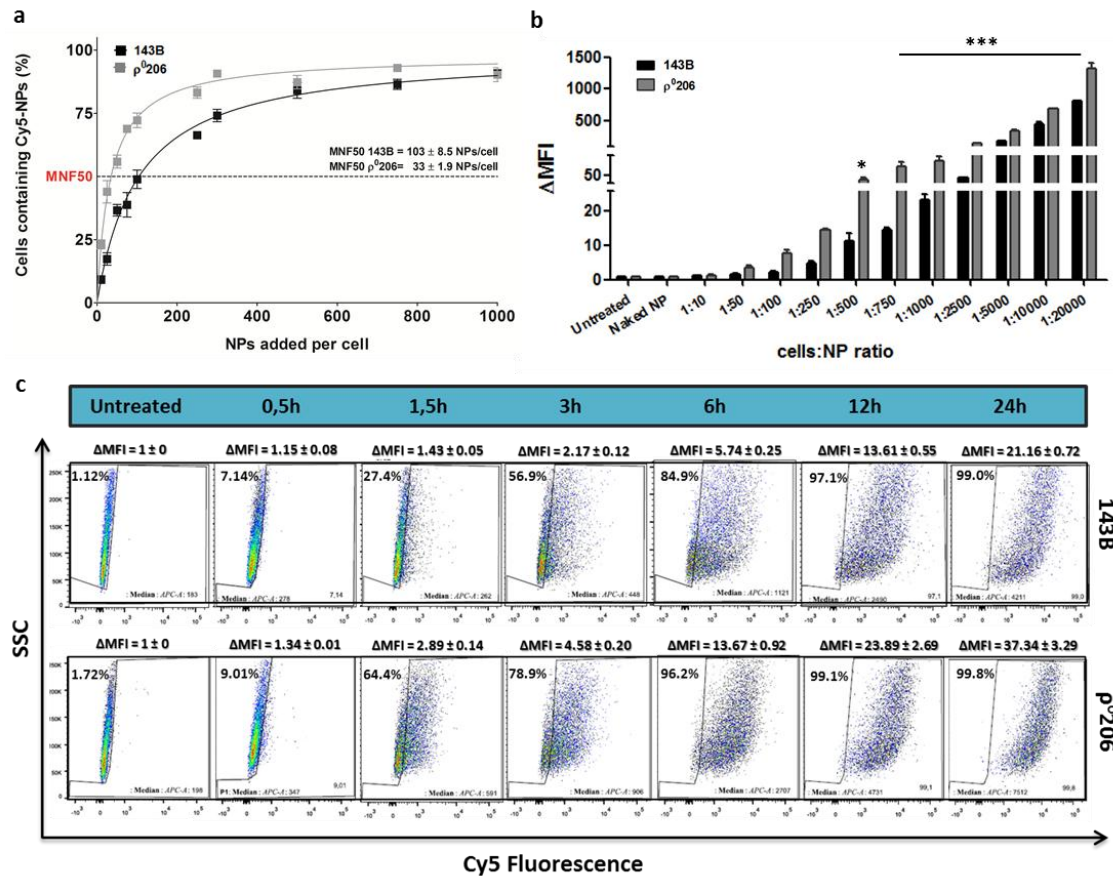


Fig. 31. Evaluation of Cy5-NPs cellular uptake in 143B and p⁰206 cell lines analyzed by flow cytometry. (a) Percentage of cells containing Cy5-NPs versus cell to NP ratios is displayed. The data (mean ± S.E.M) are represented as hyperbola model to study the saturation of cellular uptake behavior. 143B, $r^2 = 0.9458$; p⁰206, $r^2 = 0.9616$. MNF50: Multiplicity of Nanofection Fifty. **(b)** Bar representation to compare Δ MFI between 143B (black) and p⁰206 (grey) cell lines. Statistical significance was determined by Bonferroni's multiple comparison test between the same treatments of the different cell lines, $n = 8$, (*p value < 0.05, *** p value < 0.001). **(c)** Representative flow cytometry dot plots obtained with 143B and p0206 cells incubated with 1:100 cell: Cy5-NPs ratio at different time points. SSC, side scatter, cellular complexity. Δ MFI, increment of median fluorescence intensities. Results are expressed as mean ± S.E.M.

To investigate the cytotoxicity induced by intracellular entrance of nanoparticles in 143B and p0206 cells, long-term incubation assay was performed using unlabeled NPs. Later, cell cycle was evaluated by flow cytometry following propidium iodine staining. Evidence of cell dead was not observed in any cell line (**Fig. 32a**). In addition, none of them presented a significant increment in the subG1 population after NPs treatment, showing any toxic effect. Instead, perfect matches between cell cycle profile of untreated and nanofected cells were observed after seven days of incubation (**Fig. 32b**). No significant difference between cell percentages in each phase of the cell cycle in any condition was observed. Additionally, a long-term tetrazolium-based toxicity assay to assess mitochondrial function was performed in NP treated cells compared to untreated cells using different NP:cell ratios. Same proliferation level was maintained in all conditions tested and no substantial metabolic changes due to NP treatment were observed (**Fig. 32c**). Taken together, these results suggest that nanoparticles do not

present cytotoxic effects in the cell lines tested and cell-NP interaction does not adversely affect cell viability.

In other hand, primary uptake studies were focused on optimizing a non-toxic NP ratio from which monodispersed labeled population independent of the type cellular could be obtained. This goal was achieved when both respiration deficient cells and parental cells were incubated with 50000 NPs/cell for 1 hour (**Fig. 32d**).

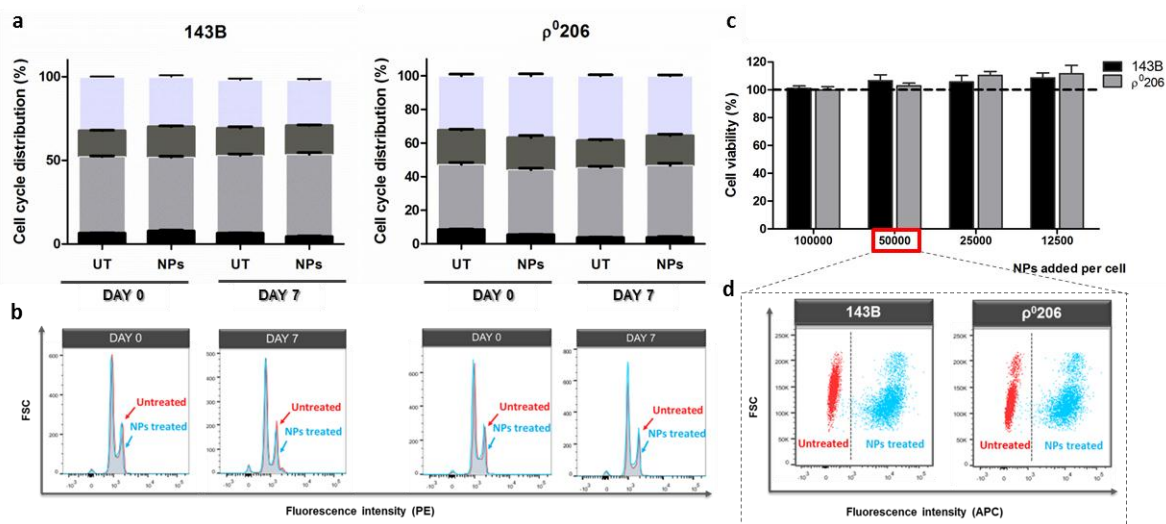


Figure 32. Effect of NP treatment on cell viability and proliferation during time course experiment. (a) Cell cycle distribution before and after long-term nanoparticle incubation. The percentages of cells in different phases of the cell cycle were determined from the histograms by flow cytometry. Graphs summarize data from initial (Day 0) and final (Day 7) experimental time points. **(b)** Ploidy histogram of the relative DNA content was determined in cells incubated with NPs (blue) compared with untreated cells (red). **(c)** Proliferation of NP treated cells (1:10000, 1:50000, 1:25000 and 1:12500 NPs added per cell) referred to untreated cells (100%) measured by MTT assay. **(d)** Representative overlay dot plot obtained after flow cytometry analysis of untreated (red) and Cy5-NP treated cells (blue). Bars represent mean \pm S.E.M of results from 3 independent experiments with duplicated points. UT: untreated cells. FSC: Forward scatter. Cy5-NPs: fluorescence nanoparticles.

From these results, we can conclude that even though the ability to uptake was shown to be dependent on the type cellular, the nanofection load can be controlled in a robust manner through concentration and incubation time in our cell models. Furthermore, the amount of nanoparticles that was internalized following 24 hours of treatment was always more higher than 99%, underlining that the PS-nanoparticles could be tested as a delivery system, able to be transported inside the our cell models with remarkable efficacy.

2.2.DEVELOPMENT AND EVALUATION OF CONTROLLED DRUG DELIVERY SYSTEM FOR COMBINED METABOLIC-BASED THERAPY

Polystyrene nanoparticles have proved to be an efficient and controlled delivery system, able to efficiently target different cargos in diverse cell lines, without altering cell viability (see Introduction section 3.3). Hence, using these functionalized NPs, we expect to improve the efficacy of traditional antiproliferative cancer therapies. We focus on doxorubicin (DOX) as anticancer agent, which remains as one of the most effective chemotherapeutic drugs of the past 50 years together with its antimetabolic engagement that has been recently reported

(Yang, 2016). The enhanced anticancer efficacy of doxorubicin *in vitro* and *in vivo* through GOT1 suppression using the shRNA, which inhibits drug-induced oxidative stress, was reported. The enhancement in therapeutic efficacy is based on the inability of the cells to detoxify doxorubicin-stimulated ROS, thus confirming targeting metabolic strategies can improve conventional chemotherapeutics efficiency. This fact makes doxorubicin the ideal drug candidate to develop this aim.

2.2.1. Preparation of DOX-conjugated nanoparticles

DOX was conjugated to PEGylated polystyrene NPs via pH-sensitive hydrazone linkage. For this purpose, NPs were functionalised with hydrazide functional group by treatment of carboxyl functionalized NPs with hydrazine. Then DOX was conjugated with hydrazide functionalized NPs (**Functionalised NP**) by the formation of hydrazone bond (**Fig. 33a**) following a protocol optimised by the chemistry team of our research group. PEGylation avoids possible steric impediments. Drug incorporation efficiency was determined by flow cytometry according to nanoparticle fluorescence since DOX is intrinsically fluorescent (Motlagh et al., 2016). DOX-NP showed fluorescence increased compared to Functionalized NPs, thereby DOX incorporation was confirmed (**Fig. 33b**).

The delivery system is based on this pH-sensitive linker and is schematically presented in **Figure 33c**. This hydrazine bond is relatively stable under neutral condition (such as pH 7.4, modeling blood) and cleavable under mildly acidic condition (such as pH 5.0, in the tumor microenvironment). To test the stability of the chemical bond under physiological conditions and the release of DOX from nanoparticle, DOX-conjugated nanoparticles were incubated at 37°C with a pH 7.4 buffer (the extracellular pH of normal tissue) and a pH 5.0 buffer (the acidic environment). Release of DOX was measured by flow cytometry thanks to DOX related-NP fluorescence. After 96 hours of incubation in acidic buffer, nanoconjugate exhibited a fluorescence decrease due to DOX release. In contrast, same fluorescence pattern was observed between untreated nanoparticles (remain water) and treated with PBS pH 7.4, displaying that DOX is stably bound to the NPs under physiological conditions (**Fig. 33d**).

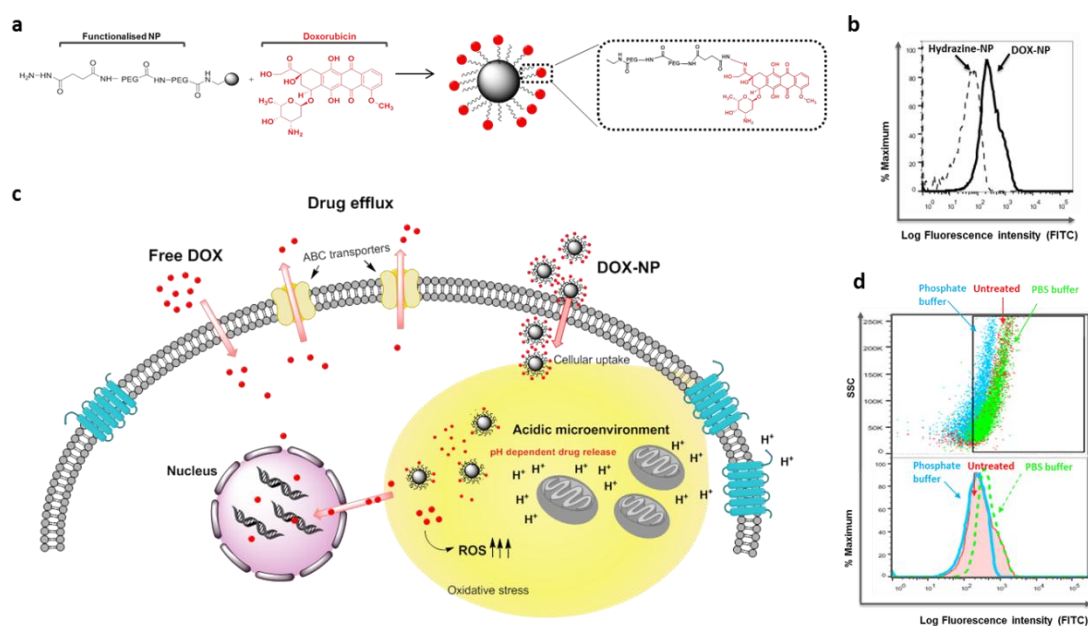


Figure 33. Schematic presentation of the drug delivery system. (a) Synthesis of functionalized polystyrene DOX-NPs. Reagents and conditions: 1:1 Doxorubicin in PBS pH 6, 50°C, 1000 rpm O/N. PEG, polyethylene glycol. **(b)** Histogram overlaid of hydrazine functionalized nanoparticles before (dashed line) and after (solid line) doxorubicin conjugation. **(c)** Representation of nanoparticle drug delivery system in a tumor cell compared to doxorubicin free treatment. **(d)** Dot plot (top) and histogram overlaid panel (bottom) representing DOX-NP populations under different pH treatment (acidic buffer, blue; neutral buffer, green; untreated, red) in order to check DOX release from the nanodevices. SSC, side scatter.

2.2.2. Effect of DOX-Nanoparticles on cell viability

Firstly, experimental drug loading (amount of DOX in the final NP formulation) of synthesized DOX-NP was calculated by HPLC analysis. A calibration curve of doxorubicin was done and known concentration of nanoparticles were incubated with PBS 5.2 for 48 hours and amount of doxorubicin release was quantified (see Material and Methods for details). It was found that the DOX concentration from 0.1 mL of DOX-NPS was 18.4 μ M. By applying the method developed in our group (Unciti et al, 2015) the number of nanoparticle (NPs/ μ L) was determined. Then it can be calculated the amount of drug release per nanoparticle (3.31×10^{-11} nmol/NP).

Doxorubicin effect on respiration deficient and parental cell lines was evaluated by measuring cell mediated reduction of resazurin sodium dye. Free DOX showed a dose dependent effect on cell proliferation and completely inhibited cell growth at concentrations in the range 500 nM (**Fig. 34a**). Half-maximum growth inhibitory concentration (IC₅₀) was 16.61 nM in 143B cells and 26.80 nM in ρ^0 206 cells. However, when DOX was managed using NP system delivery, the IC₅₀ was 0.24 nM in 143B cells and 0.19 nM in ρ^0 206 cells, which correspond to 4285 and 3365 NPs added per cell respectively (**Fig. 35b**).

To establish the concentration in which proliferation was inhibited in at least 90% of population (IC₉₀) using DOX-NPs. This IC₉₀ was in the range 35000-40000 NPs/cell in both cell lines. Theoretical DOX loading corresponding to free DOX was calculated as previously described, being determined in the range 12 nM. DOX-NP showed more cytotoxicity than free DOX under cell culture conditions. DOX-NP achieved a two-fold reduction of the IC₅₀ value compared with free DOX demonstrating the higher efficacy of the carrier.

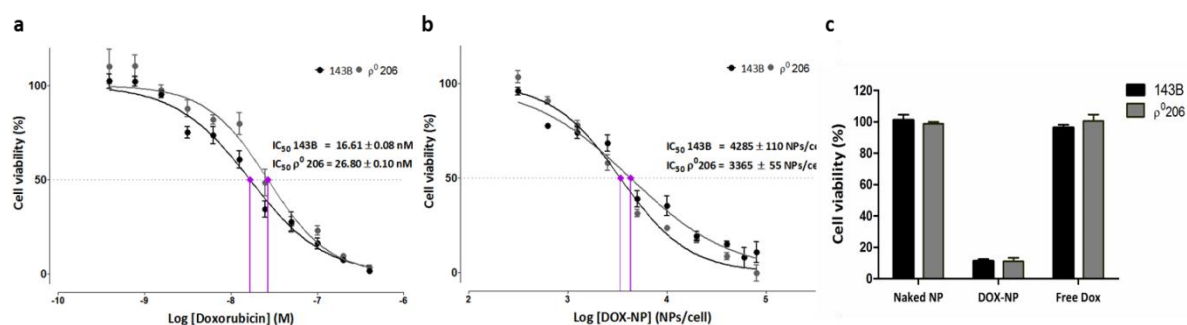


Figure 35. Effect of free and conjugated DOX on cell viability. (a) Dose response curves (cell viability percent versus NAM concentration) of doxorubicin free treatment and **(b)** of DOX-NP treatment in our cell models. The IC₅₀ value was determined by log (inhibitor) vs. normalized response-Variable slope using the GraphPad Software. **(c)** Cellular

viability impact of DOX-NP treatment compared to similar concentration of free DOX corresponding to 40000 NPs/cell.

2.2.3. Anti-MCT1 as alternative metabolic cancer therapy.

Given our results about new key proteins related to tumor metabolic reprogramming in respiration deficient cells, we propose the development of several treatment strategies targeting these new metabolic key in order to improve current cancer therapies. Towards this end, firstly we suggest use of antibodies directed against new metabolic key targets, such as MCT1, using nanoparticles as carriers.

Prior to the nanodevices development, we wanted to confirm the differential basal expression of MCT1 in our cell models. We found that MCT1 expression showed significantly higher in respiration deficient cell model compared to parental cells. This fact was observed both mRNA expression levels by quantitative PCR analysis (**Fig. 36a**) and protein levels measured by flow cytometry (**Fig. 36b-c**). This experiment led us also to check that the antibody was able to efficiently recognize the epitope of MCT1 protein in our cell models.

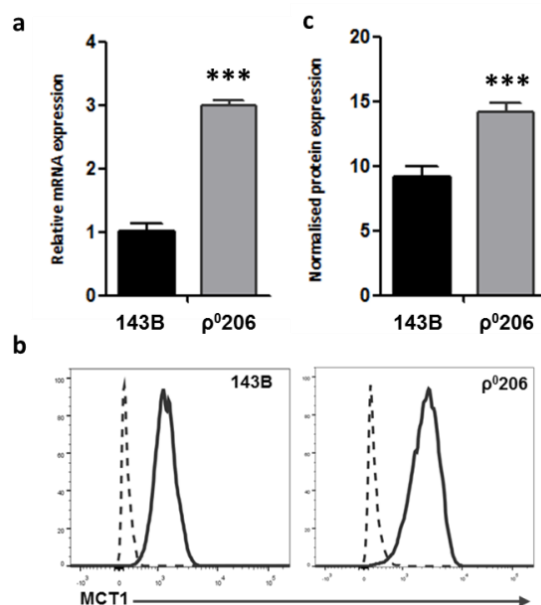


Figure 36. Comparison of MCT1 expression by flow cytometry and RT-qPCR on model cell lines. (a) Graph showing relative changes in mRNA expression of 143B and ρ⁰206. Results are presented as fold change mRNA expression ($2^{-\Delta\Delta CT}$), ***p < 0.001, normalised to β-Actin. Different protein levels were observed by flow cytometry by **(b)** histogram plots, where the dotted line represents the isotype control, and the black line denotes MCT1 recognition, and **(c)** by mean fluorescence intensity, which correlates with the amount of protein expression. ***p < 0.001, normalised to isotype control.

2.2.4. Preparation and evaluation of antibody conjugated nanoparticles.

Once differential expression was demonstrated, generation of anti MCT1 nanoparticles (henceforth MCT1-NP) in solid-phase multistep synthesis was conducted. Modern bioconjugation approach so-called biorthogonal “copper-free click chemistry” such as Huisgen 1,3-dipolar cycloaddition, was used to antibody conjugation due to its great versatility for nanoparticle functionalization. Click chemistry between bicyclo[6.1.0]nonyne (BCN)-modified

nanoparticles (henceforth BCN-NP) and azide-functionalized antibody was carried out (**Fig 37a**). Purified Mouse IgG1 was simultaneously coupled in order to be used as an irrelevant control antibody of the same isotype. To assess whether antibodies had been successfully coupled to BCN-NP, indirect labeling using a compatible fluorochrome-labeled secondary antibody was performed by flow cytometry. Fluorescence intensity differences between BCN-NP and antibody-conjugated NPs were significantly observed (**Fig. 37b**), confirming antibodies were successfully coupled.

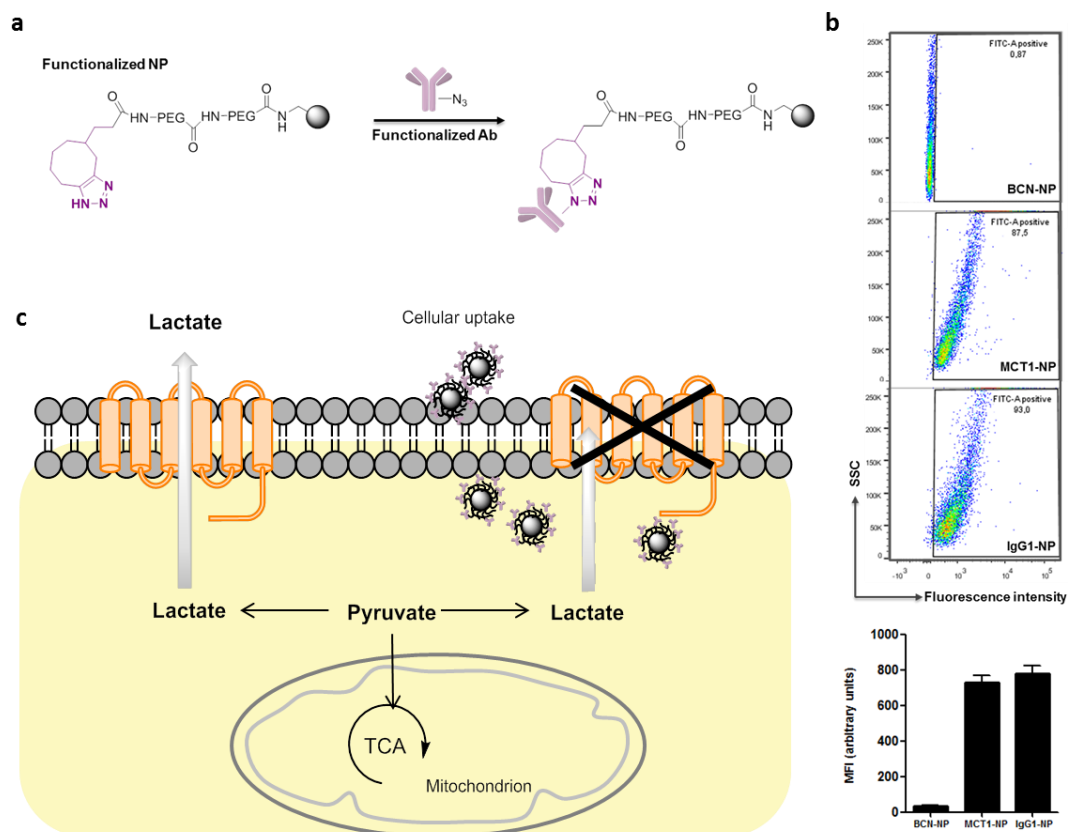


Figure 37. Nanoparticle based-platform to develop biology therapies based on metabolic targets. (a) Schematic representation of the conjugation of BCN-NP to N₃-functionalised antibody (more details in materials and methodology section 16). **(b)** Checking of coupling efficiency in MCT1-NP and IgG1-NP compared to functionalized NP (BCN-NP). Nanoparticles were incubated with conjugated secondary antibody and assessed by flow cytometry. SSC, side scatter. MFI, median of fluorescence intensity. **(c)** Representation of the NP bound antibody-mediated signaling inhibition. The growth impairment could be occurred because of blocking the conformation event to transport the molecules across the membrane or by interfering with ligand binding, lactate or pyruvate in this case.

The idea of using antibodies that target metabolic transporters is to prevent the metabolites movement across the cellular membrane (**Fig. 37c**). We expected that nanoparticle carried the antibodies which work by physically blocking the interaction between the receptor and its activating ligand or by sterically preventing translocation. For that purpose, respiration deficient cells compared to parental cells were treated with different ratio of MCT1-NPs and their cell viability was evaluated. Surprisingly we found that the same effect on cell viability was maintained between 80000 and 40000 NPs added per cell in both models, being more dramatic in p⁰206 cells (**Fig. 38a**). In addition, we tested whether 40000 MCT1-NPs added per cell caused viability disruption compared to control NPs. Interestingly, the effective cytotoxicity of MCT1-NP in respiration deficient cells was significantly more pronounced than

143B cells (**Fig. 38b**) and, using this NP ratio, no toxic effects were observed in any control conditions. Hence, and according also to primary uptake studies (**Fig. 31**), we decided to establish 40000 NPs added per cell as the amount of nanoparticles to use in the viability assays.

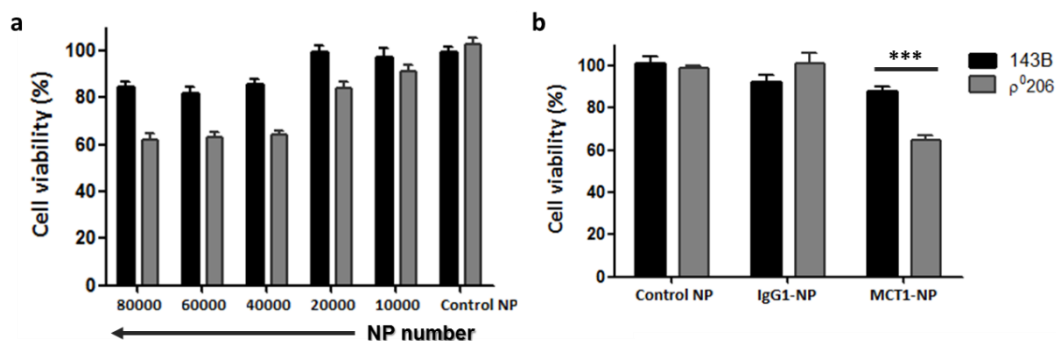


Figure 38. Effect of antibody coupled to nanoparticle on cell viability. Graphs represent the cytotoxicity results for respiration deficient cells and 143B parental cell line incubated with (a) increasing amounts of MCT1-NP and (b) 40000 NPs/cell of MCT1-NP compared with IgG1-NP and antibody unbound functionalized NP (Control NP). Data are the mean \pm S.E.M of three separate experiments. *** $p < 0.001$.

2.2.5. Engineering the combination of metabolic-based therapies using multifunctionalized nanoparticles

Interest in monoclonal antibody therapies have emerged in clinical practice due to they could be administered in combination with other chemotherapies with synergistic activities. In this regard, we designed a multifunctionalized cross-linker nanoparticle that lets to carry both MCT1 antibody and doxorubicin (**Fig. 39a**). The protocol for multifunctionalisation (see section II introduction 3.2.) established by our research group in order to conjugate firstly doxorubicin by pH-sensitive linker, and after the azide-functionalized antibody in aqueous conditions was performed. The effect on cell viability of the outcoming MCT1-DOX-NP was tested in our cell models, and more toxicity was observed in combined NP treatment than MCT1-NP. However, compared to DOX-NP strategy, combined multifunctionalized nanoparticle did not improve the treatment efficiency (**Fig. 39b**).

As showed in the first section, transamination reactions play an important role in cancer metabolism, especially in cells with impaired respiration maintaining redox balance. GOT1-dependent cell protection against doxorubicin by neutralization of drug-induced ROS has been proposed. Then, we wondered whether doxorubicin could be altering redox balance beyond induce oxidative stress by increasing the intracellular levels of ROS. In this case, inhibition of transamination reaction could be combined with doxorubicin in order to improve the treatment efficacy. In this context, anti-MCT1 therapy was also tested as these transporters are especially important to exogenous pyruvate import needed to maintain redox balance in respiration deficient models.

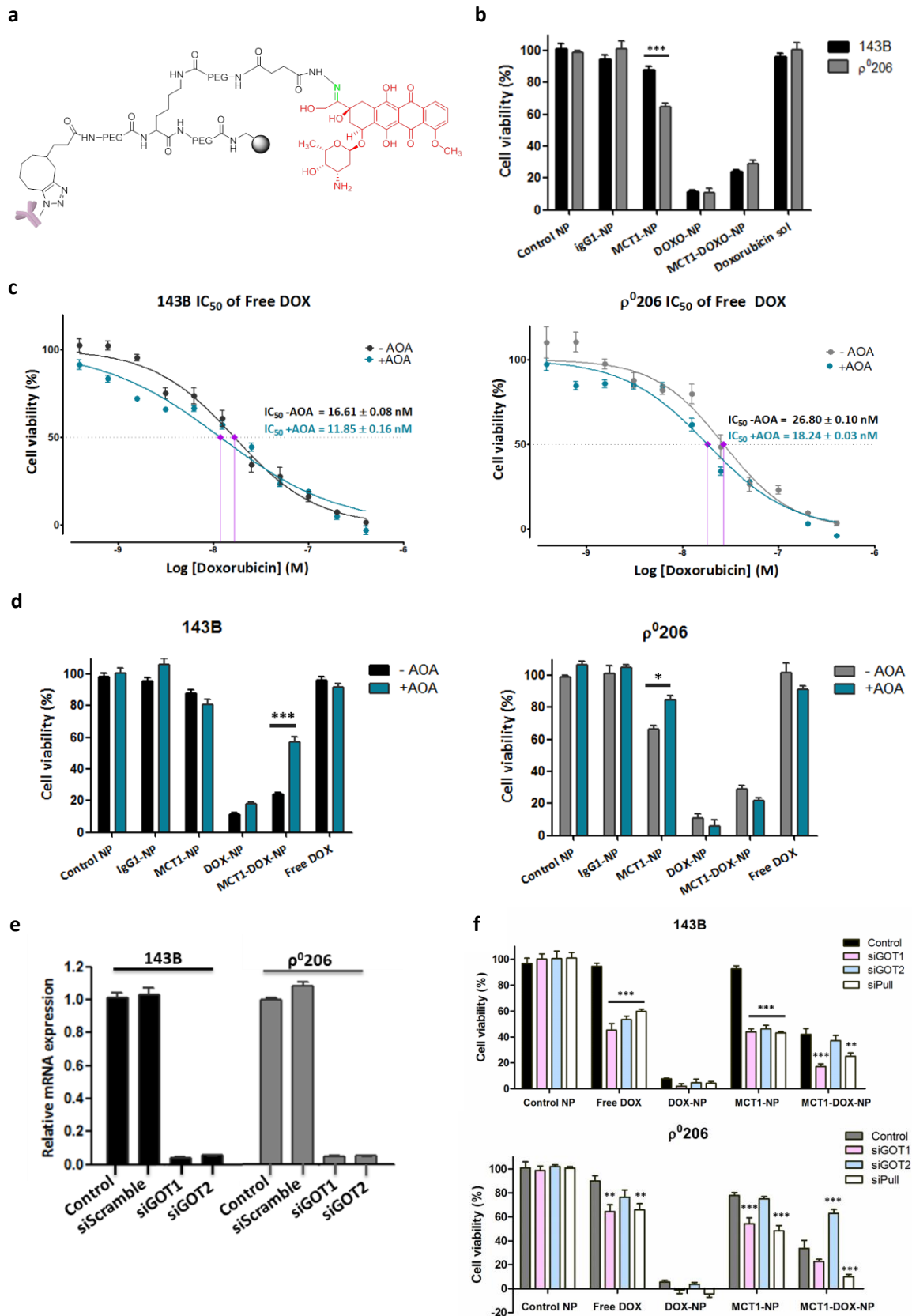


Figure 39. Development and evaluation of controlled drug delivery system for combined metabolic-based therapy. (a) Synthesis of multifunctionalized polystyrene MCT1-DOX-NP (see materials and methodology section 16 for more details about reagents and conditions). Red, doxorubicin molecule. Green, cleavage site. **(b)** Cytotoxicity

for 143B and ρ^0206 incubated with combined NP compared to single treatment (MCT1-NP and DOX-NP). Controls are unbound functionalized NP (Control NP), irrelevant antibody bound functionalized NP (IgG1-NP) and free DOX at 5.0mg mL⁻¹ DOX-equivalents. **(c)** Relative proliferation and maximal inhibitory concentration (IC₅₀) of doxorubicin treated cells in the absence or presence of AOA. **(d)** Cytotoxic effect on cell viability in cells incubated with different combined NPs in presence or absence of AOA. **(e)** 143B and ρ^0206 cells were transfected with GOT1, GOT2 and scramble siRNA and examined for GOT1 and GOT2 mRNA expression by qPCR. **(f)** Study of the cytotoxic effect on cell viability in GOTs-induced silencing cells, which were incubated with different multifunctionalized NPs. Experiments were performed in triplicate and the results are expressed as the mean \pm SEM. * $p < 0.05$, ** $p < 0.01$, *** $p < 0.001$.

Firstly, effect of transamination reactions inhibition with aminooxyacetate (AOA) on doxorubicin efficacy was examined by performing dose-response curves and measuring the IC₅₀ values. Cells under AOA treatment showed a slight decrease in the IC₅₀, being more marked in respiration deficient cells (**Fig. 39c**). However, our cytotoxicity studies with DOX-NP showed no important differences when AOA was presented in the treatment (**Fig. 39d**). Unexpectedly, 143B cellular viability increased in presence of AOA when cells were incubated with combined MCT1-DOX-NP. The same effect was also observed when ρ^0206 cells were treated with MCT1-NP (**Fig. 39d**), suggesting possible antagonist effect between AOA and MCT1 antibody/possible AOA secondary effects in MCT1 antibody.

To avoid unspecific outcome of AOA, we investigated the effect of GOT1 and GOT2 inhibition on doxorubicin efficacy by RNAi-mediated gene silencing. 143B and ρ^0206 cells were used by transfection with specific siRNA against GOT1, GOT2, both GOTs (Pull), and siRNA with a nonsense/scrambled sequence (control). The siRNA effectiveness to inhibit the expression of GOT1 and GOT2 was confirmed by measuring the mRNA levels (**Fig. 39e**). Then, the effect of specific GOTs inhibition on cell proliferation under NPs treatment was evaluated (**Fig. 39f**). 143B cells generally showed more sensitivity during all NP treatments, indicating that both transaminases and MCT transporters play an important role in cell survival during doxorubicin treatment. By contrast, respiration deficient cells showed to be much more dependent on GOT1 when they were treated with both single and combined NPs. Interestingly, opposite impact was observed in ρ^0206 when GOT2-specific siRNA was used together with MCT1-DOX-NP, suggesting GOT1 activity is enough to maintain protection against doxorubicin (**Fig. 39f**).

From these results, we can conclude that the doxorubicin immobilization on the polystyrene nanoparticle improves therapeutic drug efficacy, causing higher toxicity than free DOX-equivalent. Furthermore, we have demonstrated that the new keys in tumor metabolic reprogramming have to be considered as potential candidates for combined strategies, opening new window of opportunities in metabolic-based cancer therapies. At this point, many alternatives could be implemented to continue the development of these “metabolic-nanodevices”, but we aimed to explore further interesting applications taking advantage of antibodies in the nanotechnology field.

2.3. DEVELOPMENT AND VALIDATION OF MULTIFUNCTIONALIZED NANODEVICES FOR TARGETED DRUG DELIVERY SYSTEM TO TUMOR CELLS WITH SELECTIVE METABOLIC PROFILES

Given the importance of monocarboxylate transporters in respiration deficient cells or highly glycolytic-dependent cells in general, we decided to investigate whether we could take advantage from this hallmark compared with other tissues. To that end, we designed active drug delivery system using monoclonal antibodies against these proton-linked plasma membrane transporters on the nanoparticle surface to specifically target malignant cells focused on this metabophenotype. To further specificity we defined to use monoclonal antibody against CD147, targeting this ancillary protein required for the MCT1 functionality.

2.3.1. Implementation of a valid CD147-targeting system

Our first goal was to determine the basal expression of CD147 in our cell models. As was observed in MCT1 studies, a slight increase was found in CD147 expression in respiration deficient cells compared to parental cell model (**Fig. 40a**). Furthermore, CD147 expression levels were assessed in other cell lines with different metabophenotypes in order to establish controls with lower presence of CD147. Different expression patterns were observed in the non-transformed (mouse and human fibroblasts) and transformed cell lines (breast and lung cancer cells) tested (**Fig. 40a**). According to the findings, we decided to select MCF7 as tumor cell model, which shows much lower aerobic glucose consumption rates and less aerobic glycolytic-dependence (Gatenby and Gillies, 2004; Guppy et al., 2002). On the other hand, MEF was selected as absolute negative control because of amino-acids sequence that is recognized by our CD147-antibody does not resemble the mouse protein, thereby without being able to bind to the epitope.

Once negative controls were established, we wanted to validate CD147 protein expression levels by flow cytometry. The quantification of protein levels revealed similar differences between cell lines tested, verifying higher expression in p⁰206 cells compared to 143B and lower and non-existent CD147 expression in MCF7 and MEF respectively (**Fig. 40b-c**).

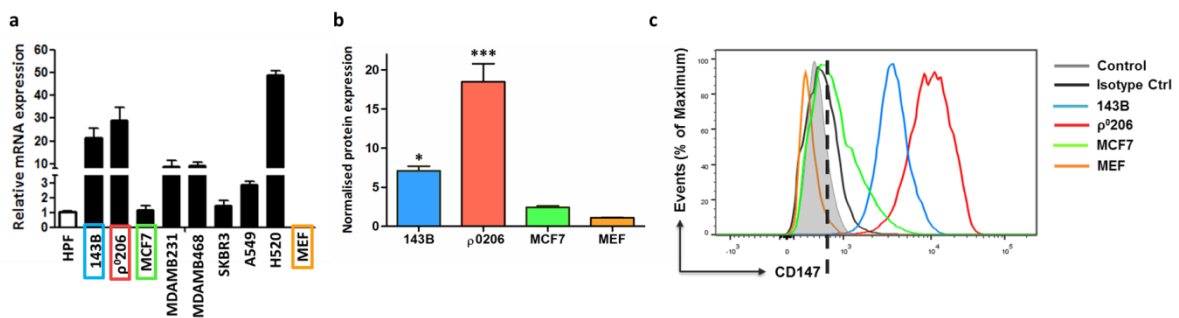


Figure 40. Characterization of CD147 expression of the different cell lines by qPCR and flow cytometry. (a) Representation of quantitative PCR analyses ($2^{-\Delta\Delta C_t}$ value) for CD147 gene expression in different non-transformed and cancer cell lines. **(b)** Protein expression levels in selected cell lines measured by mean fluorescence intensity, which correlates with the amount of CD147 protein normalised to isotype control. **(c)** Protein expression comparison of 143B and p⁰206 cells with proposed negative controls, MEF and MCF7 cell lines. t-student test performed and SEM are represented. *p value < 0.05, ***p value < 0,001.

2.3.2. Preparation and evaluation of CD147 based targeted nanoparticles.

Next, the targeted system was synthesized by conjugation of BCN-functionalized nanoparticle with azide-functionalized CD147 antibody (henceforth CD147-NP) as previously mentioned. As **Figure 41a** shows, the Cy5 fluorophore was also coupled to functionalized NP for tracking cellular nanoparticle uptake. The protocol for multifunctionalisation (see section 3.2. Multifunctionalisation strategy) established by our research group in order to conjugate firstly Cy5 and the azide-functionalized antibody in aqueous conditions was performed. Antibody coupling efficiency was certainly observed by indirect labeling using a compatible fluorochrome-labeled secondary antibody and irrelevant antibody of the same isotype as control (**Fig. 41c-d**). Furthermore, antibody integrity after azide functionalization was checked. Antibody degradation or fragmentation was not observed due to the incorporation of azide groups and total amount of functionalized CD147 was successfully bound in these conditions (**Fig. 41b**). On the other hand, antibody function was totally maintained after azide functionalization, showing intact/undamaged antigen-antibody recognition (**Fig. 41e**).

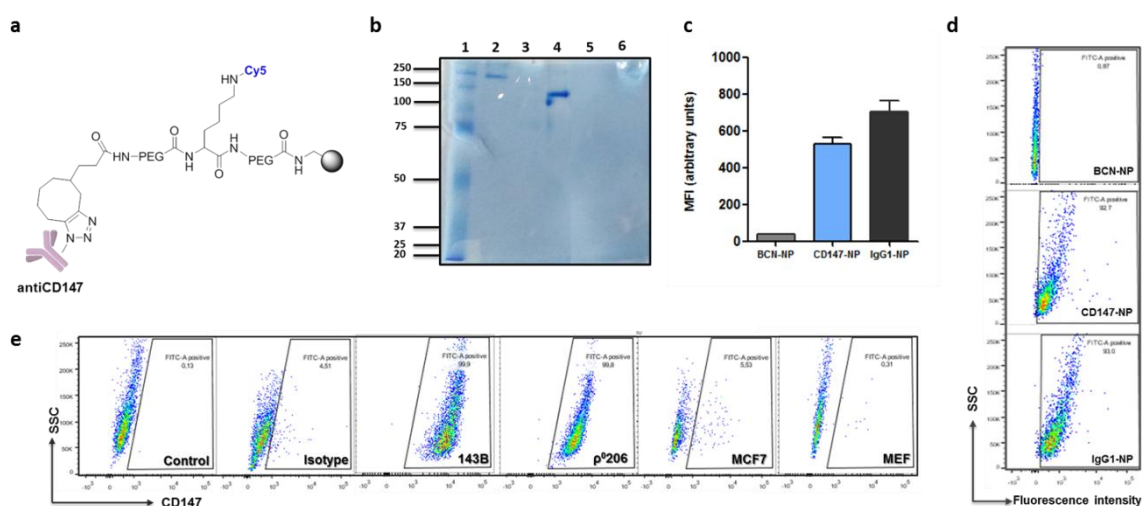


Figure 41. Development of CD147 based-targeted system. (a) Synthesis of multifunctionalized polystyrene CD147-NP (see materials and methodology section 16 for more details about reagents and conditions). Blue, Cyanine dye. **(b)** Polyacrylamide gel electrophoresis (SDS-PAGE) analysis of functionalized CD147 antibody, with protein ladder (lane 1), untreated CD147 antibody (Lane 2), flow-through from column purification of N₃-CD147 (lane 3), N₃-CD147 (lane 4) and supernatant after N₃-CD147 coupling to BCN-NP before (lane 5) and after (lane 6) wash step. **(c)** and **(d)** checking of coupling efficiency in CD147-NP and IgG1-NP compared to BCN-NP by nanoparticle incubation with conjugated secondary antibody and tested by flow cytometry **(e)** Indirect intracellular staining of CD147 in selected cell lines using functionalized anti-CD147. SSC, side scatter. MFI, median of fluorescence intensity.

2.3.3. Checking of CD147-targeting system based on metabolic phenotypes

Here we evaluated the efficiency of CD147-targeting system in cells which overexpress CD147 (143B and p⁰206 cell lines) compared to cells which have low CD147 expression levels (MCF7) and those which are not able to be recognized by our system (MEF).

Firstly, we wanted to determine which is the adequate ratio cell:NP whereby uptake differences would be measurable. For that purpose, overexpressing-CD147 cells were

incubated for 1.5 hours with different NP amounts and nanoparticle uptake was analyzed by flow cytometry. Fluorescence nanoparticles were used as a positive control of uptake ability. Interestingly, we found that CD147-NP were efficiently internalized compared to the isotype control. Further, the percentage of CD147-NP nanofected cells was gradually increased when CD147 was more plentiful, while IgG1-NP treatment remained steady in all cases (Fig. 42a).

To determine whether observed CD147-NP uptake is antigen-dependent, we compared NP internalization to control cell models (Fig. 42b-d). In accordance with their CD147 density on the cell surface, highest CD147-NP uptake was observed in ρ^0206 cells (60%), followed by 143B (50%) with a slightly significant difference. On the other hand, no antibody-mediated accumulation was observed in both MEF (20%) and MCF7 (15%) cells, showing a significant decrease in CD147-NP internalization in comparison with overexpressing-CD147 cells (Fig. 42b). These differences were also manifested when positive cell populations for antibody-coupled (CD147-NP) and uncoupled (BCN-NP) nanoparticles were displayed for each cell model (Fig. 42c). Furthermore, for the detection of non-specific cellular uptake, control nanoparticle with irrelevant antibody of the same isotype coupled was used. Non-specific uptake remained quite low in all cell lines tested. Thus, the CD147-NP uptake appears to be related to CD147 expression (Fig. 42d).

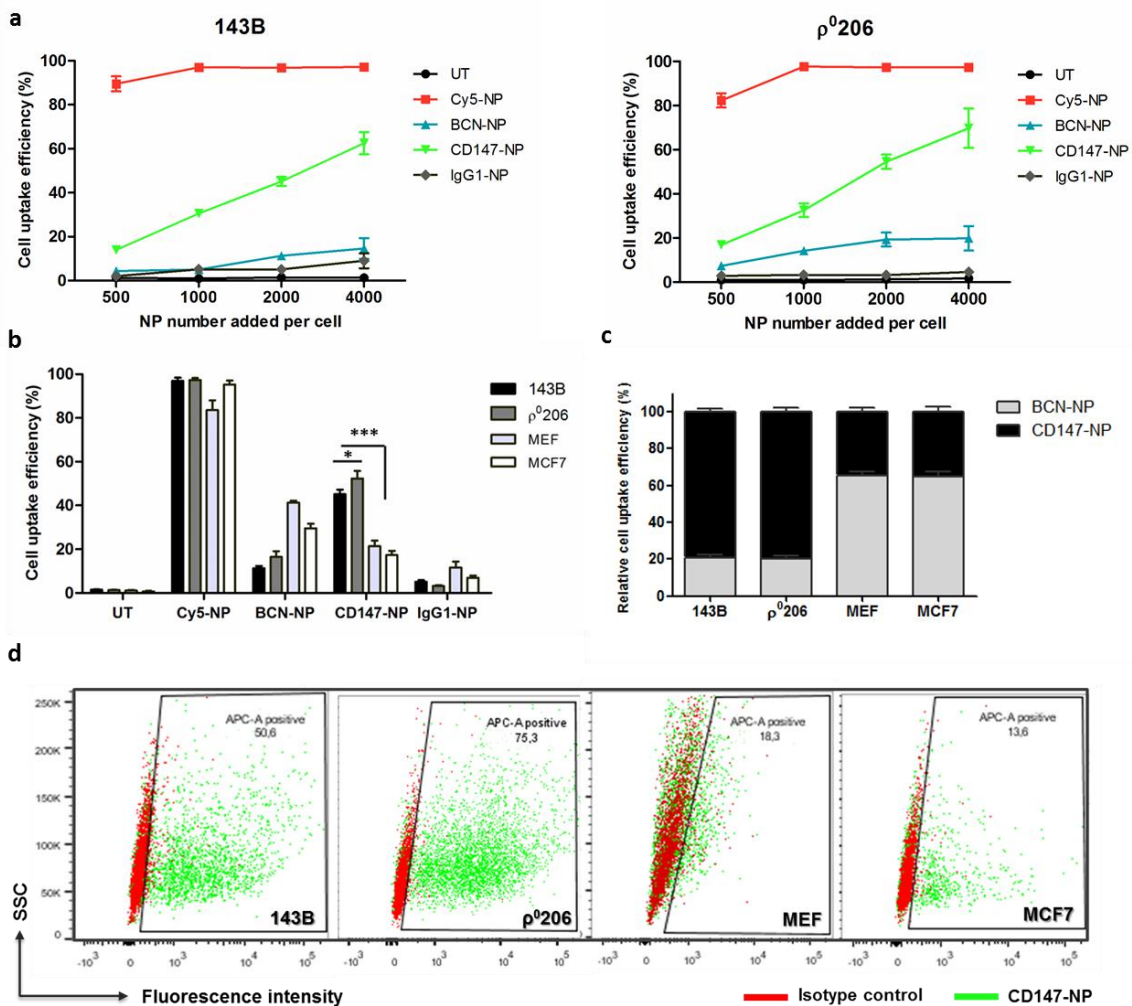
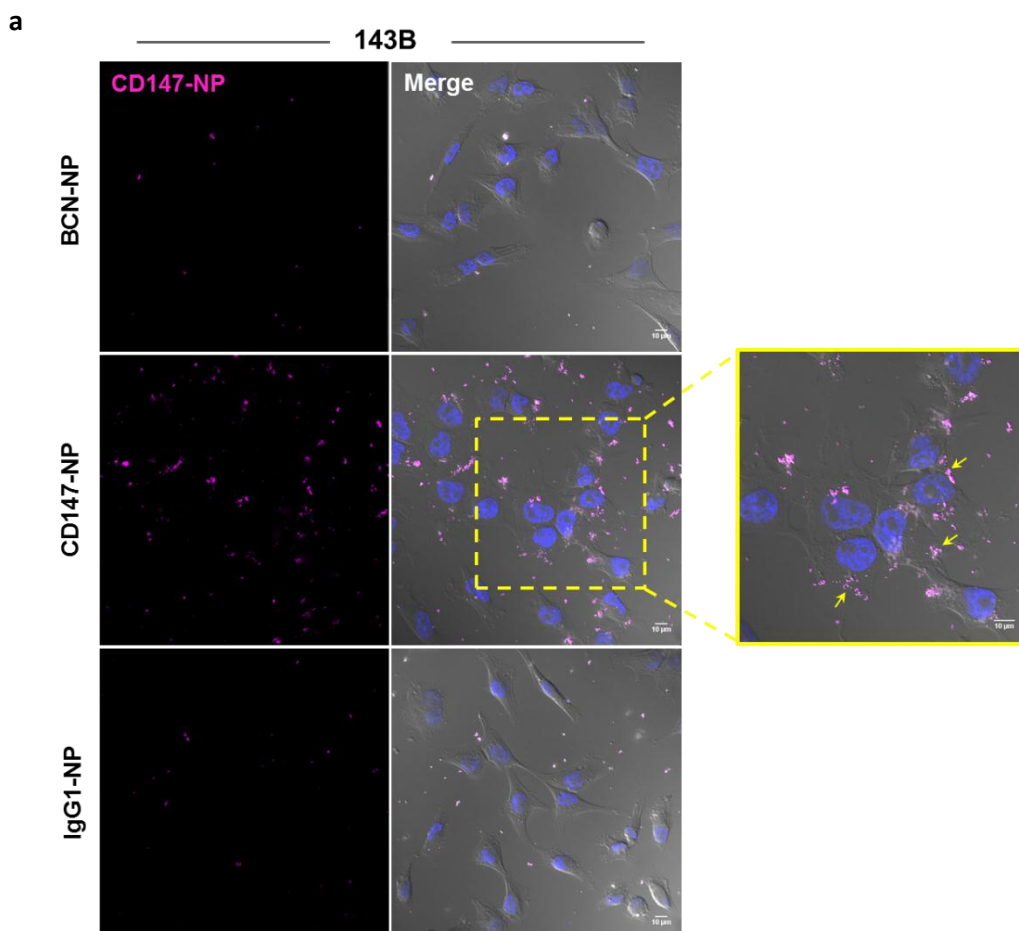
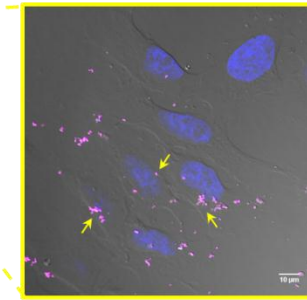
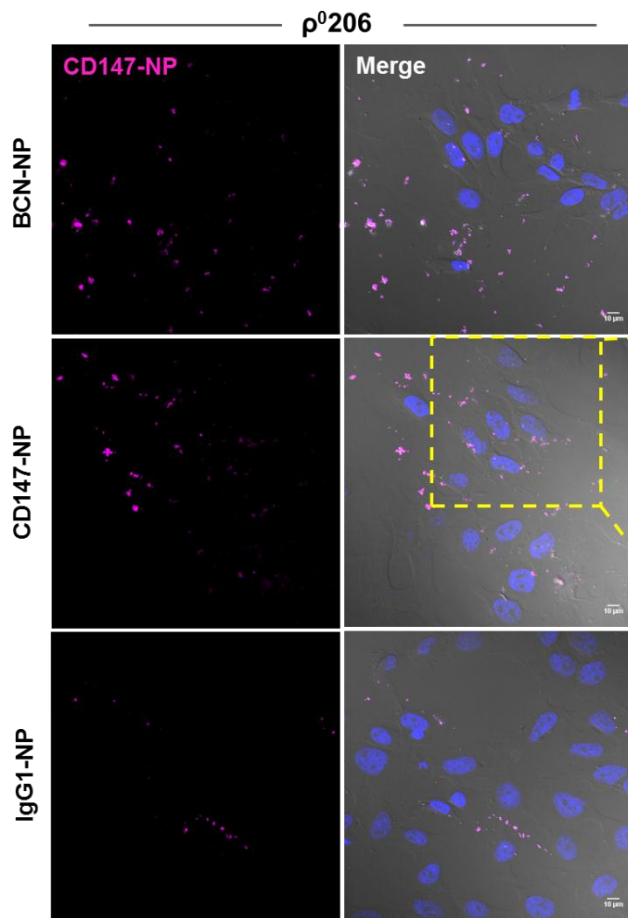


Figure 42. Cell targeting and internalization of CD147-NPs in cell culture. (a) Study of the level of NP cellular internalization versus time of incubation in overexpressing-CD147 cell models through flow cytometry. (b-d) 143B, ρ^0206 , MEF and MCF7 cell lines were incubated with 2000 NPs added per cell during 1.5 hours, and then analyzed by flow cytometry: (b) Comparison of cellular uptake efficiency of CD147-NP versus different NP controls; (c) CD147-NP cellular uptake related to uncoupled antibody nanoparticle (BCN-NP) internalization; (d) Representative flow cytometry overlaid dot plots displaying cell populations treated with CD147-NP (green) and IgG1-NP (red) as a control. Experiments were performed in quadrupled and the results are expressed as the mean \pm SEM. * $p < 0.05$, *** $p < 0.001$.

To assess the relative internalization rates of the nanoparticle formulations and their intracellular localization, additional analyses were performed by confocal laser scanning microscopy. On the one hand, intracellular CD147-NP localization in overexpressing-CD147 models was confirmed, whereas both isotype IgG1 (IgG1-NP) and unbound antibody nanoparticles (BCN-NP) were found in the extracellular space (Fig. 43a-b). In contrast, no differences in cellular internalization between all treatment tested were observed in negative controls for CD147 expression (MEF and MCF7) (Fig. 43c-d). Furthermore, to corroborate that fluorescence detected from both flow cytometry and these confocal images was generated by NPs located inside cells rather than NPs absorbed on the cell membrane, a spatial location analysis was carry out. Confocal images for three orthogonal axes of the CD147-NP uptake in overexpressing-CD147 cell lines showed entire intracellular location of these NPs (Fig. 44).



b



c

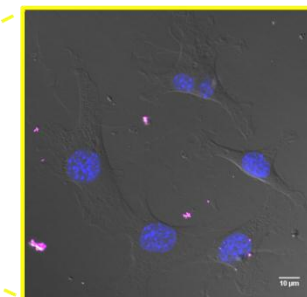
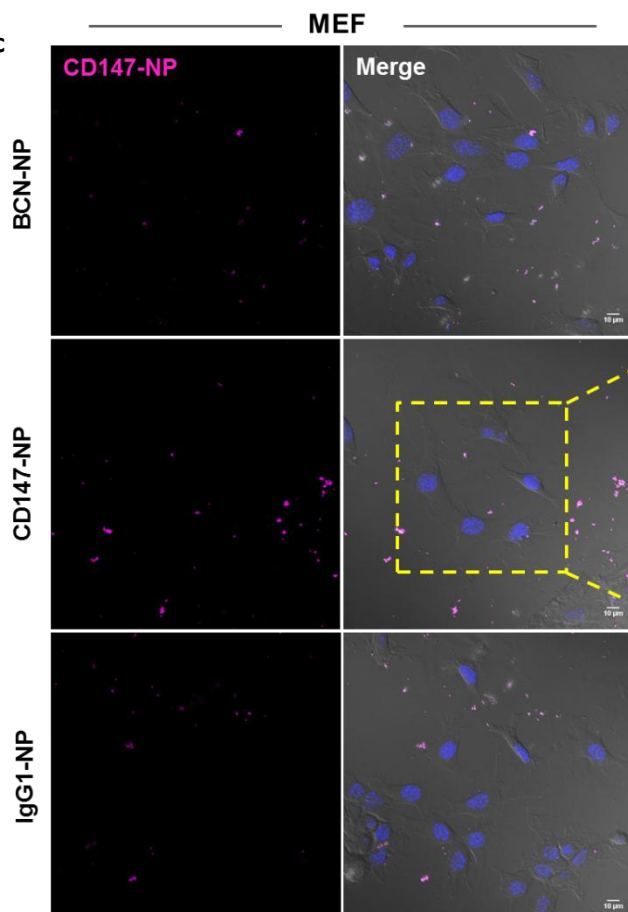


Figure 43. Confocal microscopy of the cellular uptake behavior of CD147-NP and the controls BCN-NP and IgG1-NP in (a) 143B (b) ρ⁰206, (c) MEF and (d) MCF7. 63X magnification representative images show: left panels, merge, DIC (Differential interference contrast), blue, DAPI nuclei and red, Cy5-NPs overlaid. Right panel: red channel, Cy5-NPs. Scale bar, 10 μm.

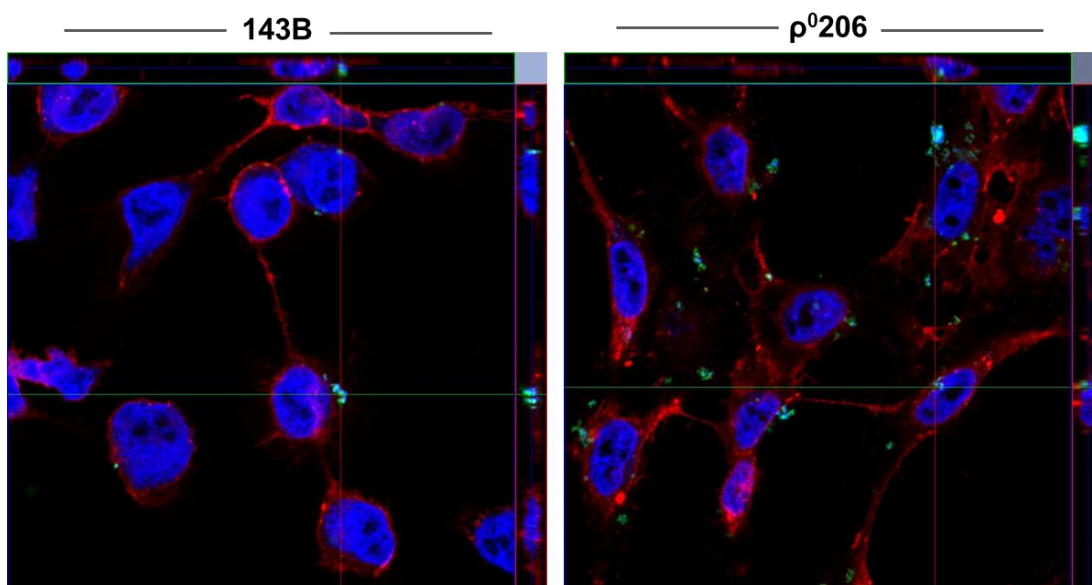
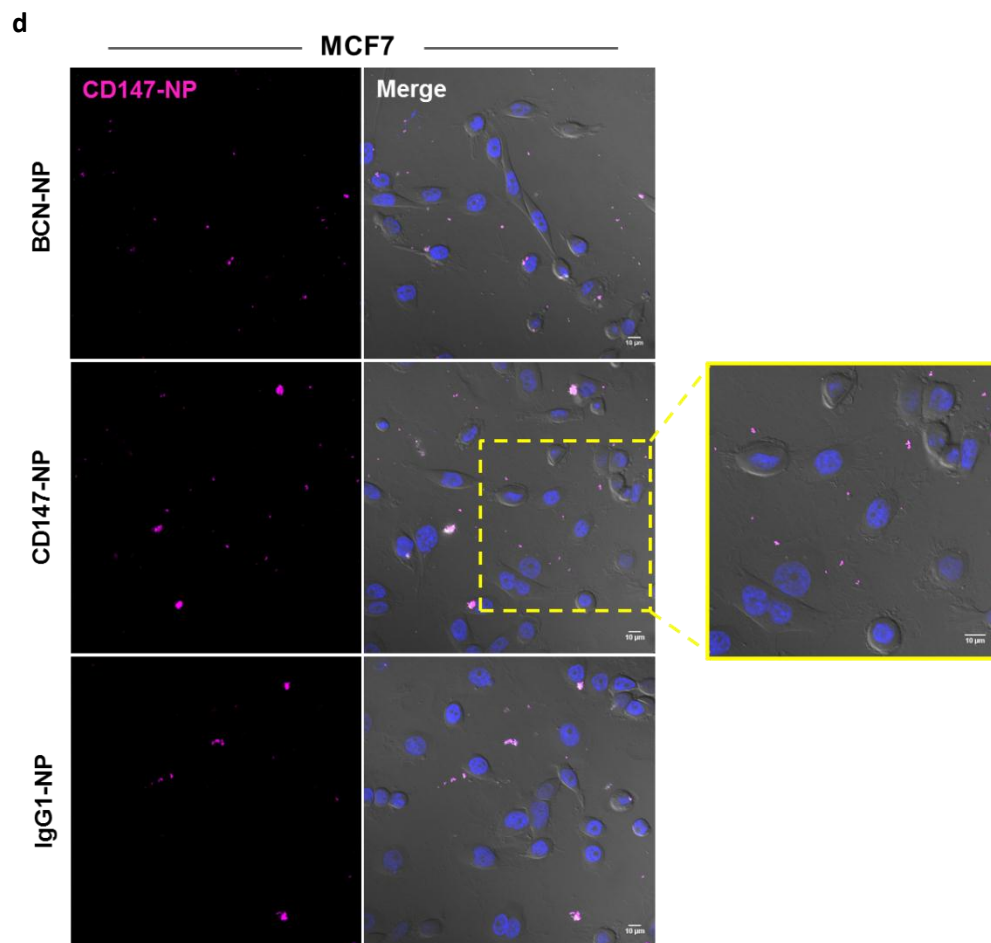


Figure 44. Orthogonal view (*xy*, *xz* and *yz*) of the confocal microscope images showing the intersection planes at the position of the yellow cross-line. Maximum intensity projection of the *z*-stack from blue (DAPI, nuclei), red (membrane labelling) and green (CD147-NP) is displayed.

Although the data reported so far suggest a selective NP uptake due to specific cell targeting, we also proceed with a deeper study that could provide more relevant information. Hence, the specificity of the cellular uptake was further investigated by competitive binding experiments with antibody in culture media solution. Cells were preincubated with anti-CD147 for 30 min (+CD147) and afterwards treated with different nanoparticles in the same conditions as in control assay (-CD147). Under the conditions of antibody preincubation, cell binding sites were effectively blocked, preventing epitope recognition from the nanodevices and thereby avoiding the CD147-NP internalization. Cellular uptake of antibody-modified nanoparticles with preincubation of anti-CD147 was reduced to same uptake levels as seen with unbound CD147 nanoparticles (IgG1-NP and BCN-NP) in overexpressing-CD147 cell models (**Fig. 45**). Furthermore, uptake levels of the rest of NPs tested remained consistent despite antibody preincubation. Therefore, taking together these data suggest that a specific and receptor-mediated binding of CD147-NP internalization can be supposed. In addition, these results led us to follow developing a selective drug delivery system using polystyrene nanoparticles.

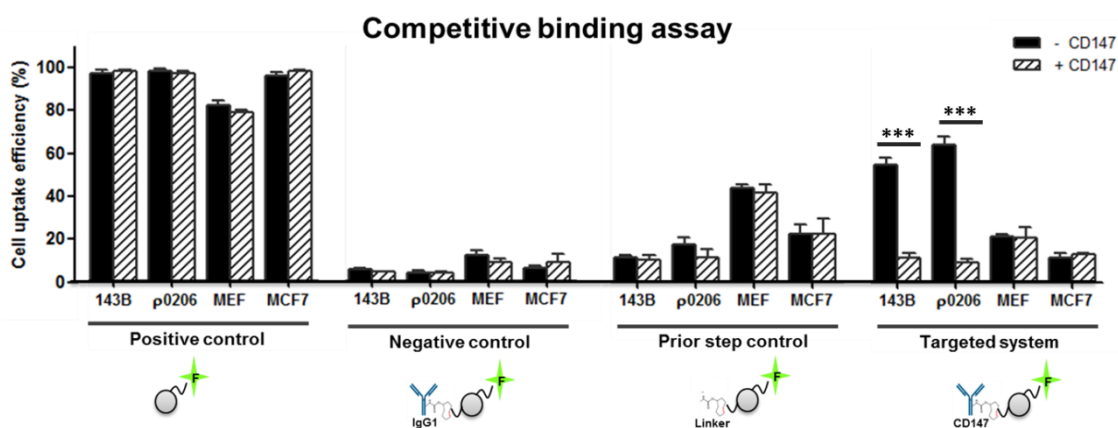


Figure 45. Competitive binding assay in overexpressing-CD147 cell models (143B and p⁰206) and negative controls for CD147 expression (MEF and MCF7). Bars show a comparison of cellular uptake of antibody-conjugated (CD147-NP), irrelevant antibody-conjugated (IgG1-NP), unbound (BCN-NP, linker) nanoparticles and Cy5-NP (2000 NPs/cell, 1.5h incubation time) with and without preincubation with anti-CD147 (0.5 µg/ml). The percentages are relativized to untreated control in each cell line. t-student test performed and SEM are represented, n= 6 samples. ***p value < 0.001.

2.3.4. Selective drug delivery system based on CD147 targeting

In addition to the previous sections, that provided a relevant contribution regarding the use of polystyrene nanoparticles as nanocarrier targeting a metabolic ligand, we finally analyzed whether these nanocarriers ensure efficient intracellular delivery of a drug. In this new approach for delivery, a multifunctionalized nanoparticle was developed, where both chemotherapeutic agent (doxorubicin) and metabolic targeting ligand (anti-CD147) are attached to the surface of the delivery vehicle (**Fig. 46a**). In this model, the nanocarrier CD147-DOX-NP will be internalized by overexpressing-CD147 cells, carrying DOX and enhancing drug permeability and retention. DOX will be release in the intracellular space due to pH-responsive hydrolysis.

In a first approach, to gain further insight into the benefit of DOX-NP release in vitro, the viable cell counts of cell models following incubation with DOX-NP and free DOX were compared using the 50% inhibitory concentration (IC₅₀) value. We found that lower doxorubicin-equivalent concentration was necessary to achieve IC₅₀ in all cell lines tested by using polystyrene nanoparticles as carrier (**Fig. 47b & Table**). Then, DOX-NP again proved greater effective cytotoxicity than free DOX in our cell models, highlighting the advantages of anticancer drugs delivery through a nanoparticle-based platform compared with traditional chemotherapeutics.

By flow cytometry and confocal microscopy, we previously demonstrated that the CD147-NP specifically binds 143B and p⁰206 cells whereas both IgG1 isotype control and antibody unbound nanoparticles scarcely exhibit cellular uptake, proving minimal nonspecific interaction. To examine the benefit of nanoparticle-conjugated DOX for cell type-specific targeting, the effective cytotoxicity against overexpressing-CD147 cancer cells versus negative expression controls (MEF and MCF7) were compared in the presence of either nanoparticle conjugated DOX or CD147-DOX-NP.

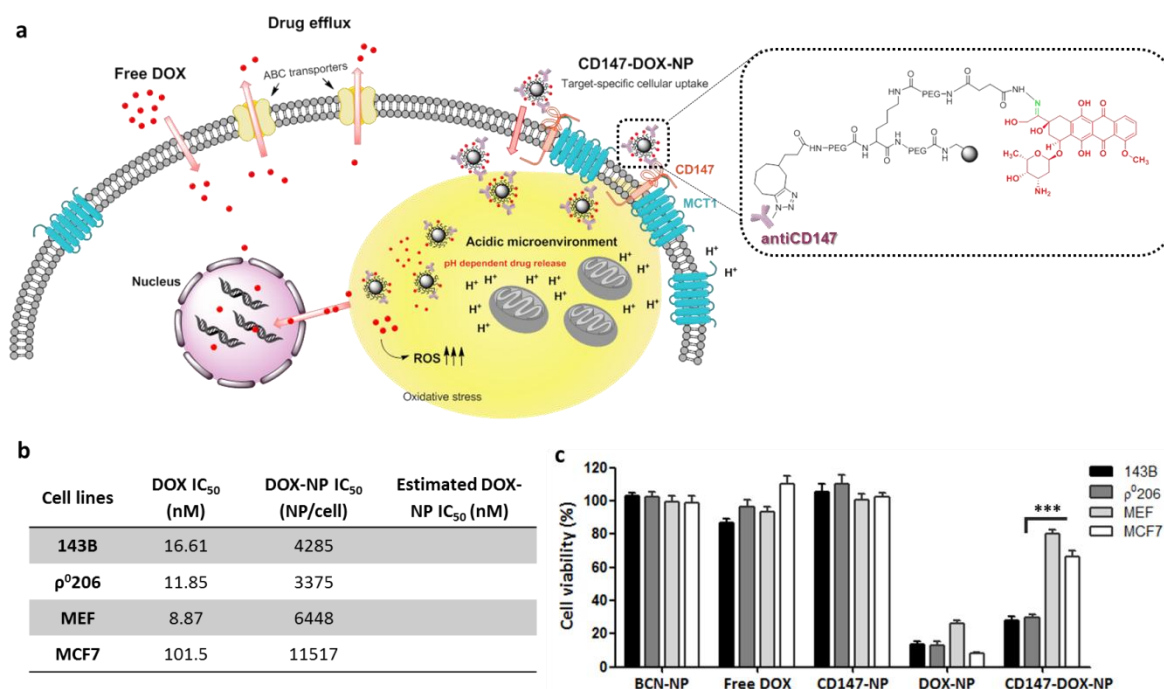


Figure 47. Multifunctionalized polystyrene nanoparticles as carrier targeted system based on metabolic phenotypes. (a) Representation of controlled drug delivery system targeting CD147 protein using polystyrene NPs versus traditional chemotherapeutic strategies. Doxorubicin (red) is coupled via pH-sensitive hydrazone linkage (green) along with polyethylene glycol (PEG), and azide functionalized anti-CD147 is coupled by click chemistry to BCN-modified nanoparticle. **(b)** Effect of free and nanoparticle-conjugated DOX (and DOX-equivalent concentration) on cell viability, presented as IC₅₀ concentration. **(c)** Cytotoxicity results for overexpressing-CD147 cell lines (143B and p⁰206) and negative controls (MEF and MCF7) incubated with 40000 NPs/cell of control NPs (BCN-NP), free DOX-equivalent concentration, CD147-NP, DOX-NP and CD147-DOX-NP.

Interestingly, the effective cytotoxicity of CD147-DOX-NP against MCF7 and MEF cells was significantly less pronounced than that against overexpressing-CD147 cells. Furthermore, DOX-NP treatment resulted in significantly reduced MCF7 and MEF cell viability relative to controls, whereas similarly treated cells were not affected by exposure to CD147-NP or free DOX-equivalent dose, maintaining the same viability as the controls (Fig. 47c). CD147-DOX-NP cytotoxicity effect due to doxorubicin release was also demonstrated as far as CD147-NP failed to trigger cell death in any cell line tested.

While DOX-NP and free DOX-equivalent dose showed similar cytotoxicity against both overexpressing-CD147 cells and negative expression control cells, the combined CD147-DOX-NP is significantly more cytotoxic against 143B and p⁰206 cells than MEF and MCF7 cells, suggesting the benefit of nanoparticle-conjugated DOX for cell type-specific targeting. Therefore, this observation in combination with the results of the present study shows, that the proposed antibody-modified nanoparticles hold promise for a specific metabolic cell targeting in combination with an effective intracellular drug delivery.

DISCUSSION

The major disadvantage of many antitumor drugs is that they are usually impaired or exported before targets have been reached. Because of that, heavy concentrations are necessary to manage antitumor effect, and consequently triggering high toxicity, which often leads to serious side effects. A prominent approach to reduce undesired effects is to use a drug carrier system, typically nanoparticles or liposomes, to selectively transport the drug to the target organ or cell type. Successful drug targeting results in a lower dosage required to achieve a therapeutic response, and as a result side effects are reduced by decreasing drug load in non-target tissues. The objective of this second part was to develop metabolism-based cancer therapy in order to provide alternatives to existing treatment that prevent these undesired effects.

Polystyrene nanoparticles have been chosen as nanosystem model in this thesis due to the fact that efficient conjugation of bioactive molecules of different nature can be achieved without damage of the transported biological material and, additionally, due to the efficient cellular uptake and easy detection by fluorescent based techniques without altering cell viability. These NPs have been shown to be “engulfed” via a passive but rapid mechanism and transported throughout the cell (Alexander et al., 2010), proving to be efficiently internalized. Moreover, they provide a reliable way to perform long-term cell tracking and imaging such as monitoring of enzymatic activity (Cárdenas-Maestre et al., 2014) or drug delivery (Gregori et al., 2015). Thus, polystyrene nanoparticles have been widely used by our research group on probing, detecting, imaging and drug delivery system *in vitro* and *in vivo* (Alexander et al., 2009; Borger et al., 2011; Sanchez-Martin et al., 2013, 2009b; Tsakiridis et al., 2009). Regarding our cell line models, efficient uptake of multifunctionalized polystyrene nanoparticles was demonstrated. In fact, respiration deficient cells showed to be more permissive of the nanofection, displaying a lower MNF50 than parental 143B. Thus, nanoparticle internalization seems to be cell line-dependent, suggesting the need to carry out exhaustive studies of cellular uptake in comparative cellular models or tissues. Nevertheless, monodispersed labeled

populations regardless of cell type could be achieved in nanoparticle saturated ratios. Additionally, cell viability after incubation with polystyrene NPs was completely comparable to control untreated cells even in saturation conditions. Importantly, the total lack of cytotoxicity in nanofected cells reinforced that such NPs are efficient biocompatible cellular release devices.

The anticancer drug doxorubicin has been widely used in clinical for treatment of a variety of tumors. However, its toxicity to healthy tissue and the development of multidrug resistance during prolonged treatment have limited its therapeutic use, preventing treatment at high dosages (Persidis, 1999). Therefore, in recent years, significant efforts have concentrated on nanoscale delivery systems of DOX such as DOXIL[®], a clinically approved nanodrug for the treatment of refractory ovarian (Barenholz, 2012). Accordingly, we expected to validate polystyrene nanoparticle as controlled drug delivery system through *in vitro* optimization of DOX conjugation and release. For delivery into recipient cancer cells, DOX was effectively conjugated via pH-sensitive hydrazone linkage as already reported (Patil et al., 2012; Ulbrich et al., 2004) and successfully cleavage was proved. This hydrazone bond used as cleavable linker for stimuli-responsive depending on pH takes advantage of high glycolytic-dependent cells. Activities of various metabolic pathways, such as generation of lactate owing to the ATP production in the cytoplasm by glycolysis, tend to acidify the cytoplasm (Casey et al., 2010), thereby promoting ideal microenvironment to release DOX intracellularly. In addition, DOX-NPs were found stable under physiological conditions and higher treatment efficacy than free DOX-equivalent was demonstrated. Unfortunately, evidences suggest that coupled DOX was not fully released, although obtained free amount showed to successfully inhibit *in vitro* cancer cell growth of several carcinoma cell lines. Percentage of drug release could be improved since polystyrene nanoparticles allow for using many further alternative chemical bonds. PS nanoparticles could be tested as a delivery system, able to be transported inside cell models with remarkable efficacy.

Trying to improve targeted metabolism therapies, we combined traditional DOX treatment with antibody-based therapy against MCT1 using multifunctionalized nanoparticles. In the single therapy, we observed that respiration deficient cells were partially susceptible to MCT1-NPs, according to higher expression of MCT1 transporter found in these cells. In addition, to improve our results in anti-MCT1 therapy, alternative strategy could be to design new antibodies raised against aspartate and arginine residues (D302/R306), which mapping within domain of MCT1 of human origin and are present as an ion pair in the channel. These residues are involved in the translocation cycle and known to be essential for the catalysis activity (Halestrap, 2012). Further studies are needed to determine the action mechanism by which the viability disruption is obtained in order to properly convey the potential of this therapy to other key transporters in tumor metabolism, such as glucose or glutamine transporters (Yoshida, 2015). On the other hand, anti-MCT1- DOX NPs combined therapy was not as effective as DOX-NPs, suggesting possible steric hindrance to the DOX release or even lower DOX loading due to the presence of the coupled-antibody.

In this regard, given that suppression of GOT1 enhances the anticancer efficacy of doxorubicin by lack of recover drug-induced oxidative stress (**Fig. 48a**) (Yang, 2016), we approached alternative combinatory therapy by targeting GOT1 in 143B and p⁰206. In accordance with this

previously reported study in triple-negative breast cancer, our results confirmed that silencing of GOT1 increased DOX-NP efficacy in GOT1-dependent cells. Surprisingly, increase of DOX-MCT1-NP efficiency was observed during GOT1 knockdown, suggesting that pyruvate import impairment enhances doxorubicin sensitivity. More interestingly, cells became much more sensitive to MCT1-NP treatment under GOT1 inhibition (in 143B even during GOT2 suppression), thereby confirming the key role of pyruvate to sustain proliferation when aspartate transamination is disrupted. Accordingly, given the importance of GOT1 in respiration deficiency metabolism, future approaches could be oriented towards the conjugation of DOX or anti-MCT1 therapy and siRNA targeted against GOT1 as described by our group (Alexander et al., 2009), to treat tumors with respiration deficiency phenotype.

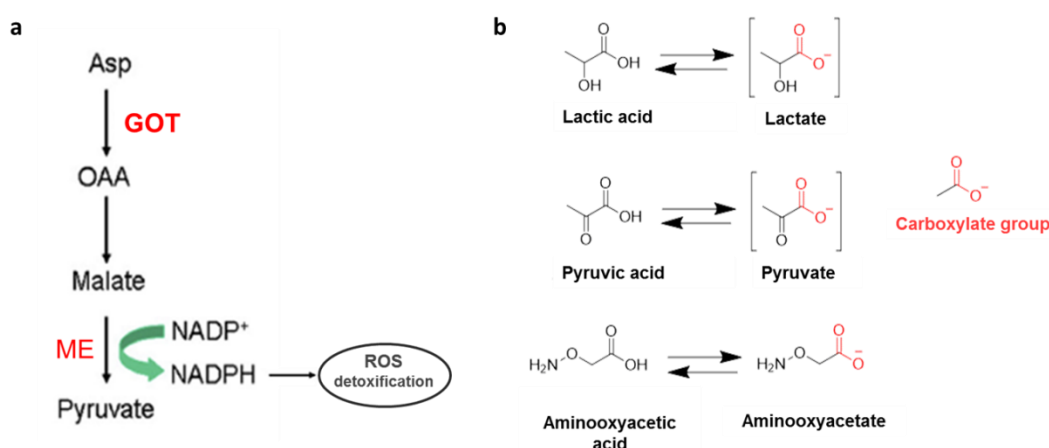


Figure 48. Inhibition of GOT1 as an alternative combinatory therapy using multifunctionalized nanoparticles. (a) Schematic representation of GOT1 signaling adapted from (Yang, 2016). Gln, glutamine; Asp, aspartate; OAA, oxaloacetate; ME, malic enzyme. **(b)** Carboxylate group presents in AOA makes it susceptible to be transported as is the case of pyruvate and lactate.

To further validate the increased efficacy of doxorubicin following GOT1 knockdown, enzymatic inhibition by AOA was assessed under different NP treatments. No significant differences were found when AOA was present. Further studies should be carried out in the future to validate the use of GOT1 as an alternative therapy.

Multifunctionalized DOX conjugated immuno-nanoparticle represents a valid method for targeted co-transport of chemotherapeutics and antibodies. Therefore, this nanotechnology based approach allows to combine specific tumor targeting with selective drug delivery. As already introduced, the specific metabolic targeting of cancer cells will be a breakthrough in cancer therapy. In an attempt to formulate a carrier system for site-selective delivery, fluorescent polystyrene nanoparticles capable of targeting highly glycolytic-dependent cells, such as 143B and p⁰206, were developed. For this purpose we applied a monoclonal antibody which specifically recognizes the CD147 subunit of MCT1 transporters, overexpressed by cells with this phenotype (Le Floch et al., 2011). A novel strategy for attaching antibodies to nanoparticles was successfully applied. The conjugation of anti-CD147 on the nanoparticle surface, its stability and recognition properties were tested, proving the effectiveness of this carrier system for targeted delivery. To know the number of antibodies that cover the

nanoparticle surface was not as important as to determine the efficiency of recognition of the antigen, since some of them after coupling may be misguided in their own bonding and hidden areas of antigen binding (Jazayeri et al., 2016). Both flow cytometry and confocal microscopy results verify the specificity and the biological activity of this novel nanoparticle system, since unspecific IgG1-modified nanoparticles did not show cellular internalization. Additional competitive binding assay demonstrated remarkable increment of the specificity cellular uptake in 143B and p⁰206 compared to negative controls due to the overexpressed CD147 on the cytoplasmic membrane of these cells.

Even more interesting results have been obtained with DOX and CD147 antibody combination conjugated to nanoparticles. These CD147-DOX-NPs were specifically internalized by CD147 overexpressing cancer cells (143B and p⁰206) inducing cell death through DOX release, while viability of cells without CD147 expression (MCF7 and MEF) was entirely maintained with due to a much lower affinity for CD147-DOX-NP. Additionally it is remarkable the fact that a dramatic effect in cellular viability of negative controls (MCF7 and MEF) was effectively observed during DOX-NP treatment. This finding suggests that the presence of antibody used here addressed the drug only to the cells overexpressing CD147, so targeted delivery of the drug is accomplished. Hence, the results presented in this section demonstrate the proof of concept for the feasibility of the drug-conjugated polystyrene nanoparticles using to deliver anticancer drugs selectively. Because of new generation liposomes showed only comparable or even poor therapeutic efficiency referred to free drug or conventional vesicles in clinical trials (Chang and Yeh, 2012), we believe these polystyrene nanoparticle are a promising tool for efficient targeted drug delivery. Due to the antibody directed specificity of the nanoparticles, our novel drug carrier system could be more efficient compared to the current available PEGylated liposomal doxorubicin carrier (Doxil or Caelyx). Additionally, these nanoparticles show a higher loading capacity with a lower tendency of drug leakage than liposomes, besides a better stability (Anhorn et al., 2008).

On the other hand, drugs bound directly to antibodies without using nanoparticles or intermediates have been already tested. In that case, antibodies themselves can be used as drug-carrier systems (Peters and Brown, 2015). Nevertheless, linking of several drug molecules to an immunoglobulin may result in a loss of antibody activity. In addition, multifunctionalization to combine more therapies is also limited. These problems can be solved by conjugation of antibody and drug simultaneously to carrier systems such as nanoparticles.

The treatment with monoclonal antibodies recognizing tumor-associated markers is a common strategy in cancer therapy. To date, efforts to address nanoparticle formulations concerning to drug targeting ligands have been focused mostly on EGFR and HER2 (Anhorn et al., 2008; Gerber, 2008; Master and Sen Gupta, 2012). However, we provided a novel approach based on targeted ancillary protein CD147/Basigin, which is required for monocarboxylate transporters functionality. Overexpression of this protein is strongly needed in tumor cells with aggressive glycolytic phenotype, which makes it an interesting key target to develop promising alternative nanocarriers. Thus, an active targeting with the advantage of an efficient accumulation of drugs in target cells has been achieved.

This study provided a proof-of-concept that CD147-NPs used in conjunction with antitumor drug can provide the ability to target tumors with a predominant glycolytic phenotype in a robust manner. We expect that the DOX-functionalized nanoparticles together with anti-CD147 chemically conjugated on the nanoparticle surface may prolong the circulation time, reduce DOX systemic toxicity, and facilitate active targeting, thereby making the formulation a therapeutically effective platform for *in vivo* application. Thus, we can conclude that we have developed a novel specific drug carrier system, which allowed us a specific transport of doxorubicin to CD147 overexpressing tumor cells. Accordingly, a reduction of the dosis of doxorubicin required in cancer therapy is presumed, triggering consequently a reduction of the drug secondary side effects.

At this point, we require more analytical work to understand which metabolic pathways are activated in different tumor types, so that we can more efficiently identify new tumor targets, novel ligands, and new strategies for targeting that are efficacious and specific for tumors with minimal toxicity for normal tissues.

AIM 3. DEVELOPMENT OF AN EFFICIENT NANOTECHNOLOGY FLUORESCENCE-BASED METHOD TO TRACK CELL PROLIFERATION.

RESULTS

Herein, we present a novel approach to monitor cell proliferation based on the use of fluorescent bifunctionalized crosslinked polystyrene NPs. The alternative method is inspired by the use of cell-labelling dyes to quantify cell proliferation by fluorescence techniques but avoiding the limitations of the mentioned dyes by applying nanotechnology. We focus on the optimization and validation of this novel method using different cell lines. Furthermore, a protocol for monitoring cell proliferation in a long-term assay has been successfully established.

3.1. OPTIMIZATION OF A NOVEL NANOTECHNOLOGY APPROACH TO TRACK CELLULAR PROLIFERATION BY FLOW CYTOMETRY USING FLUORESCENCE LABELLED NANOPARTICLES

3.1.1. Generation of fluorescence nanoparticles

A monodispersed population of 200 nm amino functionalized cross-linked PS-NPs (PDI 0.089) ((1) **Fig. 49a**) was obtained by dispersion polymerization as previously described (Unciti-Broceta et al., 2012a). NPs were firstly functionalized with a polyethylene glycol (PEG) spacer PEGylation of PS-NPs ((2) **Fig. 49a**), following a Fmoc solid phase protocol and using Oxyma/DIC as coupling reagents. This PEGylation increases the biocompatibility of the NPs, thereby facilitating their transport across cell membranes. The NPs were bifunctionalized following an orthogonal strategy based on the use of 1-(4,4-dimethyl-2,6-dioxacyclohexylidene)ethyl (Dde) and Fluorenylmethyloxycarbonyl (Fmoc) protecting groups (Díaz-Mochón et al., 2004). This bifunctionalization allowed the labelling of the nanoparticle by conjugation of a near infrared fluorophore (Cy5) (activated as NHS ester) while keeping a defined amount of free amino groups to keep the positive surface charge of the nanoparticle. The stability of these nanoparticles upon different temperatures was confirmed. These nanoparticles were stable at storage conditions (4°C, 2% solid content in water) and also at conditions of cell incubation (37°C in culture media supplemented with serum) (**Fig. 49d-e and, Table 4**) (more details of synthesis, characterization and stability studies in materials and methodology section 16).

Considering the requirements of fluorescent dye labelling procedures, the number of fluorescent NPs per cell and the incubation time required for obtaining a 100% of nanofected cells were calculated. Firstly, the number of fluorescent NPs per μL was calculated using a spectrometric based method recently reported by our research group (Unciti-Broceta et al., 2015).

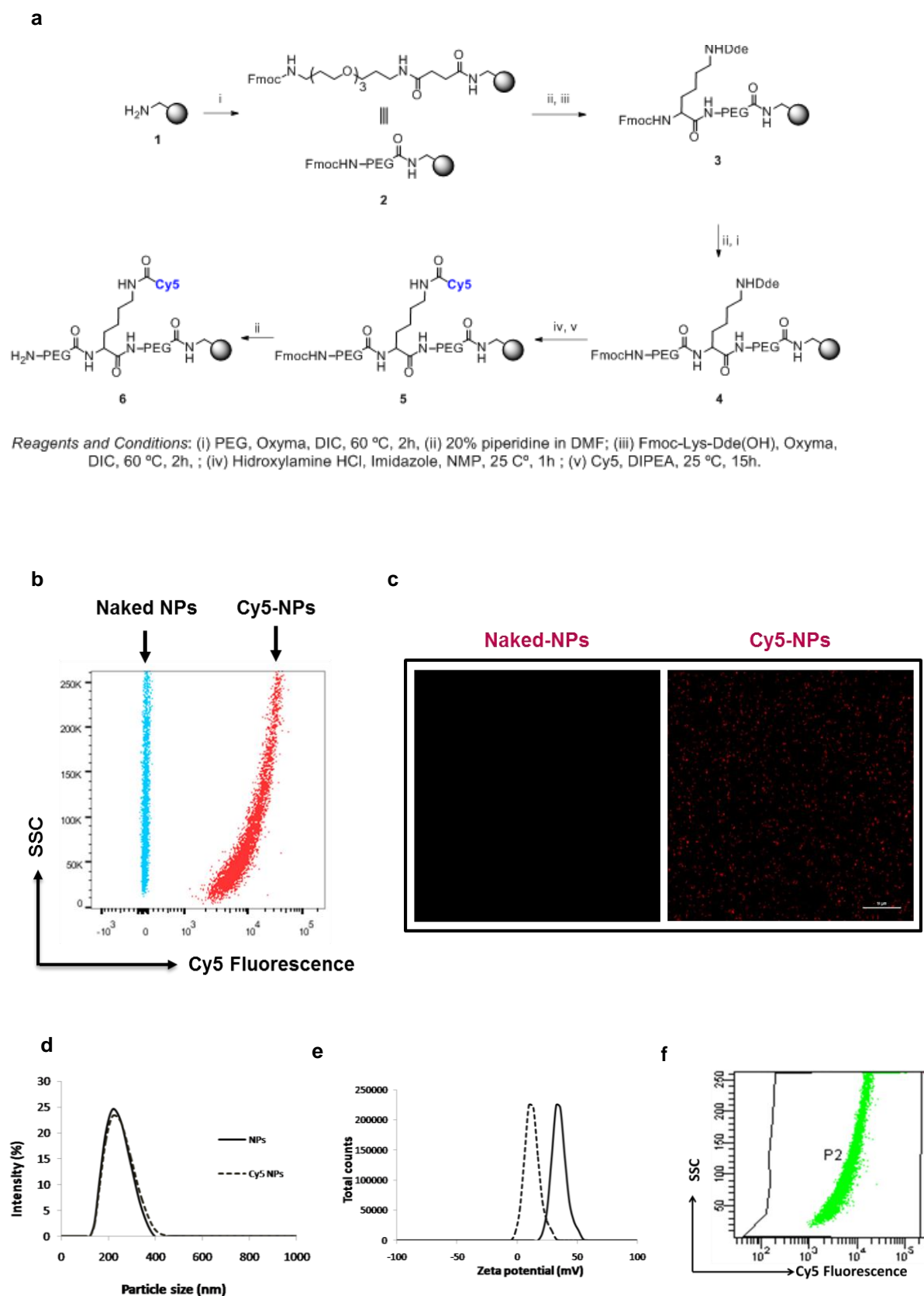


Fig. 49. Fluorescence nanoparticles synthesis and characterization. (a) Schematic synthesis of fluorescence NPs. Abbreviations: PS, polystyrene; PEG, Fmoc-1-amino-4,7,10-trioxo-13-tridecamine succinic acid, polyethylene glycol; NP, nanoparticle. **(b)** Representative overlay dot plot obtained after flow cytometry analysis of naked NPs (blue) and

Cy5-NPs (Red). (c) Confocal fluorescence microscopy of naked NPs and Cy5-NPs. DIC, Differential Interference Contrast. Scale bar, 10 μ m. (d) Particle size distribution (nm) and (e) Zeta potential values of amino NPs (NPs) and Fluorescent labelled amino NPs (Cy5 NPs). (f) Flow cytometry analysis of Cy5-NPs suspended in culture media supplemented with serum after 7 days incubated at 37°C. SSC, side scatter.

Time (days) 37°C	Size (nm)*	PDI	Zeta potential (mV)
0	205.6	0.051	19.3
1	206.1	0.069	18.9
2	202.3	0.087	19.6
3	204.9	0.102	17.8
4	205.1	0.056	18.5
5	202.9	0.075	19.1
6	206.8	0.098	18.4
7	205.4	0.063	19.7

* Dynamic Light Scattering analysis

Table 4. Study of stability of Cy5-NPs suspended in culture media supplemented with serum versus time (temperature 37°C). The *in vitro* stability studies show that, the Cy5-NPs were highly stable under the experimental conditions adopted. PDI: polydispersity index.

3.1.2. Optimization of Cy5-NP labeling

To optimize cellular uptake, three different ratios of fluorescent NPs per cell (1:12500, 1:25000 and 1:50000; cells: fluorescent NPs) were interrogated at a fixed incubation time of 60 minutes using human breast cancer cell lines: MCF-7, MDA-MB-468 and MDA-MB-231. Following incubation, cells were analyzed by flow cytometry and the percentage of cells which are nanofected -nanofection percentage- was calculated (**Fig. 50a**). The data show that although there are high percentage of cells nanofected in all tested conditions, the required 100% value was reached when using the 1:25000 ratio (cell:fluorescent NPs). Although 100% of cells are nanofected at one point, NPs uptake continues and the nanofection load increases proportionally to the number of NPs. For this reason, an analysis of the median of fluorescence intensity increments (Δ MFI=MFI nanofected/MFI non-nanofected) was performed to obtain information about nanofection load (**Fig. 50b**). This analysis reveals that the larger the number of NPs, the greater the cellular uptake. It observes that the increase of the nanofection load - Δ MFI units- is doubled when the fluorescent NPs per cell is doubled (**Fig. 50b**). This feature allows controlling nanofection loads which is crucial to determine the labelling incubation times. As expected, the uptake capability -nanofection load- of the different cell lines differ between them so these times need to be adjusted for each cell type.

To further optimize the nanofection protocol, we performed a deeper study of the nanofection behaviour in a time course assay to determine the influence of the incubation time. We analyzed the nanofection percentage and nanofection load at different established time points (10, 20, 30, 40, 50, 60 and 75 minutes) using the ratio 1:25000 (cell:fluorescent NPs) (**Fig. 50c,d**). The Δ MFI analysis shows that the phenomenon of doubling nanofection load also occurs when the time is doubled (**Fig. 50c**). On the other hand, after 30 minutes of incubation, the 100% of all adherent cell lines were nanofected (**Fig. 50e**). The proportional increase of the nanofection load relative to the incubation time confirms the possibility to control the specific value of Δ MFI units obtained also changing the incubation time.

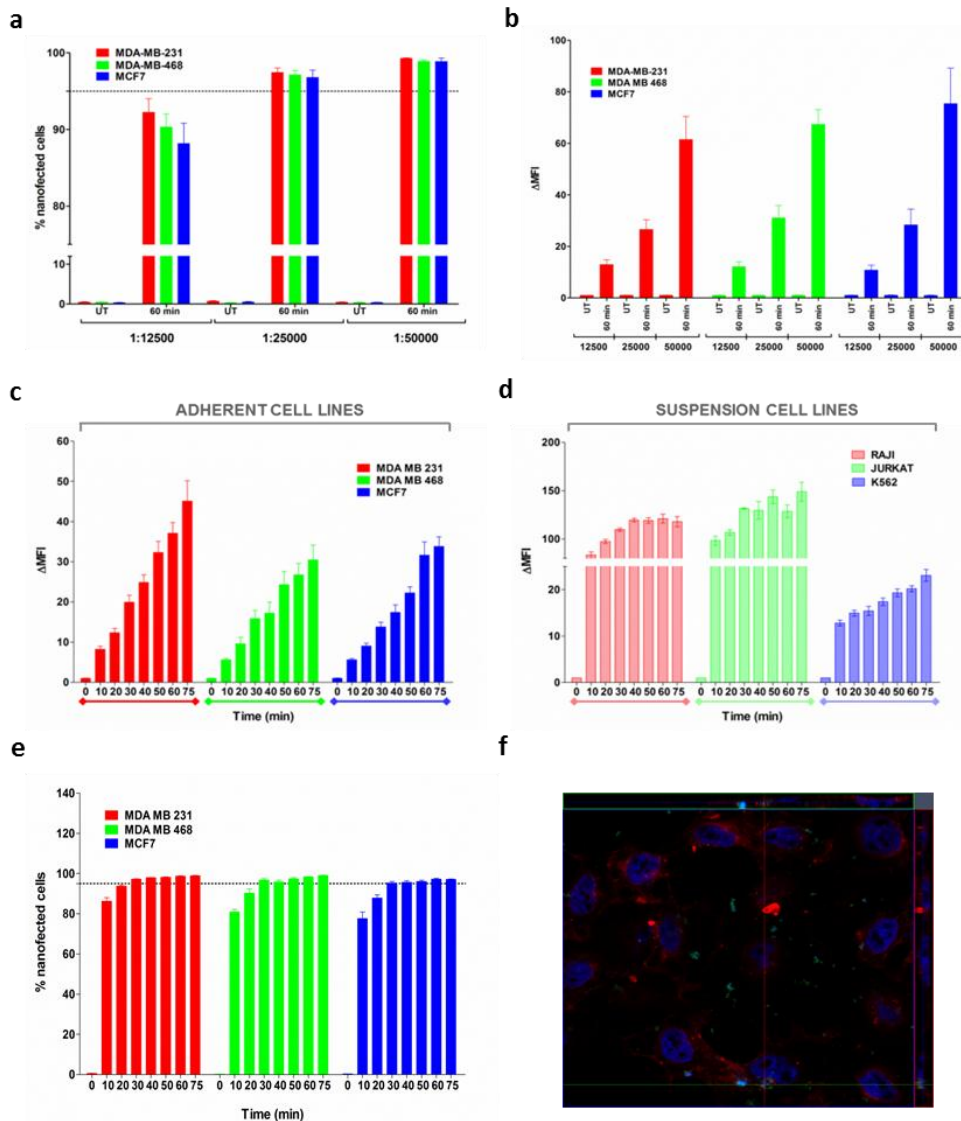


Figure 50. Figure 1. Optimisation of the nanofection method in the different tested cell lines. (a) Analysis of Cy5-NPs cellular uptakes by MDA-MB-231 (red), MDA-MB-468 (green) and MCF7 (blue). Cy5-NPs, at different ratios per cell, were incubated and analysed by flow cytometry and percentage of cells containing Cy5-NPs is displayed. Saturation percentage is represented above dotted line. **(b)** Study of median of fluorescence intensity increments (Δ MFI) at different Cy5-NPs ratios per cell (12500, 25000 and 50000) compared to cells without NP-treatment. Values for cells incubated with Cy5-NPs for 60 minutes and untreated cells (UT) are shown. **(c,d)** Study of median of fluorescence intensity increments (Δ MFI) at different incubation time points. **(c)** Strong colours panel shows results for adherent cell line models and **(d)** light colours panel represents suspension cell line models. **(e)** Analysis fluorescence-NPs cellular uptakes by adherent cell lines at different time points. Percentage of cells containing Cy5-NPs versus cell to Cy5-NPs ratio is displayed in a bar representation to compare cellular uptake. >95% of Cy5 positive cells was reached at 30 minutes from 1:25000 ratio (cell: Cy5-NPs), represented by dotted line. Results are expressed as mean \pm S.E.M. **(f)** Representative confocal section image and orthogonal projections of MCF7 to analyze Cy5-NPs cellular uptake. Channels (red, PKH26 Red Fluorescent Cell Linker -membrane stained-; blue, DAPI -nuclei-; and green, Cy5-NPs).

Once this method was optimised with adherent cells, human erythroleukemic cell line K562 was used as suspension cell model in order to evaluate the options of the method. Results obtained with K562 presented the same features as when using adherent cells in terms of nanofection load and percentage (**Fig. 50d**). Furthermore, to verify the feasibility of this

method, suspension hard-to-transfect cells, such as lymphoma cell lines Jurkat and Raji, were evaluated. Proportional increase of the nanofection load related to incubation time was also shown (Fig. 50d). In both cases, the best ratio cell:fluorescent NPs was 1:25000 and optimum incubation time was 30 minutes. To corroborate that fluorescence detected by flow cytometry was generated by NPs located inside cells rather than NPs absorbed on the cell membrane, a confocal microscopy analysis was carry out. Confocal images for three orthogonal axes of the nanoparticle uptake are shown in figure 50f, noting the intracellular location of these NPs.

An important aspect to keep in mind when developing methods for proliferation monitoring is their potential cytotoxicity. The cell cycle was evaluated by flow cytometry following propidium iodide staining. Evidence of cell dead was not observed in any cell line (Fig. 51a). None of them presented a significant increment in the subG1 population after NPs treatment, showing any toxic effect. Instead, perfect matches between cell cycle profile of untreated and nanofected cells were observed after seven days of incubation. There is not a significant difference between the percentage of cells in each phase of the cell cycle in any condition ($p < 0.05$) (Fig. 51a-b). Additionally, a long-term tetrazolium-based toxicity assay to assess mitochondrial function was performed in NP treated cells compared to untreated cells using two different NP:cell ratios. Same proliferation level was maintained in all conditions tested and no substantial metabolic changes due to NP treatment were observed (Fig. 51c). These results suggest that nanofection load can be controlled in a robust manner through concentration and incubation time and cell-NP interaction does not adversely affect cell viability.

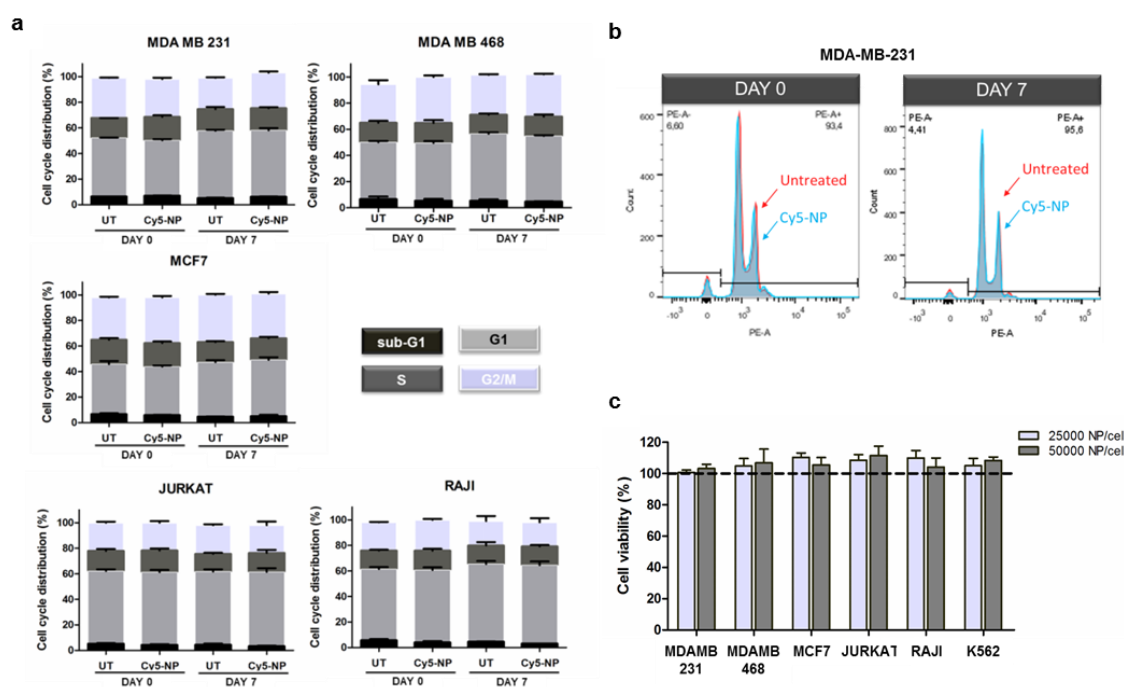


Figure 51. Effect of NP treatment on cell viability and proliferation during time course experiment. (a) Cell cycle distribution in cell lines before and after long term nanoparticle incubation. The percentages of cells in different phases of the cell cycle were determined from the histograms by flow cytometry. Adherent cell lines (upper and middle panels) and suspension hard to transfect cell lines (lower panels) were tested. Graphs summarize data from initial (Day 0) and final (Day 7) experimental time points. Bars represent mean \pm SEM of results from 3 independent experiments with duplicated points. UT: untreated cells. Cy5-NPs: fluorescence nanoparticles. **(b)** Ploidy histogram of the relative DNA content was determined in cells incubated with NPs (blue) compared with untreated cells (red).

Cell cycle profiles showed identical viability in cells with and without NP treatment. Figure shows a representative adherent cell line (MDA-MB-231). Identical effect was observed in the rest of the cell lines tested. **(c)** Proliferation of NP treated cells (1:2500 and 1:5000 NPs added per cell) referred to untreated cells (100%) measured in adherent and suspension cell lines.

3.1.3. Predictive calculation of optimum range of nanofection

In this study, Δ MFI analysis revealed that median of fluorescence intensity decreases over time, and importantly this empirical observation was evident in all cell lines tested. Surprisingly, this fluorescence decay was differed dependent on cell line. These data supported possibility of use doubling time as a key parameter for cellular-based assays using NPs in order to optimize cellular uptake. Previous simulations predicts an exponential decay of the average number of nanoparticles per cell with a decay constant given by where is the cell population doubling time (Geng et al., 2016). Therefore, we propose a mathematic approximation to predict the correct NPs amount to be able to monitor cell proliferation. Accordingly, previous optimization assay will not be required for using this method with new cell lines. As mentioned above, time-point assay can be determined by calculating the nanofection load values together with population doubling time. Cells can theoretically be monitored until complete dilution of fluorescents NPs, i.e. when Δ MFI decrease to 1 unit. This end point is reached when median fluorescence intensity of nanofected cells is equal to median fluorescence intensity of non-nanofected cells (background). However, this fluorescent NPs dilution is also influenced by population doubling times of cell lines. In the division process of a nanofected cell, a parent-progeny transfer of NPs is produced. After each division, the nanofection load halves into daughter cells reducing fluorescence intensities -nanofection load- to half. This results in an exponential decay of the fluorescence division after division. This force us to consider the ratio “nanofection load: population doubling times” for long-term assay.

With this purpose, we calculate population doubling times of adherent and suspension cell lines. We observed that considering the number of cell divisions of each cell line in specific period of time, we can estimate the optimal range of nanofection load - Δ MFI units- that we need in order to monitor cells during that period of time. Applying the general formula that is used for exponential growth and decay formula we know the optimal Δ MFI value require at the start of the experiment:

$$Y=Y_0k^x$$

Y = Δ MFI units at the end of the experiment (equal to 1).

Y_0 = Δ MFI units at the start of the experiment.

κ = Reduction rate constant (equal to 0.5; after each division the Δ MFI units are reduced to the half).

X = Number of divisions of each cell line in an specific period (days)

By applying this formula, an estimation of the initial range of nanofection load can be calculated. We applied that formula to our experimental data with MDA-MB-231, MDA-MB-468 and MCF-7 cell lines. The doubling time is respectively 38, 40 and 43 hours. Typical monitoring proliferation assays take 7 days. During this time, MDA-MB-231 cells divide 4.4 times, MDA-MB-468 cells 4.2 times, and MCF7 3.9 times. In contrast, suspension hard-to-transfect cells, Jurkat and Raji, proliferate faster. In consequence their doubling time is lower

(23 and 25 hours respectively) and their division ratio in 7 days higher (7.30 and 6.72 times). In particular, using this predictive approach we found that to monitor MDA-MB-231, MBA-MB-468 and MCF7 cells, an initial nanofection load of around 21.4, 18.4 and 15 Δ MFI units, respectively, would be required. In the case of suspension hard-to-transfect cells, which have greater division ratio, higher Δ MFI units would be required (158.1 for Jurkat cells and 105.4 for Raji cells) (**Table 5**). Remarkably, using the ratio 1:25000 (cell:fluorescent NPs), these Δ MFI values were obtained for all cell lines with a 30 minutes incubation time (**Fig. 51c-d**). These results confirm the predictive value of this mathematic approach. Using this exponential decay formula, an estimation of a range of fluorescence intensity initial can be successfully calculated.

$$y = y_0 \times k^x \rightarrow 1 = y_0 \times 0.5^{\text{division number}}$$

Doubling time (hour)	Cell divisions in 7 days	0.5 ^{division number}	Y0 in MFI units	
48	3,5	0,09	11,3	
47	3,6	0,08	11,9	
46	3,7	0,08	12,6	
45	3,7	0,08	13,3	
44	3,8	0,07	14,1	
43	3,9	0,07	15,0	⇒ MCF7
42	4,0	0,06	16,0	
41	4,1	0,06	17,1	
40	4,2	0,05	18,4	⇒ MDA-MB-468
39	4,3	0,05	19,8	
38	4,4	0,05	21,4	⇒ MDA-MB-231
37	4,5	0,04	23,3	
36	4,7	0,04	25,4	
35	4,8	0,04	27,9	
34	4,9	0,03	30,7	
33	5,1	0,03	34,1	
32	5,3	0,03	38,1	
31	5,42	0,02	42,8	
30	5,60	0,02	48,5	
29	5,79	0,02	55,4	
8	6,0	0,02	64,0	
27	6,2	0,01	74,7	
26	6,5	0,01	88,1	
25	6,7	0,01	105,4	⇒ RAJI
24	7,0	0,01	128,0	
23	7,3	0,01	158,1	⇒ JURKAT
22	7,6	0,01	199,0	

Table 5. Calculation of range of MFI units needed to 7 days proliferation monitoring experiment by exponential decay formula depending on cellular doubling time. Different doubling time values are showed in the first column. Median of fluorescence intensity, showed in the last column, is calculated based on exponential decay formula (on the top), regarding 7 days of the proliferation monitoring. Calculated doubling time for each cell line used in cell monitoring experiments is outlined. Therefore, considering the number of cell divisions of each cell line in that specific period of days, an estimated optimal range of nanofection load -ΔMFI units- needed was obtained.

3.2. VALIDATION AND IMPLEMENTATION OF THE METHOD IN DIFFERENT CELL TYPES AND CELL PROLIFERATION ASSAYS

3.2.1. Tracking cell proliferation in a long-term assay

Once all parameters were efficiently established (concentration and time of incubation together with doubling time), we tested this novel method for tracking cell proliferation. For this purpose, a long-term assay of cellular monitoring was performed. Adherent and hard-to-transfect suspension cells were nanofected (25,000 NPs per cell, 30 minutes). Following nanofection, fluorescent NPs were distributed to daughter cells resulting in a progressive halving of the progeny fluorescence. This reduction of fluorescence intensity was quantified by flow cytometry. In order to monitor cell populations, harvesting was done at different time points (every 24 hours). Firstly, percentage and load of nanofection were analysed at initial time (Day 0). Flow cytometry plots and fluorescence intensity decay are shown in **Figure 52a-c**. During the progression of the assay, the reduction of nanofection load was clearly observed (**Fig. 52a**). Δ MFI was near 1 at day 7, validating the use of exponential decay formula to optimize the nanofection parameters (**Fig. 52b-c**).

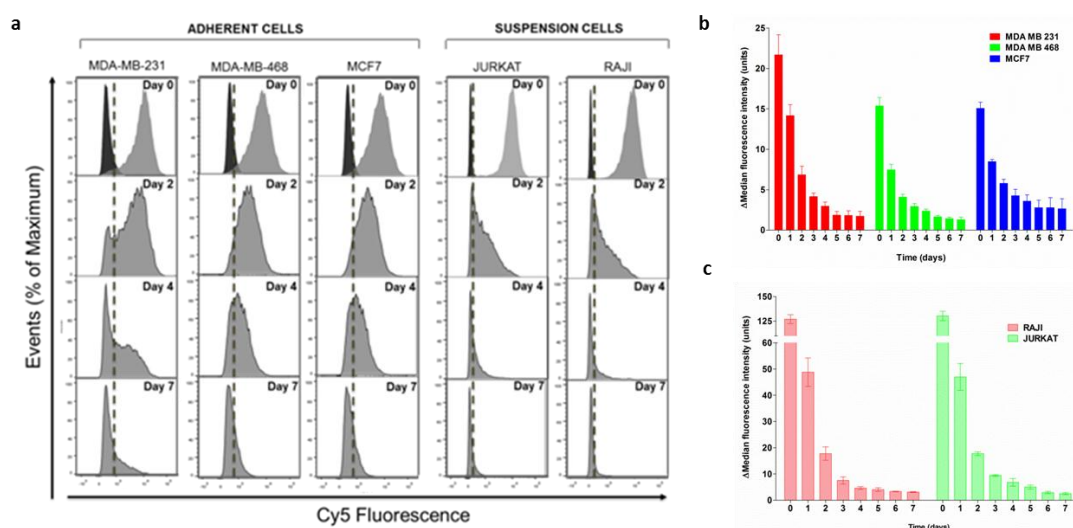


Figure 52. Validation of the nanofection method to monitor cell proliferation. (a) Representative histogram plots of untreated cells (dark peak) compared to Cy5-NPs treated cells (light peaks) at day 0, 2, 4 and 7. Reduction of the nanofection load was observed over the days. (b,c) Flow cytometry was performed every 24 hours and increment of median fluorescence intensity measured (Δ MFI) is represented for (b) adherent cell lines and (c) suspension hard to transfect cell lines.

To reinforce the feasibility of this method, an assay to monitor the reduction of cell proliferation was set up. For this purpose, cell proliferation was reduced by treatment with Mitomycin C (MCC), a cytotoxic drug that induces cell cycle arrest in G2/M phase as consequence of DNA damage. In a first stage, the cytotoxic effect of this drug was determined by flow cytometry analysis using propidium iodide staining (**Fig. 53a**). The arrest in G2/M impedes that cells initiate mitosis, producing a stop of cell division. According to this, cells do not proliferate after MMC treatment; therefore, if the cells are nanofected, they should maintain the nanofection load after MMC treatment. With this purpose we monitored

cells (red histogram) and cells treated with Mitomycin C for 96h (blue histogram). **(b)** Flow cytometry analysis of untreated and nanofected cell lines after Mitomycin C treatment. Open dashed histograms represent 7 days incubation time point, whereas the filled histograms depict initial experimental time point. Each panel shows a comparison between untreated cells (grey filled histogram) and cells treated with Cy5-NP (25000 added per cell) for 30 min (blue filled histogram). The graphs show that fluorescence intensity decrease after 7 days of incubation due to cell division (dashed red histogram) compared to initial fluorescence. In contrast, in cells which cell cycle is arrested, nanoparticles have not been split and fluorescence intensity is maintained over time (dashed blue histogram). Each histogram is representative of at least 3 experiments and shows percentage of maximum (Y axis) versus log fluorescence intensity (X axis) for 10.000 viable cells. **(c)** Increment of median fluorescence intensity (Δ MFI) versus Cy5-NPs treated cells at initial proliferation time-point (0), after 4 days of proliferation (96h) and after 4 days of MMC treatment. Results are expressed as mean \pm S.E.M. Statistical significance was determined by Bonferroni's multiple comparison test between the different treatments of each cell lines.

3.2.2. Monitoring primary lymphocytes proliferation

Success of adaptive immune system depends on lymphocyte proliferation. The ability to accurately predict proliferative behavior of lymphocytes has important implications for human health research. Standard methods to measure cell proliferation based on fluorescent dyes are particularly toxic in this kind of cell (Parish, 1999). Therefore, alternative methods which were not cytotoxic are required. This fact led us to assess our method for measuring lymphocyte proliferation. For this purpose, in the first stage, the nanoparticle uptake capacity of isolated human primary PBMC (monocyte depleted-peripheral blood mononuclear cells) was tested.

PBMCs were incubated with Cy5-NP and the efficiency of NPs internalization was analysed by confocal fluorescence microscopy and flow cytometry. A confocal fluorescence microscopy confirmed the nanoparticles intracellular localization just after nanofection (**Fig. 54a**). In parallel, a flow cytometry analysis was performed. It was found that our nanofection parameters managed to reach 90% nanofected population (**Fig. 54b-c**). Nanofected population percentages can increase by varying incubation time and number of added NPs per cell.

Once the efficiency of cellular labelling using NPs was proven, and in order to assess our method for measuring lymphocyte proliferation, the PBMCs were nanofected and stimulated to induce their proliferation. The analysis was performed following 7 days after PHA-induced proliferation. The nanofection load practically disappeared due to the induced lymphocyte proliferation. In fact, fluorescence intensity decrease was gradually observed over days due to Cy5-NPs dilution between the progeny as consequence of induced cell division (**Fig. 54d**). At day 7, the histogram plot shows a slight peak of positive population which corresponds to non-proliferative cells, something expected due to the fact that, following stimulation step, not all cell population participate in the division (**Fig. 54e**). Overall, the data confirms the absence of deleterious effect of Cy5-NPs in the PBMC viability.

In order to confirm our data, comparison of our nanotechnology-based method with the wide accessible and most popular method to measure lymphocyte proliferation (intracellular fluorescent dye, CFSE) was performed (Parish, 1999; Parish et al., 2009; Quah et al., 2007). We confirmed that substantial cell proliferation was evident only after 3 days of culture as common feature of T and B cells responding to mitogens and specific antigens. CFSE dye dilution was observed in the tested successive time points (**Fig. 6f**). The data validates the applicability of the method to measure lymphocyte proliferation.

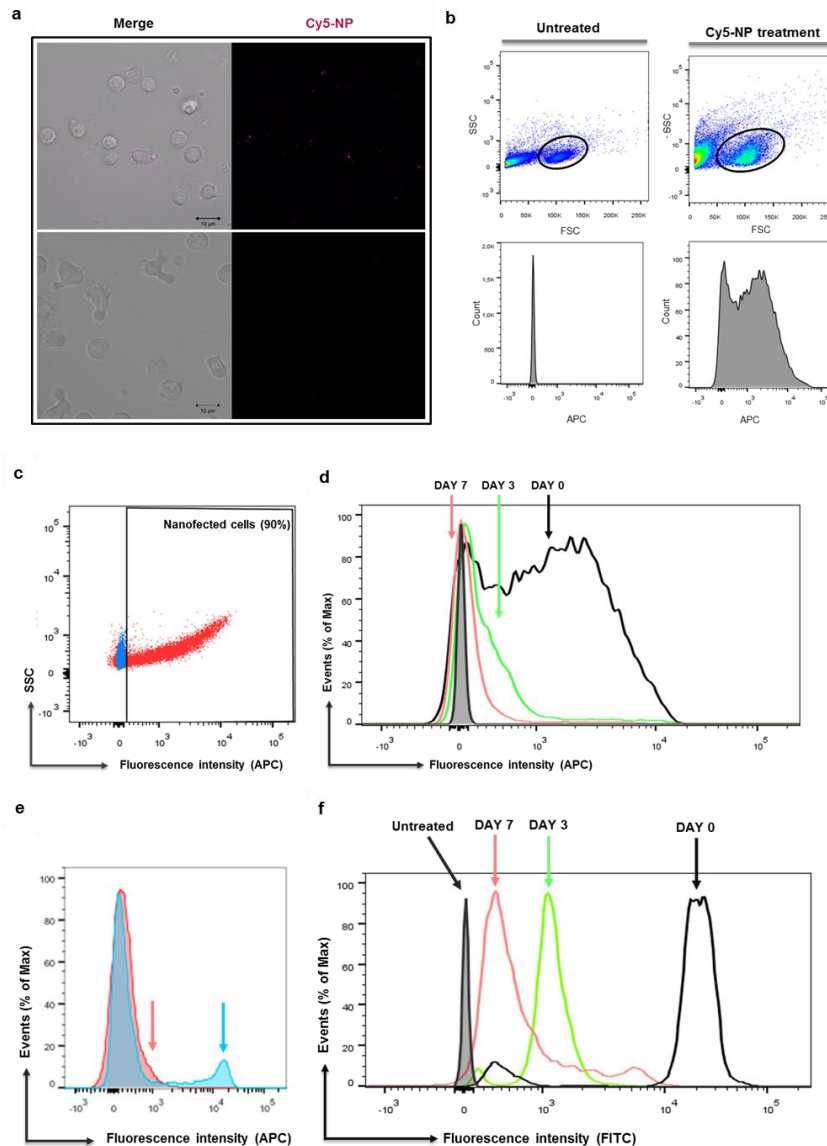


Figure 54. Figure 3. Demonstration of Cy5 labelling lymphocytes and proliferation detection and monitoring of proliferating lymphocytes. (a) Confocal fluorescence microscopy to confirm Cy5-NPs internalization by freshly isolated lymphocytes (top panel) and demonstration of Cy5-NPs dilution after 7 days caused by proliferation of lymphocytes stimulated (bottom panel). Left panel: Merge, composition of the two recorded channels (DIC–Differential interference contrast– and red, Cy5-NPs). Right panel: red channel, Cy5-NPs. Scale bar, 10 μ m. (b) Analysis of the specific lymphocyte populations depending on treatment provided. Freshly isolated lymphocytes were subjected to the same procedure without nanoparticles (represented in left panel) and they were considered as untreated cells; right panel shows lymphocytes after 30 min Cy5-NP incubation. The results show lymphocytes population is not affected when Cy5-NPs were used. (c) Nanofected population (red) after 30 minutes of Cy5-NPs incubation versus untreated cells (blue) represented by dot plots. (d) Fluorescence intensity dilution over days in PHA-induced lymphocytes (open histograms) versus untreated cells (filled grey histogram). Results are from a representative experiment. (e) Histogram plot comparing both PHA-induced nanofected (blue) and non nanofected (unlabelled) cells (red) after 7 days. Higher blue peak represents stimulated nanofected cells which have diluted their fluorescence. Blue arrow shows a slight peak corresponding to fluorescence measurement of non-dividing lymphocytes. Red arrow highlights unlabeled population, which provides a measurement of the autofluorescence of an activated lymphocyte population. (f) CFSE labelling dilution (FITC fluorescence) over days in PHA-induced lymphocytes (open histograms) versus untreated cells (filled grey histogram).

DISCUSSION

A good candidate for tracking cell proliferation using fluorescence techniques must have certain specific characteristics such as (1) have bright fluorescent features, (2) being readily taken up by cells, (3) being evenly distributed within progeny cells, (4) displaying slow dilution rates and (5) being non cytotoxic (Progatzky et al., 2013; Tario et al., 2012). The main advantages of using nanoparticles rather than classical approaches are that: a) they are more stable than fluorophore in solution (Cárdenas-Maestre et al., 2014), b) the fluorescence signal does not decrease rapidly during the first 24 hours after labelling, then zeroth generation can be set up using cell sample from day 0 (Chung et al., 2017) and c) they can be used to track a broad range of cellular types without any cytotoxic effect allowing its application in many biological/biomedical research fields (Unciti-Broceta et al., 2015). To the best of our knowledge, cell clone formation assay based on nanotechnology imaging technique by using Quantum dot, has been the only reported to date to study the proliferative features (Geng et al., 2016). In this work, we have evaluated a nanotechnology based method to monitor cell proliferation by analysing these properties that a good candidate for tracking cell proliferation must offer. To do so, we have used 200 nm PS NPs labelled with a near infra-red fluorophore (Cy5) to be able to evaluate these nanodevices by fluorescent techniques. However, other fluorophores of different nature could be used instead of Cy5. On the other hand, the role of surface charge of polystyrene nanoparticles on cellular uptake is still controversial. Carboxylated PS-NPs were ingested to a higher degree by alveolar type I cells (Kemp et al., 2008), whereas preferential uptake of cationic PS-NPs has been observed in Madin Darby canine kidney cells (Fazlollahi et al., 2011b). However, as previously reported, we have found that the presence of free amino groups on the NP surfaces is essential to allow an efficient cell labelling (He et al., 2010). Based on these findings, we have designed a nanodevice that contain a defined amount of free amino groups to ensure an efficient cellular uptake with high rate, allowing an effective internalisation and consequently an efficient cell labelling to be able to monitor cell proliferation in long term assays. Nanoparticles do not present cytotoxic effects in the cell lines tested, being this fact an essential characteristic therefore making them an ideal method to monitor cell proliferation. Interestingly this method could be implemented using nanoparticles of different nature as far as they do not affect cell viability.

We demonstrated that these nanodevices are readily taken up by the cells, and they present slow dilution and non-effect on the cell function. On the other hand, it is already accepted NPs are split between daughter cells when the parent cell divides [26]. Whether their distribution is equal during cell division still remains controversial. Future work could be focused on the determination of nanoparticle dose in a statistical framework by imaging microscopy using our fluorescent NPs as nanotracker. Nevertheless our results support the efficiency of this method. We have proven that the measurement of Δ MFI is a reliable parameter to monitoring the linearity over time, regardless of eventual asymmetry. MFI is more robust than mean values and heterogeneity from cell to cell is considered [27]. On the other hand, because of it is known that used hard-to-transfect cells are specialized in avoid uptake, we considered NPs could be remained associated to membrane cells. Hence, we have discriminated between NPs absorbed on the cell membrane or NPs internalized inside the cell, providing solid correlation between fluorescent signal observed and proliferation. Regarding cell cycle stage, differences in cellular nanoparticle uptake levels have been previously reported [26]. However, these

differences are not evident during the first 5 h of exposure. Consequently, as shorter incubation time is needed in this methodology (only 30 minutes), there is not influence of cell cycle phase in the uptake of these nanoparticles.

Changing parameters such as concentration and time of incubation, the nanofection load can be controlled in a robust manner in order to reach an optimum MFI initial value. We have demonstrated that 25000 NPs and short period of nanofection time (30 min) were adequate to achieve satisfactory MFI values to monitor cell proliferation during 7 days. Likewise, same MFI values could be accomplished applying lower number NPs added per cell and higher incubation time. Even so, the highest ratio that has been used for this method is 50000 NPs added per cell. However, in previous work, higher concentration without observing any cytotoxic effect was successfully used (Unciti-Broceta et al., 2015). Accordingly, the use of this method allows the fluorescence labelling of cells with high intensity and reproducibility (very low variance). In fact, this is a method of broad application as the unique cell requirement to be able to monitor cell proliferation using this nanotracker is efficient internalisation (Treuel et al., 2013).

Because of these nanoparticles are not exocytosed by cells as previously was reported (Kim et al., 2011a), make them an excellent candidate for cell proliferation monitoring, as the only thing diluting the signal is the division of the cell in two daughter cells. The fact that these nanoparticles are not toxic for any cell lines tested so far is also of remarkably importance as they do not affect the cell function. Indeed, lymphocyte viability after NP internalization and PHA-induced proliferation has been demonstrated. This observation suggests that NPs are non-toxic in systems cultured with less serum (such as PMBC), as it was previously reported (Hsiao and Huang, 2013), allowing this methodology to be considered in different physiological media.

It is important to mention that, due to the fact that these fluorescent nanoparticles are labelled with a far red dye, then a multicolour flow cytometry assay can be set up as before reported (Geng et al., 2016), but without interference of the nanodevices with other fluorophores labelled reagents (such as fluorescein-labelled antibodies), therefore avoiding cell autofluorescence.

Finally, we have proposed the use of NP-based cell tracker as a potential tool to monitor lymphocyte proliferation minimizing toxicity, and thereby being required lower initial lymphocytes number to assess. Our methodology has also proven beneficial for *in vitro* studies as possible alternative for the current cell tracking using fluorescent protein and membrane dyes (Parish et al., 2009; Tario et al., 2011).

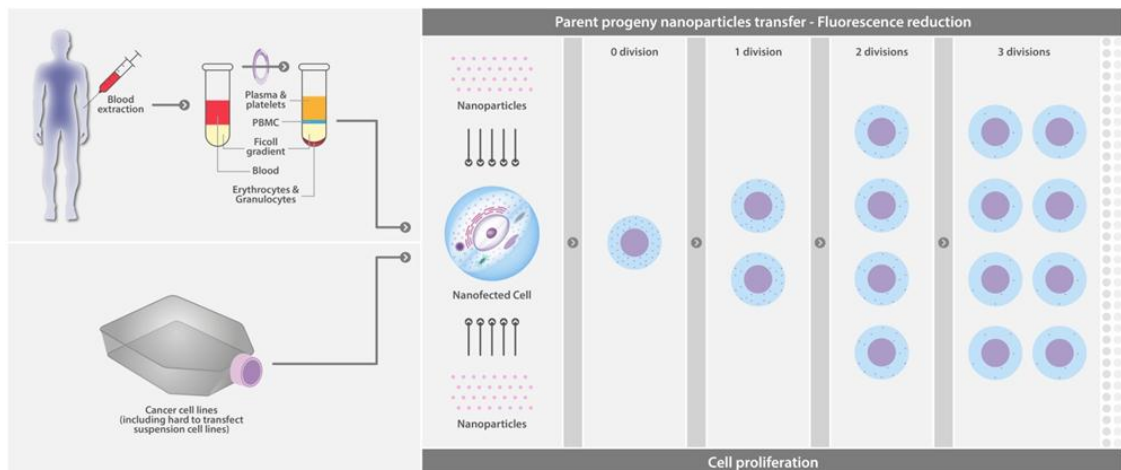


Figure 55. Schematic of method for tracking cell proliferation using a nanotechnology approach.

To conclude, the method has been validated in several adherent cells and also in suspension cells including hard-to-transfect cells. Even more interesting is the fact that monitoring of cell proliferation of lymphocytes has been successfully achieved (so far the only efficient method to do this lymphocytes monitoring is CFSE staining). The method was also validated in a cell-based assay which determined the induced cellular arrest through MMC effect, showing the power of the method for long-term cellular assays (**Fig. 55**). Furthermore, this new method does not alter the cell cycle hence presenting no cytotoxic effects. This fact corresponds to previously findings where NPs were never found associated with any components of the mitotic apparatus and no abnormal cell division was detected after their internalization (Liu et al., 2011).

In conclusion, an alternative method to monitor cell proliferation, which can be used with a large variety of cell lines for long term cellular assays, is presented. We propose the use of nanoparticles as an accessible tool to track cell proliferation for any laboratory which could access nanotechnology-based approaches.

CONCLUSIONS

SECTION I:

- Respiration-deficient ρ^0 206 cancer cells display a pronounced glycolytic phenotype and a truncated TCA with only a reductive branch. This phenotype resulted viable by reprogramming of alternative metabolic pathways, which provide the necessary NAD⁺/NADH balance.
- A successful metabolic rewiring in respiration deficient cancer cells is based on a strong dependence of pyruvate and glutamine to sustain a high proliferation rate. Pyruvate is required to maintain high glycolytic flux by NAD⁺ regeneration, avoiding the impact on cell viability of aspartate consumption beyond its support for aspartate biosynthesis. Glutamine serves as fundamental resource to fuel a reductive TCA.
- Dependence on pyruvate import is a fundamental requirement to ensure the successful adaptation avoiding a metabolic collapse during respiration impairment. This fact highlights the importance of the monocarboxylate transporters (such as MCT1) as metabolic target in emerging cancer therapies.
- Aspartate plays a pivotal role in tumor metabolism to maintain cell proliferation. Alternative reductive pathway of aspartate consumption is exhibited upon mitochondrial respiration impairment. In this scenario, the lack of available electron acceptors not only restricts aspartate biosynthesis, but also reprograms consumption of available aspartate to maintain NAD⁺ production.
- Pyruvate supports aspartate synthesis by cytosolic aspartate aminotransferase (GOT1), thus generating an increased dependence on aspartate-to-oxaloacetate route in respiration deficient cells. Importantly, GOT1 therefore plays a key role in cells with inhibited respiration, thus displaying to be synthetically lethal.
- Oncogenes HIF-1 α and c-Myc, which are involved in metabolic signaling pathways that contribute to cancer development, are induced in respiration deficient ρ^0 206 cells regardless of oxygen tension.
- Respiration is paradoxically required in both proliferating and cancer cells to sustain a high glycolytic biosynthetic metabolism.

SECTION II

- Polystyrene nanoparticles have been uptaken with remarkable efficiency by our cancer cell models, based on respiration deficient cells with an extreme metabolic phenotype (143B and ρ^0 206 cells). The nanofection load can be controlled in a robust manner through concentration and incubation time in our cell models.
- The chemotherapeutic drug Doxorubicin has been effectively conjugated to polystyrene nanoparticles via a pH-sensitive linker and efficiently delivery into our cell

models. Doxorubicin release mediated by nanoparticles improves therapeutic drug efficacy, reducing the dose required to achieve the inhibitory concentration 50 (IC50).

- The antibody directed against the metabolic key target MCT1 has been successfully conjugated to polystyrene nanoparticles. The effective cytotoxicity of MCT1-NP in respiration deficient cells was significantly more pronounced than 143B cells, according to higher expression of MCT1 transporter found in these cells.
- A bifunctionalised anti-MCT1-DOX nanodevice was been successfully prepared. However, this combined therapy was not as effective as DOX-NPs, suggesting possible steric hindrance to the DOX release or even lower DOX loading due to the presence of the coupled-antibody.
- A multifunctionalized nanodevice to target a specific metabolic ligand overexpressed in tumor cells has been efficiently developed. In particular, monoclonal antibody which specifically recognizes the CD147 subunit of MCT1 transporters has been conjugated to nanoparticles. A specificity cellular uptake in 143B and p⁰206 compared to negative controls due to the overexpressed CD147 on the cytoplasmic membrane of these cells has been observed.
- A novel specific drug carrier system for specific transport of doxorubicin to CD147 overexpressing tumor cells has been efficiently developed. CD147-NPs used in conjunction with antitumor drug doxorubicin can provide the ability to target tumors with a predominant glycolytic phenotype in a robust manner.

SECTION III

- Polystyrene nanoparticles have been successfully functionalized to assess *in vitro* long-term monitoring of cell proliferation. These nanoparticles are stable and not alter the cell cycle hence presenting no cytotoxic effects for any cell lines tested so far.
- An efficient and novel nanotechnology fluorescence based method to track cell proliferation has been validated in several adherent cells and also in suspension cells including hard-to-transfect cells and lymphocytes.
- The use of nanoparticles as an accessible tool to track cell proliferation for any laboratory which could access nanotechnology-based approaches has been proposed.

CONCLUSIONES

SECCIÓN I

- Células tumorales deficientes en respiración muestran un fenotipo glucolítico muy pronunciado además de un ciclo de los ácidos tricarboxílicos truncado debido a la pérdida de actividad en la cadena transportadora de electrones mitocondrial. Este fenotipo es mantenido gracias a vías metabólicas alternativas las cuales garantizan un balance NAD⁺/NADH adecuado.
- La reprogramación metabólica en células tumorales deficientes en respiración está basada en una fuerte dependencia al piruvato y a la glutamina para sustentar su alto nivel de proliferación. Además de su papel en la síntesis de aspartato, el piruvato es necesario para mantener el alto flujo glicolítico regenerando NAD⁺. La glutamina sirve como recurso fundamental para alimentar un TCA reductor.
- Importación de piruvato es un requisito fundamental para asegurar la reprogramación exitosa evitando un colapso metabólico durante el deterioro de la respiración. Este hecho pone de manifiesto la importancia de los transportadores de monocarboxilatos (tales como MCT1) para ser usados como dianas metabólicas en las terapias antitumorales emergentes.
- El aspartato juega un papel fundamental en el metabolismo tumoral para mantener la proliferación celular. Durante la falta de respiración mitocondrial, aspartato es consumido mediante una vía reductora alternativa. En este escenario, la falta de aceptores de electrones disponibles no sólo restringe la biosíntesis de aspartato, sino que también reprograma el consumo de aspartato disponible para mantener la producción de NAD⁺.
- El piruvato apoya la generación de aspartato a través de la enzima aspartato aminotransferasa citosólica (GOT1), lo que provoca una mayor dependencia de la ruta aspartato-oxaloacetato durante la reprogramación metabólica producida tras la disfunción de la respiración mitocondrial. Es importante destacar que GOT1 desempeña un papel clave en las células con disfunción en la respiración, mostrando por tanto ser sintéticamente letal durante la inhibición de la respiración.
- Los oncogenes HIF-1 α y c-Myc, los cuales están implicados en vías de señalización metabólicas que contribuyen al desarrollo del cáncer, son inducidos durante la disfunción mitocondrial independientemente de la cantidad de oxígeno presente.
- La respiración es necesaria tanto en células proliferativas como tumorales para mantener su alto metabolismo biosintético glicolítico.

SECCIÓN II

- Las nanopartículas de poliestireno han sido eficientemente internalizadas por nuestro modelo de células cancerígenas basado en células deficientes en la respiración con un fenotipo metabólico extremo (células 143B y p⁰206). El nivel de internalización se

puede controlar de forma robusta a través de la concentración y el tiempo de incubación en nuestros modelos celulares.

- El fármaco quimioterapéutico doxorubicina se ha conjugado eficazmente a las nanopartículas de poliestireno a través de un enlace sensible al pH y ha sido eficientemente internalizado por nuestros modelos celulares. La inmovilización de doxorubicina en la nanopartícula de poliestireno mejora la eficacia del fármaco terapéutico, reduciendo la dosis requerida para alcanzar la concentración inhibitoria 50 (CI50).
- El anticuerpo dirigido contra la diana metabólica MCT1 se ha conjugado con éxito a nanopartículas de poliestireno. La citotoxicidad efectiva de MCT1-NP en células con deficientes respiratoria fue significativamente más pronunciada que en las células 143B, de acuerdo con la mayor expresión del transportador MCT1 que se encuentra en estas células.
- Un nanosistema anti-MCT1-DOX bifuncionalizado ha sido preparado con éxito. Sin embargo, esta terapia combinada no fue tan eficaz como las DOX-NPs, lo que sugiere posible impedimento estérico para la liberación de DOX o incluso que se haya reducido la cantidad de fármaco conjugado debido a la presencia del anticuerpo acoplado.
- La preparación de un nanosistema multifuncionalizado para dirigir un ligando metabólico específico sobreexpresado en células tumorales se ha llevado a cabo con éxito. En particular, el anticuerpo monoclonal que reconoce específicamente la subunidad CD147 de transportadores MCT1 se ha conjugado eficientemente a las nanopartículas. Se observó una captación celular específica en células 143B y p⁰206 en comparación con controles negativos debido a la sobreexpresión de CD147 en la membrana citoplasmática de estas células.
- Se ha desarrollado eficientemente un nuevo sistema de liberación selectiva de fármacos para el transporte específico de doxorubicina a células tumorales que sobreexpresan CD147. Las CD147-NP utilizadas en combinación con fármacos antitumorales pueden proporcionar la capacidad de dirigirse selectivamente a tumores con un fenotipo glicolítico predominante.

SECCIÓN III

- Nanopartículas de poliestireno han sido eficientemente funcionalizadas para ser usadas *in vitro* en la monitorización a largo plazo de la proliferación celular. Estas nanopartículas son estables y no alteran el ciclo celular, sin presentar además efectos citotóxicos en ninguna de las líneas celulares testadas hasta ahora.
- Un eficiente nuevo método basado en el uso de la nanotecnología para evaluar la proliferación celular ha sido validado en varias células adherentes y en suspensión, incluyendo células difíciles de transfectar y linfocitos.

- Proponemos por tanto el uso de nanopartículas como una herramienta accesible para monitorizar la proliferación celular que puede ser desarrollada en cualquier laboratorio que pueda acceder a estrategias nanotecnológicas.

MATERIAL & METHODS

1. Cell culture

Osteosarcoma 143B cell line, human breast cancer cell lines MCF-7, MDA-MB-468 and MDA-MB-231, and immortalized MEF cells were cultured in Dulbecco's Modified Eagle's Medium (DMEM) (GIBCO) supplemented with 10% fetal bovine serum and 1% penicillin/streptomycin. ρ^{0206} cells were also supplemented with 2% pyruvate and 50 $\mu\text{g}/\text{mL}$ of uridine. Suspension cells, the B-lymphoblastic cell line Raji and leukemia cell lines K562 and Jurkat were cultured in RPMI-1640 (GIBCO), 10% FBS and 1% penicillin/streptomycin supplemented. All cells were maintained at 37°C and 5% CO₂ and 95% relative humidity. All cell lines were regularly tested negative for mycoplasma infection.

2. Genotype analysis by PCR

DNA from 143B and ρ^{0206} pellets was purified using AllPrep DNA kit (Qiagen), according to the manufacturer's protocol. Gene fragments encoding the control region DLP6 were amplified from DNA with the specific primers DLP6-forward (5'-CCACTTCCACACAGACATC') and DLP6-Reverse (5' GTATGGGGTTAGCAGCGG -3'). Polymerase chain reaction (PCR) was performed with AmpliTaq polymerase (Promega) and the followings PCR parameters: 95°C, 5 min; 35 cycles at 95°C, 45 s, 55°C, 45 s and 72°C, 10 s. PCR reaction products were checked by 1% agarose gel electrophoresis.

3. Cell growth curves and doubling time

Once the cell lines reached 80 to 90% of confluence, they were collected and plated at initial density of 1×10^5 cells in 10 cm² plates. Counts were performed for 24 h for 7 days in a Neubauer camera by TB dye exclusion to count total viable cells. Results were represented by a non-linear regression curves. The quantification of doubling time as a measure of cell growth for each cell line was calculated as described (Mehrara et al., 2007).

4. Cell-Cycle distribution measurements

Cell cycle analysis by quantitation of DNA content was performed using propidium iodide staining. Cells were harvested, washed twice with PBS, and fixed with 70% cold ethanol added drop wise to the pellet while vortexing. After overnight refrigeration at -20°C, cells were washed again with PBS and cell nuclei were stained for 15 min in the dark with 50 $\mu\text{g}/\text{mL}$ propidium iodide containing 100 U/ml of ribonuclease A, and added into a flow cytometry tube. DNA content was measured by flow cytometry (BD FACS Canto II) and the percentages of cells in the G₀/G₁, S and G₂/M phases were determined from DNA content histograms using FlowJo software.

5. Cellular viability measurement by phosphatidylserine exposure assay

Annexin V-FITC/7AAD double-staining was performed with an Annexin V-FITC Kit (BD Bioscience, USA). Cells were incubated with different selective medias for 96 h. For analysis of viability, cells were harvested by combining floating cells in the medium and adherent cells detached by trypsinization, rinsed twice with PBS, and resuspended in 1x Annexin buffer

(Hepes 10 mM, NaCl 150 mM, KCl 5 mM, MgCl₂ 1 mM, CaCl₂ 1.8 mM). The cells were labeled with 1/200 of FITC-conjugated Annexin V and 1/200 of 7AAD according to the manufacturer's instructions. After incubation in the dark for 15 min at room temperature, 400 μ L of 1x binding buffer was added and the samples were immediately analyzed with a flow cytometer (BD FACS Canto II). The Annexin V-FITC⁻/7AAD⁻ population was regarded as viable cells, while the Annexin V-FITC⁺/7AAD⁻ and Annexin V-FITC⁺/7AAD⁺ populations were taken as measurements of apoptotic cells. Data were analyzed with FlowJo software.

6. Proliferation and migration/invasion assays

Real-time cell proliferation and invasion properties were assessed using the xCELLigence system (ACEA Biosciences, California, USA). xCelligence device provides a real-time proliferative, adherent and migration behavior of cells using specialized 16-well plates known as the E-plate (for proliferation) and CIM plates (migration). These plates consist of an underlying sheet of microelectrodes that detect cell interaction upon contact. When cells interact with the underlying electrode surface, it impedes the ability of the electrodes to sense the surrounding conductive culture media, reported as cell impedance, and it corresponds to cell number and strength of the interaction. Proliferation assays were performed with 2×10^4 in 143B and 3×10^4 in ρ^{0206} cells/well seeded in E-plates. 24 hours later, media was replaced according to specific deprivation conditions and real-time proliferation was followed to 96 hours. Migration assays were performed according to manufacturer's advice. Upper chamber of the CIM-plates were uncoated or a Matrigel (BD, USA) (1:20) layer was created during 4 hours at 37 °C. A total of 2×10^4 cells were seeded in each well of the upper chamber in serum-free media. Fresh DMEM was added to each well of the lower chamber. The CIM-plates were left in an incubator for 1 h to allow cell attachment. The impedance value of each well was automatically monitored by the xCELLigence system for duration of 66 h and expressed as a Cell Invasion index.

7. Tumor sphere culturing

143B and ρ^{0206} cells (5×10^4 cells/well) were plated into 10-cm dishes previously coated with Poly(2-hydroxyethyl methacrylate) (PHEMA) (Sigma-Aldrich) to facilitate sphere formation (Folkman and Moscona, 1978). Briefly, polyHEMA was dissolved in 95% ethanol at 12% (w/v). A working solution was made by a further dilution of 1:10 in 95% ethanol and was added to tissue culture dishes at 3 ml per 10-cm dish. A hydrophobic surface was formed after the polyHEMA solution dried out at 56°C incubator and subsequently UV-sterilized. The sphere medium, serum-free and growth factors enriched, was prepared with DMEM-F12 +Glutamax (GIBCO) containing 4x B27 supplement (GIBCO), 10 ng/mL basic fibroblast growth factor 2 (bFGF), 20 ng/mL epidermal growth factor (EGFR), 25 ng/ml insulin (PeproTech Inc.) and 2 ng/mL heparin sodium (Changzhou Qianhong Bio-Pharma) (Weiswald et al., 2015). ρ^{0206} media was also supplemented with 2% pyruvate and 50 μ g/mL uridine. After 10 days, the tumor spheres were collected by centrifugation at $300 \times g$ and RNA was extracted as described.

8. RNA extraction, cDNA synthesis and quantitative PCR

Total RNA from mouse and human cells was isolated using miRNeasy extraction kit (Qiagen) and quantified using a NanoDrop 2000c spectrophotometer (Thermo). When required, RNA quality was evaluated by electrophoresis, loading 200 ng in a 2% agarose gel in TAE buffer (tris base, EDTA and acetic acid). Single-strand cDNA synthesis was performed using oligo dT-adaptor primers and the iScript cDNA kit (Roche) according to the manufacturer's protocols, starting from 500 to 1000 ng of original RNA. The cDNA was amplified with gene-specific primers (see primer list included at the end of this section) and Fast SybrGreen in the 7900HT system (Applied Biosystems). In every assay, we used 30 ng of cDNA per reaction, including non-template-controls. Each sample was run in triplicates in every experiment and each experiment was repeated at least three times. The mRNA expression in each sample was normalized to endogenous housekeeping gene β -actin. Relative mRNA expression was analyzed using $2^{-\Delta\Delta Ct}$ method as described previously (Livak and Schmittgen, 2001). Error bars show the standard error of the mean (SEM).

9. Western Blotting

Protein was extracted with RIPA buffer containing 1mM PMSF, 1 μ g/ml aprotinin and 10 μ g/ml leupeptin incubated for 10 min in ice. After centrifugation at 15,000 rpm at 4°C for 10 min, the supernatants were recovered. Extraction of nuclear fraction of proteins was performed by resuspension of cellular pellet in buffer A [10 mM HEPES-KOH (pH 7.8), 10 mM KCl, 0.1 mM EDTA (pH 8.0), and 0.1% NP40], and then vigorously mixed. After centrifugation at 1300 rpm for 5 min, the supernatants were discarded (cytoplasmic proteins). The pellets were resuspended in buffer B [50 mM HEPES-KOH (pH 7.8), 420 mM KCl, 0.1 mM EDTA (pH 8.0), 5 mM $MgCl_2$, and 20% glycerol] and gently mixed at 4°C for 30 min. After centrifugation at 15,000 rpm at 4°C for 30 min, the supernatants were recovered as nuclear proteins. All samples were measured using a Pierce BSA protein assay kit (ThermoFisher) at a 455 nm wavelength using the infinite 200Pro nanoquant (Tecan). A total of 50-100 μ g proteins were diluted in 4 \times Laemmli buffer (Bio-Rad) and heat-shock treated during 10 minutes at 95°C. Proteins were resolved by sodium dodecyl sulfate polyacrylamide gel electrophoresis (SDS-PAGE) and transferred to polyvinylidene difluoride membranes (PVDF) (BioRad). Membranes were blocked with Tris-buffered saline-Tween 20 (TBST, 0.1% Tween 20) containing 5% low-fat milk (room temperature during 1 hour) and incubated with the following primary antibodies: monoclonal mouse anti-human HIF-1 α (NB100-105, Novus), monoclonal rabbit anti-human c-Myc (5605, cell signaling) and monoclonal mouse anti-human β -Actin (A2228, Sigma-Aldrich). All primary antibodies were incubated at 4°C shaking overnight and secondary antibodies RT during 1 hour. Between every incubation step, the membranes were three times with TBST for 10 min each. After incubation with appropriate secondary peroxidase-conjugated antibodies, signal was detected with the SuperSignal West Dura Chemiluminescence Kit (ThermoFisher). For the image acquisition we used the LAS4000 system (General electric). Membranes are incubated with the SuperSignal reagent into the dark camera for one minute and the images were acquired every 10 seconds in a sequential burst until the signal was saturated. For signal quantification, WB images were processed with ImageJ software (NIH, USA). A rectangular area was drawn along the signal of all lanes which represented a positive signal. The intensity was measured for each lane and normalized with the β -Actin signal. The images shown in the

western blots correspond to the best signal intensity and thus the exposure time varies among membranes and antibodies.

10. Monitorization of K-Ras activation

K-Ras Activation Assay Kit (Cell Biolabs) was performed to detect active K-Ras according to the manufacturer's instructions. Raf1 RBD Agarose beads were used to selectively isolate and pull-down the active form of Ras from endogenous lysates. Subsequently, the precipitated GTP-Ras was detected by western blot analysis using an Anti-K-Ras specific polyclonal antibody.

11. mTOR determination

Ser2448 of mTOR protein in cell lysates were quantified using the enzyme-linked immunosorbent assay kits (Abcam) following the manufacture's instruction. Control samples were treated with 50 nM calyculin A for 15 minutes in order to obtain positive signal due to Ser2448 phosphorylation with calyculin A treatment. Serial diluted positive control was used to assess the calibration curve to interpolate the mTOR relative levels of pSer2448.

12. siRNA transfection

Cells were plated at a concentration of $1-1.5 \times 10^5$ cells per well in six-well tissue culture plates in standard culture conditions above for 24 hours. Cells were then transfected with siRNA for a final concentration of 100 nM using RNAiMax reagent (Invitrogen) as a transfection reagent according to the manufacturer's protocol. siRNA constructs were obtained from a predesigned siRNA library (Sigma-Aldrich) and Silencer Select negative control (Scramble siRNA) were included as negative control. Six hours post transfection, cells were counted and plated for next assays. Efficiency of gene extinction was evaluated by qPCR. Proliferation assays were performed 48 h after transfection.

13. Cell viability assay

Monitoring cell viability was performed using CellTiter-Blue® Cell Viability Assay (Promega). This quantitative fluorometric method is based on the ability of living cells to convert a redox dye (resazurin) into a fluorescent end product, which is measured 570 nm directly from 96-well plates. Cells were seeded in solid 96-well plate at the concentration previously optimized, depend on the end-point of corresponding analysis. CellTiter was assessed according to the manufacturer's protocol, and the fluorescence amount obtained was proportional to the number of viable cells. Viability was expressed respect to the percentage of untreated cells (100%). Control wells were included on each plate to measure the fluorescence from serum-supplemented culture medium in the absence of cells.

14. Metabolite identification and quantification by Liquid Chromatography-Mass Spectrometry

Measurements were as described previously (Sullivan et al., 2015). 143B and ρ^{0206} cells were respectively seeded at 3×10^4 and 4.5×10^4 cells/well in 6 well dishes and growth in complete media during 48 hours. The medium was replaced by fresh standard medium or by media with specific cultured conditions (AOA inhibition or metabolite deprivation) overnight before pulse. Then, cells were washed 2 times in PBS and media was changed to proliferation assay media

with or without the indicated treatments. In all cases, media containing same concentration of unlabeled metabolite was used as control. After 1 hour for $^{13}\text{C}_6$ -glucose and $^{13}\text{C}_3$ -pyruvate, 6 hours for $^{13}\text{C}_5$ -glutamine, and 12 hours for $^{13}\text{C}_4$ -aspartate (Sigma-aldrich), cells were washed in ice cold PBS and polar metabolites were extracted from cells using 1 mL of ice cold extraction buffer (50% methanol, 30% acetonitrile, 20% water, all MS grade). After scraping the cells, they were collected and centrifuged for 5 min at 4 °C at 13,000rpm. Supernatant was recovered and 30 μl was transferred into a LC-MS tube prior to sample analysis. A Dionex UltiMate 3000 ultra-high performance liquid chromatography system connected to a Q Exactive benchtop Orbitrap mass spectrometer, equipped with an Ion Max source and a HESI II probe (Thermo Fisher Scientific) was used to determine and quantify the isotopologues of the metabolites. Samples were separated by chromatography by injecting 10 μl of sample on a SeQuant ZIC-pHILIC Polymeric column (2.1 \times 150 mm 5 μM , EMD Millipore). Flow rate was set to 150 $\mu\text{l}/\text{min}$, temperatures were set to 25 °C for column compartment and 4 °C for autosampler sample tray. Mobile Phase A consisted of 20 mM ammonium carbonate, 0.1% ammonium hydroxide. Mobile Phase B was 100% acetonitrile. The mobile phase gradient (%B) was set in the following protocol: 0-20 min.: linear gradient from 80% to 20% B; 20-20.5 min.: linear gradient from 20% to 80% B; 20.5-28 min.: hold at 80% B. Mobile phase was introduced into the ionization source set to the following parameters: sheath gas = 40, auxiliary gas = 15, sweep gas = 1, spray voltage = -3.1kV, capillary temperature = 275 °C, Slens RF level = 40, probe temperature = 350 °C. Metabolites were monitored using full scan in negative mode in the range of 285-700 m/z, with the resolution set at 140,000, the AGC target at 1,000,000, and the maximum injection time at 250 msec. A minimum of triplicate samples were required for each condition for statistical analysis. Relative quantitation of metabolites was performed with XCalibur QuanBrowser 2.2 (Thermo Fisher Scientific) using a 5 ppm mass tolerance and referencing an in-house retention time library of chemical standards. The relative comparison between samples of metabolite peak areas of the extracted ion chromatogram at the appropriate retention time was displayed and for statistical significance, unpaired Student's t test was used.

For untargeted metabolism, after data acquisition, the results were processed by using XCMS and 13XCMS bioinformatic softwares as described (Huang et al., 2014), to perform nonlinear retention time alignment and identify peaks that are changing between the groups of samples measured. The m/z values for the peaks of interest were searched in Metlin/Isometlin metabolite databases to obtain putative identifications. Then identified metabolites were verified by further comparison with online fragmentation pattern databases (Metlin and MassBank) using known standard or fragmentation fingerprint (MS²). For targeted metabolomics, metabolites of interest were identified by accurate mass and retention time, and compared to commercial standards which were acquired to confirm peak identification.

15. Nanoparticle characterization

15.1. Solid content (SC) of the emulsion (%) (mg/mL)

A known volume of a suspension of polystyrene nanoparticles in water (usually 0.5 mL) was placed in a small Petri dish (previously tared), covered with aluminium foil, dried at 80°C for 15

hours and reweighed to give the mass of microspheres. The solid content was then calculated according to the following equation:

% SC = $(m/V_s) \times 100$, where m = mass of microspheres (mg), V_s = Volume of suspension (mL),

15.2. Scanning Electron microscopy (SEM)

Microspheres as a suspension in water (100 μ L) were spread on a carbon disk (11 mm), mounted on SEM pins and dried at 50°C in the vacuum oven overnight. The samples were gold sputter coated prior to analysis (between 20-25 nm layer). Samples were analysed by the Microscopy service of the CIC of the University of Granada in the Faculty of Pharmacy.

15.3. Calculation of loading (mmol/g) of microspheres using Fmoc test

Fmoc-X-microspheres (where x is Fmoc-Gly-OH, Fmoc-PEG-OH or Fmoc-Lys(Dde)-OH, etc) were resuspended in 1 mL of 20% piperidine in DMF (3 x 20 min) after which the nanoparticles were washed by centrifugation three times, the supernatants combined and quantification of Fmoc release analysed by UV spectrophotometry. The loading was calculated according to the following equation:

Loading (mmol/g) = $(A_{302} \times V) / (\epsilon_{302} \times W) \times 1000$

A_{302} : Absorbance measured at 302 nm, V_{mL} : Volume of combined supernatants, ϵ_{302} : Molar Extinction Coefficient (7800 M⁻¹cm⁻¹) and W_{mg} : Mass of nanoparticles.

15.4. Qualitative ninhydrin test

The reaction control was determined by qualitative ninhydrin test. Small samples of microspheres in MeOH (12 μ L, 4% sc) in a 0.5 mL capacity eppendorf were washed with methanol and centrifuged after which 6 μ L of reagent A and 2 μ L of reagent B were added. Mix well and heat to 100 °C for 3 min. Blue stained NPs indicate the presence of primary amines and yellow stained NPs indicates the absence or free primary amino groups.

15.5. Measurement of particle size distribution

A sample of polystyrene microspheres in water (5 μ L) was suspended in 995 μ L of deionised water and placed in a disposable sizing cuvette. Dynamic Light Scattering (DLS) was measured on a Zetasizer Nano ZS ZEN 3500.

15.6. Measurement of Zeta Potential

A sample of polystyrene microspheres in water (1 μ L) was suspended in 999 μ L of 10% PBS pH 7.4 solution in molecular biology grade water and place in a clear disposable zeta cell. The zeta potential was measured on a Zetasizer Nano ZS ZEN 3500.

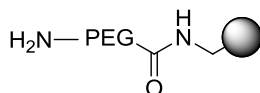
16. Protocols for functionalization and conjugation of bioactive cargoes to nanoparticles

16.1. Deprotection steps

Fmoc deprotection was achieved by treating microspheres with 20% piperidine/DMF (1 mL; 3 x 20 min). Microspheres were obtained by centrifugation and subsequently washed with DMF (3 x 1 mL), MeOH (3 x 1 mL), deionized water (3 x 1 mL).

Dde deprotection on microspheres in presence of Fmoc protecting group: Dde deprotection was facilitated by treating microspheres with the Dde deprotection solution mixture (1.25 g (1.80 mmol) of $\text{NH}_2\text{OH}\cdot\text{HCl}$ and 0.918 g (1.35 mmol) of imidazole were suspended in 5 mL of NMP, and the mixture was sonicated until complete dissolution. Just before reaction, 5 volumes of this solution were diluted with 1 volume of DMF (1 mL) for 1 hour at r.t. on a rotary wheel, then microspheres were washed with DMF (1 mL) and the entire process repeated under the same conditions. Microspheres were obtained by centrifugation and subsequently washed with DMF (3 x 1 mL), methanol (3 x 1 mL), deionised water (3 x 1 mL) and finally DMF (3 x 1 mL). Next, ninhydrin test was performed to check the presence of primary amine.

16.2. PEGylation of nanoparticles

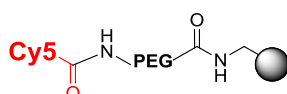


Amino functionalised nanoparticles (205 nm; S.D: 0.035 μm ; C.V: 19.0%, 1 mL, 4% SC, 0.025 mmol/g, 1 eq) were washed in DMF (1 mL x 3 times) and suspended in DMF (1 mL). Separately, the Fmoc-PEG spacer (Fmoc-4,7,10-trioxa-1,13-tridecanediamine succinamic acid) (10 eq) was dissolved in DMF (1 mL), then oxyma (10 eq; Apollo Scientific) was added and the solution mixture mixed for 4 minutes at r.t. before the addition of DIC (10 eq; Sigma-Aldrich) and mixed for 8-10 minutes at r.t. The solution mixture was then added to amino nanoparticles and suspension mixed on the Thermomixer at 1400 rpm for 2 hours at 60°C. Nanoparticles were washed with DMF (3 x 1 mL). Efficiency of coupling was checked by ninhydrin test.

Fmoc deprotection was achieved by treating nanoparticles with 20% piperidine/DMF (1 mL; 3 x 20 min). Microspheres were obtained by centrifugation and subsequently washed with DMF (3 x 1 mL), MeOH (3 x 1 mL), deionised water (3 x 1 mL). Efficiency of deprotection was checked by ninhydrin test.

Note: Double or triple PEGylation is achieved by carry this protocol on two or three times respectively.

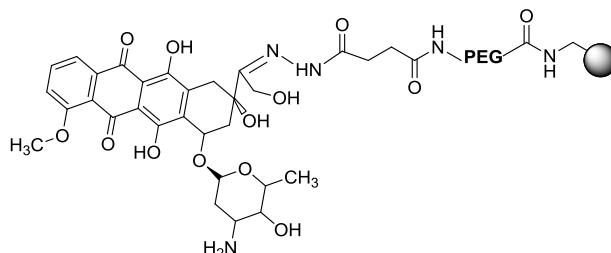
16.3. Preparation of Cy5-NPs



The labelling of the microspheres with Cy5 was carried out by suspension of NPs in DMF (1 mL). Separately, NHS activated Cy5 (5 eq, Lumiprobe) was dissolved in anhydrous DMF (1 mL),

then DIPEA (5 eq; Apollo Scientific) was added and the solution mixture mixed for 10 minutes at r.t. before added to amino NPs and suspension mixed on the Thermomixer at 1400 rpm for 2 hours at 60°C. NOTE: It is very important to carry on all this process in dark. Avoid exposure to light. Fmoc deprotection was achieved by treating microspheres with 20% piperidine/DMF (1 mL; 3 x 20 min). Microspheres were obtained by centrifugation and subsequently washed with DMF (3 x 1 mL), MeOH (3 x 1 mL), deionised water (3 x 1 mL).

16.4. Preparation of DOX-NPs



(a) Preparation of Hydrazone functionalised nanoparticles

Carboxyl functionalised nanoparticles were prepared by addition of Succinic Anhydride (20Eq) dissolved in DMF (1 mL) and then was added DIPEA (1 μ L) in the role of basic catalyst. Once the suspension is ready, it was placed in the Thermomixer 2h / 1400 rpm / 60°C. Then nanoparticles were centrifuged and washed with DMF (1mL \times 3). The activation of Succinic-nanoparticles was achieved by washing with DMF (3 \times 1mL) and centrifuged. The oxime (18.9 mg, 50 eq) was dissolved in 1 mL of DMF and the solution was sonicated and then added to the nanoparticles that were resuspended by ultrasonicator; then was added DIC (17.6 g, 50 eq) and were placed at the Thermomixer 4h, 1400 rpm at room temperature. After that, NPs were centrifuged and the supernatant was removed. At the same time, the aqueous-solution of 55% v/v of Hydrazine (7.99 μ L, 0.14 mmol, 50 Eq) was added to 0.5 mL of DMF; then the solution was added to NPs that are sonicated by ultrasonicator. After that, the mixture was placed to Thermomixer over night/ 1000 rpm/ 25°C. When the coupling is finished, NPs were washed with DMF (1 mL \times 3), MeOH (1 mL \times 3) and finally with PBS at pH 7.4 (1 mL \times 3) in which were suspended.

(b) Preparation of the Doxorubin-Nanoparticles

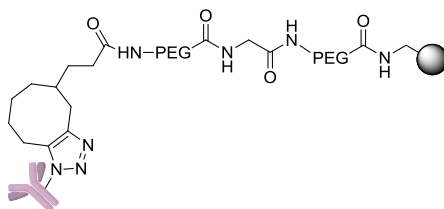
The Hydrazone-PEGylated-Nanoparticles (100 μ L) were washed with PBS at pH 6 (100 μ L \times 3) and then centrifugated. The doxorubicin (Sigma Aldrich, 3 Eq) was added in a 100 μ L of PBS buffer at pH 6, so the resulting mixture was added to NPs, sonicated by ultrasonicator and placed in Thermomixer 12 hours, 1000 rpm and 50 °C. The NPs were washed three times with warm PBS at pH 7.4, to ensure that the adsorbed doxorubicin to the surface of the NPs is removed. Then the NPs were stored in PBS at pH 7.4 appears to be the optimal pH for the stability of the hydrazone bond.

(c) *Determination of loading of doxorubicin. HPLC analysis.*

Doxorubicin-nanoparticles were incubated with pH 5.2 PBS buffer at 37 °C for 72 hours to induce hydrazine cleavage. Nanoparticles were centrifuged and supernatant was analysis by HPLC.

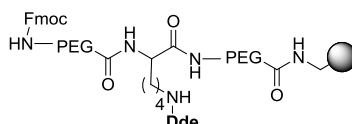
Analytical HPLC was conducted on an Agilent 1100 series HPLC system coupled to a Polymer Lab PL-ELS 1000 Evaporative Light Scattering (ELS) detector with UV detection at 220, 254, 260, 282 and 495 nm, Supelco's Discovery® C 18 (50 mm x 2.1 mm x 5 µm) was used, method S50D. Elution was performed with Solvent A (0.1% formic acid in HPLC-grade deionized water) and Solvent B (0.1% formic acid in HPLC-grade methanol) at 1 mL x min with a gradient of 5 to 95% B over 3 min, followed by 1 min isocratic at 95% B and ending with a gradient of 95 to 5% B over 1 min, then 1 min isocratic at 95% A.

16.5. Preparation of antibody-NPs



NHS-BCN ((1R,8S,9s)-Bicyclo[6.1.0]non-4-yn-9-ylmethyl N-succinimidyl carbonate (5 eq, Lumiprobe) was dissolved in anhydrous DMF (1 mL), then DIPEA (5 eq; Apollo Scientific) was added and the solution mixture mixed for 10 minutes at r.t. before added to PEGylated NPs dissolved in anhydrous DMF and suspension mixed on the Thermomixer at 1400 rpm overnight at 25°C. Then antibody was functionalized by treatment with Azide-PEG-NHS Ester (Sigma Aldrich) and purified using a ultra 0.5 Centrifugal Filter Device MW 30 or 10 depending on antibody size). Azide modified antibody and BCN functionalized nanoparticles were mixed and reacted at room temperature for 3 h and the final mixture was purified by centrifugation. Nanoparticles were resuspended in PBS 7.4. A 10% polyacrylamide gel was loaded with 50 µl of the collected supernatants diluted 1:5 with loading buffer. The electrophoresis was carried out in 1% SDS running buffer pH 8.8 and subsequently gel was staining with Coomassie.

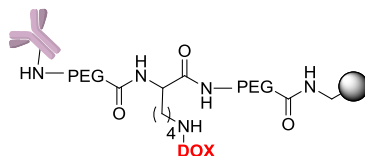
16.6. Preparation of bifunctionalized nanoparticles



PEG functionalized nanoparticles (1 mL; 1 eq) were washed in DMF (1 mL x 3 times) and suspended in DMF (1 mL). Separately, Fmoc-Lys(Dde)OH (5 eq) was dissolved in DMF (1 mL), then oxyma (5 eq; Apollo Scientific) was added and the solution mixture mixed for 4 minutes at r.t. before the addition of DIC (5 eq; Sigma-Aldrich) and mixed for 8-10 minutes at r.t. The

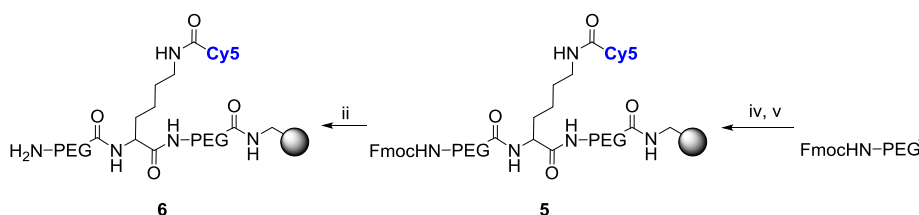
solution mixture was then added to PEGylated nanoparticles and suspension mixed on the Thermomixer at 1400 rpm for 2 hours at 60°C. Fmoc deprotection was achieved by treating nanoparticles with 20% piperidine/DMF (1 mL; 3 x 20 min). Microspheres were obtained by centrifugation and subsequently washed with DMF (3 x 1 mL), MeOH (3 x 1 mL), deionized water (3 x 1 mL). Then PEGylation step was repeated to introduce a second PEG spacer

16.7. Preparation of bifunctionalized drug and antibody nanoparticles



Following Fmoc deprotection, bifunctionalized nanoparticles were BCN functionalized following the protocols previously described (section 16.5). Then, following Dde deprotection step, drug was conjugated following protocol described in section 16.4. Finally, azide functionalized antibody was conjugated to nanoparticles following protocol described in section 16.5.

16.8. Preparation of bifunctionalized fluorescent NP



Fluorescent NPs were specifically designed for tracking cellular proliferation. PEGylation, bifunctionalization and dye conjugation were performed following a Fmoc-Dde orthogonal strategy using Oxyma/DIC as coupling reagents. Briefly, amino-methyl cross-linked polystyrene 200 nm nanoparticles were coupled with Fmoc-1-amino-4,7,10-trioxa-13-tridecamine succinic acid using standard HOBt (1-hydroxybenzotriazole)/DIC (1,3-Diisopropylcarbodiimide) chemistry. PEGylated NPs were centrifuged (13000 rpm), washed three times with dimethylformamide (DMF) before deprotecting the Fmoc group with 20% piperidine in DMF with three consecutive treatments, 20 min each, at room temperature and shaken at 1400 rpm. Fmoc deprotected NPs were then washed three times with DMF and Fmoc-Lys(Dde-OH)ref was conjugated followed by Dde deprotection and Cy5 conjugation (near infra-red dye). For the coupling, deprotected PEGylated 200 nm NPs were resuspended in DMF with DIPEA and commercially available Cy5 NHS ester (Lumiprobe) was added. The coupling was performed overnight at room temperature and at 1400 rpm. Finally, NPs (fluorescent near infra-red polystyrene NPs, referred in the main text as Cy5-NPs) were Fmoc deprotected with 20 % piperidine in DMF (x3) and two times washed with DMF. Culture suitable NPs were obtained by washing steps with methanol, ethanol, 70 % ethanol and resuspension in sterile water. The stability of the Cy5-NPs incubated in culture media over a period of time of 7 days at 37°C was monitored using flow cytometry.

The effectiveness of the Cy5 conjugation was checked by flow cytometry with a FACSCanto II flow cytometer (BD FACS Canto II) and by fluorescence microscopy with Confocal Scanning Microscope Zeiss LSM 710. As control Fmoc deprotected PEGylated 200 nm NPs, referred as naked NPs, were used. Dynamic Light Scattering (DLS) and Zeta potential were measured on a Zetasizer Nano ZS ZEN 3500 in molecular biology grade water in a disposable sizing cuvette for hydrodynamic size measurements or clear disposable zeta cuvette for zeta potential measurements. The stability of nanoparticles at 37 °C in culture medium was tested at different time points by measuring the hydrodynamic size and zeta potential.

17. Determination of fluorescent NPs concentration (NPs/ μ L) by spectrophotometric method

Fluorescent NPs concentration (NPs per microliter) was determined by a spectrophotometric method as described previously by our group (Unciti-Broceta et al., 2015). Briefly, measurement of turbidity optical density at 600 nm of polystyrene NP suspensions was performed, based on nephelometric principals. Light going through NP suspensions is scattered via reflection, refraction and diffraction phenomena and the intensity of the scattered light, which are proportional to number of NPs in suspension, is recorded by standard spectrophotometers. In this way, calibrate standard curves were obtained for amino-methyl cross-linked polystyrene NPs of 450 nm and 200 nm by NP known concentrations. Calibration curves fitted linear regression models by which the number of NPs per microliter corresponding to one unit of OD600 for each size could be determined. Thus, these curves using initial batches of NP suspensions permitted us to estimate the number of NPs in final batches, which underwent multiple handling procedures, by OD600 measurement of 1 μ L.

18. Flow cytometry staining protocol for protein detection

Cells were harvest and washed in 1x PBS in 1.5 mL microtubes. Then, pellets were incubated in 200 μ L of ice cold FACS Buffer (1% BSA, 10% FBS in PBS). If the protein is present in the cytoplasmic, 0.1% Triton X is added to blocking buffer to cell permeation. Cells were incubated on ice for 1 h. Pellets were washed by centrifugation at 1500 rpm for 5 min at 4°C. Primary labeled antibodies were diluted in 100 μ L of FACS Buffer according to manufacturer's instructions and incubated on ice for 30 min. After incubation, cells were washed three times and resuspended in 100 μ L of FACS buffer containing fluorochrome-labeled secondary antibody at the optimal dilution. After 30 min of incubation at room temperature, cells were washed three times and resuspended in 200 μ L of ice cold FACS buffer and analyzed by flow cytometry on the same day. For checking antibody conjugation, nanoparticles were processed in the same way as cellular pellets. Per measurement, 10,000 cells or NPs were acquired by flow cytometry (FASC CANTO II Becton Dickinson) and mean fluorescence intensity as well as percentage of cells with positive signal in the FITC channel calculated using FlowJo Software.

19. Nanoparticle uptake study by flow cytometry

Adherents cell lines were washed with phosphate buffered saline (PBS 1X), detached with Trypsin-EDTA (0.25%, phenol red), counted and diluted with media to a final concentration of 1×10^5 cells per mL. 500 μ L of each cell line suspension were plated in 24 well plates and

incubated for 18 h. Then, media was replaced with 500 μL of fresh media mixture containing specific number of NPs previously quantified. The cells were incubated with the NPs at the established incubation times in a humidified incubator at 5% CO_2 and 37°C. Suspension cells were harvested, washed with PBS1X, counted and diluted with serum free media to a final concentration of 1×10^6 cells per mL. 600 μL of each cell line suspension were placed in 1.5 mL conical culture tube (Eppendorf). Then, the specific number of NPs was added and cells were incubated in a humidified incubator at 5% CO_2 and 37°C. As control were used naked NPs (at the specific ratio cell/NPs), and cells without nanoparticles treatment.

After incubation with NPs, for adherent cells, the media was aspirated and cells were washed with PBS 1X, and detached with Trypsin-EDTA at 37°C for 5 minutes; for suspension cells, the media was removed by centrifugation and once washed with PBS 1X. In the case of suspension hard-to-transfect cells, additional wash step adding a reducing agent (tris(2-carboxyethyl)phosphine, Fluorochem) was done in order to quench possible binding nanoparticles in the membrane extracellular side, avoiding fluorescence interference from unincorporated NPs. Then, each sample was fixed in 2% paraformaldehyde (PFA) at room temperature for 10 minutes and protected from the light. Samples were analyzed via flow cytometry with a FACSCanto II flow cytometer (Becton Dickinson). Each experiment was done in duplicate per ratio and incubation time and repeated at least three times per cell line.

The MNF_{50} index, defined as the number of NPs capable of nanofecting 50% of the cell population (Unciti-Broceta et al., 2015), was estimated by fitting percentages of nanofected cells versus ratio to a hyperbola equation model.

20. Nanoparticle internalization study by confocal microscopy

Cells were washed with phosphate buffered saline (PBS 1X), detached with trypsin/EDTA, counted and diluted with media to a final concentration of 10^5 cells per mL. 500 μL of each cell line suspension were seeded onto glass poly-L-lysine-coated coverslips in 24 well plates and incubated for 18 h. Then, media was replaced with a fresh media mixture containing the amount of Cy5-NPs corresponding to each experiment. Unconjugated NPs, referred as naked NPs (at maximum cell/NPs ratio used in Cy5-NPs), and cells without nanoparticles treatment were used as controls. Following the corresponding incubation time, the media was aspirated and cells were washed with PBS 1X, and fixed in 4% paraformaldehyde at room temperature for 30 min. Fixed cells were washed with PBS 1X and coverslips were mounted with ProLong Gold antifade mountant with DAPI (Life technologies). Microscopy assays were performed with Confocal Scanning Microscope Zeiss LSM 710 Axio Observer (Carl Zeiss, Jena, Germany). Image acquisition was performed using a Plan-Apochromat 63x/1.40 objective, numerical aperture of DIC M27 of oil immersion and software ZEN 2010 (Carl Zeiss, Jena, Germany). Images were subsequently processed by software ZEN 2012 Blue Edition (Carl Zeiss, Jena, Germany) or ImageJ version 1.49b. Samples containing fluorescent nanoparticles and DAPI nuclear staining were using a 405 nm Diode laser-line (30.0 mW), a 543 nm HeNe laser-line (1.2 mW) for DIC images. Each experiment was done in duplicate per ratio and repeated three times per cell line. Optical sections were displayed in three orthogonal projections [xy-projections (main panel), xz-projections (top panel), and yz-projections (right panel)] to distinguish between

extracellular and internalized nanoparticles. The yellow lines indicate the positions of the xz and yz planes.

21. Competitive binding assay

Cells were seeded in regular culture media in 24-well plates, and were cultured at 37 °C in an atmosphere of 5% CO₂ and 95% air for 18 h. After attachment, cells were incubated in 0.5 mL of regular media containing 0.15 µg/µL free anti-CD147. The incubation was carried out for 30 min followed by washing with culture media. Then, NPs were added at corresponding concentration and incubated for 1.5 h. After that, cells were collected and fixed as explained before. Cells were analyzed by flow cytometry (FACS CANTO, Becton Dickinson, Mississauga, CA, USA) and FlowJo software.

22. Fluorescent nanoparticle-based proliferation assay

Cells were properly disposed to nanoparticle incubation as described above, using 1:25000 cell:NPs ratio and 30 minutes of nanofection. Immediately after the incubation had finished, a sample of nanofected cells was fixed and named time 0. After that, the rest of the nanofected cells were plated and maintained using appropriate culture conditions for each cell line. Every day, a sample of the nanofected cells was fixed and named as the corresponding harvesting day (day 1, 2, 3, 4, 5, 6 and 7). Untreated and arresting cells treated with 0.5 µg/mL of mitomycin C (Sigma) were used as a control. Once the assay was finished, all the samples were analyzed by flow cytometry. Data acquisition and analysis was performed using the BP 660/20 nm (APC filter) on a BD FACS Canto II Flow Cytometer with BDFACSDiva™61 software. Harvest cells from culture wells can also be analyzed directly without fixation step by flow cytometry for cell proliferation.

23. In vitro lymphocyte proliferation assay

Peripheral blood mononuclear cells (PMBCs) were provided from cell bank of the Centre for Scientific Instrumentation (CIC) of the University of Granada. Cryovials of PMBC were thawed according to manufacture instructions. Cells were resuspended in free serum DMEM at 1×10^6 cell/mL, and incubated 1 hour at 37°C horizontally. Monocytes were adherent to plastic flask and lymphocytes were collected from culture. After collecting lymphocytes from PBMC isolated cells, concentration was adjusted to 1×10^6 cells/mL and labelled with 25000 NP added per cell for 30 minutes at 37°C. Following washing steps, Cy5-NPs-labeled cells were resuspended in culture medium and divided into proliferating and resting cells. PHA-P was added to culture media in a final concentration of 2%. Cell proliferation was examined on days 0, 3, 5, and 7 after nanofection. Cy5-NP-labeled, unstimulated cells as a control, as well as stimulated cells (both unlabeled and Cy5-NP-labeled) were analyzed by flow cytometry. CFSE assay was performed according to the manufacturer's instructions as a control of monitoring proliferation lymphocyte model assay. Experiment was performed in quadruplicate from four independent PMBC batch.

24. Statistical analysis

Graphs and statistical difference data were performed using GraphPad Software according to the following explanation. Percentage data of cells containing fluorescent-NPs were

represented versus cell/Cy5-NPs ratio in a bar representation, and statistical significant differences were stabilised by two-way ANOVA Bonferroni's multiple comparison test in the different treatments between the same cell lines. Furthermore, median fluorescence intensity (MFI) was exhaustive analyzed comparing the MFI increment (Δ MFI, MFI sample/MFI untreated). Two-way ANOVA Bonferroni's multiple comparison test was applied to study statistical significance. A p-value of ≤ 0.05 was considered significant. Results are given as means \pm standard error of the mean (SEM). Sample size, which indicates experimental replicates from a single representative experiment, was 3 unless otherwise specified. The results of all experiments were validated by independent repetitions.

REFERENCES

- Abramson, H.N. (2011). The Lipogenesis Pathway as a Cancer Target. *J. Med. Chem.* *54*, 5615–5638.
- Adam, J., Yang, M., Bauerschmidt, C., Kitagawa, M., O’Flaherty, L., Maheswaran, P., Özkan, G., Sahgal, N., Baban, D., Kato, K., et al. (2013). A Role for Cytosolic Fumarate Hydratase in Urea Cycle Metabolism and Renal Neoplasia.
- Alano, C.C., Tran, A., Tao, R., Ying, W., Karliner, J.S., Swanson, R.A., Swanson, R., Anderson, K., Green, M., Huynh, F., et al. (2007). Differences among cell types in NAD⁺ compartmentalization: A comparison of neurons, astrocytes, and cardiac myocytes. *J. Neurosci. Res.* *85*, 3378–3385.
- Alexander, L.M., Sánchez-Martín, R.M., and Bradley, M. (2009). Knocking (Anti)-Sense into Cells: The Microsphere Approach to Gene Silencing. *Bioconjug. Chem.* *20*, 422–426.
- Alexander, L.M., Pernagallo, S., Livigni, A., Sánchez-Martín, R.M., Brickman, J.M., and Bradley, M. (2010). Investigation of microsphere-mediated cellular delivery by chemical, microscopic and gene expression analysis. *Mol. BioSyst.* *6*, 399–409.
- Allen, E.L., Ulanet, D.B., Pirman, D., Mahoney, C.E., Coco, J., Si, Y., Chen, Y., Huang, L., Ren, J., Choe, S., et al. (2016). Differential Aspartate Usage Identifies a Subset of Cancer Cells Particularly Dependent on OGDH. *Cell Rep.* *17*, 876–890.
- Altman, B.J., Stine, Z.E., and Dang, C. V. (2016). From Krebs to clinic: glutamine metabolism to cancer therapy. *Nat. Rev. Cancer* *16*, 619–634.
- Anastasiou, D., and Cantley, L.C. (2012). Breathless cancer cells get fat on glutamine. *Cell Res.* *22*, 443–446.
- Anastasiou, D., Poulgiannis, G., Asara, J.M., Boxer, M.B., Jiang, J., Shen, M., Bellinger, G., Sasaki, A.T., Locasale, J.W., Auld, D.S., et al. (2011). Inhibition of Pyruvate Kinase M2 by Reactive Oxygen Species Contributes to Cellular Antioxidant Responses. *Science* (80-). *334*.
- Anastasiou, D., Yu, Y., Israelsen, W.J., Jiang, J.-K., Boxer, M.B., Hong, B.S., Tempel, W., Dimov, S., Shen, M., Jha, A., et al. (2012). Pyruvate kinase M2 activators promote tetramer formation and suppress tumorigenesis. *Nat. Chem. Biol.* *8*, 839–847.
- Anhorn, M.G., Wagner, S., Kreuter, J., Langer, K., and von Briesen, H. (2008). Specific Targeting of HER2 Overexpressing Breast Cancer Cells with Doxorubicin-Loaded Trastuzumab-Modified Human Serum Albumin Nanoparticles. *Bioconjug. Chem.* *19*, 2321–2331.
- Arruebo, M., Valladares, M., and González-Fernández, Á. (2009). Antibody-Conjugated Nanoparticles for Biomedical Applications. *J. Nanomater.* *2009*, 1–24.
- Au, K.K., Liong, E., Li, J.Y., Li, P.S., Liew, C.C., Kwok, T.T., Choy, Y.M., Lee, C.Y., and Fung, K.P. (1997). Increases in mRNA levels of glucose transporters types 1 and 3 in Ehrlich ascites tumor cells during tumor development. *J. Cell. Biochem.* *67*, 131–135.
- Baenke, F., Peck, B., Miess, H., and Schulze, A. (2013). Hooked on fat: the role of lipid synthesis in cancer metabolism and tumour development. *Dis. Model. Mech.* *6*, 1353–1363.
- Ban, H.S., Xu, X., Jang, K., Kim, I., Kim, B.-K., Lee, K., Won, M., Heiden, M. Vander, Cantley, L., Thompson, C., et al. (2016). A Novel Malate Dehydrogenase 2 Inhibitor Suppresses Hypoxia-

- Inducible Factor-1 by Regulating Mitochondrial Respiration. *PLoS One* *11*, e0162568.
- Bardella, C., Pollard, P.J., and Tomlinson, I. (2011). SDH mutations in cancer. *Biochim. Biophys. Acta - Bioenerg.* *1807*, 1432–1443.
- Barenholz, Y. (Chezy) (2012). Doxil® — The first FDA-approved nano-drug: Lessons learned. *J. Control. Release* *160*, 117–134.
- Beijersbergen, R.L., Wessels, L.F.A., and Bernards, R. (2017). Synthetic Lethality in Cancer Therapeutics. *Annu. Rev. Cancer Biol* *1*, 141–161.
- Birsoy, K., Wang, T., Possemato, R., Yilmaz, O.H., Koch, C.E., Chen, W.W., Hutchins, A.W., Gultekin, Y., Peterson, T.R., Carette, J.E., et al. (2012). MCT1-mediated transport of a toxic molecule is an effective strategy for targeting glycolytic tumors. *Nat. Genet.* *45*, 104–108.
- Birsoy, K., Possemato, R., Lorbeer, F.K., Bayraktar, E.C., Thiru, P., Yucel, B., Wang, T., Chen, W.W., Clish, C.B., and Sabatini, D.M. (2014). Metabolic determinants of cancer cell sensitivity to glucose limitation and biguanides. *Nature* *508*, 108–112.
- Birsoy, K., Wang, T., Chen, W.W., Freinkman, E., Abu-Remaileh, M., and Sabatini, D.M. (2015). An Essential Role of the Mitochondrial Electron Transport Chain in Cell Proliferation Is to Enable Aspartate Synthesis. *Cell* *162*, 540–551.
- Borger, J.G., Cardenas-Maestre, J.M., Zamoyska, R., and Sanchez-Martin, R.M. (2011). Novel Strategy for Microsphere-Mediated DNA Transfection. *Bioconjug. Chem.* *22*, 1904–1908.
- Bradley, M., Alexander, L., Duncan, K., Chennaoui, M., Jones, A.C., and Sánchez-Martín, R.M. (2008a). pH sensing in living cells using fluorescent microspheres.
- Bradley, M., Alexander, L., and Sanchez-Martin, R.M. (2008b). Cellular Uptake of Fluorescent Labelled Biotin–Streptavidin Microspheres. *J. Fluoresc.* *18*, 733–739.
- Brand, K. (1985). Glutamine and glucose metabolism during thymocyte proliferation. Pathways of glutamine and glutamate metabolism. *Biochem. J.* *228*, 353–361.
- Briere, J.-J., Favier, J., Bénit, P., El Ghouzzi, V., Lorenzato, A., Rabier, D., Di Renzo, M.F., Gimenez-Roqueplo, A.-P., and Rustin, P. (2005). Mitochondrial succinate is instrumental for HIF1 nuclear translocation in SDHA-mutant fibroblasts under normoxic conditions. *Hum. Mol. Genet.* *14*, 3263–3269.
- Brigger, I., Dubernet, C., and Couvreur, P. (2002). Nanoparticles in cancer therapy and diagnosis. *Adv. Drug Deliv. Rev.* *54*, 631–651.
- Bunik, V., Artiukhov, A., Aleshin, V., and Mkrtychyan, G. (2016). Multiple Forms of Glutamate Dehydrogenase in Animals: Structural Determinants and Physiological Implications. *Biology (Basel)*. *5*, 53.
- Cabeza, L., Ortiz, R., Prados, J., Delgado, Á. V., Martín-Villena, M.J., Clares, B., Perazzoli, G., Entrena, J.M., Melguizo, C., and Arias, J.L. (2017). Improved antitumor activity and reduced toxicity of doxorubicin encapsulated in poly(ε-caprolactone) nanoparticles in lung and breast cancer treatment: An in vitro and in vivo study. *Eur. J. Pharm. Sci.* *102*, 24–34.
- Cairns, R.A., Harris, I.S., and Mak, T.W. (2011). Regulation of cancer cell metabolism. *Nat. Rev. Cancer* *11*, 85–95.
- Cantley, L.C. (2002). The Phosphoinositide 3-Kinase Pathway. *Science (80-)*. *296*, 1655–1657.

- Cardaci, S., Zheng, L., MacKay, G., van den Broek, N.J.F., MacKenzie, E.D., Nixon, C., Stevenson, D., Tumanov, S., Bulusu, V., Kamphorst, J.J., et al. (2015). Pyruvate carboxylation enables growth of SDH-deficient cells by supporting aspartate biosynthesis. *Nat. Cell Biol.* *17*, 1317–1326.
- Cardenas-Maestre, J.M., Panadero-Fajardo, S., Perez-Lopez, A.M., Sanchez-Martin, R.M., Chou, L.Y.T., Ming, K., Chan, W.C.W., Cheng, Y., Zhao, L., Li, Y., et al. (2011). Sulfhydryl reactive microspheres for the efficient delivery of thiolated bioactive cargoes. *J. Mater. Chem.* *21*, 12735.
- Cárdenas-Maestre, J.M., Pérez-López, A.M., Bradley, M., and Sánchez-Martín, R.M. (2014). Microsphere-Based Intracellular Sensing of Caspase-3/7 in Apoptotic Living Cells. *Macromol. Biosci.* *14*, 923–928.
- Casey, J.R., Grinstein, S., and Orlowski, J. (2010). Sensors and regulators of intracellular pH. *Nat. Rev. Mol. Cell Biol.* *11*, 50–61.
- Cavalli, L.R., Varella-Garcia, M., and Liang, B.C. (1997). Diminished tumorigenic phenotype after depletion of mitochondrial DNA. *Cell Growth Differ.* *8*, 1189–1198.
- Chandel, N.S., and Schumacker, P.T. (1999). Cells depleted of mitochondrial DNA ($\rho 0$) yield insight into physiological mechanisms. *FEBS Lett.* *454*, 173–176.
- Chaneton, B., Gottlieb, E., Mazurek, S., Harada, K., al., et, Noguchi, T., al., et, Noguchi, T., al., et, Yamada, K., et al. (2012). Rocking cell metabolism: revised functions of the key glycolytic regulator PKM2 in cancer. *Trends Biochem. Sci.* *37*, 309–316.
- Chang, H.-I., and Yeh, M.-K. (2012). Clinical development of liposome-based drugs: formulation, characterization, and therapeutic efficacy. *Int. J. Nanomedicine* *7*, 49–60.
- Chen, W.W., Freinkman, E., Wang, T., Birsoy, K., and Sabatini, D.M. (2016). Absolute Quantification of Matrix Metabolites Reveals the Dynamics of Mitochondrial Metabolism. *Cell* *166*, 1324–1337.e11.
- Cheng, T., Sudderth, J., Yang, C., Mullen, A.R., Jin, E.S., Matés, J.M., and DeBerardinis, R.J. (2011). Pyruvate carboxylase is required for glutamine-independent growth of tumor cells. *Proc. Natl. Acad. Sci. U. S. A.* *108*, 8674–8679.
- Cheong, J.-H., Park, E.S., Liang, J., Dennison, J.B., Tsavachidou, D., Nguyen-Charles, C., Wa Cheng, K., Hall, H., Zhang, D., Lu, Y., et al. (2011). Dual Inhibition of Tumor Energy Pathway by 2-Deoxyglucose and Metformin Is Effective against a Broad Spectrum of Preclinical Cancer Models. *Mol. Cancer Ther.* *10*.
- Chiarugi, A., Dölle, C., Felici, R., and Ziegler, M. (2012). The NAD metabolome — a key determinant of cancer cell biology. *Nat. Rev. Cancer* *12*, 741–752.
- Choy, E., Hornicek, F., MacConaill, L., Harmon, D., Tariq, Z., Garraway, L., and Duan, Z. (2012). High-throughput genotyping in osteosarcoma identifies multiple mutations in phosphoinositide-3-kinase and other oncogenes. *Cancer* *118*, 2905–2914.
- Christofk, H.R., Vander Heiden, M.G., Harris, M.H., Ramanathan, A., Gerszten, R.E., Wei, R., Fleming, M.D., Schreiber, S.L., and Cantley, L.C. (2008a). The M2 splice isoform of pyruvate kinase is important for cancer metabolism and tumour growth. *Nature* *452*, 230–233.
- Christofk, H.R., Vander Heiden, M.G., Wu, N., Asara, J.M., and Cantley, L.C. (2008b). Pyruvate

kinase M2 is a phosphotyrosine-binding protein. *Nature* *452*, 181–186.

Chung, S., Kim, S.-H., Seo, Y., Kim, S.-K., and Lee, J.Y. (2017). Quantitative analysis of cell proliferation by a dye dilution assay: Application to cell lines and cocultures. *Cytom. Part A*.

Clem, B.F., Clem, A.L., Yalcin, A., Goswami, U., Arumugam, S., Telang, S., Trent, J.O., and Chesney, J. (2011). A novel small molecule antagonist of choline kinase- α that simultaneously suppresses MAPK and PI3K/AKT signaling. *Oncogene* *30*, 3370–3380.

Clem, B.F., O'Neal, J., Tapolsky, G., Clem, A.L., Imbert-Fernandez, Y., Kerr, D.A., Klarer, A.C., Redman, R., Miller, D.M., Trent, J.O., et al. (2013). Targeting 6-Phosphofructo-2-Kinase (PFKFB3) as a Therapeutic Strategy against Cancer. *Mol. Cancer Ther.* *12*, 1461–1470.

Cohen, R., Neuzillet, C., Tijeras-Raballand, A., Faivre, S., de Gramont, A., and Raymond, E. (2015). Targeting cancer cell metabolism in pancreatic adenocarcinoma. *Oncotarget* *6*, 16832–16847.

Coller, H.A. (2014). Is cancer a metabolic disease? *Am. J. Pathol.* *184*, 4–17.

Coloff, J.L., Murphy, J.P., Braun, C.R., Harris, I.S., Shelton, L.M., Kami, K., Gygi, S.P., Selfors, L.M., and Brugge, J.S. (2016). Differential Glutamate Metabolism in Proliferating and Quiescent Mammary Epithelial Cells. *Cell Metab.* *23*, 867–880.

Couvreux, P. (2013). Nanoparticles in drug delivery: Past, present and future. *Adv. Drug Deliv. Rev.* *65*, 21–23.

Currie, E., Schulze, A., Zechner, R., Walther, T.C., and Farese, R.V. (2013). Cellular Fatty Acid Metabolism and Cancer. *Cell Metab.* *18*, 153–161.

Dang, C. V. (2010). Rethinking the Warburg Effect with Myc Micromanaging Glutamine Metabolism. *Cancer Res.* *70*, 859–862.

Dang, C. V., Kim, J., Gao, P., and Yustein, J. (2008). The interplay between MYC and HIF in cancer. *Nat. Rev. Cancer* *8*, 51–56.

Dang, L., White, D.W., Gross, S., Bennett, B.D., Bittinger, M.A., Driggers, E.M., Fantin, V.R., Jang, H.G., Jin, S., Keenan, M.C., et al. (2009). Cancer-associated IDH1 mutations produce 2-hydroxyglutarate. *Nature* *462*, 739–744.

Davis, M.E., Zuckerman, J.E., Choi, C.H.J., Seligson, D., Tolcher, A., Alabi, C.A., Yen, Y., Heidel, J.D., and Ribas, A. (2010). Evidence of RNAi in humans from systemically administered siRNA via targeted nanoparticles. *Nature* *464*, 1067–1070.

Daye, D., and Wellen, K.E. (2012). Metabolic reprogramming in cancer: Unraveling the role of glutamine in tumorigenesis. *Semin. Cell Dev. Biol.* *23*, 362–369.

DeBerardinis, R.J., and Chandel, N.S. (2016). Fundamentals of cancer metabolism. *Sci. Adv.* *2*, e1600200.

DeBerardinis, R.J., and Cheng, T. (2010). Q's next: the diverse functions of glutamine in metabolism, cell biology and cancer. *Oncogene* *29*, 313–324.

DeBerardinis, R.J., and Thompson, C.B. (2012). Cellular Metabolism and Disease: What Do Metabolic Outliers Teach Us? *Cell* *148*, 1132–1144.

DeBerardinis, R.J., Mancuso, A., Daikhin, E., Nissim, I., Yudkoff, M., Wehrli, S., and Thompson,

- C.B. (2007a). Beyond aerobic glycolysis: Transformed cells can engage in glutamine metabolism that exceeds the requirement for protein and nucleotide synthesis. *Proc. Natl. Acad. Sci.* *104*, 19345–19350.
- DeBerardinis, R.J., Mancuso, A., Daikhin, E., Nissim, I., Yudkoff, M., Wehrli, S., and Thompson, C.B. (2007b). Beyond aerobic glycolysis: transformed cells can engage in glutamine metabolism that exceeds the requirement for protein and nucleotide synthesis. *Proc. Natl. Acad. Sci. U. S. A.* *104*, 19345–19350.
- DeBerardinis, R.J., Lum, J.J., Hatzivassiliou, G., and Thompson, C.B. (2008a). The Biology of Cancer: Metabolic Reprogramming Fuels Cell Growth and Proliferation. *Cell Metab.* *7*, 11–20.
- DeBerardinis, R.J., Sayed, N., Ditsworth, D., and Thompson, C.B. (2008b). Brick by brick: metabolism and tumor cell growth. *Curr. Opin. Genet. Dev.* *18*, 54–61.
- Desai, N. (2012). Challenges in Development of Nanoparticle-Based Therapeutics. *AAPS J.* *14*, 282–295.
- Díaz-Mochón, J.J., Bialy, L., and Bradley, M. (2004). Full Orthogonality between Dde and Fmoc: The Direct Synthesis of PNA–Peptide Conjugates. *Org. Lett.* *6*, 1127–1129.
- Düvel, K., Yecies, J.L., Menon, S., Raman, P., Lipovsky, A.I., Souza, A.L., Triantafellow, E., Ma, Q., Gorski, R., Cleaver, S., et al. (2010). Activation of a Metabolic Gene Regulatory Network Downstream of mTOR Complex 1. *Mol. Cell* *39*, 171–183.
- Eales, K.L., Hollinshead, K.E.R., and Tennant, D.A. (2016). Hypoxia and metabolic adaptation of cancer cells. *Oncogenesis* *5*, e190.
- Ecker, D.M., Jones, S.D., and Levine, H.L. (2015). The therapeutic monoclonal antibody market. *MAbs* *7*, 9–14.
- Emerling, B.M., Weinberg, F., Snyder, C., Burgess, Z., Mutlu, G.M., Viollet, B., Budinger, G.R.S., and Chandel, N.S. (2009). Hypoxic activation of AMPK is dependent on mitochondrial ROS but independent of an increase in AMP/ATP ratio. *Free Radic. Biol. Med.* *46*, 1386–1391.
- Espelin, C.W., Leonard, S.C., Geretti, E., Wickham, T.J., and Hendriks, B.S. (2016). Dual HER2 Targeting with Trastuzumab and Liposomal-Encapsulated Doxorubicin (MM-302) Demonstrates Synergistic Antitumor Activity in Breast and Gastric Cancer. *Cancer Res.* *76*, 1517–1527.
- Evan, G.I., and Vousden, K.H. (2001). Proliferation, cell cycle and apoptosis in cancer. *Nature* *411*, 342–348.
- Fan, J., Ye, J., Kamphorst, J.J., Shlomi, T., Thompson, C.B., and Rabinowitz, J.D. (2014). Quantitative flux analysis reveals folate-dependent NADPH production. *Nature* *510*, 298–302.
- Fantin, V.R., and Leder, P. (2006). Mitochondriotoxic compounds for cancer therapy. *Oncogene* *25*, 4787–4797.
- Fantin, V.R., St-Pierre, J., and Leder, P. (2006). Attenuation of LDH-A expression uncovers a link between glycolysis, mitochondrial physiology, and tumor maintenance. *Cancer Cell* *9*, 425–434.
- Fazlollahi, F., Angelow, S., Yacobi, N.R., Marchelletta, R., Yu, A.S.L., Hamm-Alvarez, S.F., Borok, Z., Kim, K.-J., and Crandall, E.D. (2011a). Polystyrene nanoparticle trafficking across MDCK-II.

Nanomedicine Nanotechnology, *Biol. Med.* 7, 588–594.

Fazlollahi, F., Angelow, S., Yacobi, N.R., Marchelletta, R., Yu, A.S.L., Hamm-Alvarez, S.F., Borok, Z., Kim, K.-J., and Crandall, E.D. (2011b). Polystyrene nanoparticle trafficking across MDCK-II. *Nanomedicine Nanotechnology, Biol. Med.* 7, 588–594.

Feron, O. (2009). Pyruvate into lactate and back: From the Warburg effect to symbiotic energy fuel exchange in cancer cells. *Radiother. Oncol.* 92, 329–333.

Flavin, R., Peluso, S., Nguyen, P.L., and Loda, M. (2010). Fatty acid synthase as a potential therapeutic target in cancer. *Futur. Oncol.* 6, 551–562.

Fleige, E., Quadir, M.A., and Haag, R. (2012). Stimuli-responsive polymeric nanocarriers for the controlled transport of active compounds: Concepts and applications. *Adv. Drug Deliv. Rev.* 64, 866–884.

Le Floch, R., Chiche, J., Marchiq, I., Naiken, T., Naïken, T., Ilc, K., Ilk, K., Murray, C.M., Critchlow, S.E., Roux, D., et al. (2011). CD147 subunit of lactate/H⁺ symporters MCT1 and hypoxia-inducible MCT4 is critical for energetics and growth of glycolytic tumors. *Proc. Natl. Acad. Sci. U. S. A.* 108, 16663–16668.

Folkman, J., and Moscona, A. (1978). Role of cell shape in growth control. *Nature* 273, 345–349.

Fontana, F., Liu, D., Hirvonen, J., and Santos, H.A. (2017). Delivery of therapeutics with nanoparticles: what's new in cancer immunotherapy? *Wiley Interdiscip. Rev. Nanomedicine Nanobiotechnology* 9, e1421.

Frank, D., Tyagi, C., Tomar, L., Choonara, Y.E., du Toit, L.C., Kumar, P., Penny, C., and Pillay, V. (2014). Overview of the role of nanotechnological innovations in the detection and treatment of solid tumors. *Int. J. Nanomedicine* 9, 589–613.

Frezza, C., and Gottlieb, E. (2009). Mitochondria in cancer: Not just innocent bystanders. *Semin. Cancer Biol.* 19, 4–11.

Frezza, C., Zheng, L., Folger, O., Rajagopalan, K.N., MacKenzie, E.D., Jerby, L., Micaroni, M., Chaneton, B., Adam, J., Hedley, A., et al. (2011). Haem oxygenase is synthetically lethal with the tumour suppressor fumarate hydratase. *Nature* 477, 225–228.

Fulda, S., Galluzzi, L., and Kroemer, G. (2010). Targeting mitochondria for cancer therapy. *Nat. Rev. Drug Discov.* 9, 447–464.

Gaglio, D., Soldati, C., Vanoni, M., Alberghina, L., Chiaradonna, F., Deberardinis, R., Lum, J., Hatzivassiliou, G., Thompson, C., Ramanathan, A., et al. (2009). Glutamine Deprivation Induces Abortive S-Phase Rescued by Deoxyribonucleotides in K-Ras Transformed Fibroblasts. *PLoS One* 4, e4715.

Gaglio, D., Metallo, C.M., Gameiro, P.A., Hiller, K., Danna, L.S., Balestrieri, C., Alberghina, L., Stephanopoulos, G., and Chiaradonna, F. (2011). Oncogenic K-Ras decouples glucose and glutamine metabolism to support cancer cell growth. *Mol. Syst. Biol.* 7, 523.

Galluzzi, L., Kepp, O., Heiden, M.G. Vander, and Kroemer, G. (2013). Metabolic targets for cancer therapy. *Nat. Rev. Drug Discov.* 12, 829–846.

Gameiro, P.A., Yang, J., Metelo, A.M., Pérez-Carro, R., Baker, R., Wang, Z., Arreola, A.,

- Rathmell, W.K., Olumi, A., López-Larrubia, P., et al. (2013). In Vivo HIF-Mediated Reductive Carboxylation Is Regulated by Citrate Levels and Sensitizes VHL-Deficient Cells to Glutamine Deprivation. *Cell Metab.* *17*, 372–385.
- Gao, P., Tchernyshyov, I., Chang, T.-C., Lee, Y.-S., Kita, K., Ochi, T., Zeller, K.I., De Marzo, A.M., Van Eyk, J.E., Mendell, J.T., et al. (2009). c-Myc suppression of miR-23a/b enhances mitochondrial glutaminase expression and glutamine metabolism. *Nature* *458*, 762–765.
- Gao, Z., Zhang, L., and Sun, Y. (2012). Nanotechnology applied to overcome tumor drug resistance. *J. Control. Release* *162*, 45–55.
- Garber, K. (2016). Cancer anabolic metabolism inhibitors move into clinic. *Nat. Biotechnol.* *34*, 794–795.
- Garten, A., Petzold, S., Körner, A., Imai, S.-I., and Kiess, W. (2009). Nampt: linking NAD biology, metabolism and cancer. *Trends Endocrinol. Metab.* *20*, 130–138.
- Gatenby, R.A., and Gillies, R.J. (2004). Why do cancers have high aerobic glycolysis? *Nat. Rev. Cancer* *4*, 891–899.
- Gaude, E., and Frezza, C. (2014). Defects in mitochondrial metabolism and cancer. *2*, 1–9.
- Geng, X.-F., Fang, M., Liu, S.-P., and Li, Y. (2016). Quantum dot-based molecular imaging of cancer cell growth using a clone formation assay. *Mol. Med. Rep.* *14*, 3007–3012.
- Gennet, N., Alexander, L.M., Sánchez-Martín, R.M., Behrendt, J.M., Sutherland, A.J., Brickman, J.M., Bradley, M., and Li, M. (2009). Microspheres as a vehicle for biomolecule delivery to neural stem cells. *N. Biotechnol.* *25*, 442–449.
- Gerber, D.E. (2008). Targeted therapies: a new generation of cancer treatments. *Am. Fam. Physician* *77*, 311–319.
- Gilliam, L.A.A., Moylan, J.S., Patterson, E.W., Smith, J.D., Wilson, A.S., Rabbani, Z., and Reid, M.B. (2012). Doxorubicin acts via mitochondrial ROS to stimulate catabolism in C2C12 myotubes. *AJP Cell Physiol.* *302*, C195–C202.
- van Gisbergen, M.W., Voets, A.M., Starmans, M.H.W., de Coo, I.F.M., Yadak, R., Hoffmann, R.F., Boutros, P.C., Smeets, H.J.M., Dubois, L., and Lambin, P. (2015). How do changes in the mtDNA and mitochondrial dysfunction influence cancer and cancer therapy? Challenges, opportunities and models. *Mutat. Res. Mutat. Res.* *764*, 16–30.
- Goldberg, M.S., and Sharp, P.A. (2012). Pyruvate kinase M2-specific siRNA induces apoptosis and tumor regression. *J. Exp. Med.* *209*, 217–224.
- Gossage, L., Eisen, T., and Maher, E.R. (2014). VHL, the story of a tumour suppressor gene. *Nat. Rev. Cancer* *15*, 55–64.
- Gottlieb, E., and Tomlinson, I.P.M. (2005). Mitochondrial tumour suppressors: a genetic and biochemical update. *Nat. Rev. Cancer* *5*, 857–866.
- Greenhouse, W.V. V., and Lehninger, A.L. (1976). Occurrence of the Malate-Aspartate Shuttle in Various Tumor Types. *Cancer Res.* *36*.
- Greenhouse, W.V. V., and Lehninger, A.L. (1977). Magnitude of Malate-Aspartate Reduced Nicotinamide Adenine Dinucleotide Shuttle Activity in Intact Respiring Tumor Cells. *Cancer Res.* *37*.

- Gregori, M., Bertani, D., Cazzaniga, E., Orlando, A., Mauri, M., Bianchi, A., Re, F., Sesana, S., Minniti, S., Francolini, M., et al. (2015). Investigation of Functionalized Poly(*N*, *N* - dimethylacrylamide)- *block* -polystyrene Nanoparticles As Novel Drug Delivery System to Overcome the Blood-Brain Barrier In Vitro. *Macromol. Biosci.* *15*, 1687–1697.
- Guerra, F., Arbini, A.A., and Moro, L. (2017). Mitochondria and cancer chemoresistance. *Biochim. Biophys. Acta - Bioenerg.*
- Gui, D.Y., Sullivan, L.B., Luengo, A., Hosios, A.M., Bush, L.N., Gitego, N., Davidson, S.M., Freinkman, E., Thomas, C.J., and Vander Heiden, M.G. (2016). Environment Dictates Dependence on Mitochondrial Complex I for NAD⁺ and Aspartate Production and Determines Cancer Cell Sensitivity to Metformin. *Cell Metab.* *24*, 716–727.
- Guppy, M., Leedman, P., Zu, X., and Russell, V. (2002). Contribution by different fuels and metabolic pathways to the total ATP turnover of proliferating MCF-7 breast cancer cells. *Biochem. J* *364*, 309–315.
- Haas, R., Cucchi, D., Smith, J., Pucino, V., Macdougall, C.E., and Mauro, C. (2016). Intermediates of Metabolism: From Bystanders to Signalling Molecules. *Trends Biochem. Sci.* *41*, 460–471.
- Halestrap, A.P. (2012). The monocarboxylate transporter family-Structure and functional characterization. *IUBMB Life* *64*, 1–9.
- Hanahan, D., and Weinberg, R.A. (2011a). Hallmarks of Cancer: The Next Generation. *Cell* *144*, 646–674.
- Hanahan, D., and Weinberg, R.A. (2011b). Hallmarks of cancer: the next generation. *Cell* *144*, 646–674.
- Harwood, H.J., Organe, S., Timmermans, L., Scheys, K., Peeters, A., Brusselmans, K., Verhoeven, G., and Swinnen, J. V. (2004). Acetyl-CoA carboxylase inhibition for the treatment of metabolic syndrome. *Curr. Opin. Investig. Drugs* *5*, 283–289.
- Hatzivassiliou, G., Zhao, F., Bauer, D.E., Andreadis, C., Shaw, A.N., Dhanak, D., Hingorani, S.R., Tuveson, D.A., and Thompson, C.B. (2005). ATP citrate lyase inhibition can suppress tumor cell growth. *Cancer Cell* *8*, 311–321.
- Hay, N. (2016). Reprogramming glucose metabolism in cancer: can it be exploited for cancer therapy? *Nat. Rev. Cancer* *16*, 635–649.
- He, C., Hu, Y., Yin, L., Tang, C., and Yin, C. (2010). Effects of particle size and surface charge on cellular uptake and biodistribution of polymeric nanoparticles. *Biomaterials* *31*, 3657–3666.
- Hedekov, C.J. (1968). Early effects of phytohaemagglutinin on glucose metabolism of normal human lymphocytes. *Biochem. J.* *110*, 373–380.
- Vander Heiden, M.G. (2011). Targeting cancer metabolism: a therapeutic window opens. *Nat. Rev. Drug Discov.* *10*, 671–684.
- Vander Heiden, M.G., and Deberardinis, R.J. (2017). Understanding the Intersections between Metabolism and Cancer Biology.
- Vander Heiden, M.G., Cantley, L.C., and Thompson, C.B. (2009). Understanding the Warburg Effect: The Metabolic Requirements of Cell Proliferation. *Science* (80-). *324*, 1029–1033.
- Vander Heiden, M.G., Locasale, J.W., Swanson, K.D., Sharfi, H., Heffron, G.J., Amador-Noguez,

- D., Christofk, H.R., Wagner, G., Rabinowitz, J.D., Asara, J.M., et al. (2010). Evidence for an Alternative Glycolytic Pathway in Rapidly Proliferating Cells. *Science* (80-). 329, 1492–1499.
- Vander Heiden, M.G., Lunt, S.Y., Dayton, T.L., Fiske, B.P., Israelsen, W.J., Mattaini, K.R., Vokes, N.I., Stephanopoulos, G., Cantley, L.C., Metallo, C.M., et al. (2011). Metabolic pathway alterations that support cell proliferation. *Cold Spring Harb. Symp. Quant. Biol.* 76, 325–334.
- Hidalgo, M. (2010). Pancreatic Cancer. *N. Engl. J. Med.* 362, 1605–1617.
- Hirschhaeuser, F., Sattler, U.G.A., and Mueller-Klieser, W. (2011). Lactate: A Metabolic Key Player in Cancer. *Cancer Res.* 71, 6921–6925.
- Hitosugi, T., Kang, S., Vander Heiden, M.G., Chung, T.-W., Elf, S., Lythgoe, K., Dong, S., Lonial, S., Wang, X., Chen, G.Z., et al. (2009). Tyrosine Phosphorylation Inhibits PKM2 to Promote the Warburg Effect and Tumor Growth. *Sci. Signal.* 2.
- Hitosugi, T., Zhou, L., Elf, S., Fan, J., Kang, H.-B., Seo, J.H., Shan, C., Dai, Q., Zhang, L., Xie, J., et al. (2012). Phosphoglycerate Mutase 1 Coordinates Glycolysis and Biosynthesis to Promote Tumor Growth. *Cancer Cell* 22, 585–600.
- Hong, C.S., Graham, N.A., Gu, W., Espindola Camacho, C., Mah, V., Maresh, E.L., Alavi, M., Bagryanova, L., Krotee, P.A.L., Gardner, B.K., et al. (2016). MCT1 Modulates Cancer Cell Pyruvate Export and Growth of Tumors that Co-express MCT1 and MCT4.
- Hosios, A.M., Hecht, V.C., Danai, L.V., Johnson, M.O., Rathmell, J.C., Steinhauser, M.L., Manalis, S.R., and Vander Heiden, M.G. (2016). Amino Acids Rather than Glucose Account for the Majority of Cell Mass in Proliferating Mammalian Cells. *Dev. Cell* 36, 540–549.
- Hrkach, J., Von Hoff, D., Mukkaram Ali, M., Andrianova, E., Auer, J., Campbell, T., De Witt, D., Figa, M., Figueiredo, M., Horhota, A., et al. (2012). Preclinical development and clinical translation of a PSMA-targeted docetaxel nanoparticle with a differentiated pharmacological profile. *Sci. Transl. Med.* 4, 128ra39.
- Hsiao, I.-L., and Huang, Y.-J. (2013). Effects of serum on cytotoxicity of nano- and micro-sized ZnO particles. *J. Nanopart. Res.* 15, 1829.
- Huang, X., Chen, Y.-J., Cho, K., Nikolskiy, I., Crawford, P.A., and Patti, G.J. (2014). X¹³ CMS: Global Tracking of Isotopic Labels in Untargeted Metabolomics. *Anal. Chem.* 86, 1632–1639.
- Hwang, C.-I., Boj, S.F., Clevers, H., and Tuveson, D.A. (2016). Preclinical models of pancreatic ductal adenocarcinoma. *J. Pathol.* 238, 197–204.
- Isaacs, J.S., Jung, Y.J., Mole, D.R., Lee, S., Torres-Cabala, C., Chung, Y.-L., Merino, M., Trepel, J., Zbar, B., Toro, J., et al. (2005a). HIF overexpression correlates with biallelic loss of fumarate hydratase in renal cancer: Novel role of fumarate in regulation of HIF stability. *Cancer Cell* 8, 143–153.
- Isaacs, J.S., Jung, Y.J., Mole, D.R., Lee, S., Torres-Cabala, C., Chung, Y.-L., Merino, M., Trepel, J., Zbar, B., Toro, J., et al. (2005b). HIF overexpression correlates with biallelic loss of fumarate hydratase in renal cancer: Novel role of fumarate in regulation of HIF stability. *Cancer Cell* 8, 143–153.
- Ishihara, Y., Tsuji, M., Kawamoto, T., and Yamazaki, T. (2016). Involvement of reactive oxygen species derived from mitochondria in neuronal injury elicited by methylmercury. *J. Clin. Biochem. Nutr.* 59, 182–190.

- Israelsen, W.J., Dayton, T.L., Davidson, S.M., Fiske, B.P., Hosios, A.M., Bellinger, G., Li, J., Yu, Y., Sasaki, M., Horner, J.W., et al. (2013). PKM2 Isoform-Specific Deletion Reveals a Differential Requirement for Pyruvate Kinase in Tumor Cells. *Cell* 155, 397–409.
- Iyer, N. V., Kotch, L.E., Agani, F., Leung, S.W., Laughner, E., Wenger, R.H., Gassmann, M., Gearhart, J.D., Lawler, A.M., Yu, A.Y., et al. (1998). Cellular and developmental control of O₂ homeostasis by hypoxia-inducible factor 1 alpha. *Genes Dev.* 12, 149–162.
- Jazayeri, M.H., Amani, H., Pourfatollah, A.A., Pazoki-Toroudi, H., and Sedighimoghaddam, B. (2016). Various methods of gold nanoparticles (GNPs) conjugation to antibodies. *Sens. Bio-Sensing Res.* 9, 17–22.
- Jeong, S.M., Hwang, S., Park, K., Yang, S., Seong, R.H., Hidalgo, M., Jemal, A., Siegel, R., Xu, J., Ward, E., et al. (2016). Enhanced mitochondrial glutamine anaplerosis suppresses pancreatic cancer growth through autophagy inhibition. *Sci. Rep.* 6, 30767.
- Jhaveri, A., Deshpande, P., and Torchilin, V. (2014). Stimuli-sensitive nanopreparations for combination cancer therapy. *J. Control. Release* 190, 352–370.
- Jose, C., and Bellance, N. (2011). Choosing between glycolysis and oxidative phosphorylation: A tumor's dilemma? *Biochim. Biophys. Acta - Bioenerg.* 1807, 552–561.
- Kemp, S.J., Thorley, A.J., Gorelik, J., Seckl, M.J., O'Hare, M.J., Arcaro, A., Korchev, Y., Goldstraw, P., and Tetley, T.D. (2008). Immortalization of Human Alveolar Epithelial Cells to Investigate Nanoparticle Uptake. *Am. J. Respir. Cell Mol. Biol.* 39, 591–597.
- Kennedy, K.M., and Dewhirst, M.W. (2010). Tumor metabolism of lactate: the influence and therapeutic potential for MCT and CD147 regulation. *Future Oncol.* 6, 127–148.
- Khan, S.M., Smigrodzki, R.M., and Swerdlow, R.H. (2007). Cell and animal models of mtDNA biology: progress and prospects. *Am. J. Physiol. - Cell Physiol.* 292.
- Kim, J., Tchernyshyov, I., Semenza, G.L., and Dang, C. V. (2006). HIF-1-mediated expression of pyruvate dehydrogenase kinase: A metabolic switch required for cellular adaptation to hypoxia. *Cell Metab.* 3, 177–185.
- Kim, J.A., Åberg, C., Salvati, A., and Dawson, K.A. (2011a). Role of cell cycle on the cellular uptake and dilution of nanoparticles in a cell population. *Nat. Nanotechnol.* 7, 62–68.
- Kim, J.A., Åberg, C., Salvati, A., and Dawson, K.A. (2011b). Role of cell cycle on the cellular uptake and dilution of nanoparticles in a cell population. *Nat. Nanotechnol.* 7, 62–68.
- King, M.P., and Attardi, G. (1989). Human cells lacking mtDNA: repopulation with exogenous mitochondria by complementation. *Science* 246, 500–503.
- King, M.P., and Attardi, G. (1996). Isolation of human cell lines lacking mitochondrial DNA. *Methods Enzymol.* 264, 304–313.
- King, A., Selak, M.A., and Gottlieb, E. (2006). Succinate dehydrogenase and fumarate hydratase: linking mitochondrial dysfunction and cancer. *Oncogene* 25, 4675–4682.
- Korangath, P., Teo, W.W., Sadik, H., Han, L., Mori, N., Huijts, C.M., Wildes, F., Bharti, S., Zhang, Z., Santa-Maria, C.A., et al. (2015). Targeting Glutamine Metabolism in Breast Cancer with Aminooxyacetate. *Clin. Cancer Res.* 21, 3263–3273.
- Kroemer, G., and Pouyssegur, J. (2008). Tumor Cell Metabolism: Cancer's Achilles' Heel. *Cancer*

Cell 13, 472–482.

Kroll, W., Löffler, M., and Schneider, F. (1983). Energy parameters, macromolecular synthesis and cell cycle progression of in vitro grown Ehrlich ascites tumor cells after inhibition of oxidative ATP synthesis by oligomycin. *Zeitschrift Fur Naturforschung. Sect. C, Biosci.* 38, 604–612.

Labbé, R.F., Vreman, H.J., and Stevenson, D.K. (1999). Zinc protoporphyrin: A metabolite with a mission. *Clin. Chem.* 45, 2060–2072.

Lane, A.N., and Fan, T.W.-M. (2015). Regulation of mammalian nucleotide metabolism and biosynthesis. *Nucleic Acids Res.* 43, 2466–2485.

Le, A., Cooper, C.R., Gouw, A.M., Dinavahi, R., Maitra, A., Deck, L.M., Royer, R.E., Vander Jagt, D.L., Semenza, G.L., and Dang, C. V. (2010). Inhibition of lactate dehydrogenase A induces oxidative stress and inhibits tumor progression. *Proc. Natl. Acad. Sci.* 107, 2037–2042.

Le, A., Lane, A.N., Hamaker, M., Bose, S., Gouw, A., Barbi, J., Tsukamoto, T., Rojas, C.J., Slusher, B.S., Zhang, H., et al. (2012). Glucose-Independent Glutamine Metabolism via TCA Cycling for Proliferation and Survival in B Cells. *Cell Metab.* 15, 110–121.

Lehuédé, C., Dupuy, F., Rabinovitch, R., Jones, R.G., and Siegel, P.M. (2016). Metabolic Plasticity as a Determinant of Tumor Growth and Metastasis. *Cancer Res.* 76, 5201–5208.

Levine, A.J., and Puzio-Kuter, A.M. (2010). The Control of the Metabolic Switch in Cancers by Oncogenes and Tumor Suppressor Genes. *Science* (80-.). 330.

Li, J., and Zhu, Z. (2010). Research and development of next generation of antibody-based therapeutics. *Acta Pharmacol. Sin.* 31, 1198–1207.

Li, F., Wang, Y., Zeller, K.I., Potter, J.J., Wonsey, D.R., O'Donnell, K.A., Kim, J.-W., Yustein, J.T., Lee, L.A., and Dang, C. V (2005). Myc stimulates nuclearly encoded mitochondrial genes and mitochondrial biogenesis. *Mol. Cell. Biol.* 25, 6225–6234.

Li, Y.C., Fung, K.P., Kwok, T.T., Lee, C.Y., Suen, Y.K., and Kong, S.K. (2002). Mitochondrial targeting drug lonidamine triggered apoptosis in doxorubicin-resistant HepG2 cells. *Life Sci.* 71, 2729–2740.

Liberti, M. V., and Locasale, J.W. (2016). The Warburg Effect: How Does it Benefit Cancer Cells? *Trends Biochem. Sci.* 41, 211–218.

Linehan, W.M., Srinivasan, R., and Schmidt, L.S. (2010). The genetic basis of kidney cancer: a metabolic disease. *Nat. Rev. Urol.* 7, 277–285.

Liu, Q., Harvey, C.T., Geng, H., Xue, C., Chen, V., Beer, T.M., and Qian, D.Z. (2013). Malate dehydrogenase 2 confers docetaxel resistance via regulations of JNK signaling and oxidative metabolism. *Prostate* 73, 1028–1037.

Liu, Y., Li, W., Lao, F., Liu, Y., Wang, L., Bai, R., Zhao, Y., and Chen, C. (2011). Intracellular dynamics of cationic and anionic polystyrene nanoparticles without direct interaction with mitotic spindle and chromosomes. *Biomaterials* 32, 8291–8303.

Liu, Y., Cao, Y., Zhang, W., Bergmeier, S., Qian, Y., Akbar, H., Colvin, R., Ding, J., Tong, L., Wu, S., et al. (2012). A Small-Molecule Inhibitor of Glucose Transporter 1 Downregulates Glycolysis, Induces Cell-Cycle Arrest, and Inhibits Cancer Cell Growth In Vitro and In Vivo. *Mol. Cancer*

Ther. *11*, 1672–1682.

Livak, K.J., and Schmittgen, T.D. (2001). Analysis of Relative Gene Expression Data Using Real-Time Quantitative PCR and the $2^{-\Delta\Delta CT}$ Method. *Methods* *25*, 402–408.

Lo, Y.-W., Lin, S.-T., Chang, S.-J., Chan, C.-H., Lyu, K.W., Chang, J.-F., May, E.W.S., Lin, D.-Y., Chou, H.-C., and Chan, H.-L. (2015). Mitochondrial proteomics with siRNA knockdown to reveal ACAT1 and MDH2 in the development of doxorubicin-resistant uterine cancer. *J. Cell. Mol. Med.* *19*, 744–759.

Locasale, J.W., and Cantley, L.C. (2011). Metabolic Flux and the Regulation of Mammalian Cell Growth. *Cell Metab.* *14*, 443–451.

Löffler, M., and Schneider, F. (1982). Further characterization of the growth inhibitory effect of rotenone on in vitro cultured Ehrlich ascites tumour cells. *Mol. Cell. Biochem.* *48*, 77–90.

Loos, C., Syrovets, T., Musyanovych, A., Mailänder, V., Landfester, K., Nienhaus, G.U., and Simmet, T. (2014a). Functionalized polystyrene nanoparticles as a platform for studying bio-nano interactions. *Beilstein J. Nanotechnol.* *5*, 2403–2412.

Loos, C., Syrovets, T., Musyanovych, A., Mailänder, V., Landfester, K., Nienhaus, G.U., and Simmet, T. (2014b). Functionalized polystyrene nanoparticles as a platform for studying bio-nano interactions. *Beilstein J. Nanotechnol.* *5*, 2403–2412.

Lopes-Rodrigues, V., Di Luca, A., Mleczko, J., Meleady, P., Henry, M., Pesic, M., Cabrera, D., van Liempd, S., Lima, R.T., O'Connor, R., et al. (2017). Identification of the metabolic alterations associated with the multidrug resistant phenotype in cancer and their intercellular transfer mediated by extracellular vesicles. *Sci. Rep.* *7*, 44541.

López-Alarcón, L., and Eboli, M.-L. (1986). Oxidation of Reduced Cytosolic Nicotinamide Adenine Dinucleotide by the Malate-Aspartate Shuttle in the K-562 Human Leukemia Cell Line. *Cancer Res.* *46*.

Lu, D., Wen, X., Liang, J., Gu, Z., Zhang, X., and Fan, Y. (2009). A pH-sensitive nano drug delivery system derived from pullulan/doxorubicin conjugate. *J. Biomed. Mater. Res. Part B Appl. Biomater.* *89B*, 177–183.

Lu, H., Forbes, R.A., and Verma, A. (2002). Hypoxia-inducible Factor 1 Activation by Aerobic Glycolysis Implicates the Warburg Effect in Carcinogenesis. *J. Biol. Chem.* *277*, 23111–23115.

Lukey, M.J., Katt, W.P., and Cerione, R.A. (2016). Targeting amino acid metabolism for cancer therapy. *Drug Discov. Today*.

Lunt, S.Y., and Vander Heiden, M.G. (2011). Aerobic Glycolysis: Meeting the Metabolic Requirements of Cell Proliferation. *Annu. Rev. Cell Dev. Biol.* *27*, 441–464.

Luo, J., Hong, Y., Lu, Y., Qiu, S., Chaganty, B.K.R., Zhang, L., Wang, X., Li, Q., and Fan, Z. (2017). Acetyl-CoA carboxylase rewires cancer metabolism to allow cancer cells to survive inhibition of the Warburg effect by cetuximab. *Cancer Lett.* *384*, 39–49.

Lussey-Lepoutre, C., Hollinshead, K.E.R., Ludwig, C., Menara, M., Morin, A., Castro-Vega, L.-J., Parker, S.J., Janin, M., Martinelli, C., Ottolenghi, C., et al. (2015a). Loss of succinate dehydrogenase activity results in dependency on pyruvate carboxylation for cellular anabolism. *Nat. Commun.* *6*, 8784.

- Lussey-Lepoutre, C., Hollinshead, K.E.R., Ludwig, C., Menara, M., Morin, A., Castro-Vega, L.-J., Parker, S.J., Janin, M., Martinelli, C., Ottolenghi, C., et al. (2015b). Loss of succinate dehydrogenase activity results in dependency on pyruvate carboxylation for cellular anabolism. *Nat. Commun.* *6*, 8784.
- Lyssiotis, C.A., Son, J., Cantley, L.C., and Kimmelman, A.C. (2013). Pancreatic cancers rely on a novel glutamine metabolism pathway to maintain redox balance. *Cell Cycle* *12*, 1987–1988.
- Mamot, C., Ritschard, R., Wicki, A., Stehle, G., Dieterle, T., Bubendorf, L., Hilker, C., Deuster, S., Herrmann, R., and Rochlitz, C. (2012). Tolerability, safety, pharmacokinetics, and efficacy of doxorubicin-loaded anti-EGFR immunoliposomes in advanced solid tumours: a phase 1 dose-escalation study. *Lancet Oncol.* *13*, 1234–1241.
- Martinez-Outschoorn, U.E., Peiris-Pagés, M., Pestell, R.G., Sotgia, F., and Lisanti, M.P. (2016). Cancer metabolism: a therapeutic perspective. *Nat. Rev. Clin. Oncol.* *14*, 11–31.
- Master, A.M., and Sen Gupta, A. (2012). EGF receptor-targeted nanocarriers for enhanced cancer treatment. *Nanomedicine (Lond).* *7*, 1895–1906.
- Matoba, S., Kang, J.-G., Patino, W.D., Wragg, A., Boehm, M., Gavrilova, O., Hurley, P.J., Bunz, F., and Hwang, P.M. (2006). p53 Regulates Mitochondrial Respiration. *Science* (80-). *312*, 1650–1653.
- Matsumura, Y., Gotoh, M., Muro, K., Yamada, Y., Shirao, K., Shimada, Y., Okuwa, M., Matsumoto, S., Miyata, Y., Ohkura, H., et al. (2004). Phase I and pharmacokinetic study of MCC-465, a doxorubicin (DXR) encapsulated in PEG immunoliposome, in patients with metastatic stomach cancer. *Ann. Oncol. Off. J. Eur. Soc. Med. Oncol.* *15*, 517–525.
- Mayers, J.R., Wu, C., Clish, C.B., Kraft, P., Torrence, M.E., Fiske, B.P., Yuan, C., Bao, Y., Townsend, M.K., Tworoger, S.S., et al. (2014). Elevation of circulating branched-chain amino acids is an early event in human pancreatic adenocarcinoma development. *Nat. Med.* *20*, 1193–1198.
- MEDES, G., THOMAS, A., and WEINHOUSE, S. (1953). Metabolism of neoplastic tissue. IV. A study of lipid synthesis in neoplastic tissue slices in vitro. *Cancer Res.* *13*, 27–29.
- van der Meel, R., Vehmeijer, L.J.C., Kok, R.J., Storm, G., and van Gaal, E.V.B. (2013). Ligand-targeted particulate nanomedicines undergoing clinical evaluation: Current status. *Adv. Drug Deliv. Rev.* *65*, 1284–1298.
- Mehrara, E., Forssell-Aronsson, E., Ahlman, H., and Bernhardt, P. (2007). Specific Growth Rate versus Doubling Time for Quantitative Characterization of Tumor Growth Rate. *Cancer Res.* *67*.
- Menendez, J.A., and Lupu, R. (2007). Fatty acid synthase and the lipogenic phenotype in cancer pathogenesis. *Nat. Rev. Cancer* *7*, 763–777.
- Meng, F., Zhong, Y., Cheng, R., Deng, C., and Zhong, Z. (2014). pH-sensitive polymeric nanoparticles for tumor-targeting doxorubicin delivery: concept and recent advances. *Nanomedicine* *9*, 487–499.
- Metallo, C.M., Gameiro, P.A., Bell, E.L., Mattaini, K.R., Yang, J., Hiller, K., Jewell, C.M., Johnson, Z.R., Irvine, D.J., Guarente, L., et al. (2011). Reductive glutamine metabolism by IDH1 mediates lipogenesis under hypoxia. *Nature* *481*, 380.
- Michelakis, E.D., Webster, L., and Mackey, J.R. (2008). Dichloroacetate (DCA) as a potential

metabolic-targeting therapy for cancer. *Br. J. Cancer* 99, 989–994.

Milane, L., Duan, Z., and Amiji, M. (2011). Development of EGFR-Targeted Polymer Blend Nanocarriers for Combination Paclitaxel/Lonidamine Delivery To Treat Multi-Drug Resistance in Human Breast and Ovarian Tumor Cells. *Mol. Pharm.* 8, 185–203.

Moreno-Sánchez, R., Rodríguez-Enríquez, S., Marín-Hernández, A., and Saavedra, E. (2007). Energy metabolism in tumor cells. *FEBS J.* 274, 1393–1418.

Motlagh, N.S.H., Parvin, P., Ghasemi, F., and Atyabi, F. (2016). Fluorescence properties of several chemotherapy drugs: doxorubicin, paclitaxel and bleomycin. *Biomed. Opt. Express* 7, 2400–2406.

Mullen, A.R., Wheaton, W.W., Jin, E.S., Chen, P.-H., Sullivan, L.B., Cheng, T., Yang, Y., Linehan, W.M., Chandel, N.S., and DeBerardinis, R.J. (2011a). Reductive carboxylation supports growth in tumour cells with defective mitochondria. *Nature* 481, 385.

Mullen, A.R., Wheaton, W.W., Jin, E.S., Chen, P.-H., Sullivan, L.B., Cheng, T., Yang, Y., Linehan, W.M., Chandel, N.S., and DeBerardinis, R.J. (2011b). Reductive carboxylation supports growth in tumour cells with defective mitochondria. *Nature* 481, 385.

Mullen, A.R., Wheaton, W.W., Jin, E.S., Chen, P.-H., Sullivan, L.B., Cheng, T., Yang, Y., Linehan, W.M., Chandel, N.S., and DeBerardinis, R.J. (2011c). Reductive carboxylation supports growth in tumour cells with defective mitochondria. *Nature* 481, 385.

Mullen, A.R., Hu, Z., Shi, X., Jiang, L., Boroughs, L.K., Kovacs, Z., Boriack, R., Rakheja, D., Sullivan, L.B., Linehan, W.M., et al. (2014). Oxidation of Alpha-Ketoglutarate Is Required for Reductive Carboxylation in Cancer Cells with Mitochondrial Defects. *Cell Rep.* 7, 1679–1690.

Müller, H. (1998). Use of L-asparaginase in childhood ALL. *Crit. Rev. Oncol. Hematol.* 28, 97–113.

Muñoz-Pinedo, C., El Mjiyad, N., and Ricci, J.-E. (2012). Cancer metabolism: current perspectives and future directions. *Cell Death Dis.* 3, e248.

Mura, S., Nicolas, J., and Couvreur, P. (2013). Stimuli - responsive nanocarriers for drug delivery.

Nakano, A., Tsuji, D., Miki, H., Cui, Q., Sayed, S.M. El, Ikegame, A., Oda, A., Amou, H., Nakamura, S., Harada, T., et al. (2011). Glycolysis Inhibition Inactivates ABC Transporters to Restore Drug Sensitivity in Malignant Cells. *PLoS One* 6, e27222.

Narayanan Vijayakumar, S., Sethuraman, S., and Krishnan, U.M. Metabolic pathways in cancers: key targets and implications in cancer therapy.

Nicholls, C., Pinto, A.R., Li, H., Li, L., Wang, L., Simpson, R., and Liu, J.-P. (2012). Glyceraldehyde-3-phosphate dehydrogenase (GAPDH) induces cancer cell senescence by interacting with telomerase RNA component. *Proc. Natl. Acad. Sci.* 109, 13308–13313.

Niemirowicz, K., Markiewicz, K., Wilczewska, A., and Car, H. (2012). Magnetic nanoparticles as new diagnostic tools in medicine. *Adv. Med. Sci.* 57, 196–207.

Ott, P.A., Carvajal, R.D., Pandit-Taskar, N., Jungbluth, A.A., Hoffman, E.W., Wu, B.-W., Bomalaski, J.S., Venhaus, R., Pan, L., Old, L.J., et al. (2013). Phase I/II study of pegylated arginine deiminase (ADI-PEG 20) in patients with advanced melanoma. *Invest. New Drugs* 31,

425–434.

Owen, O.E., Kalhan, S.C., and Hanson, R.W. (2002). The key role of anaplerosis and cataplerosis for citric acid cycle function. *J. Biol. Chem.* 277, 30409–30412.

Papandreou, I., Cairns, R.A., Fontana, L., Lim, A.L., and Denko, N.C. (2006). HIF-1 mediates adaptation to hypoxia by actively downregulating mitochondrial oxygen consumption. *Cell Metab.* 3, 187–197.

Parish, C.R. (1999). Fluorescent dyes for lymphocyte migration and proliferation studies. *Immunol. Cell Biol.* 77, 499–508.

Parish, C.R., Glidden, M.H., Quah, B.J.C., Warren, H.S., Parish, C.R., Glidden, M.H., Quah, B.J.C., and Warren, H.S. (2009). Use of the Intracellular Fluorescent Dye CFSE to Monitor Lymphocyte Migration and Proliferation. In *Current Protocols in Immunology*, (Hoboken, NJ, USA: John Wiley & Sons, Inc.), p. 4.9.1-4.9.13.

Park, S.Y., Chang, I., Kim, J.-Y., Kang, S.W., Park, S.-H., Singh, K., and Lee, M.-S. (2004). Resistance of mitochondrial DNA-depleted cells against cell death: role of mitochondrial superoxide dismutase. *J. Biol. Chem.* 279, 7512–7520.

Pasca, M., Magliano, D., and Logsdon, C.D. (2013). Roles for KRAS in Pancreatic Tumor Development and Progression.

Patil, R., Portilla-Arias, J., Ding, H., Konda, B., Rekechenetskiy, A., Inoue, S., Black, K.L., Holler, E., and Ljubimova, J.Y. (2012). Cellular delivery of doxorubicin via pH-controlled hydrazone linkage using multifunctional nano vehicle based on poly(β -l-malic acid). *Int. J. Mol. Sci.* 13, 11681–11693.

Pavlova, N.N., and Thompson, C.B. (2016). The Emerging Hallmarks of Cancer Metabolism. *Cell Metab.* 23, 27–47.

Pelicano, H., Martin, D.S., Xu, R.-H., and Huang, P. (2006). Glycolysis inhibition for anticancer treatment. *Oncogene* 25, 4633–4646.

Persidis, A. (1999). Cancer multidrug resistance. *Nat. Biotechnol.*

Peters, C., and Brown, S. (2015). Antibody-drug conjugates as novel anti-cancer chemotherapeutics. *Biosci. Rep.* 35.

Petersen, G.H., Alzghari, S.K., Chee, W., Sankari, S.S., and La-Beck, N.M. (2016). Meta-analysis of clinical and preclinical studies comparing the anticancer efficacy of liposomal versus conventional non-liposomal doxorubicin. *J. Control. Release* 232, 255–264.

Petros, J.A., Baumann, A.K., Ruiz-Pesini, E., Amin, M.B., Sun, C.Q., Hall, J., Lim, S., Issa, M.M., Flanders, W.D., Hosseini, S.H., et al. (2005). mtDNA mutations increase tumorigenicity in prostate cancer. *Proc. Natl. Acad. Sci. U. S. A.* 102, 719–724.

Phan, L.M., Yeung, S.-C.J., and Lee, M.-H. (2014). Cancer metabolic reprogramming: importance, main features, and potentials for precise targeted anti-cancer therapies. *Cancer Biol. Med.* 11, 1–19.

Petrovito, L., Cano-Cortés, V., Gamberi, T., Magherini, F., Bianchi, L., Bini, L., Sánchez-Martín, R.M., Fasano, M., and Modesti, A. (2015). Cellular response to empty and palladium-conjugated amino-polystyrene nanospheres uptake: A proteomic study. *Proteomics* 15, 34–43.

- Piktel, E., Niemirowicz, K., Wątek, M., Wollny, T., Deptuła, P., and Bucki, R. (2016). Recent insights in nanotechnology-based drugs and formulations designed for effective anti-cancer therapy. *J. Nanobiotechnology* *14*, 39.
- Pollak, N., Dölle, C., and Ziegler, M. (2007). The power to reduce: pyridine nucleotides – small molecules with a multitude of functions. *Biochem. J.* *402*.
- Pollard, P.J., Spencer-Dene, B., Shukla, D., Howarth, K., Nye, E., El-Bahrawy, M., Deheragoda, M., Joannou, M., McDonald, S., Martin, A., et al. (2007). Targeted Inactivation of Fh1 Causes Proliferative Renal Cyst Development and Activation of the Hypoxia Pathway. *Cancer Cell* *11*, 311–319.
- Progatzy, F., Dallman, M.J., and Lo Celso, C. (2013). From seeing to believing: labelling strategies for in vivo cell-tracking experiments. *Interface Focus* *3*, 20130001.
- Quah, B.J.C., Warren, H.S., and Parish, C.R. (2007). Monitoring lymphocyte proliferation in vitro and in vivo with the intracellular fluorescent dye carboxyfluorescein diacetate succinimidyl ester. *Nat. Protoc.* *2*, 2049–2056.
- Rabinovich, S., Adler, L., Yizhak, K., Sarver, A., Silberman, A., Agron, S., Stettner, N., Sun, Q., Brandis, A., Helbling, D., et al. (2015). Diversion of aspartate in ASS1-deficient tumours fosters de novo pyrimidine synthesis. *Nature* *527*, 379–383.
- Ren, D., Kratz, F., and Wang, S.-W. (2011). Protein Nanocapsules Containing Doxorubicin as a pH-Responsive Delivery System. *Small* *7*, 1051–1060.
- Ren, D., Kratz, F., and Wang, S.-W. (2014). Engineered drug-protein nanoparticle complexes for folate receptor targeting. *Biochem. Eng. J.* *89*, 33–41.
- Rezaei, N., Bonilla, F.A., Seppänen, M., de Vries, E., Bousfiha, A.A., Puck, J., and Orange, J. (2017). Introduction on Primary Immunodeficiency Diseases. In *Primary Immunodeficiency Diseases: Definition, Diagnosis, and Management*, N. Rezaei, A. Aghamohammadi, and L.D. Notarangelo, eds. (Berlin, Heidelberg: Springer Berlin Heidelberg), pp. 1–81.
- Rhind, N., and Russell, P. (2012). Signaling pathways that regulate cell division. *Cold Spring Harb. Perspect. Biol.* *4*.
- Röhrig, F., and Schulze, A. (2016). The multifaceted roles of fatty acid synthesis in cancer. *Nat. Rev. Cancer* *16*, 732–749.
- Roudier, E., and Perrin, A. (2009). Considering the role of pyruvate in tumor cells during hypoxia. *Biochim. Biophys. Acta - Rev. Cancer* *1796*, 55–62.
- Roy Chowdhury, S.K., Raha, S., Tarnopolsky, M.A., and Singh, G. (2007). Increased expression of mitochondrial glycerophosphate dehydrogenase and antioxidant enzymes in prostate cancer cell lines/cancer. *Free Radic. Res.* *41*, 1116–1124.
- Sadhukha, T., and Prabha, S. (2014). Encapsulation in nanoparticles improves anti-cancer efficacy of carboplatin. *AAPS PharmSciTech* *15*, 1029–1038.
- Samid, D., Ram, Z., Hudgins, W.R., Shack, S., Liu, L., Walbridge, S., Oldfield, E.H., and Myers, C.E. (1994). Selective activity of phenylacetate against malignant gliomas: resemblance to fetal brain damage in phenylketonuria. *Cancer Res.* *54*, 891–895.
- Sanchez-Martin, R., Cano-Cortés, V., Marchal, J.A., and Perán, M. (2013). In Vitro Nanoparticle-

- Mediated Intracellular Delivery into Human Adipose-Derived Stem Cells. In *Methods in Molecular Biology* (Clifton, N.J.), pp. 41–47.
- Sanchez-Martin, R.M., Muzerelle, M., Chitkul, N., How, S.E., Mittoo, S., and Bradley, M. (2005). Bead-Based Cellular Analysis, Sorting and Multiplexing. *ChemBioChem* *6*, 1341–1345.
- Sanchez-Martin, R.M., Alexander, L., Muzerelle, M., Cardenas-Maestre, J.M., Tsakiridis, A., Brickman, J.M., and Bradley, M. (2009a). Microsphere-Mediated Protein Delivery into Cells. *ChemBioChem* *10*, 1453–1456.
- Sanchez-Martin, R.M., Alexander, L., Muzerelle, M., Cardenas-Maestre, J.M., Tsakiridis, A., Brickman, J.M., and Bradley, M. (2009b). Microsphere-mediated protein delivery into cells. *ChemBioChem* *10*, 1453–1456.
- Sánchez-Martín, R.M., Cuttle, M., Mittoo, S., and Bradley, M. (2006). Microsphere-Based Real-Time Calcium Sensing. *Angew. Chemie Int. Ed.* *45*, 5472–5474.
- Scarlett, D.-J., Herst, P., Tan, A., Prata, C., and Berridge, M. (2004). Mitochondrial gene-knockout (ρ^0) cells: A versatile model for exploring the secrets of trans-plasma membrane electron transport. *BioFactors* *20*, 213–220.
- Scheinberg, D.A., Grimm, J., Heller, D.A., Stater, E.P., Bradbury, M., and McDevitt, M.R. (2017). Advances in the clinical translation of nanotechnology. *Curr. Opin. Biotechnol.* *46*, 66–73.
- Schulze, A., and Harris, A.L. (2012). How cancer metabolism is tuned for proliferation and vulnerable to disruption. *Nature* *491*, 364–373.
- Scott, D.A., Richardson, A.D., Filipp, F. V., Knutzen, C.A., Chiang, G.G., Ronai, Z.A., Osterman, A.L., and Smith, J.W. (2011). Comparative Metabolic Flux Profiling of Melanoma Cell Lines: BEYOND THE WARBURG EFFECT. *J. Biol. Chem.* *286*, 42626–42634.
- Selak, M.A., Armour, S.M., MacKenzie, E.D., Boulahbel, H., Watson, D.G., Mansfield, K.D., Pan, Y., Simon, M.C., Thompson, C.B., and Gottlieb, E. (2005). Succinate links TCA cycle dysfunction to oncogenesis by inhibiting HIF- α prolyl hydroxylase. *Cancer Cell* *7*, 77–85.
- Seltzer, M.J., Bennett, B.D., Joshi, A.D., Gao, P., Thomas, A.G., Ferraris, D. V., Tsukamoto, T., Rojas, C.J., Slusher, B.S., Rabinowitz, J.D., et al. (2010). Inhibition of Glutaminase Preferentially Slows Growth of Glioma Cells with Mutant IDH1. *Cancer Res.* *70*, 8981–8987.
- Semenza, G.L. (2009). Regulation of cancer cell metabolism by hypoxia-inducible factor 1. *Semin. Cancer Biol.* *19*, 12–16.
- Semenza, G.L., Vaupel, P., Mayer, A., Helmlinger, G., Yuan, F., Dellian, M., Jain, R.K., Semenza, G.L., Kim, J.W., Tchernyshyov, I., et al. (2008). Tumor metabolism: cancer cells give and take lactate. *J. Clin. Invest.* *118*, 3835–3837.
- Seyfried, T.N., and Mukherjee, P. (2005). Targeting energy metabolism in brain cancer: review and hypothesis. *Nutr. Metab. (Lond)*. *2*, 30.
- Shackelford, D.B., and Shaw, R.J. (2009). The LKB1–AMPK pathway: metabolism and growth control in tumour suppression. *Nat. Rev. Cancer* *9*, 563–575.
- Shen, Y.-C., Ou, D.-L., Hsu, C., Lin, K.-L., Chang, C.-Y., Lin, C.-Y., Liu, S.-H., and Cheng, A.-L. (2013). Activating oxidative phosphorylation by a pyruvate dehydrogenase kinase inhibitor overcomes sorafenib resistance of hepatocellular carcinoma. *Br. J. Cancer* *108*, 72–81.

- Shi, J., Kantoff, P.W., Wooster, R., and Farokhzad, O.C. (2016). Cancer nanomedicine: progress, challenges and opportunities. *Nat. Rev. Cancer* *17*, 20–37.
- Shim, H., Dolde, C., Lewis, B.C., Wu, C.S., Dang, G., Jungmann, R.A., Dalla-Favera, R., and Dang, C. V (1997). c-Myc transactivation of LDH-A: implications for tumor metabolism and growth. *Proc. Natl. Acad. Sci. U. S. A.* *94*, 6658–6663.
- Simões, R. V., Serganova, I.S., Kruchevsky, N., Leftin, A., Shestov, A.A., Thaler, H.T., Sukenick, G., Locasale, J.W., Blasberg, R.G., Koutcher, J.A., et al. (2015). Metabolic Plasticity of Metastatic Breast Cancer Cells: Adaptation to Changes in the Microenvironment. *Neoplasia* *17*, 671–684.
- Singh, G. (2014). Mitochondrial FAD-linked Glycerol-3-phosphate Dehydrogenase: A Target for Cancer Therapeutics. *Pharmaceuticals (Basel)*. *7*, 192–206.
- Solaini, G., Baracca, A., Lenaz, G., and Sgarbi, G. (2010). Hypoxia and mitochondrial oxidative metabolism. *Biochim. Biophys. Acta - Bioenerg.* *1797*, 1171–1177.
- Son, J., Lyssiotis, C.A., Ying, H., Wang, X., Hua, S., Ligorio, M., Perera, R.M., Ferrone, C.R., Mullarky, E., Shyh-Chang, N., et al. (2013). Glutamine supports pancreatic cancer growth through a KRAS-regulated metabolic pathway. *Nature* *496*, 101–105.
- Sonnenschein, C., and Soto, A.M. (1999). *The society of cells: cancer and control of cell proliferation* (Bios Scientific Pub Limited).
- Sonveaux, P., Végran, F., Schroeder, T., Wergin, M.C., Verrax, J., Rabbani, Z.N., De Saedeleer, C.J., Kennedy, K.M., Diepart, C., Jordan, B.F., et al. (2008). Targeting lactate-fueled respiration selectively kills hypoxic tumor cells in mice. *J. Clin. Invest.* *118*, 3930–3942.
- Sousa, F., Castro, P., Fonte, P., Kennedy, P.J., Neves-Petersen, M.T., and Sarmento, B. (2016). Nanoparticles for the delivery of therapeutic antibodies: Dogma or promising strategy? *Expert Opin. Drug Deliv.* 1–14.
- Stanley, I.A., Ribeiro, S.M., Giménez-Cassina, A., Norberg, E., and Danial, N.N. (2014). Changing appetites: the adaptive advantages of fuel choice. *Trends Cell Biol.* *24*, 118–127.
- Stavrovskaya, A.A. (2000). Cellular mechanisms of multidrug resistance of tumor cells. *Biochemistry. (Mosc)*. *65*, 95–106.
- Stephen R. Popielarski, Suzie H. Pun, † and, and Davis*, M.E. (2005). A Nanoparticle-Based Model Delivery System To Guide the Rational Design of Gene Delivery to the Liver. 1. Synthesis and Characterization.
- Stewart, J.B., Alaei-Mahabadi, B., Sabarinathan, R., Samuelsson, T., Gorodkin, J., Gustafsson, C.M., and Larsson, E. (2015). Simultaneous DNA and RNA Mapping of Somatic Mitochondrial Mutations across Diverse Human Cancers. *PLOS Genet.* *11*, e1005333.
- Stine, Z.E., Walton, Z.E., Altman, B.J., Hsieh, A.L., and Dang, C. V. (2015). MYC, Metabolism, and Cancer. *Cancer Discov.* *5*.
- Sullivan, L.B., Gui, D.Y., Hosios, A.M., Bush, L.N., Freinkman, E., and Vander Heiden, M.G. (2015). Supporting Aspartate Biosynthesis Is an Essential Function of Respiration in Proliferating Cells. *Cell* *162*, 552–563.
- Sullivan, L.B., Gui, D.Y., and Heiden, M.G. Vander (2016). Altered metabolite levels in cancer: implications for tumour biology and cancer therapy. *Nat. Rev. Cancer* *16*, 680–693.

- Sun, R.C., Fadia, M., Dahlstrom, J.E., Parish, C.R., Board, P.G., and Blackburn, A.C. (2010). Reversal of the glycolytic phenotype by dichloroacetate inhibits metastatic breast cancer cell growth in vitro and in vivo. *Breast Cancer Res. Treat.* *120*, 253–260.
- Sun, T., Zhang, Y.S., Pang, B., Hyun, D.C., Yang, M., and Xia, Y. (2014). Engineered Nanoparticles for Drug Delivery in Cancer Therapy. *Angew. Chemie Int. Ed.* *53*, n/a-n/a.
- Suzuki, T., Iwazaki, A., Katagiri, H., Oka, Y., Redpath, J.L., Stanbridge, E.J., and Kitagawa, T. (1999). Enhanced expression of glucose transporter GLUT3 in tumorigenic HeLa cell hybrids associated with tumor suppressor dysfunction. *Eur. J. Biochem.* *262*, 534–540.
- Talekar, M., Boreddy, S.R., Singh, A., and Amiji, M. (2014). Tumor aerobic glycolysis: new insights into therapeutic strategies with targeted delivery. *Expert Opin. Biol. Ther.* *14*, 1145–1159.
- Tario, J.D., Muirhead, K.A., Pan, D., Munson, M.E., Wallace, P.K., and Wallace, P.K. (2011). Tracking immune cell proliferation and cytotoxic potential using flow cytometry. *Methods Mol. Biol.* *699*, 119–164.
- Tario, J.D., Humphrey, K., Bantly, A.D., Muirhead, K.A., Moore, J.S., and Wallace, P.K. (2012). Optimized Staining and Proliferation Modeling Methods for Cell Division Monitoring using Cell Tracking Dyes. *J. Vis. Exp.*
- Tedeschi, P.M., Markert, E.K., Gounder, M., Lin, H., Dvorzhinski, D., Dolfi, S.C., Chan, L.L.-Y., Qiu, J., DiPaola, R.S., Hirshfield, K.M., et al. (2013). Contribution of serine, folate and glycine metabolism to the ATP, NADPH and purine requirements of cancer cells. *Cell Death Dis.* *4*, e877.
- Tennant, D.A., Durán, R. V., and Gottlieb, E. (2010a). Targeting metabolic transformation for cancer therapy. *Nat. Rev. Cancer* *10*, 267–277.
- Tennant, D.A., Durán, R. V, and Gottlieb, E. (2010b). Targeting metabolic transformation for cancer therapy. *Nat. Publ. Gr.*
- Thorn, C.F., Oshiro, C., Marsh, S., Hernandez-Boussard, T., McLeod, H., Klein, T.E., and Altman, R.B. (2011). Doxorubicin pathways: pharmacodynamics and adverse effects. *Pharmacogenet. Genomics* *21*, 440–446.
- Thornburg, J.M., Nelson, K.K., Clem, B.F., Lane, A.N., Arumugam, S., Simmons, A., Eaton, J.W., Telang, S., and Chesney, J. (2008). Targeting aspartate aminotransferase in breast cancer. *Breast Cancer Res.* *10*, R84.
- Tong, X., Zhao, F., and Thompson, C.B. (2009). The molecular determinants of de novo nucleotide biosynthesis in cancer cells. *Curr. Opin. Genet. Dev.* *19*, 32–37.
- Treuel, L., Jiang, X., and Nienhaus, G.U. (2013). New views on cellular uptake and trafficking of manufactured nanoparticles. *J. R. Soc. Interface* *10*.
- Tsakiridis, A., Alexander, L.M., Gennet, N., Sanchez-Martin, R.M., Livigni, A., Li, M., Bradley, M., and Brickman, J.M. (2009). Microsphere-based tracing and molecular delivery in embryonic stem cells. *Biomaterials* *30*, 5853–5861.
- Ulbrich, K., Etrych, T., Chytil, P., Jelínková, M., and Říhová, B. (2004). Antibody-targeted Polymer–doxorubicin Conjugates with pH-controlled Activation. *J. Drug Target.* *12*, 477–489.

- Unciti-Broceta, A., Johansson, E.M. V, Yusop, R.M., Sánchez-Martín, R.M., and Bradley, M. (2012a). Synthesis of polystyrene microspheres and functionalization with Pd0 nanoparticles to perform bioorthogonal organometallic chemistry in living cells. *Nat. Protoc.* 7, 1207–1218.
- Unciti-Broceta, A., Díaz-Mochón, J.J., Sánchez-Martín, R.M., and Bradley, M. (2012b). The Use of Solid Supports to Generate Nucleic Acid Carriers. *Acc. Chem. Res.* 45, 1140–1152.
- Unciti-Broceta, J.D., Cano-Cortés, V., Altea-Manzano, P., Pernagallo, S., Díaz-Mochón, J.J., and Sánchez-Martín, R.M. (2015). Number of nanoparticles per cell through a spectrophotometric method - A key parameter to assess nanoparticle-based cellular assays. *Sci. Rep.* 5.
- Viale, A., Pettazzoni, P., Lyssiotis, C.A., Ying, H., Sánchez, N., Marchesini, M., Carugo, A., Green, T., Seth, S., Giuliani, V., et al. (2014). Oncogene ablation-resistant pancreatic cancer cells depend on mitochondrial function. *Nature* 514, 628–632.
- Vousden, K.H., and Ryan, K.M. (2009). p53 and metabolism. *Nat. Rev. Cancer* 9, 691–700.
- Wallace, D.C. (2012). Mitochondria and cancer. *Nat. Rev. Cancer* 12, 685–698.
- Wang, A.Z., Gu, F., Zhang, L., Chan, J.M., Radovic-Moreno, A., Shaikh, M.R., and Farokhzad, O.C. (2008). Biofunctionalized targeted nanoparticles for therapeutic applications. *Expert Opin. Biol. Ther.* 8, 1063–1070.
- Wang, J., Wang, T.T., Gao, P.F., Huang, C.Z., Kim, W.J., Baker, D.L., Parrill, A.L., Huang, X., Gao, G., Gao, B., et al. (2014). Biomolecules-conjugated nanomaterials for targeted cancer therapy. *J. Mater. Chem. B* 2, 8452–8465.
- Wang, J.-B., Erickson, J.W., Fuji, R., Ramachandran, S., Gao, P., Dinavahi, R., Wilson, K.F., Ambrosio, A.L.B., Dias, S.M.G., Dang, C. V., et al. (2010). Targeting Mitochondrial Glutaminase Activity Inhibits Oncogenic Transformation. *Cancer Cell* 18, 207–219.
- Wang, T., Marquardt, C., and Foker, J. (1976). Aerobic glycolysis during lymphocyte proliferation. *Nature* 261, 702–705.
- Warburg, O. (1924). Über den Stoffwechsel der Carcinomzelle. *Naturwissenschaften* 12, 1131–1137.
- Warburg, O. (1956a). On the Origin of Cancer Cells. *Science* (80-). 123.
- Warburg, O. (1956b). On respiratory impairment in cancer cells. *Science* 124, 269–270.
- Ward, P.S., Patel, J., Wise, D.R., Abdel-Wahab, O., Bennett, B.D., Collier, H.A., Cross, J.R., Fantin, V.R., Hedvat, C. V., Perl, A.E., et al. (2010). The Common Feature of Leukemia-Associated IDH1 and IDH2 Mutations Is a Neomorphic Enzyme Activity Converting α -Ketoglutarate to 2-Hydroxyglutarate. *Cancer Cell* 17, 225–234.
- Ward, P.S., Thompson, C.B., Adam, J., Hatipoglu, E., O’Flaherty, L., Ternette, N., Sahgal, N., Lockstone, H., Baban, D., Nye, E., et al. (2012). Metabolic reprogramming: a cancer hallmark even warburg did not anticipate. *Cancer Cell* 21, 297–308.
- Weinberg, F., Hamanaka, R., Wheaton, W.W., Weinberg, S., Joseph, J., Lopez, M., Kalyanaraman, B., Mutlu, G.M., Budinger, G.R.S., and Chandel, N.S. (2010). Mitochondrial metabolism and ROS generation are essential for Kras-mediated tumorigenicity. *Proc. Natl. Acad. Sci. U. S. A.* 107, 8788–8793.
- Weiswald, L.-B., Bellet, D., and Dangles-Marie, V. (2015). Spherical cancer models in tumor

biology. *Neoplasia* 17, 1–15.

Wheaton, W.W., Weinberg, S.E., Hamanaka, R.B., Soberanes, S., Sullivan, L.B., Anso, E., Glasauer, A., Dufour, E., Mutlu, G.M., Budigner, G.S., et al. (2014). Metformin inhibits mitochondrial complex I of cancer cells to reduce tumorigenesis. *Elife* 3, e02242.

Wilczewska, A.Z., Niemirowicz, K., Markiewicz, K.H., and Car, H. (2012). Nanoparticles as drug delivery systems. *Pharmacol. Rep.* 64, 1020–1037.

Wilson, M.C., Meredith, D., Fox, J.E.M., Manoharan, C., Davies, A.J., and Halestrap, A.P. (2005). Basigin (CD147) is the target for organomercurial inhibition of monocarboxylate transporter isoforms 1 and 4: the ancillary protein for the insensitive MCT2 is EMBIGIN (gp70). *J. Biol. Chem.* 280, 27213–27221.

Wise, D.R., and Thompson, C.B. (2010). Glutamine addiction: a new therapeutic target in cancer. *Trends Biochem. Sci.* 35, 427–433.

Wise, D.R., DeBerardinis, R.J., Mancuso, A., Sayed, N., Zhang, X.-Y., Pfeiffer, H.K., Nissim, I., Daikhin, E., Yudkoff, M., McMahon, S.B., et al. (2008). Myc regulates a transcriptional program that stimulates mitochondrial glutaminolysis and leads to glutamine addiction. *Proc. Natl. Acad. Sci.* 105, 18782–18787.

Wolf, A., Agnihotri, S., Micallef, J., Mukherjee, J., Sabha, N., Cairns, R., Hawkins, C., and Guha, A. (2011). Hexokinase 2 is a key mediator of aerobic glycolysis and promotes tumor growth in human glioblastoma multiforme. *J. Exp. Med.* 208, 313–326.

Wong, K.-K., Engelman, J.A., and Cantley, L.C. (2010). Targeting the PI3K signaling pathway in cancer. *Curr. Opin. Genet. Dev.* 20, 87–90.

Wong, N., De Melo, J., and Tang, D. (2013). PKM2, a Central Point of Regulation in Cancer Metabolism. *Int. J. Cell Biol.* 2013, 242513.

Wu, W., and Zhao, S. (2013). Metabolic changes in cancer: beyond the Warburg effect. *Acta Biochim. Biophys. Sin. (Shanghai)*. 45, 18–26.

Xie, G., Zhou, B., Zhao, A., Qiu, Y., Zhao, X., Garmire, L., Shvetsov, Y.B., Yu, H., Yen, Y., and Jia, W. (2015). Lowered circulating aspartate is a metabolic feature of human breast cancer. *Oncotarget* 6, 33369–33381.

Xu, F., Wang, F., Yang, T., Sheng, Y., Zhong, T., and Chen, Y. (2014). Differential drug resistance acquisition to doxorubicin and paclitaxel in breast cancer cells. *Cancer Cell Int.* 14, 538.

Yacobi, N.R., DeMaio, L., Xie, J., Hamm-Alvarez, S.F., Borok, Z., Kim, K.-J., and Crandall, E.D. (2008). Polystyrene nanoparticle trafficking across alveolar epithelium. *Nanomedicine Nanotechnology, Biol. Med.* 4, 139–145.

Yadav, K., Singhal, N., Rishi, V., and Yadav, H. (2001). Cell Proliferation Assays. In *eLS*, (John Wiley & Sons, Ltd), p.

Yahagi, N., Shimano, H., Hasegawa, K., Ohashi, K., Matsuzaka, T., Najima, Y., Sekiya, M., Tomita, S., Okazaki, H., Tamura, Y., et al. (2005). Co-ordinate activation of lipogenic enzymes in hepatocellular carcinoma. *Eur. J. Cancer* 41, 1316–1322.

Yallapu, M.M., Gupta, B.K., Jaggi, M., and Chauhan, S.C. (2010). Fabrication of curcumin encapsulated PLGA nanoparticles for improved therapeutic effects in metastatic cancer cells. *J.*

Colloid Interface Sci. 351, 19–29.

Yang, Y. (2016). Enhancing doxorubicin efficacy through inhibition of aspartate transaminase in triple-negative breast cancer cells. *Biochem. Biophys. Res. Commun.* 473, 1295–1300.

Yang, M., and Vousden, K.H. (2016). Serine and one-carbon metabolism in cancer. *Nat. Rev. Cancer* 16, 650–662.

Yang, C., Sudderth, J., Dang, T., Bachoo, R.M., McDonald, J.G., DeBerardinis, R.J., and DeBerardinis, R.J. (2009). Glioblastoma Cells Require Glutamate Dehydrogenase to Survive Impairments of Glucose Metabolism or Akt Signaling. *Cancer Res.* 69, 7986–7993.

Yang, Y., Valera, V.A., Padilla-Nash, H.M., Sourbier, C., Vocke, C.D., Vira, M.A., Abu-Asab, M.S., Bratslavsky, G., Tsokos, M., Merino, M.J., et al. (2010). UOK 262 cell line, fumarate hydratase deficient (FH-/FH-) hereditary leiomyomatosis renal cell carcinoma: in vitro and in vivo model of an aberrant energy metabolic pathway in human cancer. *Cancer Genet. Cytogenet.* 196, 45–55.

Yang, Y., Valera, V., Sourbier, C., Vocke, C.D., Wei, M., Pike, L., Huang, Y., Merino, M.A., Bratslavsky, G., Wu, M., et al. (2012). A novel fumarate hydratase-deficient HLRCC kidney cancer cell line, UOK268: a model of the Warburg effect in cancer. *Cancer Genet.* 205, 377–390.

Ying, H., Kimmelman, A.C., Lyssiotis, C.A., Hua, S., Chu, G.C., Fletcher-Sananikone, E., Locasale, J.W., Son, J., Zhang, H., Coloff, J.L., et al. (2012). Oncogenic Kras maintains pancreatic tumors through regulation of anabolic glucose metabolism. *Cell* 149, 656–670.

Yoshida, G.J. (2015). Metabolic reprogramming: the emerging concept and associated therapeutic strategies. *J. Exp. Clin. Cancer Res.* 34, 111.

Yuan, W., Wu, S., Guo, J., Chen, Z., Ge, J., Yang, P., Hu, B., and Chen, Z. (2010). Silencing of TKTL1 by siRNA inhibits proliferation of human gastric cancer cells in vitro and in vivo. *Cancer Biol. Ther.* 9, 710–716.

Yusop, R.M., Unciti-Broceta, A., Johansson, E.M. V., Sánchez-Martín, R.M., and Bradley, M. (2011). Palladium-mediated intracellular chemistry. *Nat. Chem.* 3, 241–245.

Zhan, T., Digel, M., Küch, E.-M., Stremmel, W., and Füllekrug, J. (2011). Silybin and dehydrosilybin decrease glucose uptake by inhibiting GLUT proteins. *J. Cell. Biochem.* 112, 849–859.

Zhang, H., Gao, P., Fukuda, R., Kumar, G., Krishnamachary, B., Zeller, K.I., Dang, C.V., and Semenza, G.L. (2007). HIF-1 Inhibits Mitochondrial Biogenesis and Cellular Respiration in VHL-Deficient Renal Cell Carcinoma by Repression of C-MYC Activity. *Cancer Cell* 11, 407–420.

Zhang, X., de Mito, A., Olofsson, M.H., Gullbo, J., D’Arcy, P., and Linder, S. (2015). Targeting Mitochondrial Function to Treat Quiescent Tumor Cells in Solid Tumors. *Int. J. Mol. Sci.* 16, 27313–27326.

Zheng, L., MacKenzie, E.D., Karim, S.A., Hedley, A., Blyth, K., Kalna, G., Watson, D.G., Szlosarek, P., Frezza, C., and Gottlieb, E. (2013). Reversed argininosuccinate lyase activity in fumarate hydratase-deficient cancer cells. *Cancer Metab.* 1, 12.

Zhou, Z., Kennell, C., Lee, J.-Y., Leung, Y.-K., and Tarapore, P. (2017). Calcium phosphate-polymer hybrid nanoparticles for enhanced triple negative breast cancer treatment via co-

delivery of paclitaxel and miR-221/222 inhibitors. *Nanomedicine Nanotechnology, Biol. Med.* *13*, 403–410.

Zohreh, N., Hosseini, S.H., and Pourjavadi, A. (2016). Hydrazine-modified starch coated magnetic nanoparticles as an effective pH-responsive nanocarrier for doxorubicin delivery. *J. Ind. Eng. Chem.* *39*, 203–209.

Zong, W.-X., Rabinowitz, J.D., and White, E. (2016). Molecular Cell Review Mitochondria and Cancer. *Mol. Cell* *61*, 667–676.

Zu, X.L., and Guppy, M. (2004). Cancer metabolism: facts, fantasy, and fiction. *Biochem. Biophys. Res. Commun.* *313*, 459–465.